UNIVERSITY OF HULL

Fractal Analyses of Some Natural Systems

being a Thesis submitted for the degree of PhD

in the University of Hull

by

SHI-CHING WU

MSc. (BANGOR, U.C.N.W., U.K.)
BSc. (N.T.U., TAIWAN, R.O.C.)

January 1999

Acknowledgements

I would like to express my gratitude to everyone who helped in the writing of this thesis. However, it is virtually impossible. The list below is just the tip of the iceberg of my sincere appreciation.

Special thanks are given to my supervisor, Professor Jack Hardisty who, with patience and experience, guided me through all obstacles. Thanks to Dr. David Taylor who was also my supervisor until he moved to Singapore in 1997. Sincere thanks to Dr. Annette Parkes who got involved in the final stage of correction and helped completing the thesis. Many thanks must be given to some fellow researchers for their support, for example, Mr. Daniel Patty, Dr. Shanthi Thambiah, and Professor Mia Patty. My colleagues, for their moral support and valuable discussions, deserve my sincere thanks, too. They include Ms. Salfarina Abdul-Gapor, Dr. Ian C. Drummond, Mr. Duncan Fuller, Mr. Rob Marchant, Ms. Helen Rouse, Mr. Neil Tunstall, Mr. Bin Wu, and Dr. Yue Zho. Best wishes to them. Fellow students of different nations also gave me an insight into their cultures. The departmental staff gave me valuable help, too. I am especially grateful to computer programmers, Mr. Nick Hughes, Mr. Dick Middleton, and Dr. James Duncan Whyatt. Many thanks are given to the many technical and secretarial staff who always cheer me up. I am also thankful to the staff in the Computer Centre of the University. They include, to name but a few, Mr. Stewart Doyle, Mr. Robert Allan Reese, and Mr. Alexander Sharaz. Some native English people have been more than just a source of consultancy. They include Mrs. Margaret Freeman, Mrs. Lucian Martinez, Mrs. Katherine Spry and Mrs. Paddy Long, who corrected my spoken and written English.

I also acknowledge the environment on and outside the campus, which stimulated my study in Hull. For example, the computer network on campus brought me into the world community without having to travel around physically. Also, the entire thesis has been produced using the TEX and LATEX typesetting systems, which are softwares in the public domain.

Although my parents are unlikely able to understand the thesis, they are undoubtedly my greatest support in the pursuit of knowledge, and much else. I thank them for the great autonomy they have given me.

Last but not least, this thesis could not have been prepared without the full financial support from the Ministry of Education, Taiwan, the Republic of China.

Abstract

Fractal dimensions are estimated by the box-counting method for real world data sets and for mathematical models of three natural systems. The natural systems are nearshore sea wave profiles, the topography of Shei-pa National Park in Taiwan, and the normalised difference vegetation index (NDVI) image of a fresh fern. The mathematical models which represent the natural systems utilise multi-frequency sinusoids for the sea waves, a synthetic digital elevation model constructed by the mid-point displacement method for the topography and the Iterated Function System (IFS) codes for the fern leaf. The results show that similar fractal dimensions are obtained for discrete sub-sections of the real and synthetic one-dimensional wave data, whilst different fractal dimensions are obtained for discrete sections of the real and synthetic topographical and fern data. The similarities and differences are interpreted in the context of system evolution which was introduced by Mandelbrot (1977). Finally, the results for the fern images show that use of fractal dimensions can successfully separate void and filled elements of the two-dimensional series.

Contents

List of Figures

List of Tables

Introduction

Chapter 1

Introduction

I do not know what I may seem to the world but to myself I am as a small boy playing on the shore whose attention is now and then diverted by a rounder pebble or shinier stone while the whole ocean of truth lies undiscovered before me. Isaac Newton (1642-1727).

Mandelbrot (1977) introduced the concept of fractal analysis of natural and synthetic systems and, since that time, the estimation of "fractal dimension" has become one of many methods which have been used to explore the invariant nature of objects. The literature is extensive: in 1996, for example, 478 articles used the phrase "fractal dimension" in the title, in the keywords or in the abstract in the Science Citation Index (SCI) of the Institute for Scientific Information (ISI) database of the Bath Information and Data Services (BIDS) in England. In most articles, the fractal dimension is estimated either from a single object using a single method, or from many objects using different methods, whereas in practice the fractal dimension can be derived for many objects through a single method. Within this thesis the single method known as the box-counting method will be used to estimate the fractal dimension of three natural systems. Although such analysis of natural systems provides useful description, it is necessary to construct models of the systems to test the understanding. In this thesis, the fractal dimensions of three numerical analogues for natural systems are also analysed. This analysis provides great insight into the generated systems that could be obtained from the real world data.

Among the many natural systems which could have been analysed, three data sets were chosen for this thesis. Firstly, the real and synthetic profiles of nearshore sea waves were analysed, followed by the real and synthetic topographic landform data, and the image of a fern leaf. The fractal dimension was determined for each data set by the box-counting method in order to compare the results for distinct sub-sections of the data and to compare the results obtained with natural and synthetic data. To achieve this, some statistical methods were used to compare results of natural data with their mathematical models.

The **objectives** of the thesis are, therefore, firstly to estimate the fractal dimensions of three natural systems and secondly to compare these results with corresponding analyses of mathematical models of the same three systems.

The thesis is organised into eight Chapters. Chapter One provides an overview and the remaining chapters are grouped into three Parts.

The methodology is explored in **Part I**, which is further divided into two chapters. Chapter Two is devoted to a general discussion of scientific methods and fractal analysis, whilst Chapter Three focuses on the details of the methods used. In Chapter Two, a brief review of scientific methods is introduced and followed by the essentials of Fractal Geometry, which can be illustrated by the Mandelbrot set (Mandelbrot, 1977). The Chapter continues with the description of the natural systems of interest and the reasons of selection.

Chapter Three concentrates on the methods used in the analyses of the selected data sets, which include the estimation of fractal dimension and statistical analyses. The fractal dimension is estimated by the box-counting method for all data sets, though various methods might be used for each of them. The results are compared using statistical methods, which include one-sample and two-sample tests.

Part II presents the results in Chapters Four, Five and Six, for the analyses of sea wave profiles, the topographic data and the image of a fern respectively. Each chapter has a similar format: the introduction, the real data, the synthetic models, the analysis, the results and a concise discussion. However, the comprehensive comparison with other published work will appear later, in Chapter Seven.

Wave profiles are analysed in Chapter Four, which starts with an introduction to the history of wave recording, followed by the measurement of natural waves at Teignmouth in England. This chapter continues with a section of analyses including the estimation of fractal dimensions and the conventional time series. The results of the analyses and a discussion conclude the chapter.

The study on *landform data* is detailed in Chapter Five. An introduction is followed by details of the study area and the construction of a digital elevation model (DEM) in this area, which precedes the generation of synthetic DEMs. The subsequent analysis is followed by the results and a discussion.

The *fern image* is analysed in Chapter Six. A brief introduction is followed by the construction of the normalised difference vegetation index (NDVI) image of a real fern and the simulation of a synthetic fern using the Iterated Function System (IFS) codes. This chapter continues with the analysis and the results, and concludes with a discussion.

Part III concludes the thesis. In Chapter Seven, a synthesis of all the results is presented. The synthesis is followed by a comparison with other work, from which the contribution of the present study as well as the possibility for future research is identified. The concluding remarks are presented in Chapter Eight.

The objectives of the thesis are to calculate the fractal dimensions of three natural systems and to compare these results with corresponding analyses of synthetic models of the same natural systems. The similarities and differences of the estimated fractal dimensions of three real and synthetic systems will be examined in the context of system evolution introduced by Mandelbrot (1977).

Part I

The Methodology and Methods

Chapter 2

The Methodology

If Newton had not used the word attraction, *everyone in [the French] Academy would have opened his eyes to the light; but unfortunately he used in London a word to which an idea of ridicule was attached in Paris.*

Voltaire (1694-1778) in 1730 (Mandelbrot, 1983, p.5).

2.1 Introduction

This chapter introduces a view of the scientific method, which began rooted in the inductive-deductive procedure to be formalised by Aristotle (348–322 BC). The the procedure has rarely been challenged until Newton (1642-1727), who addressed the polarised positions and argued that scientific procedure should include both inductive and deductive stages (Losee, 1980, p.81). At about the same time, Descartes (1569-1650), proposed the concept of hypotheses testing (Losee, 1980, pp.77-78). The falsificationism by Karl Popper (1902-1994) completes the last element of the contemporary scientific method for most work (TSP, 1996). This thesis, therefore, aims to exercise the scientific method following Aristotle by proposing falsifiable hypotheses which will be tested against the real world and the synthetic data.

The following major section outlines the formulation of the Chaos Theory and the theory of Fractal Geometry. Although the Fractal Geometry is arguably connected with the Chaos Theory, nowadays those two theories are examined with the conventional scientific methods and appear to be powerful enough to describe the type of chaotic dynamics which were first recorded in 1903 by Henri Poincaré (Hellemans & Bunch, 1988, p.403). Various types of system evolution can be illustrated in the Mandelbrot set, from which data are selected.

This chapter concludes with the selection of three natural systems, followed by the description of current understanding of those systems. Three natural systems corresponding to the three types of system evolution revealed in the Mandelbrot set are selected; they are the nearshore sea wave profile, the topographic data and the image of a fern leaf.

2.2 The Methodology

It is a perfectly common practice in science to inquire how things come about. However, it does not seem to apply to situations such as choosing the research methodology. While some scientists are content with whatever they were given by the authority of their field, some prefer to be more consciously aware of how the methodology they choose in conducting a research was formulated. After having discussed, below, the history of philosophy of science, the methodological structure of the thesis is derived.

2.2.1 A History of Philosophy of Science

Aristotle viewed scientific inquiry as a progression from observation to general principles and back to observations (Losee, 1980, p.6) and maintained that the scientist should induce explanatory principles from the phenomena to be explained, and then deduce statements about the phenomena from premisses that include these principles. Aristotle's inductive-deductive procedure is represented in Figure 2.1, from Losee (1980, p.6).

Aristotle argued that it is by induction that generalisations about form[1] are drawn from sense experience (Losee, 1980, p.7). In the second stage of scientific inquiry, the generalisations reached by induction are used as premisses for the deduction of statements about the initial observations.

[1] According to Aristotle, every particular thing is a union of matter and form. Matter is what makes the particular a unique individual and form is what makes the particular a member of a class of similar entities (Losee, 1980, p.7).

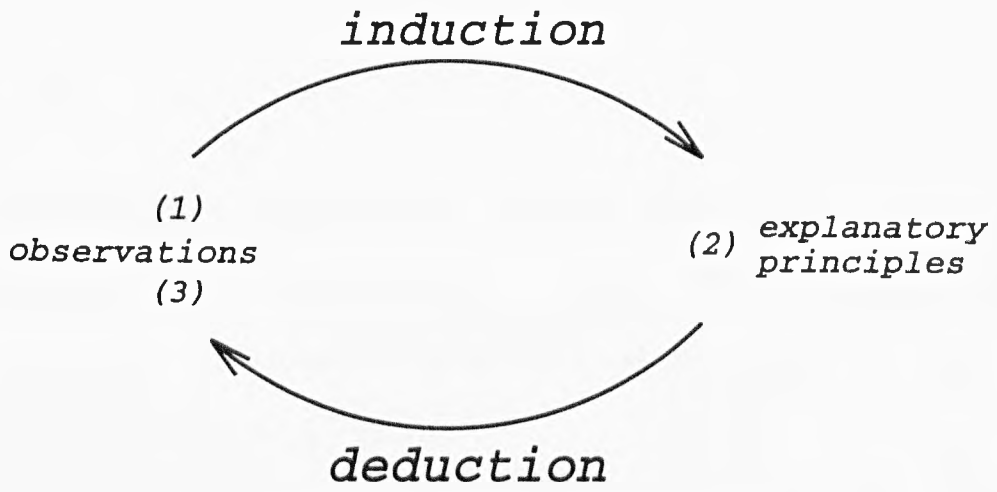

Figure 2.1: Aristotle's Inductive-Deductive Procedures.

A widely held thesis among ancient writers was that the structure of a completed science ought to be a deductive system of statements. Aristotle emphasised the deduction of conclusions from first principles.[2] Many writers in late antiquity believed that the ideal of deductive systematisation had been realised in the geometry of Euclid (*c.* 300 BC) and the statics of Archimedes (287-212 BC).

Euclid and Archimedes had formulated systems of statements – comprising axioms, definitions, and theorems – organised so that the truth of the theorems follows from the assumed truth of the axioms (Losee, 1980, p.23). With regard to the third and last aspect[3] of the ideal of deductive systematisation, that is, that theorems agree with observations, it seems merely to have been assumed by Euclid, Archimedes, and their immediate successors that such terms as "point", "line", "weight", and "rod" do have empirical correlates (Losee, 1980, p.24). This dualism claiming that the phenomenal realm is at best an "imitation" or "reflection"

[2] Aristotle held that an individual science is a deductively organised group of statements. At the highest level of generality are the first principles of **all** demonstrations–the Principles of Identity, Non-contradiction, and the Excluded Middle. These are principles applicable to **all** deductive arguments. Refer to Losee (1980, p.12) for more details.

[3] The other two are 1) that the axioms and theorems are deductively related; and 2) that the axioms themselves are self-evident truths (Losee, 1980, p.24).

of the "real world" had important repercussions in the thought of Galileo Galilei (1564-1642) and René Descartes (1596-1650).

Aristotle's method was affirmed and developed further in the Medieval period, mainly through the translation of his writings commencing about 1150, and through the work of Robert Grosseteste (*c.* 1168-1253) and Roger Bacon (*c.* 1214-1292), among others (Losee, 1980, pp.29-30).

The attack on Aristotelian philosophy, or rather, the affirmation of Archimedean philosophy, appeared in the seventeenth century, notably in the work of Galileo Galilei, Francis Bacon (1561-1626) and René Descartes, among others. However, Galileo's anti-Aristotelian polemic was not directed against Aristotle's inductive-deductive method. In fact, he accepted Aristotle's view of scientific inquiry as a two-stage progression from observations to general principles and back to observations. His remarks about scientific procedure were directed against practitioners of a false Aristotelianism, which encouraged a dogmatic theorising that parted science from its empirical base. Galileo affirmed the Archimedean ideal of deductive systematisation. However, a more important aspect of Galileo's Archimedean-Platonic commitment was his emphasis on the value of abstraction and idealisation in science. An important role of observation and experiment in Descartes' theory of scientific method is to suggest hypotheses specifying mechanisms that are consistent with the fundamental laws. Also, it is possible to remove discrepancies between theory and observation by altering the associated hypotheses, thus leaving intact the general laws of nature. The existence of this flexibility within the Cartesian system was one reason for its popularity during the seventeenth and the eighteenth centuries is mentioned by Losee (1980, pp.77-78).

Descartes was among the rationalists such as Benedictus Spinoza (1632–1677), and Gottfried Wilhelm Leibniz (1646–1716) who took the view that the self-evident propositions deduced by reasoning are the sole basis of all knowledge (Cottingham, 1988, p.4). Refer to, for example, Adam & Tannery (1964-76), Wilson (1978), Hellemans & Bunch (1988), Cottingham (1988) and Cottingham *et al.* (1985-91), for more details on rationalism and rationalists.

In contrast, empiricists such as Thomas Hobbes (1588–1679), John Locke (1632–1704), David Hume (1711–1776), and Bertrand Russell (1872–1970) insisted that "all our knowledge is based upon or derived ultimately from experience" (Evans, 1964, p.4). Further details on empiricism and empiricists can be found in, for example, Santillana & Zilsel (1941), Zilsel (1941) and Priest (1990).

Isaac Newton (1642-1727) made comments about scientific method that were directed primarily against Descartes and his followers. He opposed the Cartesian method by affirming Aristotle's theory of scientific method. However, by insisting that scientific procedure should include both an inductive stage and a deductive stage, Newton affirmed a position that had been defended by Grosseteste and Roger Bacon in the thirteenth century, as well as by Galileo and Francis Bacon in the beginning of the seventeenth century. In fact, this procedure which incorporates the Cartesian system of testing hypotheses has laid the foundation for the most common scientific method used today.

During the Enlightenment[4] and the beginning of the nineteenth century that followed the success of Newton's theories, there was a romantic reaction against

[4] The period of the Enlightenment is often equated with the latter part of the eighteenth century (Hellemans & Bunch, 1988, p.188).

the mechanistic and materialistic philosophy behind scientific development. The romanticists' view of nature was, to use a modern term, holistic; that is, "they believed that all nature should be viewed as a single organism and imbued with spirit" (Hellemans & Bunch, 1988, p.189). Their influence was eventually replaced by materialism and "positivism" (Hellemans & Bunch, 1988, p.271). In positivism, the use of scientific principles to explain the laws governing all phenomena supersedes the two earlier stages of knowledge: a theological stage in which phenomena are explained by divine powers and a metaphysical stage in which phenomena are explained by general philosophical ideas. Little attention was paid to the development of scientific methods until the arrival of the theory of falsificationism first expounded by Karl Popper (1902-1994).

The theory of falsificationism states that "although scientific generalizations cannot be conclusively verified, they can be conclusively falsified by a counterinstance; therefore, science is not certain knowledge but a series of 'conjectures and refutations', approaching, though never reaching, a definite truth" (TSP, 1996, p.697). In other words, falsificationism is the belief that the merit of a scientific theory lies only in how well it stands up to rigorous testing. Such thinking also implies that a theory can only be held to be scientific if it makes predictions that are testable. For Popper, psychoanalysis and Marxism are unfalsifiable and therefore unscientific. "Critics of this belief acknowledge the strict logic of this process, but doubt whether the whole of scientific method can be subsumed into so narrow a programme" (TSP, 1996, p.321). Nevertheless, Popper's revolutionary contribution to scientific methods is best illustrated by one of his critics, Thomas S. Kuhn (1922–), who argued that paradigms such as Darwinism and Newtonian theory are so dominant that "they

are uncritically accepted as true, until a 'scientific revolution' creates a new orthodoxy" (TSP, 1996, p.496). Whilst the scientific method has reasonably solidified so far, some modern scientists are eager to break loose from the rigid tradition of partitioning disciplines strongly influenced by the Linnaean classification scheme.

Over the history of science since the Renaissance, as the totality of science knowledge has grown, scientists have specialised more and more. At the same time as there has been specialisation, there has also been a merging of disciplines. Albert Einstein (1879-1955) limited his work to theoretical physics, but contributed to virtually all parts of that field; whilst astrophysics and biophysics are two examples of merging.

A recent revolution in scientific development showed that a single principle is devised to interpret various phenomena across scientific fields. Chaos Theory has been applied, for example, to meteorology, population modelling, quantum mechanics and astronomy (Crilly *et al.*, 1991). Mandelbrot (1983) also revolutionised the non-Euclidean geometry and formulated the theory of Fractal Geometry solely from the entities of the classic geometry. The applicability of the theory will be rigorously tested under the framework evolved in the long history of science.

2.2.2 The Methodological Structure of the Thesis

This thesis exercises perhaps the most common approach in science, described in the previous section and illustrated in Figure 2.2. The methodology is utilised to estimate the fractal dimensions of real measurements and the corresponding mathematical models, and to make comparisons between them. The methodological structure appears to transcribe the ancient Greek inductive-deductive procedure.

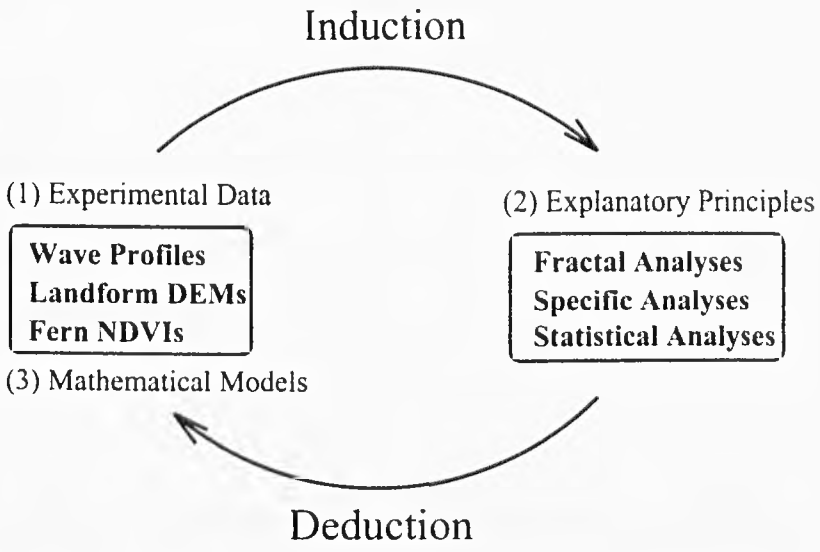

Figure 2.2: The Methodological Structure of the Thesis.

However, it is more akin to the proposal by Isaac Newton, who integrated the Greek "either-inductive-or-deductive" approach and insisted that scientific procedure should include both inductive and deductive stages (Losee, 1980, p.81). Furthermore, the structure incorporates the concept of testing hypotheses formulated by René Descartes (Losee, 1980, pp.77-8).

At the methodological level, the inductive-deductive procedure is followed twice in completing the analysis of a single data set. In the inductive stage of the first run, the theoretical aspect of the fractal dimension is introduced, followed by the deductive stage of the first run, the estimation of the fractal dimension of the real world data. In order to test the applicability of the fractal dimension, the derived fractal dimension has to be compared to that of known or mathematical models. Therefore, the inductive-deductive procedure is followed for the second time, when theoretical models of natural systems are introduced then followed by the estimation of the fractal dimension of such synthetic data. This procedure is completed for each of the three data sets: wave profiles, landform data, and fern images.

Fractal Geometry centres on the estimating of fractal dimensions and also provides a guidance to the selection of data. The fundamental concept of Fractal Geometry is given in the following section, while the methods of analysis are detailed in Chapter Three. This chapter continues with the selection of data in the context of system evolution introduced in the Mandelbrot set.

2.3 Fractal Geometry: An Aspect of Nature

Although Henri Poincaré (1854–1912) (TSP, 1996, p.690) recognised in 1903 that very small inaccuracies in initial conditions can lead to vast differences in a short order, the fundamental idea of chaos was not explored much further until the 1970s and 1980s (Hellemans & Bunch, 1988, p.403). The most famous examples of chaos phenomena from the empiricist and rationalist camps are, perhaps, the Lorenzian waterwheel (Gleick, 1987, p.27) and the logistic map (May, 1992, for example), respectively. However, a deterministic system shows a totally different dynamic if the researcher either changes the experience of data collection or alters the reasoning of an equation; if, for example, in the case of the waterwheel, "irregular" movements of the bucket are regarded as "data" instead of "noise"; or, in the case of the logistic equation, one of the parameters is altered to an unusual range of value. See Figure 2.3 and refer to Appendix A for chaos arising from a deterministic system. The C programme that calculates such a system is listed in Appendix B. However, the quantification of such structure proved to be a great challenge until the science of Fractal Geometry was introduced.

Fractal Geometry, coined and developed by Mandelbrot (1977), shows that a

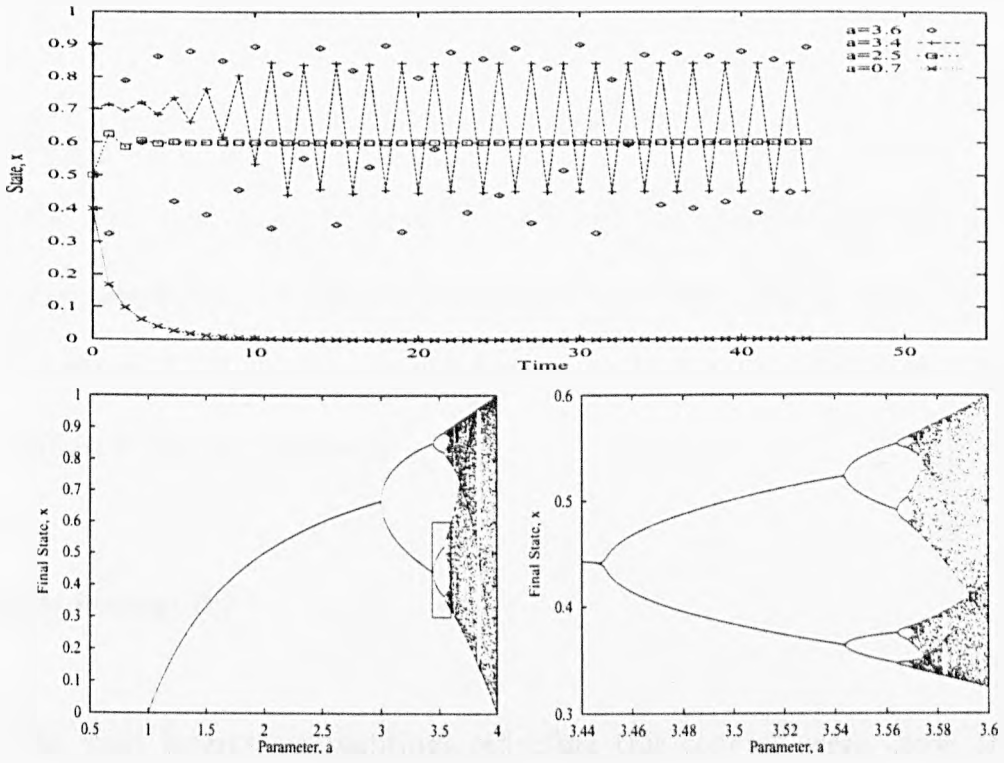

Figure 2.3: Dynamics of a Logistic System, $x_{t+1} = ax_t(1 - x_t)$.
(Top) The state variable (x) is plotted against time (t) for various values of parameters (a), representing the stable, bifurcating, and chaotic dynamics. The final state x is then plotted against a range of the parameter a (see below).
(Bottom Left) As parameter a increases from 0 to 4, its dynamics change from predictable to unpredictable. When a is greater than 3.5699456..., chaos occurs.
(Bottom Right) Self-similar structure is as seen from the window on the left.

complex structure can be generated by simple building blocks (Barnsley, 1993). Furthermore, it produces scale-invariant fractional dimensions entirely different from Euclidean integral dimensions, although it is based on the entities of classical geometry (Mandelbrot, 1983). The implication is that a complicated object of self-similar structure could be represented by the fractal dimension.

This section introduces fractals that existed before the Fractal Geometry was formulated, including those in humanities, and various objects that are of fractal nature. It continues with the definition of a fractal set, followed by the discussion on the system evolution revealed in the Mandelbrot set.

2.3.1 Fractals before Mandelbrot

The concept of fractals is scattered throughout humanistic as well as scientific works, although the term was coined by Mandelbrot (1977). It appeared, for example, in the European arts and in the oriental literatures. Many other objects were identified as of fractal nature by Mandelbrot (1983) himself, and were the source of inspiration for his creation of Fractal Geometry.

Fractals in Humanity

Perhaps the most interesting paintings reflecting this concept were those of the Dutch artist, Maurits C. Escher (1902-1972) (Escher, 1967; Schattschneider, 1990). Mandelbrot (1988) was fascinated by the tesselating plane figures which seem intuitively to have some fractal form. For example, the "Day and Night" and the "Circle Limits" woodcut series take people by surprise with the gradual changes between the dark and bright entities (Schattschneider, 1990; Jones, 1991). A much earlier artist who generated a fractal object based on regular pentagons was Albrecht Dürer (1471–1528). If we take a regular pentagon and surround that by five identical pentagons, the shape created fits almost exactly into a larger pentagon (Dixon, 1987; Jones, 1991). Imagine starting the procedure from the larger pentagon. We could draw the six smaller pentagons that sit inside the larger one. The subdivision can continue, with ever decreasing pentagons being produced. Each pentagon is a copy of the whole. If subdivision is continued *ad infinitum*, Dürer's pentagons form a truly fractal object.

However, an even earlier example was found in one of the Buddhist sutras (Ap-

pendix C). The "Array of Flowers" Sutra describes that "all [universes] are contained in one and one in all" (Harvey, 1990, p.118). This notion was echoed by some recent cosmologists. For example, Lanini *et al.* (1996; 1998) argued that "the universe is not uniform at all, but has a never-ending hierarchical structure in which galaxies group together in clusters which, in turn, group together in super clusters, and so on." They assumed that the Universe is better described in terms of a fractal set characterised by a fractal dimension. Objections were abundant, however, especially from other studies on the galaxy redshift surveys (Guzzo, 1997; Coles, 1998, for example).

The above artistic and literal descriptions reveal objects that fit into the definition of a fractal. There were also certain mathematical objects whose fractal nature led to the development of Fractal Geometry.

Objects of Fractal Nature

Several basic ideas of fractals might be viewed as mathematical and scientific implementations of loose but potent notions that date back to Aristotle and Leibniz. Aristotle had already believed that the gap between any two living species can be bridged continuously by other species. He was therefore fascinated by "in-between" animals. This principle of continuity reflected the belief in "missing links" of all sorts, including in Greek mythology the chimera, a beast with a lion's head and a goat's body (Mandelbrot, 1983, p.405). Mandelbrot (1983, p.406) found that the idea of fractional integro-differentiation had occurred to Leibniz, as soon as Leibniz had developed his version of calculus. In his free translation of one of Leibniz's letters, Mandelbrot (1983, p.405) stated that "[it is] possible to say in a way that

successive differentials are in geometric progression. One can ask what would be a differential having as its exponent a fraction. You see that the result can be expressed by an infinite series. Although this seems removed from Geometry, which does not yet know of such fractional exponents, it appears that one day these paradoxes will yield useful consequences, since there is hardly a paradox without utility."

In mathematics, Aristotle's idea finds an application in the interpolation of the sequence of integers by ratios of integers, then by limits of ratios of integers. What about Cantor, Peano, and Koch curves? Cantor's curve is "divisible without end but is not continuous" (Mandelbrot, 1983, p.406). They are among the examples of fractal objects that were devised in the pre-Mandelbrot era. A list of people and their respective relations to the concept of fractals is given in Table 2.1.

The Fractal Dust

During the late nineteenth century the theory of sets was being developed. Mathematicians delighted in producing sets with ever more weird properties, many of them now recognised as being fractal in nature. One of these is the set devised by George Cantor (1845–1918) (Lauwerier, 1991; Jones, 1991). Its construction is relatively simple: Begin with all real numbers in the interval [0,1] of the real time; Extract the interval (1/3, 2/3) which constitutes the central third of the original interval, leaving the two closed intervals [0, 1/3] and [2/3, 1]; Continue this process, at each stage extracting the central third of any interval that remains. It may not seem particularly remarkable if this is continued *ad infinitum*, but the set has some unusual properties. A piece of simple arithmetic shows that the points remaining in the Cantor set, although infinite in number, are crammed into a total length of

Date	Name	Profession	Note
		Fractal Artists	
1471–1528	Albrecht Dürer		(Jones, 1991; Dixon, 1987)
1902–1972	Maurits Escher	Nl. Artist	(Jones, 1991; Schattschneider, 1990)
		Fractal Dusts	
1845–1918	George Cantor	D. Math.	(Jones, 1991; Peitgen *et al.*, 1992)
		Fractal Curves	
1858–1932	Giuseppe Peano		Space–filling curve
1862–1943	David Hilbert		
1870–1924	Helge von Koch	Su. Math.	Nowhere differentiable curve
		Fractal in Higher Dimensions	
1882–1969	Waclaw Sierpinski	Pl. Math.	Sierpinski triangle
		Fractal in Complex Plane	
1878–1929	Pierre Fatou		
1893–1978	Gaston Julia	Fr. Math.	Julia set
		Non-integral Dimensions	
1919	Felix Hausdorff	D. Math.	Hausdorff dimension
		Mandelbrot Set	
1976	B.B. Mandelbrot	Am. Math.	Coined 'fractal' and developed Fractal Geometry

Table 2.1: A List of People who Created Fractal Objects.
Most of them were artists and mathematicians (Math.), dwelling in France (Fr.), Germany (D.), Netherland (Nl.), Poland (Pl.), Swiss (Su.) in Europe. The American (Am.) mathematician Mandelbrot (1983) was also related to French institutes.

magnitude of zero. Such points must be disconnected: there is some unfilled space between any pair of points in the set, no matter how close these points may be. The set is said to form a "dust". Thus, the Cantor set contains an infinite set of values which lie in a zero length space, yet they have a one-to-one correspondence with the set of all real values which fill the interval [0,1]. See Figure 2.4.

The Fractal Curves

In 1890 Giuseppe Peano (1858-1932) "show[ed] how thoroughly mathematicians could outrage common sense when he constructed continuous space filling curves". David Hilbert (1862-1943) later developed a similar construction, a curve which vis-

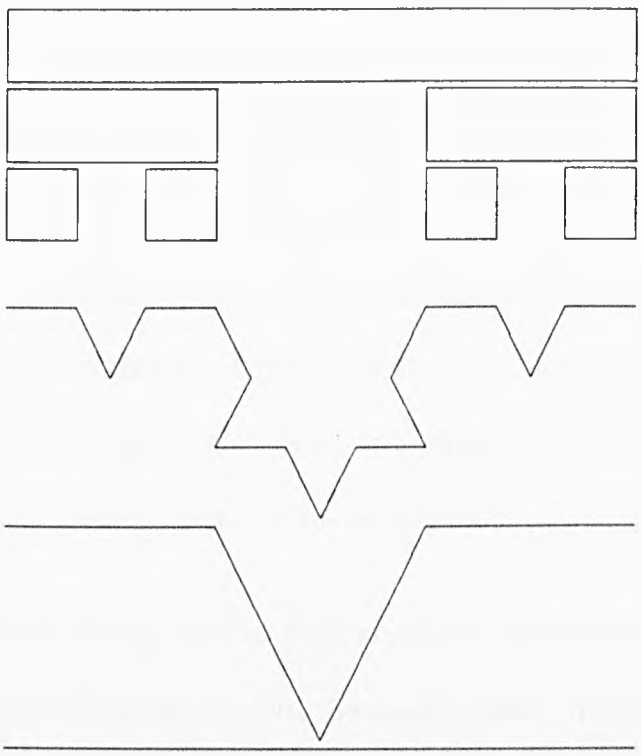

Figure 2.4: The Cantor Set and the Koch Curve.
The Cantor comb (rectangles) is obtained by repeatedly taking away the middle third of the previous rectangles. A similar process is applied to construct the Koch curve (lines), where the gap is replaced with two lines of 1/3 unit.

its every point in a square and which is nowhere differentiable. The curve generated by Helge von Koch (1870-1924) in 1904 is one of the classic fractal objects. The curve is constructed from a line segment of unit length. Then the central third of this line is extracted and replaced by two lines of length 1/3. This process is continued, the central third of any line segment being replaced at each stage by two lines of length one third of that of the segment. The protrusion of the replacement is always on the same side of the curve. Note that the points at which the final curve touches the original line are the points of the Cantor set. At each stage, the total length of the curve is multiplied by 4/3. In fact, the length of the complete Koch curve is infinite. Now consider the area between the Koch curve and the original line. At each stage, four times as many new triangles are added to the total area, the area

of each triangle added being one-ninth of those added at the previous stage. Thus, the increase in area at any stage is four-ninths of the area added at the previous stage. This leads to a geometric progression for the total area, which has a finite sum. Therefore, we have a curve of infinite length which encloses a finite area. This curve is nowhere differentiable, that is, it does not have a well defined slope at any point. It also contains an infinite number of perfect miniature images of itself. As the curve is infinite in length, any scaled down sub-image is also of infinite length. Refer to Jones (1991, p.11) and Figure 2.4 for more details.

There are many other fractal curves with similarly intriguing properties, for example, Levy's curve, Koch's quadric curve, the monkey tree curve, etc. (Lauwerier & Kaandorp, 1987; Saupe, 1988b; Jones, 1991; Peitgen *et al.*, 1992)

Fractal Objects in Higher Dimensions

Waclaw Sierpinski (1882-1969) gave his name to a number of fractal objects: the Sierpinski triangle (or gasket) and the Sierpinski carpet, formed in two-dimensional space; and the Sierpinski tetrahedron and sponge, constructed in three-dimensional space. To construct a Sierpinski triangle, extract from an original triangle the inverted half-scale copy of itself formed by joining the midpoints of the three sides. Three half-scale triangles now remain, so one-fourth of the area of the original triangle has been removed. The process is now repeated for each triangle remaining in the object. If the original area is set to A, the area removed by this process gives another geometric progression which sums up to A. That is, we have extracted a region of the same size as the whole of the original space, but we still have points left in the Sierpinski triangle. A similar procedure can be performed using a square as

the original region, which gives a "Sierpinski carpet". The Sierpinski tetrahedron is created by a similar repetitive construction and replacement strategy, starting with a tetrahedron or triangular based pyramid. The Sierpinski sponge, also known as the Menger sponge, is a close relative of this shape. Its formation is very similar to that of the Sierpinski carpet, except that the starting shape is a cube in three dimensions rather than a square in two dimensions. Refer to Jones (1991, p.14) for more details.

2.3.2 Fractals Formally Defined

This section introduces the essentials of the fractal objects; that is, fractals are exactly self-similar or statistically self-affine structures of non-integral dimensions residing in a complete matrix space.

Fractals are Self-similar Objects of Non-Integral Dimensions

The word "fractal" has its root from the Latin adjective *fractus* corresponding to the verb *frangere*, meaning "to break" (Mandelbrot, 1983). Mandelbrot (1983, p.15) stated that "a fractal is by definition a set for which the Hausdorff-Bescovitch dimension [D] strictly exceeds the topological dimension [D_T]", and "every set with a non-integer D is a fractal", although "a fractal may have an integer D"; he continued that "the dimension D_T is always an integer, but D need not be an integer." The formal definition of topological dimension is sophisticated (Hastings & Sugihara, 1993, p.29, for example); usually, objects such as a curve, a surface and a solid are assigned topological dimensions of 1, 2 and 3, respectively (Barabási & Stanley,

1995, p.31). The roots of defining dimensions that were in Euclid's Books on geometry were "as clear as mud" (Mandelbrot, 1983, p.409). However, the relationship between Euclidean space (D_E) and topological dimension is generally made clear in the statements such as "the topological dimension of an object in Euclidean space" (Hastings & Sugihara, 1993, p.29). Therefore, the following relationship is generally accepted, that is,

$$D_T \leq D \leq D_E. \tag{2.1}$$

The Hausdorff-Bescovitch dimension comprises the Hausdorff measure and its non-integral dimension formulated by Bescovitch (Mandelbrot, 1983, p.364); therefore, it was actually developed by the two mathematicians whose names are attached to it. The fractal dimension has been widely used instead of the Hausdorff-Bescovitch dimension since Mandelbrot (1983). However, researchers sometimes rephrased Mandelbrot's definition erroneously. For example, Jones (1991, p.7) quoted from Peitgen & Richter (1986) who stated that "Mandelbrot's definition of a fractal set X is one whose *Hausdorff dimension* $h(X)$ is not an integer"; and Turcotte (1992, p.74) even replaced the Hurst exponent with the Hausdorff measure.

The notion of non-integral dimension is one of the two essential characteristics of a fractal set whereas the other is self-similarity and self-affinity. A fractal object is self-similar in that subsections of the objects are similar in some sense to the whole object. No matter how small a subdivision is taken, the subsection contains no less detail than the whole. Typical examples of fractal objects are "Dürer's Pentagon" (*c.* 1500), the "Pythagorean Tree" and the "Snowflake Curve" by Helge von Koch in 1904 (Jones, 1991, p.1). These examples have exactly similar subsections, but many fractal objects, particularly those which occur naturally, have statistically similar

subsections, so that those subsections have similar forms with some variations.

In the Euclidean space of dimension E, a real ratio $r > 0$ determines a transformation called *similarity* (Hutchinson, 1981). It transforms the point $X = (X_1, \cdots X_\delta, \cdots, X_E)$ into the point $r(X) = (rX_1, \cdots, rX_\delta, \cdots, rX_E)$; hence, it transforms a set into another set. A self-similar fractal appears the same for all scales. A coastline exhibits such self-similar behaviour. Upon magnification, segments of the coastline look like segments at different scales (Poon *et al.*, 1992, p.1273). Other self-similar sets include, for example, the Cantor dust, the Koch curve, the Julia sets and the Mandelbrot set.

Similarly, in the Euclidean space of dimension, E, a collection of positive real ratios $r = (r_1, \cdots, r_\delta, \cdots, r_E)$ determines an *affinity*. It transforms each point $X = (X_1, \cdots, X_\delta, \cdots, X_E)$ into the point $r(X) = r(X_1, \cdots, X_\delta, \cdots, X_E) = (r_1X_1, \cdots, r_\delta X_\delta, \cdots, r_E X_E)$; hence, it transforms a set S into the set $r(S)$. Mandelbrot (1983, p.350) also defined the bounded and unbounded sets of both the self-similar and self-affine sets. Practical examples are vertical cuts through either relief, a surface of non-isotropic metal fracture, or records of electronic noise.

A self-affine fractal is self-similar only when scaled in one direction. This scaling behaviour of different profiles, such as surface profiles of fractured rocks, is characterised by the Hurst exponent H in the range $0 < H < 1$ (Poon *et al.*, 1992, p.1274). When H is close to 0, the surfaces are roughest while values of H close to 1 are relatively smooth. H is related to the typical changes of surface height, z, which is a single-valued function of distance, t; that is, when t is magnified by a factor r, i.e., t becomes rt, then z must be magnified by a factor r^H, i.e., z becomes $r^H z$.

More common examples of self-affine structures are records of the scalar Brownian motion $B(t)$, of the more general fractional scalar Brownian motion $B_H(t)$ whose parameter H satisfies $0 < H < 1$, and of related fractal motion (Mandelbrot, 1985, p.257). Note that, when a point moves in the xy-plane, the "trail" is the set of points (x, y) that have been visited, and the "record" will be the sets of points $(t, x(t))$ and $(t, y(t))$. Wiener's scalar Brownian motion $B(t)$ is the process within independent and stationary Gaussian increments. It has a well-known invariance property: at setting $B(0) = 0$, the random processes $B(t)$ and $b^{-1/2}B(bt)$ are identical in distribution for every ratio $b > 0$. One observes that the rescaling ratios of t and of B are different, hence the transformation from $B(t)$ to $b^{-1/2}B(bt)$ is an "affinity". This is why $B(t)$ is "statistically self-affine" (Mandelbrot, 1983; Mandelbrot, 1985, p.257).

A very important role is played in Fractal Geometry by the more general fractional Brownian motion $B_H(t)$, where $0 < H < 1$. If $B_H(0) = 0$, the random processes $B_H(t)$ and $b^{-H}B(bt)$ are identical in distribution. The value $H = 1/2$ brings $B(t)$ as a special case of $B_H(t)$, called *random walk* or *Brownian motion*. It is the random walk or the Brownian motion that is used to model self-affine fractals such as mountain terrains (Voss, 1988; Poon *et al.*, 1992). This current thesis utilises this concept to generate digital elevation models, detailed in Chapter Five.

Evertsz & Mandelbrot (1992) stated that "the idea of self-similarity is readily extended from sets to measures", which are then called "multifractals"; although the probabilistic approach to multi-fractals was first described in two papers by Mandelbrot (1974a; 1974b). Interest in multifractals has grown considerably (Held & Illangasekare, 1995; Gutierrez *et al.*, 1996; Tcheou & Brachet, 1996; Bershadskii, 1997, for example). Refer to Appendix D for some details of multifractal dimensions.

Deterministic and Random Fractals

The relationship between (deterministic) fractals and random fractals was that (exactly) scale-invariant objects are fractals and statistically scale-invariant objects are random fractals (Hastings & Sugihara, 1993, p.13). Fractals are defined by Hastings & Sugihara (1993, p.16), for example, to be scale-invariant, either self-similar or self-affine, geometric objects. A geometric object is called "self-similar" if it may be written as a union of rescaled copies of itself, with the rescaling copies isotropic or uniform in all directions. A geometric object is called "self-affine" if it may be written as a union of rescaled copies of itself, where the rescaling may be anisotropic or dependent on the direction. "Regular fractals" display exact self-similarity. "Random fractals" display a weaker, statistical version of self-similarity or, more generally, self-affinity. Although describing the same concepts, other researchers (Turcotte, 1992, for example) used terms such as "deterministic" and "statistical" fractals.

The Space where Fractals Live

In the geometrical space of real numbers, R, each point in it is a real number, or a dot on a line. The Euclidean plane, R^2, is the coordinate plane of calculus. Any pair of real numbers $x_1,\ x_2 \in R$ determines a single point in R^2, where $\in$ means "belongs to." In the complex plane, C, any point is represented by

$$x = x_1 + ix_2, \tag{2.2}$$

where $i = \sqrt{-1}$ for some pair of real numbers $x_1,\ x_2 \in R$. Any pair of numbers $x_1,\ x_2 \in R$ determines a point of C. It is obvious that C is essentially the same as

R^2, but there is an implied distinction. In C we can multiply two points x, y and obtain a new point in C,

$$x \cdot y = (x_1 + ix_2)(y_1 + iy_2) = (x_1y_1 - x_2y_2) + i(x_2y_1 + x_1y_2). \tag{2.3}$$

The Riemann Sphere, $\hat{C}$, is formally defined as $\hat{C} = C \cup \{\infty\}$. That is, it includes all the points of C together with the "point at infinity." Here is a way of constructing and thinking about $\hat{C}$. Place a sphere on the plane C, with the South Pole on the origin, and the North Pole vertically above it.

Fractal Geometry is concerned with the structure of subsets of various simple "geometrical" spaces. Such a space is denoted by X, and defined thus by Barnsley as "a space X is a set...where fractals live" (1993, p.5).

In order to understand the space "where fractals live," we need to know the definitions of "a complete metric space" and "the compact sets". Refer to Barnsley (1993) for mathematical details.

Ideal space, in which Fractal Geometry is studied, starts with some complete metric space such as the Euclidean, R^2. However, then "it becomes natural to introduce the space H" (Barnsley, 1993, p.27). Let (X, d) be a complete metric space. Thus, $H(X)$ denotes the space whose points are the compact subsets of X, other than the empty set. The *Hausdorff distance* between points A and B in $H(X)$ is defined by $h(A, B) = d(A, B) \vee d(B, A)$. The notation $x \vee y$ is used to mean the maximum of the two real numbers x and y. Barnsley (1993) referred to $(H(X), h)$ as the "space of fractals."

Although virtually all natural objects are random fractals (Hastings & Sugihara, 1993, p.16), the concept of self-similarity is best first explored through the study of

regular fractals. There are numerous mathematical fractals. The first and perhaps the most fundamental one is called the Mandelbrot set, devised by Mandelbrot (1977; 1983) in order to illustrate the concept of fractals. The systems dynamics of constructing such a set are given in the following section.

2.3.3 Systems Evolution in the Mandelbrot Set

The connection between Fractal Geometry and the systems evolution as introduced by Chaos Theory can be illustrated by the Mandelbrot set (Mandelbrot, 1983). The process of generating the Mandelbrot set incorporates exactly the elements that characterise a chaotic system: it is deterministic, non-linear and sensitive to initial conditions. The set also reveals the exact characteristics of fractals; that is, they are self-similar structures with scale-invariant measures, the fractal dimension. See the discussion below and Figure 2.5.

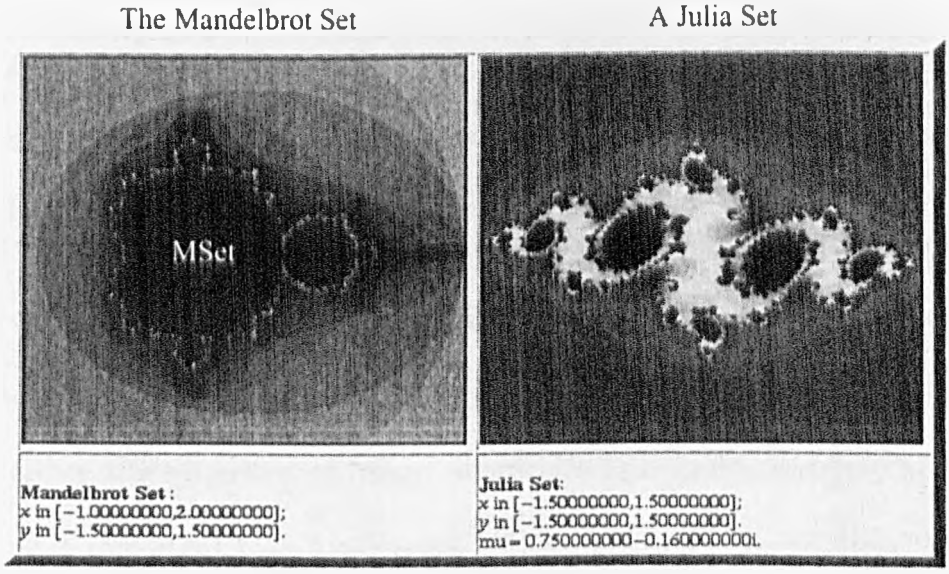

Figure 2.5: The Mandelbrot and Julia sets.
The Mandelbrot set is a "road map" to Julia sets, which can be located by the reference points (mu). Shades of greyness are equipotential surfaces, representing rates of escaping to infinity, in the dynamics of $z \mapsto z^2 + z_0$.

Generation of the Mandelbrot and Julia Sets

Fractals generated from the theories of Gaston Julia (1893-1978) and Pierre Fatou (1878-1929), dating from about 1919, are based in the complex plane. Work similar to that of Julia and Fatou had been attempted earlier, but with little success. For example, Arthur Cayley (1821-1895) was defeated by the complexity of attempting to determine which root of a complex equation would be approached from various starting points, using Newton's iterative method. Using modern computers, it is relatively easy to demonstrate that the boundaries between the regions defined in this problem are fractal in nature, but without the concept of fractals and without computer power this problem proved too complicated for Cayley in 1879 (Peitgen & Richter, 1986; Peitgen *et al.*, 1992). It was eventually solved by Hubbard, one hundred years after Cayley's attempt (Gleick, 1987; Jones, 1991).

The direct method for computer graphic generation of a Julia set on a raster device involves repeated evaluation of the non-linear deterministic function

$$z \mapsto z^2 + c, \tag{2.4}$$

where the complex c is on the reference c-plane, and complex number z is picked out on a working z-plane (Figure 2.5). Evaluation of the above equation repetitively yields a sequence of image points of z. There are two frequently occurring outcomes; that is, either the sequence of image points diverges and eventually approaches infinity, or it converges to a fixed point. There are other possibilities, such as a finite cycle of points being repeated, but the divergent and convergent sequences are the most frequently observed. While c is fixed, points $z_0 = (x_0, y_0)$ which act as starting points for such an operation can be divided into two sets: the set of points

for which the sequence diverges and the set for which the sequence does not diverge. Those points which lead to non-divergent sequences but lie next to points which create divergent sequences constitute the "Julia set" for a particular value of c. The Julia set is the boundary between the non-divergent values of z_0 and the divergent values of z_0, lying just within the set of the non-divergent values. The complete set of non-divergent starting values of z_0 is called the "filled-in" Julia set (Duoady, 1986; Jones, 1991).

Reeve (1991) used the method suggested above and showed how changing the power of z gives different effects. For example, using the function

$$z \mapsto z^k + c \tag{2.5}$$

gives k possible values of z_{n-1} for each z_n, so the random selection at each stage is from a larger set of possibilities. Experiments with a range of functions produce images resembling primitive biological life forms (Pickover, 1986; Kaandorp, 1994).

Very similar to the Julia set, the method used to generate the Mandelbrot set is

$$z \mapsto z^2 + z_0. \tag{2.6}$$

However, to create an image of the Mandelbrot set, the starting point is set to the origin of the complex plane. Sequences of image points are evaluated in the same way as for the Julia sets, except that both z and z_0 are on the z-plane. Extremely different types of systems dynamics are observed at neighbouring points, that is, the initial conditions, especially close to the set boundary.

The relationship between Julia sets and the Mandelbrot set is actually very rigid. Different values of the constant c give many different shapes of Julia set. They fall

into two essential different forms: connected and disconnected. If a Julia set is connected, then any point within the set can be joined to any other point within the set by a line which lies completely within the set, with the boundary enclosing a single "island". Other values of c give disconnected sets, reducing to a "dust" of separate points in two-dimensional space (Duoady, 1986; Peitgen & Richter, 1986; Jones, 1991; Reeve, 1991). The Mandelbrot set is "the set of values of c for which the Julia sets are connected" (Jones, 1991, p.24). If a point within the outline of the Mandelbrot set is used to define the constant for the generation of a Julia set, then the Julia set will be connected (Peitgen & Richter, 1986; Reeve, 1991). If the point is outside the Mandelbrot set, the generated Julia set is disconnected. Therefore, the Mandelbrot set has been termed its name as "the road map" or "table of content" of the Julia sets (Peitgen *et al.*, 1992, p.855). For example, the Julia set in Figure 2.5 (Right) can be located by the *mu* value on the Mandelbrot set on the left. There can be many Julia sets, although there is only one Mandelbrot set.

Systems Evolution in the Mandelbrot Set

The systems evolution depicted in the Mandelbrot set can be interpreted in the context of systems evolution using equipotential surfaces (Figure 2.6). The non-divergent part of the Mandelbrot set can be regarded as a piece of metal charged with electrons. This charge produces an electrostatic field in the surrounding space, resulting in an attracting force on any small test charge of the opposite polarity. Imagine the field is bounded by vectors indicating the direction and the strength of the force per unit test charge. The lines which follow the vectors from any given point to the charged non-divergent part are those that infinitesimally small

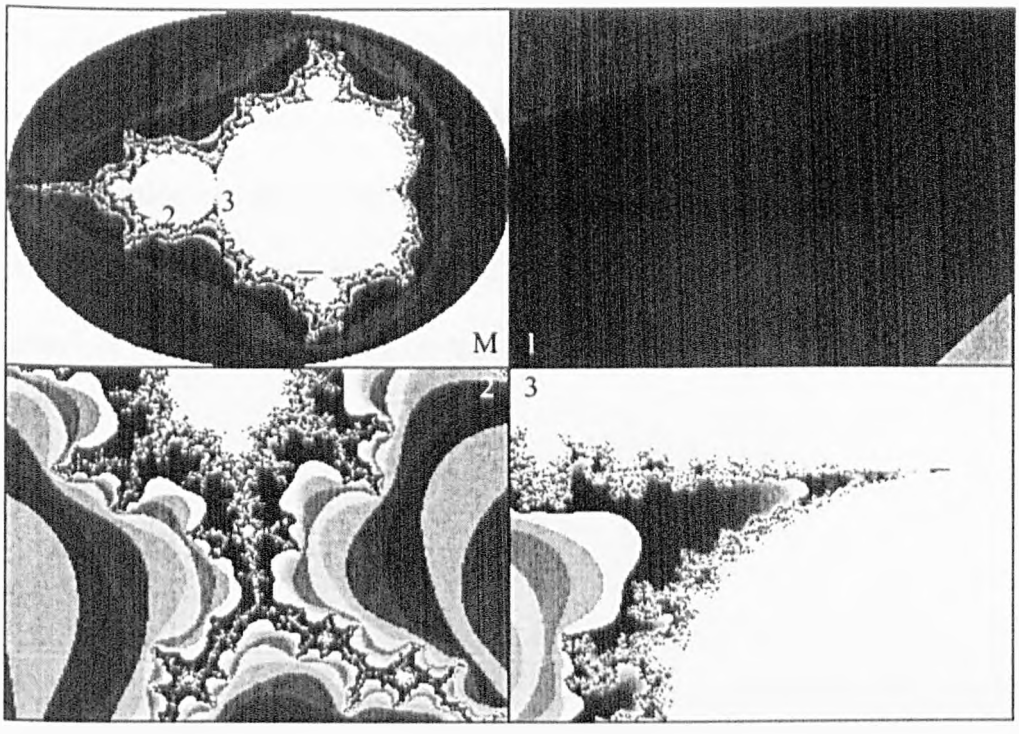

Figure 2.6: System Evolution as Depicted in the Mandelbrot Set.
Areas of similar systems (1), diverse systems (2), and the area containing the boundary between those areas (3) can be identified from the Mandelbrot set (M).

test particles would travel when exposed to the field. These lines are called "field lines". In an electrostatic field, the potential energy of an object can be defined "in terms of the external work necessary to move it from place to place against the forces of the force field", and the equipotential surfaces as "surfaces on which the potential is constant" (Peitgen *et al.*, 1992, p.801). For example, the equipotential surfaces of a point charge are spheres, and those of the infinite wire are cylinders. The equipotential surfaces of irregular objects such as the Mandelbrot set are also possible. Refer to Peitgen *et al.* (1992) for the computation of the electrostatic potential.

The equipotential surfaces give an idea of the diversity of system evolution; that is, the intensity of the field is inversely proportional to the distance between equipotential surfaces when they are drawn for equally spaced values of the potential.

In other words, sparse equipotential surfaces indicate relatively similar systems, and crowded equipotential surfaces mean relatively diverse systems. Therefore, three types of dynamics can be categorised, including the one containing the boundary between similar and diverse systems. This classification scheme also identifies the corresponding natural systems to be analysed in this thesis.

2.4 Data Types

Fractals are "everywhere" (Barnsley, 1993) to which the estimation of fractal dimension can be applied (Mandelbrot, 1983), although some (Panico & Sterling, 1995; Kurz *et al.*, 1998, for example) argued that retinal neurons and blood vessels are not fractal. Among many natural systems, three systems are found to correspond to the three types of systems dynamics identified in the Mandelbrot set: the sea wave profiles, landform as in the form of digital elevation models, and the normalised difference vegetation index (NDVI) image of ferns. The first data set is an example of temporal homogeneity. The second contains data that represent spatial heterogeneity. The third is related to plant growth rigour in space. The following three sub-sections provide current understanding of those phenomena.

2.4.1 Tides and Waves

The prediction of tidal heights makes use of the knowledge that the observed tide is the sum of a number of components or partial tides, each of whose periods precisely corresponds with the period of one of the relative astronomical motions between

earth, sun and moon (Doodson & Warburg, 1941). Table 2.2 gives some principal tidal components and respective periods in solar hours forming the basic patterns of tides (Brown *et al.*, 1989).

Name of the component	Symbol	Periods in solar hours
Principal lunar	M_2	12.42
Principal solar	S_2	12.00
Large lunar elliptic	N_2	12.66
Luni-solar semi-diurnal	K_2	11.97
Luni-solar diurnal	K_1	23.99
Principal lunar diurnal	O_1	25.82
Principal solar diurnal	P_1	24.07

Table 2.2: Some Principal Tidal Components.
After Brown *et al.* (1989, p.57).

These basic patterns of tides can be modified by local effects, particularly those of harmonic, that is, simple multiples of the frequency of the partial tides (Russell & Macmillan, 1952, p.58). For example, just west of the Isle of Wight, the principal lunar tide is about 0.5 metres, the quarter-diurnal component about 0.15 metres, and one-sixth diurnal component about 0.2 metres (Russell & Macmillan, 1952, p.59). The period of waves that break on the English Channel coasts and are generated by local winds is of the order of six seconds, while Cornish has reported on two occurrences of very large waves, namely, 19 and 22.5 seconds, breaking in Bournmouth Bay (Russell & Macmillan, 1952, p.34). Such observation is actually the measurement as a result of wave interference (Brown *et al.*, 1997).

Figure 2.7 shows an example of interference of two idealised waves: if the difference between the wavelengths of two sets of waves (or wave trains) is relatively small, the two sets will "interfere" and produce a single set of resultant waves. Where the crests of two wave trains coincide, the wave amplitudes are added and the resultant

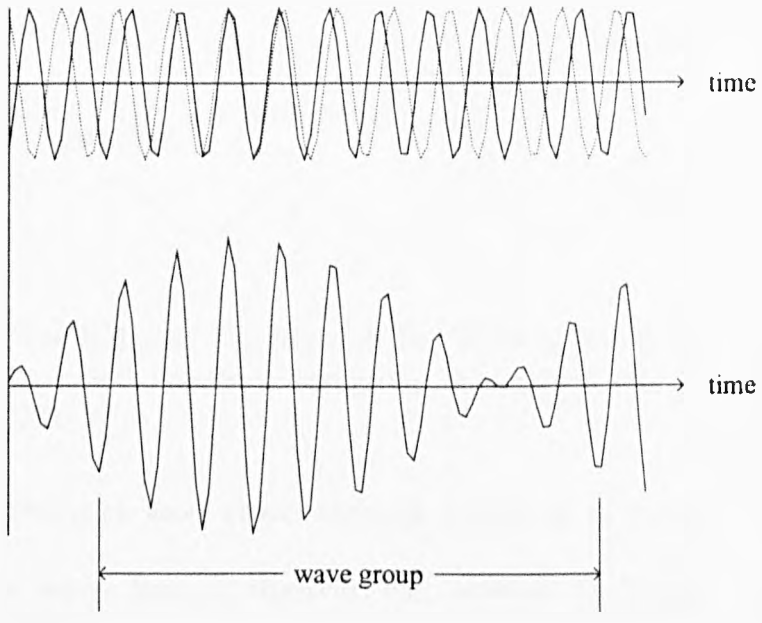

Figure 2.7: Wave Interference.
Interference occurs at the merging of two wave trains of slightly different wavelengths. Modified from Brown *et al.* (1997) and Russell & Macmillan (1952).

wave has about twice the amplitude of the two original waves. Where the two wave trains are "out of phase", that is, where the crests of one wave train coincide with the troughs of the other, the amplitudes cancel each other out, and the water surface has minimal displacement. The two component wave trains thus interact, each losing its individual identity, and combine to form a series of wave groups, separated by regions almost free from waves, as explained by Brown *et al.* (1989, p.20). The wave group advances more slowly than individual waves in the group, and thus in terms of the occurrence and propagation of waves, group speed is more significant than speeds of the individual waves in it.

Individual waves do not persist for long in the open sea, only as long as they take to pass through the group. Figure 2.8 shows the relationship between the wave speed (or phase speed) and the group speed in the open sea. As the wave advances

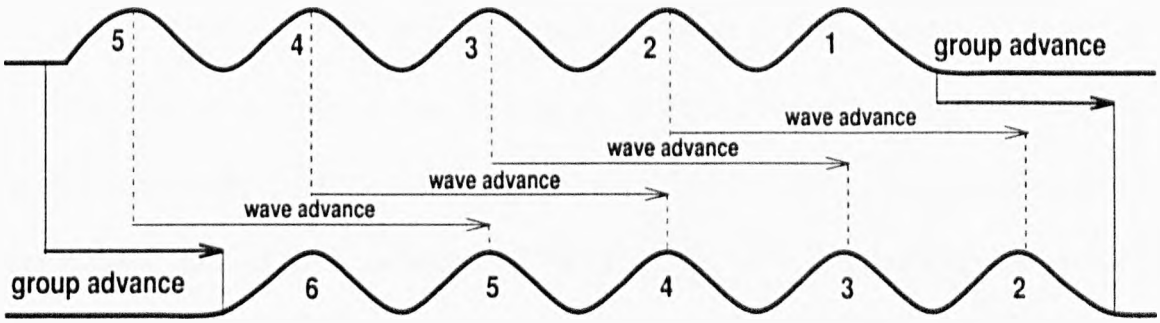

Figure 2.8: The Relationship Between the Wave Speed and the Group Speed. Wave advances twice the speed of the group in the open sea. Modified from Brown *et al.* (1997, p.20).

from left to right, each wave moves through the group to die out at the front, e.g., wave 1, as new waves form at the rear, e.g., wave 6. In this process, the distance travelled by each individual wave as it travels from rear to front of the group is twice that travelled by the group as a whole. Hence, the wave speed is twice that of the group speed. However, wave energy is contained within each group, and advances at the group speed. For more details refer to Brown *et al.* (Brown *et al.*, 1989, p.21).

Entering into shallow water, the wave dynamics start to change. As the water becomes shallower, wavelength becomes less significant and depth becomes more important in determining wave speed. As a result, wave speed in shoaling water becomes closer to group speed. Eventually, all waves travel at the same depth-determined speed, there will be no wave-wave interference, and in effect each wave will represent its own "group". Thus, in shallow water, group speed can be regarded as equal to wave speed (Brown *et al.*, 1989, p.21).

The prediction of tides in the open sea is fundamentally different from the measuring of wave heights in the shallow water as a consequence. Out in the open sea, for example, the wave-wave interference dominates the system dynamics. However complicated it may be, the wave group speed is relatively easy to predict, hence the

other characteristics of waves (Doodson & Warburg, 1941). In fact, tide tables have been produced for many areas, such as the posts surrounding the Humber estuary of England (ABP, 1997). When waves enter shallow water, depth determines the wave speed and other characteristics. Furthermore, the wave pattern is dramatically modified by the local effects of harmonics, as explained earlier in this section, and by the influence of terrestrial conditions (Doodson & Warburg, 1941). It is thus not surprising that actual measurements of wave heights differ distinctly from port to port along the coastlines in the world.

However, some wave characteristics seemingly remain unchanged in theory and are subject to further tests. In contrast to individual waves which disappear as soon as they pass through the wave group in the open sea (Brown *et al.*, 1989, p.20), the wave group carries forward all the characteristics occurring as a result of interference. In other words, individual waves lose their discrete characteristics only to produce a composite wave group that represents the waves that generate it. Such a wave group itself can be treated as an individual wave, which has repeated patterns of heights. The dynamics of one section of the wave should, therefore, be consistent with those of another. The question remaining here asks how such dynamics may be measured or quantified.

Along with some conventional methods, the fractal dimension is chosen because it is aimed at measuring the self-similarity of natural phenomena. It is anticipated that the relative homogeneous sections of nearshore waves can be characterised clearly by their similar fractal dimensions. A similar approach can then be applied to more heterogeneous systems such as landforms.

2.4.2 Landform

In this section, attention has turned from the analysis of a homogeneous system to that of a heterogeneous system. Apart from the choice of different type of data, another important aspect of the objectives is to maintain the use of one single method for calculating the fractal dimension. In other words, this thesis has actually proposed a relatively new approach of studying landform, as explained below.

There are three basic approaches to applying the fractal dimension using its digital elevation model (DEM) to analysing landform (Helmlinger *et al.*, 1993; Liu, 1992, for example). Firstly, one measurement of the fractal dimension is estimated to represent the whole DEM. Secondly, one measurement is calculated for each pixel of the DEM. This is an alternative to texture segmentation and classification of digital analysis (Pentland, 1984; Keller *et al.*, 1989; Müssigmann, 1989; Müssigmann, 1990; Linnett, 1991; Müssigmann, 1992, among others). It usually involves computing the local fractal dimension by means of the Fourier technique for each pixel to form a "dimension map" (Müssigmann, 1992), which can then be classified by common methods such as assigning breakpoints in the histogram of the derived fractal dimensions (Pentland, 1984). However, the more acceptable interpretation of the landform is that it contains bi-fractal (Beauvais & Montgomery, 1996, for example) or multi-fractal characteristics (Blacher *et al.*, 1993; Gao & Xia, 1996, for example), which are measures extended from sets (Evertsz & Mandelbrot, 1992).

The third approach is to estimate the fractal dimension of profiles from a DEM. Here the analogy is established between the sections in a wave profile and the profiles in a DEM, which can be taken either arbitrarily or systematically. The method

of arbitrary sampling includes taking transects along places of interest (Young & Harvey, 1996, for example). The method of systematic sampling involves taking profiles along both directions of the DEM; and, to the knowledge of the writer of this thesis, such an approach has yet to be seen in literature. Therefore, it is proposed here that the dynamics of landform can be revealed by the same method in which the wave is analysed.

This testable proposal is based on the current understanding of the heterogeneity in landform, which is usually characterised by its forms and processes and the relationship between them. A close examination of the complexity of sampling in time and space leads the study to focusing on forms instead of processes.

Landform Characterised as Drainage Basin Forms

Landform is usually understood by the drainage basin in which it is contained. A drainage basin is the entire area providing runoff to, and sustaining part of all of the stream flow of, the main stream and its tributaries (Gregory & Walling, 1973, p.37). The function of the drainage basin and its significance is hinted at in the synonyms that have gradually been adopted including *drainage area, catchment area* especially employed in river control engineering, and *watershed*, utilised especially in water supply engineering. The need to study the form of the drainage basin derives from two main sources: firstly, to describe the form-form relationships or morphological systems, and secondly, to analyse the form-process relationships. Numerous methods of describing drainage basins have been proposed. The subdivision of the quantitative expression of a drainage basin, proposed by Horton (1932), is to consider first the topographic characteristics of drainage basins; second, the rock and

soil characteristics; and third, the vegetation characteristics. It provides the understanding of the ways in which these characteristics are interrelated and combined to form several kinds of drainage basin terrain types.

Topographic attributes of drainage basins usually include area, length, shape and relief. Complete description of the characteristics of the drainage basin must include reference to the rocks and sediments beneath the basin; because the type of rock will determine the nature and extent of ground water storage and also the type of material available for erosion and transport within the drainage basin (Gregory & Walling, 1973, p.59). The superficial deposits and soils are often related to soil erodibility and dispersion and water transmission properties (Bryan, 1968). As in the case of soil types, the vegetation character of the drainage basin can be used to characterise a single watershed or to compare several drainage basins.

Interrelationships existing between the basin characteristics described earlier could be illustrated by the drainage network. Within the context of the drainage basin, the network was studied through application of the laws of morphometry; and complemented by stochastic analysis based upon simulated channel networks and the awareness of the dynamic character of the drainage net as a necessary pre-requisite for appreciating the effect which the network has upon the stream channel process (Gregory & Walling, 1973, p.79). Laws of drainage composition were formulated by Horton (1945), and supported by, among others, Schumm (1956) and Woldenberg (1966) who suggested that the river open system grows allometrically according to the general equation $y = ax^b$. However, Milton (1966) argued that some drainage net laws were allometrically irrelevant, and Scheidegger (1966) concluded that the actual junction of drainage channels in a network occurs in a stochastic fashion. Fur-

thermore, Shreve (1966) simulated stream networks and compared these with 172 published sets of stream numbers and concluded that the law of stream number is largely a result of random development of the topology of channel networks according to the law of chance. Smart (1969) saw that interest in the topological properties of channel networks has led partly to a shift of interest from the properties which could be explained by geological and other controls to those which can be accounted for by topological randomness. As a result, many of the interrelationships of the essentially morphologic drainage basin characteristic system underline the fact that relationships may exist between many variables because of the relationships of these variables with landform processes.

Drainage Basin Processes

The study of landform processes is typified by the measuring and quantitative evaluating both of the runoff dynamics and of sediment and solute dynamics (Gregory & Walling, 1973, p.93). The runoff dynamics are characterised by the measurements, through time, of precipitation input, evapotranspiration losses, precipitation/catchment interactions, and output of runoff. Furthermore, certain measurements are directed especially towards the assessment of the processes of erosion, transpiration and deposition within a catchment, which can be sub-divided into three areas of study (Gregory & Walling, 1973, p.145). Firstly, sediment dynamics involves sediment on slopes, sediment in channels, and the sediment yield that is the resultant of the processes of erosion, transportation and deposition. Secondly, there is solute production and transportation, and thirdly, the associated rates of erosion or degradation that can be calculated from the amount of sediment and

solute yields.

Gregory & Walling (1973, Ch.4) compiled a list of possible quantitative evaluations of drainage basin processes, which reveals the complexity of landform processes. The list includes catchment inputs, the water balance, runoff response, sediment and solute production, process interrelationships, and modelling of catchment response. The measurements and quantitative evaluating of processes are fundamental for the study of the interrelationship between process and form.

Process–Form Relationship

Relationships between drainage basin form and process are of two kinds (Gregory & Walling, 1973, p.234). Firstly, the character and magnitude of processes can be influenced by form and, secondly, the processes operating can be responsible for fashioning the form of the landform. The relationship is usually realised by the investigation of water and sediment in river channels, channel cross section, the channel reach, the drainage basin, and drainage basin mechanics. A large number of examples of relationships between form and process were given by Gregory & Walling (1973, pp.292-3).

The study of landform evolution can lead to an adjustment of basin characteristics or of drainage basin processes. Theories of drainage basin changes are based on short-term changes such as channel pattern and drainage basin pattern changes; intermediate-scale changes such as channel geometry, channel pattern and drainage basin changes; and towards the long-term changes (Gregory & Walling, 1973, p.359). Knowledge of present drainage basin form and process and of their interrelations can

provide the basis for an interpretation of the character of changes while, in addition, the analysis and dating of sedimentary deposits provides further assistance. A study of the past in the light of an understanding of the present might be necessary in developing adequate models of landform evolution. However, the methods of study must lean heavily upon the additional information provided by superficial deposits, and must sometimes employ spatial variations of the present as a basis for indicating how changes may take place over time. Therefore, the study of process and form is closely associated with the sampling variations in time and space.

Tempo-spatial Considerations in Sampling

Sampling in time is the prime concern for many process geomorphologists. The common use of continuous monitoring will overcome many of the problems of sampling in time, yet this may lead to insufficient data: observations made on a systematic basis could miss many of the extreme events that vary markedly in time. Any data collected from a short period of study constitute essentially a non-random sample of a time series and years may be required before data are sufficiently reliable to provide conclusions about the magnitude and frequency of specific events and processes. Furthermore, statistical analysis may be required to assess the reliability of data in time and to generate long-term records from a short period of measurement (Gregory & Walling, 1973, p.95).

The problems associated with sampling in space are equally important. Apart from measurements of the output of channel flow and the associated sediment and solute yields from a drainage basin, most process data collected are sample data and pertain only to small areas or points within the catchment area. Therefore,

most measurements embody techniques of random sampling to provide data that are to some degree representative of total area. Other difficulties are involved such as considerations of availability of suitable locations for instruments in terms of accessibility. Nevertheless, the measurement itself is often only the prelude to detailed processing, analysis and evaluation of the data obtained (Gregory & Walling, 1973, p.183).

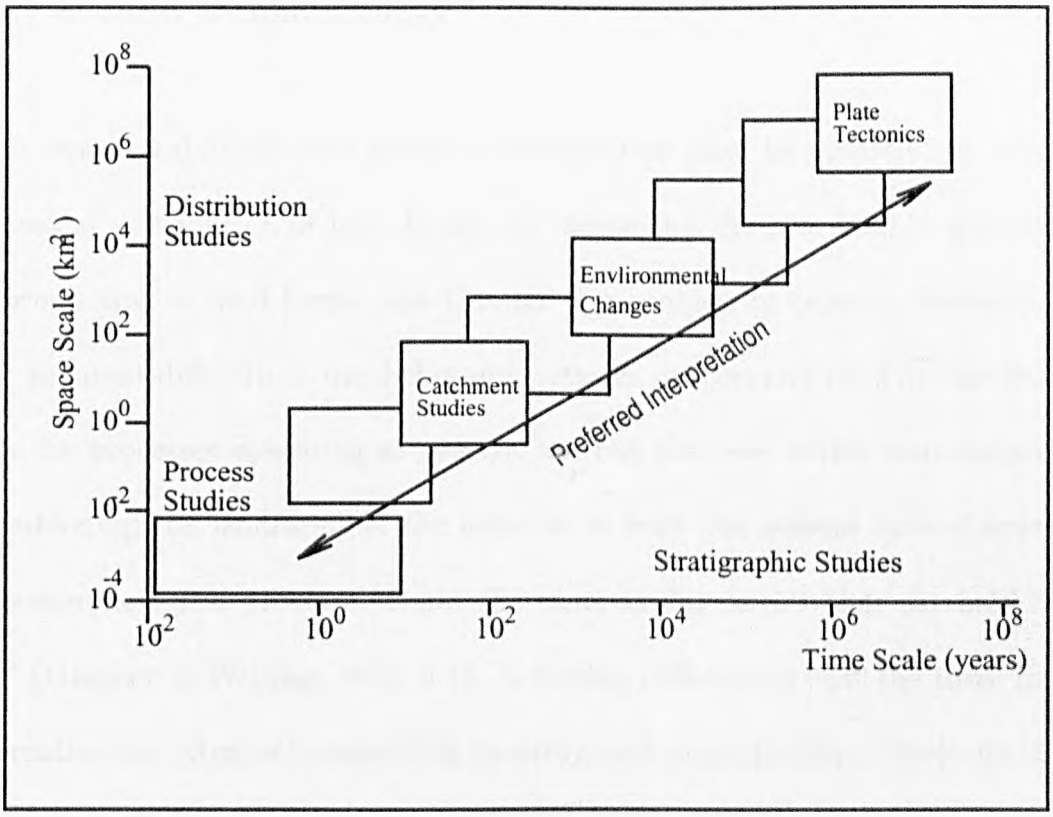

Figure 2.9: Possible Field Studies in Time and Space.
Modified from the slide by courtesy of Kirby (1999).

Possible field studies with different combinations of time and space are illustrated in Figure 2.9. According to Gregory & Walling (1973, p.298), spatial variations in the operation of fluvial processes can conveniently be considered at several levels: the micro-scale; the meso-scale of runoff, the meso-scale of sediment and solute dynamics, the continental and world scale of runoff, suspended sediment transport

and dissolved loads; and the influence of humans on rural and urban areas. The link between spatial variations and drainage basin characteristics might be revealed by careful investigation of a detailed account of the annual sediment production rates of various regions and scales (Gregory & Walling, 1973, Ch.6). Although the study of landform process is one of the desirable topics, the study of form morphology is equally challenging for reasons stated in the following section.

Study of Form Geomorphology

It has been established that landform information may be obtained by mapping the spatial distribution of land forms, by measuring the processes responsible for the production of land forms, and through the analysis of deposits However, "the most apparent difficulty is the dichotomy between process and form in that in many areas the processes operating at present are not the ones which were responsible for fashioning the landforms of the area, or at least the present rate of operation of geomorphological processes is not the same as the rates which obtained in the past" (Gregory & Walling, 1973, p.1). A further difficulty is that the three lines of information are often not susceptible to study with equal facility. The study of geomorphological processes is also more time-consuming than the study of landform; as Rice (1988, p.387) has described it, "changes [of landform] within a lifetime may be too slight for measurement." Furthermore, in landform development, the distinction between cause and effect in the shaping of landforms depends upon not only the size of the system in space but also the length of time being considered. Gregory & Walling (1973, p.21) stated that the drainage basin may present problems requiring analysis and studies conceived at different time scales, ranging from geological cyclic

and shorter cyclic to very short, steady periods of time. Such a demand on time has made the study of landform process less practical than that of form morphology.

The drainage basin is defined as "a system of complex topographic characteristics, rock type, soil, vegetation, and land use" (Gregory & Walling, 1973, p.234). Topographic characteristics individually and collectively influence catchment processes. Rock type is significant in the drainage basin statically and dynamically and both are necessarily interrelated (Gregory & Walling, 1973, p.274). The static significance is that different rock types vary in their ability to store water, which, in turn, dynamically controls the rate water outflows and dictates the rate and character of weathering, the weathering products obtained and hence the nature of the sediment and solute supplied to the stream. Similar effects can also be observed in soil, vegetation and land use. The resulting complexity is the outcome of many uncompromising sub-systems, such as rocks, soils, and vegetation, evolving at their own time scales. The current humble effort is to use the fractal dimensions obtained by the approach applied to sea waves to test such a deduction thoroughly.

The development of remote sensing technology has facilitated the study of landform even further. The digital elevation model representing the landform was generated from a pair of aerial photographs. The remote sensing technique has effectively eliminated the problems associated with sampling spatial data. One of its merits extends to the study of plant imagery, which contains the boundary between the similar background and diverse leafy area.

2.4.3 Plants

The identical approach to sea waves and topography is extended to the spectral imagery of ferns, whose complexity includes an irregular outline of the leaf. A spectral image of a plant is actually a spectral phenomenon of both temporal and spatial nature; that is, the vegetation indices are obtained for a leaf confined in two-dimensional space at a specific instant of time. The plant images are taken using the remote sensing techniques. Remote sensing usually refers to "the use of electromagnetic radiation sensors to record images of the environment which can be interpreted to yield useful information" (Curran, 1985, p.1).

The development of remote sensing began to emerge yet did not become popular until long after its inception. In 1960 when the name "remote sensing" was first coined (Fischer, 1975), it referred simply to the observation and measurement of an object without touching it (Curran, 1985, p.1). Since that date remote sensing has taken on a discipline-dependent meaning, for example, in the environmental sciences of geography (Duong & Takeuchi, 1997; Merttes *et al.*, 1998), geology (Davis *et al.*, 1993; Florinsky, 1998), botany (Lehmann & Lachavanne, 1997), civil engineering (Amos *et al.*, 1986; Profeti & MacIntosh, 1997), forestry (Holmgren & Thuresson, 1998), meteorology (Singal *et al.*, 1994; Devara *et al.*, 1998), agriculture (Tucker & Choudhury, 1987; Bouman, 1992; Das *et al.*, 1993; Bouman, 1995) and oceanography (Eppley, 1992; Ottl, 1997).

A remote sensing system using electromagnetic radiation typically has four components: a source, interactions with the earth's surface, interactions with the atmo-

sphere and a sensor (Curran, 1985).[5] A huge amount of effort has been devoted to the development of remote sensing instruments, satellite systems, photogrammetry and imagery processing and applications (Curran, 1985; Cracknell & Hayes, 1991; Barrett & Curtis, 1992; Lillesand & Kiefer, 1994). Figure 2.10 shows various sensors as related to energy sources and atmospheric transmittance. As far as plant science is concerned, the focus is on the sensors that detect visible and infrared lights, that are used for the photosynthesis process.

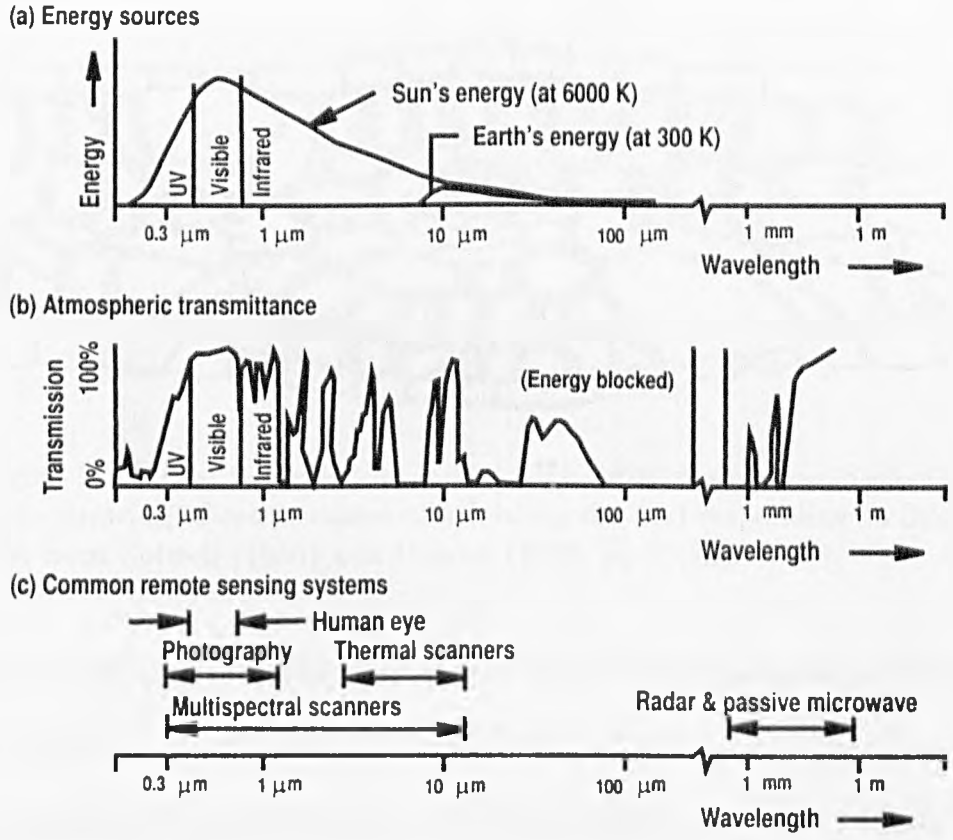

Figure 2.10: Spectral Characteristics and Remote Sensing Systems. Spectral characteristics of (a) energy sources, (b) atmospheric effects, and (c) sensing systems. Note that wavelength scale is logarithmic. Modified from Lillesand & Kiefer (1994, p.11).

[5] The source may be natural, such as the sun's reflected light or the earth's emitted heat, or man-made, like microwave radar. The interactions with the Earth's surface are characterised by the amount and characteristics of radiation emitted or reflected from the earth's surface. The atmospheric interaction mainly occurs when emitted energy passing through the atmosphere is distorted and scattered. A sensor records the emitted radiation that has interacted with the surface of the earth and the atmosphere. The interactions with the reflectance received by the sensors is further complicated by other factors such as the soil background, vegetation senescence, solar and sensor elevation and azimuth, canopy geometry and phenology.

A leaf is built of layers of structural fibrous organic matter, within which are pigmented, water-filled cells and air spaces. Figure 2.11 shows the anatomy of a

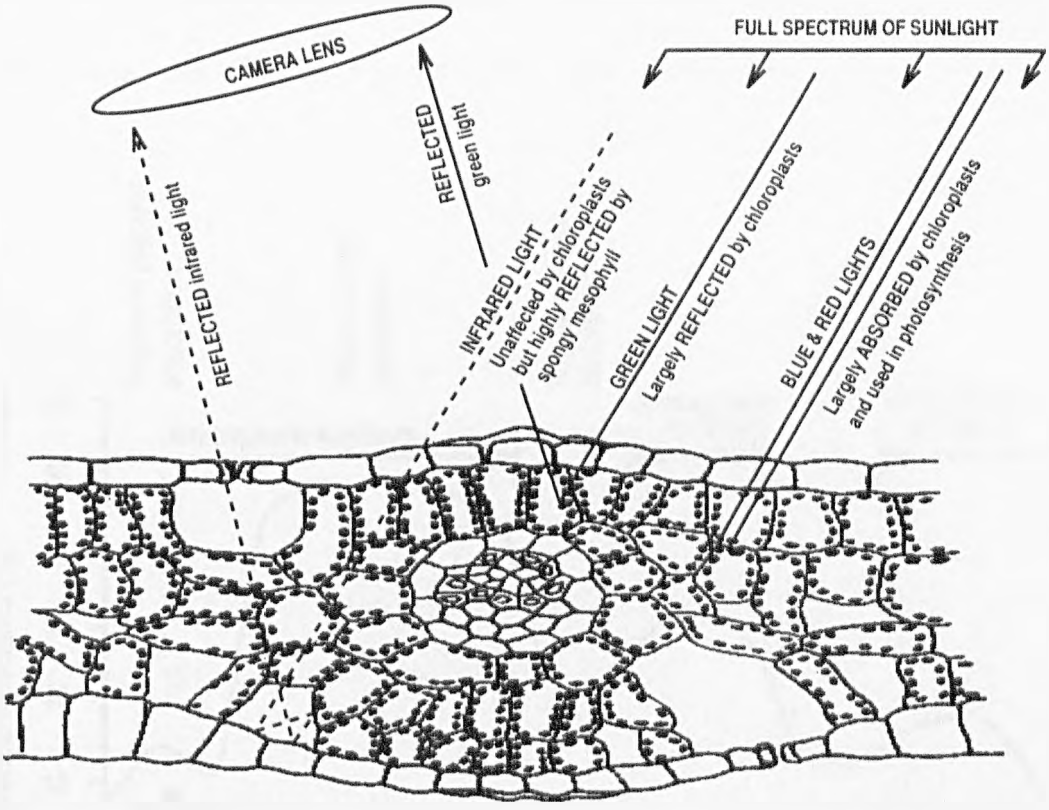

Figure 2.11: Leaf features that Affect Light Absorbance and Reflectance. Schematic drawing of cross-section of a healthy oat leaf responding to full sunlight. Modified from Colwell (1956) and Curran (1985, pp.23,26).

healthy oat leaf and the reflectance characterised by leaf features, as illustrated in Colwell (1956) and explained in Curran (1985, p.23). Each of the three features, that is, pigmentations, physiological structure and water content, have an effect on the reflectance, absorbance and transmittance properties of a green leaf.[6] The combined effects of leaf pigments and physiological structure give all healthy green leaves their characteristic reflection properties: low reflectance of red and blue light,

[6] Four primary pigments of higher plants, i.e., chlorophylls a and b, β carotene and xanthophyll, absorb visible light for photosynthesis. Chlorophylls absorb portions of blue and red light, i.e., chlorophyll a absorbs at wavelengths of 0.43 μm and 0.66 μm and chlorophyll b at wavelengths of 0.45 μm and 0.65 μm; carotene and xanthophyll both absorb blue to green light at a number of wavelengths (Whittingham, 1974). The discontinuity in the refractive indices within a leaf determines its near infrared reflectance (Curran, 1985). These discontinuities occur between membranes and cytoplasm within the upper half of the leaf and, more importantly, between individual cells and air spaces of the spongy mesophyll within the lower half of the leaf (Gausman, 1974).

medium reflectance of green light, and high reflectance of near infrared.

Figure 2.12 shows how the design of the sensors is dictated by the atmospheric absorbance, as described by Curran (1985, p.25). Leaf reflectance is reduced as a

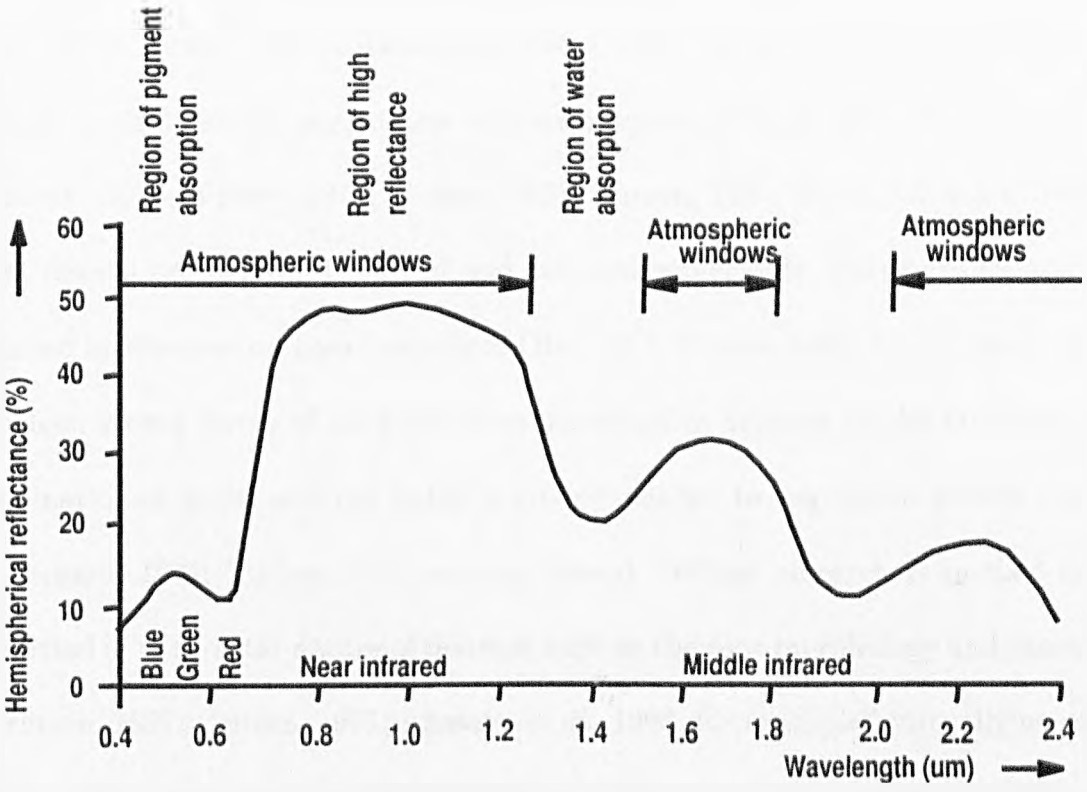

Figure 2.12: The Leaf Reflectance and Atmospheric Windows.
The hemispheric reflectance of a Rhododendron leaf and "atmospheric windows". Modified from Curran (1985).

result of absorption by three major water absorption bands that occur near wavelengths of 1.4 μm, 1.9 μm and 2.7 μm, and two minor water absorption bands that occur between wavelengths of 0.96 μm and 1.1 μm. In order to avoid water absorption in the atmosphere, the majority of sensors are limited to three atmospheric "windows" that are free of water absorption at wavelengths of 0.3 to 1.3 μm, 1.5 to 1.8 μm and 2.0 to 2.6 μm. Fortunately, within these wavebands, emitted radiation is still sensitive to leaf moisture. Vegetation spectra obtained by this range of sensors is closely linked with plant parameters such as biomass and leaf area index

(Curran, 1985, p.25). However, spectral characteristics of different wavelengths are often combined to derive vegetation indices for which the relationship with plant parameters is established.

Vegetation indices are derived from various spectral wavebands (Richard & Wiegand, 1977; Tucker, 1977; Lillesand & Kiefer, 1994, for example) and found to be related to plant growth parameters such as biomass and leaf area index (Agazzi & Franzetti, 1975; Tucker, 1977; Tucker, 1979; Curran, 1981; Elvidge & Lyon, 1985). Most indices are derived from red and infrared wavebands, which are commonly installed in scanners on board satellites (Barrett & Curtis, 1992, for instance); nevertheless, strong forms of evidence were presented in support of the fact that the combination of green and red lights is closely related to vegetation growth rigour (Kanemasu, 1974; Tucker, 1979, among others). Whilst researchers seemed more interested in the fractal nature of features such as the root morphology and canopies (Berntson, 1997; Critten, 1997; Akasaka *et al.*, 1998, for example), virtually no published article was concerned with the fractal dimension of the vegetation indices of an individual plant, The above observation provides solid support for the fractal study of the vegetation indices on the ground at a much smaller scale, using equipment commonly available to researchers; for example, some hand-held spectrometers are manufactured for use for scientific purposes, and most commercial scanners and softwares can be combined to split light into blue, green and red wavebands.

The spectral image of a fern represents a system of two major sub-systems: the inert background and the active leafy area. The inert part is extremely monotonous, whereas the leafy area can resemble a digital elevation model if projected in three-dimensional space. The difference in dynamics is to be revealed using the same

approach applied to both sea waves and digital elevation models. The fractal dimension of the boundary between the major systems can also be estimated by the same implementation method.

This major section provides the current understanding of three natural systems that correspond to the three types of dynamics revealed in the Mandelbrot set: the sea waves, topography and plant imagery. The same approach will be used for all the systems involved to test the various types of dynamics, ranging from similar through diverse to mixed dynamics. The actual analysis methods are actually described in Chapter Three.

2.5 Conclusion

The modern scientific method has evolved from the either-or approach of the deductive-reductive procedures, through the integration of the procedures and the testing of hypotheses, to the falsification of theories. The current methodology in which the objectives of this thesis are materialised follows this relatively recent scientific convention and the development of Fractal Geometry, that is usually used to quantify complex structures both in nature and as created by Chaos Theory.

Chaos Theory and Fractal Geometry, both of which were designed to assist understanding of complexity, were devised in 1970s. Chaos Theory shows that chaos can arise from processes of non-linear deterministic systems; whilst Fractal Geometry demonstrates that simple building blocks can produce complex structures. Chaos Theory focuses on the temporal characteristics of system dynamics. The

use of the phase portrait technique and Poincaré mapping also allows chaos to become the subject of spatial study. Fractal Geometry deals directly with the spatial characteristics of objects, although fractal objects cannot be created without noting the temporal aspect of the mechanism. For example, the classic Mandelbrot set is of spatial complexity which must be generated by temporal iterations.

The Mandelbrot set is the most typical example of fractal objects that are self-similar at various scales. The immediate implication is that there exists a scale-invariant measure that can be used to represent the object; as a result, the concept of fractal dimension is developed. The fractal dimension measures the scale-invariant nature of a complicated object and is in many ways more useful than the Euclidean dimension for quantifying irregular objects (Mandelbrot, 1983).

The Mandelbrot set also demonstrates three types of systems dynamics, from which three corresponding natural systems are chosen: the sea wave of similar sub-systems, the topography of diverse sub-systems, and the spectral imagery of active plant systems and inert background. The current understanding of the three natural systems presumes that those systems are suitable for revealing the complexity in systems dynamics.

The concept of the fractal dimension is then applied to those natural systems and their corresponding synthetic models. Full details of the fractal dimension and its methods of implementation will be given in the following chapter, that introduces the theme methods used throughout the thesis. These also include some valuable conventional analyses.

Chapter 3

Methods

One can ask what would be a differential having as its exponent a fraction. You see that the result can be expressed by an infinite series. Although this seems removed from Geometry, which does not yet know of such fractional exponents, it appears that one day these paradoxes will yield useful consequences, since there is hardly a paradox without utility. Thoughts that mattered little in themselves may give occasion to more beautiful ones. Gottfried Wilhelm Leibniz, 1695 (Mandelbrot, 1983, p.405).

3.1 Introduction

This chapter explains the methods used to analyse the real-world and synthetic data; where the methods include the estimation of fractal dimension and various types of statistical analyses. The fractal dimensions are estimated, using the box-counting method, for temporal data in Chapter Four and for spatial data in Chapters Five and Six. Finally the range of statistical tests used for comparison between the fractal dimensions derived from the synthetic and natural systems is also explained.

Methods specific to different data sets are given in the respective chapters. In Chapter Four, conventional qualitative and quantitative analyses are carried out on synthetic and natural sea wave profiles. In Chapter Five, general terrain information, for example, that on slopes and aspects, is obtained for synthetic and natural digital elevation models. In Chapter Six, green and red scanning channels are used to construct the normalised difference vegetation index (NDVI) image of a fern. Such an image resembles a digital elevation model and thus the methods of Chapter Five are adopted; and fractal dimensions are also estimated for the outlines of synthetic and natural ferns.

A Brief Introduction to the Data

There are three types of data; and each type comprises both measurements from natural systems and data from synthetic models. The three data sets are introduced here and detailed in Chapters Four, Five and Six, respectively.

The natural sea wave profile was measured with a pressure transducer (Hardisty,

1990b) at Teignmouth in England. The synthetic waveform is the summation of four sinusoidal waves. The sea wave is much more complex than such a simple model due to seabed friction, percolation, refraction, reflection and breaking, and the processes are detailed in Chapter Four. Box counting, statistical analysis and conventional time series analyses are applied to both the natural and the synthetic profiles in Chapter Four.

The digital elevation model of Shei-pa National Park in Taiwan comprising contours at 40-metre intervals is the second set of data used here. The synthetic digital elevation model is simulated by the mid-point displacement method (Peitgen & Saupe, 1988). General terrain information such as aspects and slopes are obtained and then, latitudinal and longitudinal transects are obtained by sectioning the digital elevation models. Fractal analysis is again applied to transects of both the natural and the synthetic digital elevation models and, finally, statistical tests of the derived fractal dimensions are performed.

The NDVI image of the fern was obtained with a digital scanner and processed by Geographic Information System (GIS) software. The fern leaf can be simulated either by random or deterministic algorithms using Iterated Function System (IFS) codes (Barnsley, 1993). Methods used in Chapter Five are applied to the fern image, because the fern image is similar to a digital elevation model in terms of digital imaging, the exception being that the background value of an NDVI image is not zero.

3.2 Fractal Methods

Linear features exist in their own right, for example, coastlines, river networks and fault traces, and a wide variety of methods to determine their fractal dimensions has been developed (Table 3.1). Linear features are objects with a topological di-

Method	Application
Area/perimeter	Digitised shoreline and contours (Goodchild, 1982) Digital cloud image (Kent & Wong, 1982) Digital images of craters on Mars (Woronow, 1981) Sinkhole perimeter (Reams, 1992)
Box counting	Digitised shoreline and contours (Goodchild, 1982) Photographs of vegetation (Morse *et al.*, 1985) Fracture patterns determined from remote imagery (Vignes-Adler & Le Page, 1991)
Divider relation	Lava flow (Bruno *et al.*, 1992) Digitised contours (Culling & Datko, 1987) Digitised shoreline and contours (Goodchild, 1982) Digitised shoreline (Kent & Wong, 1982) Line skeleton of case passage contours (Laverty, 1987; Roy *et al.*, 1987) Drainage basin perimeter (Breyer & Snow, 1992) Digitised cartographic lines (Müller, 1986; Müller, 1987)
Korcak's law Power spectrum	Area of lakes (Kent & Wong, 1982) Natural rock surface (Brown & Scholz, 1985) Digital model of sea floor (Fox & Hayes, 1985) Natural rock surface (Power *et al.*, 1987)
Variogram	Various geophysical phenomena (Burrough, 1981; Burrough, 1984) Soil profiles (Burrough, 1984) Soil pH (Culling, 1986) Digitised maps (Culling & Datko, 1987) DEMs (Klinkenberg & Goodchild, 1992) Ice sheet height profile derived from satellite data (Rees, 1992)

Table 3.1: Application of Fractal Dimensions to Some Linear Features
A selection of methods commonly used to determine the fractal dimension of linear features is presented. Modified from Klinkenberg (1994, p.24).

mension of one within Euclidean space of dimension two. A self-similar feature is generally easier to identify than a self-affine feature. If one can interchange the axes of the coordinate system used to map the feature without producing any funda-

mental changes, then the feature has the minimum requirements for self-similarity. For example, exchanging the (x, y) values which define a contour line alters little. However, the (x, y) values of a topographic profile cannot be exchanged, even though both axes may be measured in the same units. More obviously, the trace of a particle through time has axes that represent different information, time and distance. Formally, with self-affine fractals the variation in one direction scales differently from the variation in another direction (Mandelbrot, 1985; Turcotte, 1992). The distinction between self-affine and self-similar profiles is an elusive one (Mandelbrot, 1985). For analytical purposes, however, whether a profile is studied as a self-affine curve or as a self-similar curve may ultimately depend on the objective of the research (Klinkenberg, 1994, p.26).

One essential aspect of fractal features is their scaling nature. For example, the longer the topographic profile, the greater the observed variability in elevations. Building on that concept, researchers (Matsushita & Ouchi, 1989) have developed a method based on the relationship between sample size and sample variances. The method is conceptually very simple to implement and works on both self-similar and self-affine curves (Klinkenberg, 1994). Samples of various lengths (N) are taken from the curve, then the standard deviations of the coordinates along each axis, X and Y, are determined. From the two log-log plots of X and Y against N the respective slopes, V_X and V_Y, are determined. If V_X and V_Y are equal or nearly so, that is a good indication that the curve is self-similar, therefore, the fractal dimension is $1/V_X$ or $1/V_Y$. If V_X and V_Y are unequal, it implies that the coordinates scale differently. The two variances are related to each other through the Hurt scaling parameter (H) as $H = V_Y/V_X$. However, Klinkenberg argued that this method has

yet to be tested extensively (1994).

3.2.1 Algorithms for Estimating Fractal Dimensions

Method	Relation	Note
Area/perimeter relation	$A \propto P^{(2/D)}$	A, area P, perimeter
Box counting	$n \propto b^{-D}$	n, number of filled boxes b, box size
Divider relation	$L(\tau) \propto \tau^{(1-D)}$	$L(\tau)$, length of rail τ, step size
Korcak's law	$N_r(A > a) \propto a^{-(D/2)}$	$N_r(A > a)$, no. of area above size a
Line-scaling	$X \sim N^{V_X}$; $Y \sim N_{V_Y}$	X & Y, S of x- & y- coordinates V's, slopes of log-log plot
	$H' = \frac{V_Y}{V_X}$	If $H' \approx 1$, $D = \frac{1}{V}$ or $D = 2 - H'$
Power spectrum	$P(\omega) \propto \omega^{-(5-2D)}$	ω, the frequency $P(\omega)$, the power
Variogram	$< (Z_p - Z_q)^2 > \propto (d_{pq})^{(4-2D)}$	$<>$, statistical expectation Z_p & Z_q, elevation at points p and q d_{pq}, distance between p and q

Table 3.2: Some Algorithms of Estimating Fractal Dimensions
Here is a selection of algorithms used to estimate fractal dimensions. S indicates the standard deviation of a sample. Modified from Klinkenberg (1994, p.26).

Table 3.2 includes some algorithms for estimating the monofractal dimension (Mandelbrot, 1983; Feder, 1988; Turcotte, 1992; Peitgen *et al.*, 1992, for example); but most have their theoretical and/or practical limitations (Klinkenberg, 1994). It is possible that the dimension of the whole may not equal the dimension of the parts; for example, the horizontal cuts of a self-affine surface will produce a suite of self-similar curves (Klinkenberg, 1994, p.27). Matsushita *et al.* (1991) prove that the fractal dimension of the entire suite of curves will generally be greater than the fractal dimension of a single curve extracted from that suite. Example curves derived from a fractal surface of dimension 2.5 show that the fractal dimension of the entire suite is 1.50 and for the single longest curve it is 1.32 (Ouchi & Matsushita, 1991).

D of Fractal Structures

Topology is an example of both self-similar and self-affine fractals (Turcotte, 1992). In the two horizontal directions topology is often self-similar, while the vertical coordinate is statistically related to the horizontal coordinates but systematically has a smaller magnitude (Mandelbrot, 1985). Vertical cross-sections of this type are often examples of self-affine fractals (Dubuc *et al.*, 1989).

As shown in Table 3.2, most algorithms are based on the "power law", expressed in its original form of $y = cx^{-D}$ or in its logarithmic form of $\log y = C + D \log 1/x$, where D is the scaling exponent and, in fractal science, the scale-invariant measure called the fractal dimension. The calculation of D is straightforward for self-similar structures, although it needs some attention for self-affine objects.

The simplest geometrical characterisation of a fractal object is to count the minimum number of hypercubes of linear size ϵ which are required to cover the object. If the number of hypercubes is $N(\epsilon)$, then, as ϵ is varied, $N(\epsilon)$ varies as ϵ^{-D}, where D is the dimension. In the limit as ϵ tends to zero, D can be defined as follows (Mullin, 1993b):

$$D = \lim_{\epsilon \to 0} \frac{\ln N(\epsilon)}{\ln(1/\epsilon)}. \tag{3.1}$$

The value of the dimension need not be an integer. A set which has a non-integer dimension is said to be fractal and thus has the usual properties associated with such objects.

A statistically self-similar fractal such as a contour is by definition isotropic. That is, $f(rx, ry)$ is statistically similar to $f(x, y)$ in a two dimensional xy-space. The number of boxes with dimensions (x_1, y_1) required to cover the subject is N_1,

and that with dimensions (rx_1, ry_1) required to cover the subject is N_2. If the subject is a self-similar fractal,

$$N_2/N_1 = r^{-D}, \tag{3.2}$$

where D is the fractal dimension.

A statistically self-affine fractal such as a transect is not isotropic. A formal definition of a self-affine fractal in a two dimensional xy-space is that $f(rx_1, r^H y_1)$ is statistically similar to $f(x_1, y_1)$ where H is known as the Hurst scaling parameter. Note that the vast majority of researches (Hastings & Sugihara, 1993, for instance) use H as Hurst scaling parameter, while some (Turcotte, 1992, for example) refer H to Hausdorff measurement possibly incorrectly. H is related to D as $H = D_E - D$ where $0 < H < 1$ and $D_T \leq D \leq D_E + 1$ where D_T is the topological dimension and D_E is the Euclidean space. For example, in a random walk graph, if N_1 is the number of boxes with dimensions (x_1, y_1) required to cover the graph and N_2 is that with dimensions $(rx_1, r^H y_1)$, then the random walk is a self-affine fractal if $N_2/N_1 = r^{-D}$ (Turcotte, 1992).

There are two alternative derivations that give estimates of the fractal dimension. Assume that the time series is specified over the time interval, T. A necessary condition that the time series be a fractal is that its variance $V(T)$ has a power-law dependence on T (Voss, 1985a; Voss, 1985c; Voss, 1988),

$$V(T) = T^{2H} \quad or \quad \sigma(T) = T^H, \tag{3.3}$$

where the standard deviation, $\sigma(T)$ is the square root of variance $V(T)$. Another derivation of the fractal dimension of a time series can be obtained by using the box-counting method. We first produce a "rectangular box" of width T and height

$\sigma_T = \sigma(T)$ instead of square boxes of unit length, then divide the time interval into n smaller pieces, $T_n = T/n$. Then we count the boxes required to cover the time series and compute its fractal dimension according to Equation 3.1.

3.2.2 The Estimation Method

The methods for determining the fractal dimension as reviewed by other researchers (Klinkenberg, 1994; Gao & Xia, 1996, for example) can be grouped into two categories relevant to this study: methods for linear features and for features of higher dimensions. The box-counting method is the most suitable method here, because it can be applied to structures of higher as well as lower dimensions.

Methods for Linear Features

A study on the fractal analysis of time series showed that the preferred measurement of dimension for time series is the correlation method. The method utilises the property of correlation in time series. The correlation dimension is usually derived from the Grassberger-Procaccia algorithms (Grassberger & Procaccia, 1983b; Grassberger & Procaccia, 1983a). In some cases, it is obtained by means of the rescaled range (R/S) technique, devised by Hurst and introduced by Mandelbrot and Wallis (Feder, 1988; De la Fuente *et al.*, 1998). The correlation dimension including the use of the R/S technique demands data of repetitive patterns such as the annual flooding records of River Nile (Feder, 1988). It is unlikely applicable to, for example, the wave profile of a single tidal circle.

Using spectral methods to obtain the fractal dimensions of linear features is another form that is widely used (Table 3.1). Mandelbrot *et al.* (1984) cleared up some of the practical issues and formulated the link between the fractal dimension and the power spectrum. Although the spectral methods may be, they are computationally difficult and intensive. These methods require much more data preprocessing than any of the other methods, all of which work with the data "as are". Spectral methods require the raw data to be de-trended and tapered, and failure to do this properly prior to using spectral methods can greatly affect the results. Klinkenberg (1994, p.36) quoted from Peitgen & Saupe (1988) that the spectral methods "should only be applied to self-affine curves since the method will always return a fractal dimension of one for self-similar curves". The inherent complexity of time series in general and the fast Fourier transformation in particular are found in most textbooks (Cryer, 1986; Folland, 1992; Hamilton, 1994, for example).

The divider method has long been used to determine the length of cartographic lines (Klinkenberg, 1994, p.30). Richardson's (1961) investigations into the scale dependencies of border lengths, one of the key building blocks in the development of Mandelbrot's concept of fractal dimensions (Mandelbrot, 1983), has become one of the most cited references in the literature. Because of the ease with which this method can be implemented – using either physical or computational dividers – a large number of studies have used the divider method to determine fractal dimensions of features ranging from particle shapes to lava flows (Table 3.1). The divider method can be implemented in a number of ways, but the basic procedure is to "walk" the divider along the line and record the number of steps required to cover the line. By systematically increasing the width of the divider and repeating

the stepping process, the relation between step size and line length over a range of resolution can be determined. Calculation of the fractal dimension follows (Table 3.2). However, the divider method applies only over a limited range of scales, and misapplication can lead to inconsistent results (Goodchild, 1980; Beauvais & Montgomery, 1996). A common problem with the divider method is that the results are sensitive to the treatment of the remainder length (Aviles *et al.*, 1987; Klinkenberg & Goodchild, 1992; Andrle, 1992). Aviles *et al.* (1987) proposed three ways to treat the remainder problem. Andrle (1992) and Klinkenberg (1994) provided some in-depth discussions on the divider method.

Other methods for linear features or time series are also used, for example, the variogram method (Kulatilake *et al.*, 1998) and the box-counting method (Yambe *et al.*, 1995; Christ *et al.*, 1997). Both methods are also among the methods especially devised for estimating the fractal dimension of features of higher dimensions.

Methods for Features of Higher Dimensions

There are several methods of estimating the fractal dimension of structures of higher dimensions (Table 3.2). The area-perimeter method and Korcak's empirical relation for islands (Table 3.1) can be used to determine the fractal dimensions of linear features if those features form closed loops (Mandelbrot, 1983; Shook *et al.*, 1993; Stutzki *et al.*, 1998). If the data are appropriate, these are relatively simple methods to use and their implementations are simple (Table 3.2). However, the requirement that the features form closed loops restricts the usage of the above area-based methods. The variogram method is getting more popular recently (Bellehumeur & Legendre, 1998; Lobo *et al.*, 1998; Tate, 1998, for example). To implement the

variogram method, one needs to sample a large number of pairs of points of differing spacings along the profile and compute the differences in their vertical values, z. The fractal dimension is easily derived from the log-log plot of (*expected differences in* z)^2 against *the distance between the point pairs* (Table 3.2). However, in order to obtain a statistically valid average for the z differences, the point-pair distances are usually placed in a number of user-defined classes (Klinkenberg, 1994, p.37). Although the variogram method is usually applied to structures up to three dimensions (Carr & Mela, 1998), the box-counting method can be implemented easily in higher dimensions.

The Flexible Box-Counting Method

The box-counting method is widely used to determine the fractal dimension of many different phenomena (Table 3.1). Prior to its applications in fractal research, box counting was used mainly to determine quickly the area of irregular cartographic features (Klinkenberg, 1994, p.34). Since it can be applied with equal effectiveness to point sets, linear features, areas, and volumes, the box-counting method is a widely used means of determining fractal dimensions. This method is also known as the grid or reticular cell counting method (Peitgen & Saupe, 1988), and has been shown to be equivalent to the Minkowski-Bouligond (or "sausage") dimension (Dubuc *et al.*, 1989; Klinkenberg, 1994).

The box-counting method, when applied to a linear feature, is usually applied to cuts of a surface where the boxes overlie the cut lines or profiles. Systematically divide the profile lengthwise into equal parts and count the number of intersections of a horizontal line at some specified vertical value. Continue geometrically increasing

the number of divisions and re-determining the number of intersections until the minimum resolution of the data is reached. Using a log-log plot of "box size" against "the number of intersections", the fractal dimension is derived from the slope (Peitgen *et al.*, 1992). The mathematics is contained in Equation 3.1.

Several problems have been identified with the use of the box counting method. The method requires a significant amount of computer memory and computational time since a very large number of cells have to be stored. Because of this problem, some researchers (Liebovitch & Toth, 1989) have introduced a "fast" algorithm which, using a statistically-based sampling approach, does not require a complete enumeration of every cell at the higher resolutions. However, their method is best applied to a database of low fractal dimension (Klinkenberg, 1994). While this could be a problem to personal computer users, the computation in this study has not yet created any trouble on the UNIX workstation.

The problem of defining the minimum and maximum box size has been addressed (Dubuc *et al.*, 1989; Mullin, 1993b). Box counts of extreme sizes should be avoided in the slope determination. As with every other method that determines the slope in log-log plot, the box sizes should change geometrically so that they will be evenly spaced in the plot. The exclusion of extreme box counts was reported to result in too few points in the log-log plot (Klinkenberg, 1994, for example).

Problems Common to All Methods

There are several problems common to all methods utilising the regression model. The first is concerned with the remainder problem. The general tactics include

careful adjustment of sample numbers to fit the length of the counting unit, which leaves no remainder; that is, equally spaced data points in the The log-log plot can easily be produced using data length progressing geometrically.

The second is the scale problem, whose effect is more significant on experimental measurements than on theoretical objects. There is virtually no limitation on the range of scale for a theoretically generated structure; whereas the range of scaling has to be specified for naturally occurring objects. Dubuc *et al.* (1989) reported instabilities in the method when the number of data points used was small, and also found that the method was sensitive to the level of discretisation of the data. The plateau at high resolutions in the log-log plot is inevitable (Peitgen *et al.*, 1992, p.722). The log-log plots also can exhibit deviations from simple power law scaling, as revealed by systematic curvature of the structure of the standard residuals (Andrle & Abrahams, 1989; Andrle, 1992; Klinkenberg & Goodchild, 1992). Therefore, the key concern of deriving the measure of fractal dimension is with the linearity of the curves in the log-log plot.

The linearity of the log-log plot could be examined by many ways; for example, using the method of Andrle (1992), whether the fractal dimension is scale-independent can be tested (Beauvais & Montgomery, 1996). This method examines the curvature in the log-log plots for deviation from strict self-similarity, using the standardised residuals from least squares linear regression of log L versus log ε (Andrle & Abrahams, 1989; Andrle, 1992; Beauvais & Montgomery, 1996). If there is no structure to the regression residuals, then a single D is estimated using least squares linear regression of data between ε_{min} and ε_{max}, where ε_{min} is the smaller-scale cutoff, and ε_{max} is the upper limit to defining D. The log-log plots exhibiting

systematic structure to regression residuals are examined for distinct linear trend over length scales between ε_{min} and ε_{max}. New regressions are performed over each range of ε values characterised by a linear structure of residuals in the original composite regression to estimate D over those more restricted scaling domains. The threshold separating these scaling domains, ε_c, is defined as the intercept of the two linear regressions determined from the residual structure of the composite regression. The scaling thresholds defied by ε_c and ε_{max} are related to the amplitude and wavelength of the largest meander in each river platform (Beauvais & Montgomery, 1996). See Beauvais & Montgomery (1996) for more details.

In conclusion, the first problem is easily solved by adjusting data length geometrically. Although the second problem cannot be justified as easily, it will not arise if valid estimates of the fractal dimension are obtained, using the regression model.

3.2.3 The Regression Model and the Fractal Dimension

The fractal dimension is conventionally defined through linear line fitting, usually the linear regression by the method of least squares (Hastings & Sugihara, 1993; Tate, 1996, for example). The linear regression is performed on the logarithms of the data, (X_i, Y_i), where $X_i = \log_2(1/x_i)$ and $Y_i = \log_2(y_i)$, where x_i is the relative box size and y_i is the box count. The simple linear regression fits a straight line of the form (Hann & Hounam, 1991, Ex. g02caf),

$$Y = a + bX \tag{3.4}$$

to the data points. The calculated regression coefficient, b, that is, D, is defined:

$$b = D = \frac{\sum_{i=1}^{N}(X_i - \bar{X})(Y_i - \bar{Y})}{\sum_{i=1}^{N}(X_i - \bar{X})^2}, \tag{3.5}$$

and the regression constant, $a = \bar{Y} - b\bar{X}$, is obtained.

The method of least squares will fit a straight line through any set of points even when the relationship between the variables is not linear. Therefore, it requires a means of measuring the closeness of the data points to a straight line. This could be achieved by drawing a graph, although there are alternative numerical ways. For example, Tate (1996) suggested using the standard error as an alternative to the cut-off value for goodness of fit. Another numerical approach used in statistics is to examine the correlation coefficient. The correlation coefficient, r, is calculated using

$$r = \frac{N\sum_{i=1}^{N} XY - \sum_{i=1}^{N} X \sum_{i=1}^{N} Y}{\sqrt{[N\sum_{i=1}^{N} X^2 - (\sum_{i=1}^{N} X)^2]\,[N\sum_{i=1}^{N} Y^2 - (\sum_{i=1}^{N} Y)^2]}}. \tag{3.6}$$

The value of r will lie between -1 and $+1$ and have the same sign as b, the slope of the straight line given by the method of least squares. The closer r is to -1 or $+1$ the more likely it is that the data can be represented by a straight line. In practice, Eason *et al.* (1980, p.386) suggested that fitting a straight line through N data points should be considered only when the correlation coefficient (r) satisfies

$$\frac{2}{\sqrt{N-1}} \leq |r| \leq 1, \tag{3.7}$$

whilst some researchers simply reported the calculated correlation coefficients (Wilson & Dominic, 1998, for example). However, the above criterion will become useless if the data points are equal to or less than five, making the cut-off value equal to or greater than one.

Two special cut-off values of the correlation coefficients are 0.632 and 0.667, corresponding to data points of eleven and ten, because they are equivalent to the data lengths of $2^{11} = 2048$ and $2^{10} = 1024$ in a log-log plot. The former is the length found in Chapter Four, while the latter is in Chapters Five and Six.

Calculation of the Fractal Dimension by Examples

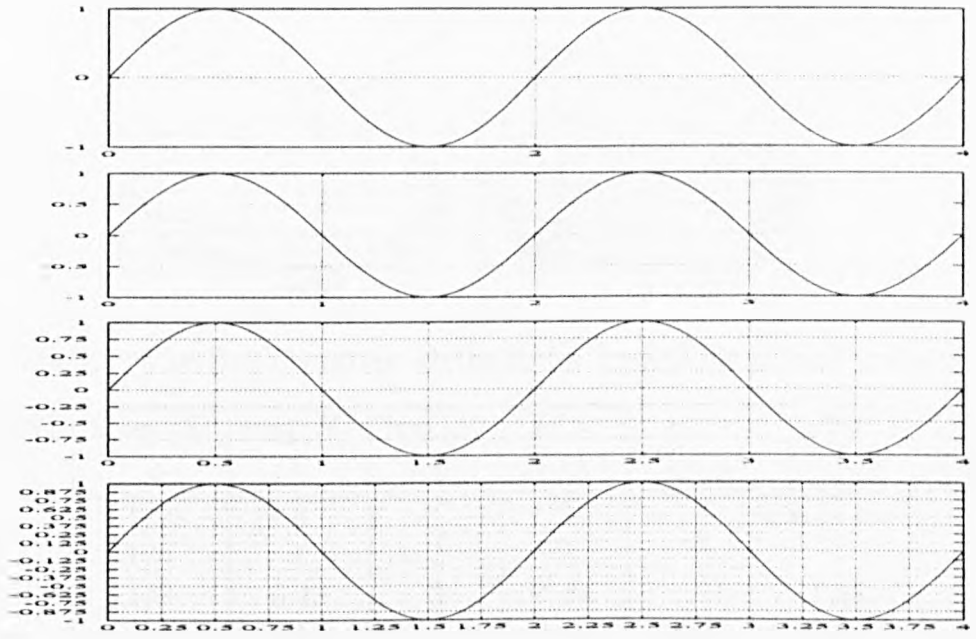

Figure 3.1: The Box Counting Method of a Sinusoidal Curve
The box size decreases geometrically in both directions.

Two examples are given here to illustrate the calculation of the fractal dimension by constructing log-log plots: a sinusoidal curve and a free-hand drawing. Figure 3.1 shows the schematic diagram of conducting the box-counting method on a sinusoidal curve. Let the time series be covered by a grid of boxes and count the number of boxes that contain part of the time series. Repeat the above procedure with varying box sizes. The fractal dimension is obtained directly by Equation 3.1, rather than by the linear regression model. The box-counting method is also applied to an irregular structure such as a two-dimensional free-hand drawing, as shown in Figure 3.2.

Table 3.3 shows the fractal dimensions directly calculated by the definition of Equation 3.1. As box sizes decrease, the calculated values decrease as well and will approach a limit, the fractal dimension. A similar conclusion is reached by the calculation of slopes using the standard geometry ($S1$ to $S3$).

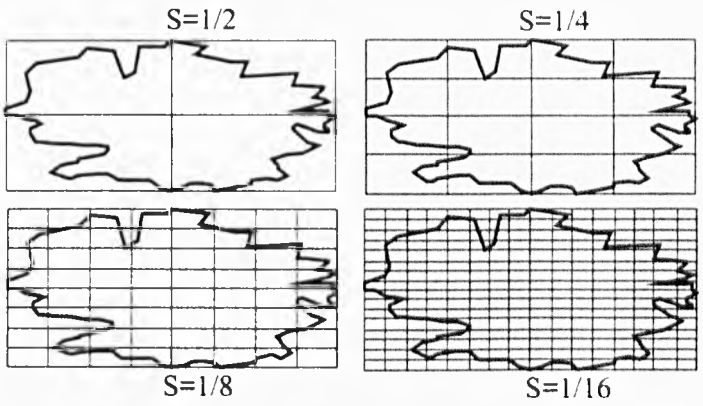

Figure 3.2: The Box Counting Method of a Two-Dimensional Feature

Counts (N)	Sizes (S)	$\log_2(N)$ (Y)	$\log_2(\frac{1}{S})$ (X)	$D' = (Y/X)$	$S1 = \frac{(Y_n-Y_1)}{(X_n-X_1)}$	$S2 = \frac{(Y_n-Y_2)}{(X_n-X_2)}$	$S3 = \frac{(Y_n-Y_3)}{(X_n-X_3)}$
4	1/2	2	1	2	(A Sine curve)		
16	1/4	4	2	2	2		
43	1/8	5.43	3	1.84	1.71	1.43	
95	1/16	6.57	4	1.64	1.52	1.28	1.14
4	1/2	2	1	2	(A 2D drawing)		
14	1/4	3.81	2	1.90	1.81		
35	1/8	5.13	3	1.71	1.52	1.32	
84	1/16	6.39	4	1.60	1.46	1.29	1.26

Table 3.3: Box Dimensions of 1D and 2D Features
The calculated fractal dimensions (D') approach a limit as box sizes decrease. This phenomenon is also seen in the slopes (S1 to S3), i.e., fractal dimensions. Note that D' is not derived from a regression model, but from Equation 3.1.

The corresponding log-lot plot is constructed in Figure 3.3. Although the slope is calculated from the regression model, its use is in doubt. The data points scatter along a straight line, and the fractal dimensions derived from the regression model seem to fall between one and two: 1.28 ($r = 0.998$) for the sinusoidal curve and 1.29 ($r = 0.999$) for the free drawing. Given the total data points of four, however, the results cannot be justified by their calculated cut-off value that exceeds one (Equation 3.7). The obvious and easy solution is to increase the counting depth. The ease of implementation strengthens the argument that the box-counting method is more suitable than other methods for the analysis of various natural phenomena corresponding to the system dynamics revealed in the Mandelbrot set.

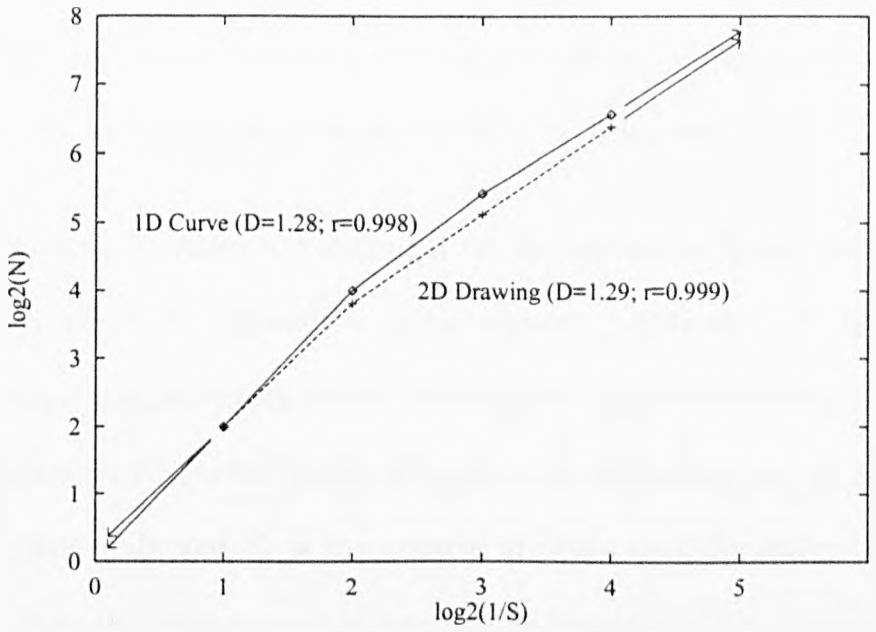

Figure 3.3: The Log-Log Plot of 1D and 2D Features.
The calculated fractal dimensions are typical for linear features; although the theoretical cut-off value cannot be computed for data points less than five.

3.2.4 Implementation of the Box-Counting Method

It is widely known that for the graph of zeros of $B(t)$, the Hausdorff-Besicovitch dimension is $1/2$, and almost as widely known that for the graph of $B(t)$ itself the Hausdorff-Besicovitch dimension is $1.5 = 1+\frac{1}{2}$. However, "the Hausdorff-Besicovitch dimension is a very non-intuitive notion because this dimension can be no use in empirical work, and is unduly complicated in the theoretical work, except for self-similar fractals" (Mandelbrot, 1985, p.258).

As to self-affine shapes, Mandelbrot (1985, p.258) stated that local and global values must be distinguished for each dimension, and that the different local values *cease to be identical.* The reason is fundamental: "square," "distance," and "circle," are vital notions in "isotropic" geometry, but they are meaningless in affine geometry. More precisely, they are meaningful for relief cross-sections, but are meaningless

for noises, because the units along the t axis and along the B-axis are set up independently of each other. "There being no intrinsic meaning to the notion of equal height and width, a square cannot be defined" (Mandelbrot, 1985, p.258).

The box dimension is meaningful for the records of $B_H(t)$, and its local value is the "correct" $2 - H$ and its global value is 1 (Mandelbrot, 1985). As to the implementation, one needs to use "rectangular" instead of the usual "square" boxes. Theoretically, if N_1 is the number of boxes with dimensions (x_1, y_1) required to cover the random walk and N_2 is the number of boxes with dimensions $(x_2 = rx_1, y_2 = r_H y_1)$, then the random walk is a self-affine fractal if $N_2/N_2 = r^{-D}$, where r is the scaling factor and D is the fractal dimension. In practice, the width and height of the box are decided by the length and the standard deviation of the time series. Firstly, we introduce a rectangular reference "box" with a width T, the length of the time series, and height $\sigma_T = \sigma(T)$, the standard deviation of the time series. Secondly, the interval of the time series T is divided into n smaller intervals with the width of $T_n = T/n$. Therefore, the size of the scaled box of smaller boxes of width T_n and height $\sigma_n = \sigma_T/n$ is decided. Note that these boxes have the same aspect ratio, *width/height*, as the reference box. Also, the standard deviation associated with the interval T_n, $\sigma_{T_n} = \sigma(T_n) = \sigma(T/n)$, is not equal to σ_n (Turcotte, 1992).

Furthermore, estimates of fractal dimensions often vary with the choice of method and details of estimation. Where this cannot be easily explained, the observed fractal dimension is of unknown accuracy and may be misleading. Tate (1996, p.794) stated that "this may partly explain the difficulties some have had fitting the fractal model to topography..., relating [fractal dimension] in any meaningful manner to process... leading some to abandon monofractals in favour of multifractals..."

This results in the observation that method-induced variations in the fractal dimension limit both the reproducibility and the testing of the monofractal model (Klinkenberg & Goodchild, 1992; Tate, 1996, p.806).

Every method appears to be, or not to be, "the" method of determining the fractal dimension of different features. However, Klinkenberg (1994, p.42) has suggested that the box dimension seems to be more appropriate for several reasons. Firstly, it represents the characters of features more precisely than Euclidean geometry. Secondly, it is relatively easy to understand and simple to implement while maintaining its representativity. Thirdly, it can be applied to both self-similar and self-affine fractals without compromising its simplicity.

Therefore, the most suitable method of estimating the fractal dimension from the three different types of data is the box-counting method, even though there are seemingly better methods specific to each type of data. For example, it is indeed truly logical that the fractal dimension is estimated using the spectral method for time series such as wave profiles; however, the method cannot be applied to estimation of the fractal dimension of a fern's shape. The concept of the box-counting method remains unchanged when it is applied to higher dimensions; that is, dimensions of hyperbolic cubes may change in higher dimensions, but the counting procedure is virtually the same. See the following for further explanations and Appendix E for the computer programme listing.

The Implementation

Negative measures in raw data are corrected by method of extrapolation before the calculation of the fractal dimension commences in the key sub-routine *BoxFD()*, using the following simple geometry

$$x_{i+2} = 2x_{i+1} - x_i, \tag{3.8}$$

if the measurement x_{i+2} is negative in origin. The very first two data points have to be either positive or zero if they are negative. Non-linear correction might be considered; however, linear relation is assumed between data of such short time span. The corrected data are then submitted to the key sub-routine *BoxFD()* for further processing.

The key sub-routine *BoxFD()* returns the fractal dimension of a time series. Essentially, it counts the minimum number of linear size (ε), constructs the log-log plot of box sizes against box counts, and calculates the fractal dimension (D) using

$$D = \lim_{\varepsilon \to 0} \frac{\log_2 N(\varepsilon)}{\log_2 (1/\varepsilon)}. \tag{3.9}$$

Here, the notion of "size" is maintained, although it is actually the "box scale", the box size relative to the largest unit box.

Several procedures are involved in this sub-routine, which are detailed as follows. Firstly, the *level* of recursion is obtained from the number of data. At each level, the *width* and *length* of the scaled smaller box are decided. Then, blocks of data are taken to be examined by the smaller box. The number of boxes needed to cover the block, *nbox*, is, therefore, derived. By adding up the *nbox* of each block, the total box *count* respective to box *size* is obtained. Standard regression is performed on

the logarithms of *count* and *size*. Fractal dimension D is the slope of the regression line. See the self-explanatory pseudo codes in Figure 3.4, while the actual computer programme is seen in Appendix E. More details are given below.

Sub-Routine: *BoxFD(X,N,S)*	Comments
$level = \log_2 N$	Level of repetition
for $i = 1$ to $level$ do	
$scale = 2^i$	Number of sub-blocks
$width = N/2^i$	Width of smaller box
$height = S/2^i$	Height of smaller box
$size[i] = 1/scale$	Size
$count[i] = 0$	Counts
for $j = 1$ to $scale$ do	Obtaining block of data
for $k = 1$ to $width$ do	
$B_j[k] = X[j * width + k]$	Block data obtained
$Stats2(B_j, width, min, max)$	Calculates min and max
$nbox = ceil(max/height) - floor(min/height)$	Counts number of boxes
$count[i] = count[i] + nbox$	Adds up number of boxes
for $i = 1$ to $level$ do	Logarithmisation
$size[i] = \log_2 size[i]$	
$count[i] = \log_2 count[i]$	
$Regress(size, count, level, D)$	Derives D
return D	Returns D
Sub-Routine: $Stats2(X, n, min, max)$	Returns min and max from data $X[n]$
Sub-Routine: $Regress(X, Y, n, D)$	Returns D from data $X[n]$ and $Y[n]$

Figure 3.4: Basic-style Pseudo Codes of the Box-Counting Method.
Sizes of the scaled smaller boxes are decided. Blocks of data, corresponding to the scaled box size, are extracted to perform the box counting function. The number of boxes is counted by taking the "ceiling" and "floor" of the maximum and minimum values, respectively, divided by the height of the scaled box.

The width (N) and height (S) of the reference box are given, where N is the number of data, and S is the standard deviation of data $X(N)$. The *level* of recursion is calculated by taking the logarithm of N to base two, that is, $level = \log_2(N)$.

At each level of recursion, the *scale* of dividing the whole data is decided, that is, $scale = 2^i$, where $i = 1, 2, ..., level$. The scaled smaller boxes are of dimensions $(width = N/2^i, height = S/2^i)$, where $i = 1, 2, ..., level$. Blocks of data of $width$, B_j,

are obtained, where $j = 1, 2, ..., n$. For each block, minimum (min) and maximum (max) of B_j are calculated by sub-routine *Stats()*. Both min and max are then divided by the *height* of the smaller box. The absolute difference between the "floor" and the "ceiling" of the divided values, respectively, is the number of boxes ($nbox$) needed to cover the block of data. Here the function $floor()$ returns the greatest integral value less than or equal to a real number x, while the function $ceil()$ returns the least integral value greater than or equal to it. The box *count* of each block is added up to produce the total number of boxes needed to cover the time series, respective to box size.

The above process is repeated until it completes the recursion. Therefore, box counts respective to box sizes are obtained. Using sub-routine *Regress*(), standard regression is performed on the logarithms of *count* and *size* to obtain fractal dimension, D, which is the slope of the regression line. The estimate of the fractal dimension is then returned by sub-routine $BoxFD()$.

Although a relatively new concept, the estimation of the fractal dimension is never detached from conventional science entities, as seen above. Some conventional methods in their own right are also useful in making comparisons of the fractal dimensions. However, any meaningful comparison of the fractal dimensions has to satisfy some basic requirement.

3.2.5 Making Comparisons of the Fractal Dimensions

There are at least two fundamental requirements in making comparisons of the fractal dimensions; that is, the range of scales and methods to derive the fractal

dimension must be identical. Andrle (1996) found that "using fractal dimension to compare even the same types of features was unreliable because of the dependency of fractal dimension on scale of measurement." Fractal dimensions were found to be sensitive to changes of scales by means of magnifying a natural object (Chan & Page, 1997) or by reducing data length of a natural system, as shown in Chapter Four; that is, the estimated fractal dimensions decrease upon increase of magnification. Such an observation would be unlikely to hold for mathematical fractals since they have no limitation on scaling up or down. For the real world data, the alternative is to state clearly the range of scale from which the fractal dimension is derived. Since the scaling technique is likely to reveal the multifractality of an object (Gao & Xia, 1996; Campbell & Shepard, 1996; Chan & Page, 1997, for example), one risks using the fractal dimension derived from one scale range in comparison with that derived from another scale range. The implication is that one has to make comparisons of the fractal dimensions derived from similar scales. Another alternative was to state clearly the threshold area associated with the derived fractal dimension (Islam *et al.*, 1993; DaRos & Borga, 1997), because "morphometric properties vary considerably with the threshold area [A_c] in channel networks, and thus values reported without their associated A_c are meaningless and should be used in hydrologic analysis with caution" (Helmlinger *et al.*, 1993).

The other requirement is related to the estimation methods. Although in theory all estimation methods are designed to reveal the scale-invariant nature of fractal objects, they actually produce slightly different measures due to the way they are implemented. Zahn & Zosch (1997) found that the fractal dimension calculated by Fourier analysis is higher than the dimension determined by the box-counting

method, yet both utilise the same digital image. The most possible reason might be that the Fourier method could provide an extrapolation procedure that "adds" data, hence produces a result different from that derived from the box-counting method, as the latter is totally dependent upon the original data points. In other words, the pixel density has far less significance in Fourier analysis than in the box-counting method. As a result, it is necessary to state explicitly the estimation method used when making a comparison.

The two basic requirements just stated are essential in enabling meaningful comparisons of fractal dimensions, reported in various sources, that might vary in methods and scales. Furthermore, it is generally accepted that a comparison should be made between identical systems, although different systems may be observed with a similar method under similar scales. Under such a restriction proposed here, relatively few articles are available for comparison with the findings in this study, as detailed in Chapter Seven, that also includes comparisons with other work for a general discussion on the application of Fractal Geometry.

Details of the fractal method have been described, including the use of the regression model on log-log plots, the box-counting method and its implementation, and the rules for making comparisons of the fractal dimensions. The following section explains the statistical techniques, the other major methods used here.

3.3 Statistical Analyses

Basic statistics such as minimum, maximum, mean, and standard deviation are obtained to illustrate the characteristics of the data and their derived fractal dimensions. The mean gives a measure of the central location of the data distribution, and the variance, whose positive square root is standard deviation, gives a measure of the spread about the mean (Eason *et al.*, 1980, p.420). Coefficient of skewness and coefficient of kurtosis are also included. The former measures the skewness of data (Bryman & Cramer, 1990, p.97). The latter is the measure of sharpness of the peak of a frequency-distribution curve (Marsh, 1988; Allen, 1990, p.658).

The difference of statistical parameters between synthetic and natural data is tested. The procedure involves, firstly, the test of normality for each sample (Eason *et al.*, 1980, Ch.24,25), which leads to the choice of a non-parametric or a parametric test between two samples. Secondly, a non-parametric or parametric two-sample test is performed accordingly. For populations of normal distribution, a parametric test is performed; otherwise, the Mann-Whitney U test is chosen, which is also designed for dealing with large sample size (Eason *et al.*, 1980, p.487). In practice, a large sample usually means the sample size is greater than or equal to thirty ($N \geq 30$) (Eason *et al.*, 1980, p.450). Details regarding the statistical tests are given below and their implementation in C programmes can be seen in Appendix F.

3.3.1 Basic Statistics

Basic statistics refer to minimum, maximum, mean and standard deviation of a given sample. Minimum and maximum are the lowest and highest values of the data in the sample, respectively, which form the range of the sample. The mean and variance of a continuous, more likely theoretical, time series are denoted as $\bar{x}(T)$ and $V(T)$, respectively, where T is time. In practice, experiment measurements are samples taken at certain intervals of time, which yield a discrete time series. Therefore, the mean and variance of a discrete time series are calculated and denoted differently as $\bar{x}$ and V, respectively. However, in either a continuous or a discrete case, standard deviation is equal to the square root of variance, that is,

$$S_2 = \sqrt{V}, \tag{3.10}$$

where $V = \frac{1}{N-1}\sum_{i=1}^{N}(x_i - \bar{x})^2$, where N is the number of samples, x_i. The standard deviation measures average amount of deviation from mean (Bryman & Cramer, 1990, p.87). Formal definitions of skewness (S_3) and kurtosis (S_4) are related to the standard deviation and given below.

Coefficient of skewness, S_3, is defined as the following (Hann & Hounam, 1991, Ex. g01aaf),

$$S_3 = \frac{\sum_{i=1}^{N}(x_i - \bar{x})^3}{(N-1){S_2}^3}. \tag{3.11}$$

If there is no skew, that is, if data are normally distributed, a value of zero or nearly zero is seen. If there is a negative value, the data are negatively skewed, that is, they "tail" to the left. If there is a positive value, the data are positively skewed, that is, they "head" to the left. See Bryman & Cramer (1990, p.97).

The coefficient of kurtosis, S_4, is given as (Hann & Hounam, 1991, Ex. g01aaf),

$$S_4 = \frac{\sum_{i=1}^{N}(x_i - \bar{x})^4}{(N-1){S_2}^4} - 3. \tag{3.12}$$

It offers an indication of whether the bulk of data are concentrated around the mean. The kurtosis of a peaked distribution is greater than 0. The average distribution has kurtosis around zero, while for *platykurtic* distributions, with widespread range of values and similar frequencies, kurtosis is smaller than zero (Allen, 1990, p.658).

A Graphic Alternative

A frequency distribution histogram is an alternative to the basic statistics, where frequency is plotted against the class intervals, that is, the grouped observations. In practice the class intervals can be of any size but are preferably chosen to give at least six equal class intervals over the range of observations (Eason *et al.*, 1980). Because of the huge amount of estimates, this histogram technique is applied specifically to the fractal dimensions derived from the digital elevation models and spectral images, where the size of the class intervals is set to twelve to cover the majority of fractal dimensions that ranges between 1.0 and 1.6.

3.3.2 Statistical Tests

Several statistical tests are performed to decide whether the difference between the synthetic and natural data is significant. Eason *et al.* (1980, p.509) gave some advice regarding the use of tests. A simple guideline is to use parametric tests when the sample sizes are large. When the sample sizes are small, unless there is

Type of test	Nature of criterion available	Number of comparison groups or samples		
		Unrelated Data		Related Data
		1 (group)	2 (groups)	2 (groups)
Non-parametric	Categorical:			
	binomial or	Binomial		
	frequency	Chi-square	Chi-square	
	Non-categorial:	KS	KS	
	ordinal or		Median*	Wilcoxon
	ranked		MW*	
Parametric	Non-categorial:			
means	interval or ratio	t, Z	$t*, Z$	t, Z
variance			F	

Table 3.4: Tests of Difference for Two Variables.
KS and MW denote the Kolmogorov-Smirnov and Mann-Whitney U tests, respectively. Those marked with " * " are used in this thesis. Modified from Bryman & Cramer (1994, p.119).

evidence to support the validity of the use of a parametric test, the corresponding non-parametric tests should be used. Often, the analysis of data by both methods will lead to the same conclusion. A summary of statistical two-sample tests is given in Table 3.4, which is modified from Bryman & Cramer (1994, p.119). The choice of tests also depends on the nature of the data.

The statistical procedure used in this thesis is summarised here. The data are tested for their distribution pattern, followed by two-sample tests. Shapiro and Wilk's W test is utilised here as the normality test. If the data are likely to be from a normal population, parametric two-sample tests are performed to compare the difference between synthetic and natural data; otherwise, non-parametric two-sample tests are carried out. In other words, if the samples are of normal distribution, the t-test is selected for small sample size ($n \leq 30$) and the z-test for large sample sizes; otherwise, non-parametric tests such as the median and Mann-Whitney U tests are used to test the difference between two samples.

In parametric tests, a hypothesis is a statement about what is believed to be the value of the population parameter before experimental data are presented (Eason *et al.*, 1980, p.465). For example, a sample of observation is drawn from a population with known variance, where the population mean μ is unknown but is thought to be μ_0. It has to be decided which of the two alternatives $\mu = \mu_0$ or $\mu \neq \mu_0$ is to be accepted; that is, the choice must be made between the null hypothesis, H_0, and one of the alternative hypotheses, H_1, respectively.

$$\begin{aligned} H_0 &: \mu = \mu_0 \\ H_1 &: \begin{cases} \mu \neq \mu_0 & or \\ \mu > \mu_0 & or \\ \mu < \mu_0 \end{cases} \end{aligned} \tag{3.13}$$

Depending on the research hypothesis, one and only one of the three alternatives is assumed. If the calculated significance level is larger than the given significance level, H_0 is accepted and H_1 is rejected.

Another category of statistical tests is called non-parametric or distribution free tests, as parameters such as the mean and variance do not need to be estimated, and assumptions about the probability distribution of the observation are unnecessary (Eason *et al.*, 1980, p.487). Hypotheses are proposed and the significance level is set. The conclusion can be drawn from the calculated significance level.

The research conclusion is reached by comparing the test statistics with the significance level of the test. The choice of significance level is, by convention, chosen arbitrarily before the analysis of data to be either 5% or 1% (Eason *et al.*, 1980, p.466). For all tests conducted here, the significance level is set to 5%, although it was suggested to use 5% for small samples and 1% or lower for larger samples (Vaus, 1993, p.191). Alternatively, the calculated significance level or the probability associated with the test statistic can be obtained, thus lead to the choice between

the null and the alternative hypotheses.

There are two types of errors associated with the choice of significance level. The former is that one might reject the assumption of no association in the population (i.e., null hypothesis) when there is no association. This is called a type I error, which is likely to happen when using a higher significance level for larger samples. On the other hand, one might accept the null hypothesis when it should be rejected. This type II error usually happens in small samples being tested against lower significance level. In the words of Chatfield (1988, p.79), for example, types I and II errors could be equated, respectively, to the statements that "a non-significant effect is not necessarily that same thing as no difference", and "a significant effect is not necessarily the same thing as an interesting effect."

Just as every statistical test risks either of the two errors, so does this thesis. For example, the analysis in the first part of Chapter Four and whole of Chapters Five and Six might risk the type I error, for the sample size is large ($N \geq 30$) and the significance level is high (5%); whereas the second part of Chapter Four might suffer from type II error. Fortunately, most statistical softwares produce the calculated significance level of a test. Therefore, one can use the alternative approach mentioned above in drawing conclusions on the hypotheses.

Normality Tests

A normal population is defined as a distribution which has zero mean and unit variance, and is denoted as $N(\mu, \sigma^2) = N(0, 1)$ (Eason *et al.*, 1980, p.434). Since the normal distribution of data is very important to statistical inference, the assumption

that the data come from a normal distribution is often examined. One way to do this is with a normal probability plot. In a normal probability plot, each observed value is paired with its expected value from the normal distribution. Although normal probability plots provide a visual basis for checking normality, it is often desirable to compute a statistical test of the hypothesis that the data are from a normal distribution. Two commonly used tests are the Lilliefors test and the Shapiro and Wilk's test. The Lilliefors test, based on a modification of Kolmogorov-Smirnov test, is used when means and variances are not known but must be estimated from the data. Refer to Norušis (1993, p.189) for more details.

Shapiro and Wilk's test shows great reliability in many situations compared to other tests of normality (Conover, 1980). Shapiro and Wilk's W statistic for the normality test requires that data are sorted into either ascending or descending order. The W statistic is defined as (Hann & Hounam, 1991, Ex. g01ddf),

$$W = \frac{(\sum_{i=1}^{N} x_i)^2}{\sum_{i=1}^{N}(x_i - \bar{x})^2}. \tag{3.14}$$

If the W statistic is small and its calculated significance level is greater than 0.05, then the null hypothesis is accepted and the alternative hypothesis H_1 is rejected. The W statistic and its related calculated significance level measures the normality of a sample, and indicates what kind of tests are needed for further comparison. That is, the parametric test will be performed if both samples are normally distributed. In all other cases, non-parametric tests are carried out.

Two-Sample Tests

There are several methods of making comparisons between two samples. The two-sample z-test is valid for all large samples and for small sample when the probability distribution of samples is normal; whereas the two-sample t-test is used instead of z-test when the sample size is small and the population variance has to be estimated by the sample variance, and the population should have a normal distribution (Eason *et al.*, 1980, pp.468,471). Another important requirement is that the variance of the two populations should be equal. In practice, the sample standard deviations should be nearly the same. All these tests are based on the assumption that samples are of normal distribution.

The two-sample t-test and z-test are to examine the difference of means between two normal populations. If the two population variances are equal, that is, $\sigma_x^2 = \sigma_y^2$, the test statistic, t, is defined (Hann & Hounam, 1991, Ex. g07caf) as

$$t_{obs} = \frac{\bar{x} - \bar{y}}{s\sqrt{(1/n_x) + (1/n_y)}}, \tag{3.15}$$

where $s^2 = \frac{(n_x-1)s_x^2+(n_y-1)s_y^2}{n_x+n_y-2}$ is the pooled variance of the two samples. Under the null hypothesis, $H_0 : \mu_x = \mu_y$, this test statistic has a t-distribution with (n_x+n_y-2) degrees of freedom. The alternative hypothesis is $H_1 : \mu_x \neq \mu_y$, and the calculated significance level, $p = P(t \geq |t_{obs}|)$, is the probability of t equal to or greater than $|t_{obs}|$, the absolute value of t_{obs}. If the population variances are not equal, the two-sample t-statistic no longer has a t-distribution and an approximate test is used. That is, the approximate test statistic, t', is defined,

$$t'_{obs} = \frac{\bar{x} - \bar{y}}{se(\bar{x} - \bar{y})}, \tag{3.16}$$

where $se(\bar{x} - \bar{y}) = \sqrt{\frac{s_x^2}{n_x} + \frac{s_y^2}{n_y}}$. A t-distribution with f degrees of freedom is used to

approximate the distribution of T', where $f = \frac{se(\bar{x}-\bar{y})^4}{\frac{s_x^2/n_x^2}{(n_x-1)}+\frac{s_y^2/n_y^2}{(n_y-1)}}$. Here the alternative hypothesis is $H_1 : \mu_x \neq \mu_y$, and the calculated significance level, p, is equal to $P(t' \geq |t'_{obs}|)$.

For large sample sizes ($n \geq 30$), the two-sample z-test is used. The z statistic is calculated as follows,

$$z = \frac{\bar{x} - \bar{y}}{\sqrt{\frac{s_x^2}{n_x} + \frac{s_y^2}{n_y}}}. \tag{3.17}$$

The hypotheses are $H_0 : \mu_x = \mu_y$ and $H_1 : \mu_x \neq \mu_y$. The calculated significance level is compared with the standard significance level associated with the z statistics, in order to reach the conclusion. For example, at a 1% significance level the z statistic must lie between -2.57 and 2.57 for H_0 to be accepted.

If the samples are not normally distributed, non-parametric tests have to be considered. In those tests, parameters such as the mean and variance do not need to be estimated and assumptions about the probability distribution of the observations can be unnecessary (Eason *et al.*, 1980, p.487). For example, the Kruskal-Wallis and the Friedman tests are methods suitable for detecting differences between several groups of observations; Contingency tables were devised as a method of handling categorised data and the Wilcoxon test is an alternative to the paired comparison t-test. Refer to Eason *et al.* (1980, Ch.24-25) for more details. Since this thesis is mainly concerned with testing the difference between the real and synthetic data, several two-sample tests are discussed below.

The two-sample Kolmogorov-Smirnov test assumes that the data to be tested consist of two independent "samples" (Hann & Hounam, 1991). The hypotheses are $H_0 : F(x) = G(y)$ against one of many alternative hypotheses such as $H_1 : F(x) \neq$

$G(y)$, where $F(x)$ and $G(y)$ represent unknown distribution functions of samples of size n_x and n_y, respectively. Given the above alternative hypothesis H_1, the largest positive deviation between the two sample cumulative distribution functions (the statistic D_{n_x,n_y}) is obtained (Hann & Hounam, 1991, Ex. g08cdf). The normal test statistic of D_{n_x,n_y} can be calculated from $Z = \sqrt{\frac{n_x+n_y}{n_x n_y}} \times D_{n_x,n_y}$. Subsequently, the conclusion can be drawn from the test; for example, the null hypothesis, H_0, is rejected under 5% significance level, if $|Z|$ is greater than 2.131.

Similar to the Kolmogorov-Smirnov distribution test is the two-sample Mann-Whitney U test, which assumes that the data consist of two independent "populations" (Hann & Hounam, 1991). The Mann-Whitney test is often suitable in cases where the two-sample parametric t-test cannot be used (Eason *et al.*, 1980, p.489). Therefore, it is the first non-parametric test used here.

The Mann-Whitney U test investigates the difference between two populations defined by the distribution functions $F(x)$ and $G(y)$, respectively. The null hypothesis under test is $H_0 : F(x) = G(y)$ and the alternative hypothesis is $H_1 : F(x) \neq G(y)$. The test procedure involves the pooled sample, average ranks being used for ties. Let r_{1i} be the rank assigned to $x_i, i = 1, 2, ..., n_1$, and r_{2j} the rank assigned to $y_j, j = 1, 2, ..., n_2$, where n_1 and n_2 are sample sizes. The test statistic U is defined as follows (Hann & Hounam, 1991, Ex. g08ahf):

$$U = \sum_{i=1}^{n_1} r_{1i} - \frac{n_1(n_1+1)}{2}. \tag{3.18}$$

The approximate normal test statistic, Z, is:

$$Z = \frac{U - mean(U) \pm \frac{1}{2}}{\sqrt{var(U)}}, \tag{3.19}$$

where $mean(U) = \frac{n_1 n_2}{2}$ and $var(U) = \frac{n_1 n_2 (n_1+n_2+1)}{12} - \frac{n_1 n_2}{n_1 n_2 (n_1+n_2-1)} \times TS$, where

$TS = \sum_{j=1}^{\tau} \frac{(t_j)(t_j-1)(t_j+1)}{12}$, where τ is the number of groups of ties in the sample and t_j is the number of ties in the jth group. However, if no ties are present, $var(U)$ reduces to $\frac{n_1 n_2 (n_1+n_2+1)}{12}$.

Another two-sample non-parametric test used in this thesis is called the median test. It investigates the difference between the medians of two independent samples of possibly unequal sizes. The test proceeds by forming a 2×2 frequency table, giving the number of scores in each sample above and below the median of the pooled sample. The hypothesis under test, H_0, is that the medians are the same, and this is to be tested against the alternative hypothesis, H_1, that they are different. Refer to Hann & Hounam (1991, Ex. g08acf) for more details.

Comparative Data

The procedures described above involve decision on the hypotheses using test statistics, which is confusing at times. However, the decision process can be made easier and clearer using data of known parameters. Two sets of data of known population parameters are used for comparative purposes: the normal scores and the random numbers from a normal distribution, that is, $N(0, 1)$. For routines that generate those data refer to Hann & Hounam (1991). Both are expected to be normally distributed, and the difference between them is not significant.

3.4 Discussion and Conclusion

In this chapter, the common methods which are used for analysing data in this thesis have been introduced, including the use of fractal analyses and of various statistical analyses. Specific methods relevant to each type of data are given in later chapters. These will include the conventional analyses of time series, digital elevation model, and spectral image.

3.4.1 On Fractal Analysis

Fractal analysis here refers to the estimation of the fractal dimension of self-affine linear features such as wave profiles, and profiles of the digital elevation model and the fern image. The analysis of the last two features involves the sectioning of a self-affine three-dimensional image. Although the distinction between self-affine and self-similar profiles is an elusive one (Mandelbrot, 1985), reducing the dimensionality means that the nature of the fractal objects might be altered (Mandelbrot, 1989). For example, horizontal slices or contours through a topographic surface or a cloud exhibit self-similar behaviour, given that those phenomena are self-affine. However, other researchers such as Klinkenberg (1994, p.25) stated that "this dimensionality-reduction process does not always alter the fractal nature since profiles of self-affine surfaces remain self-affine."

The proper estimation of the fractal dimension requires several considerations on the choice of implementation methods. For example, the box-counting method demands a large number of data points and hence computer memory; the divider

method used by Richardson (1961) is unlikely to be appropriate for digital images; and Klinkenberg (1994, p.36) advised that the spectral method "should only be applied to self-affine curves." Yet another drawback common to every method of obtaining the fractal dimension is that discretisation of the phenomena being investigated will result in a measured fractal dimension that is different from its theoretical fractal dimension (Klinkenberg, 1994, p.28). The coarser the discretisation, the greater the expected difference, and the direction that the difference will take is open to question. Gilbert (1989) found instances of both a decrease and an increase in the fractal dimension with greater decimation of the original data. Thus, to assume that discretisation achieved by removing finer details will always result in a lesser fractal dimension is inappropriate (Klinkenberg, 1994). Since the implementations of some methods are themselves discretisation of continuous expressions, that in itself may affect the derived fractal dimensions (Dubuc *et al.*, 1989). In fact, estimates of fractal dimensions often vary with the choice of method and details of estimation (Tate, 1996, p.794).

The box-counting method has proven reliable for the estimation of the fractal dimension from many fractal objects, although there are problems associated with this specific method and concerns about all methods that use the regression model, as explained earlier. The first advantage of the box-counting method is that it can be easily extended from linear features to features of higher dimensions. The second is that it can be applied to both self-similar and self-affine objects (Klinkenberg, 1994, p.42) and the third is that it is relatively easy to implement with a computer. Therefore, the box-counting method has been chosen here as the method for implementing the estimation of the fractal dimension for the various data sets. The

obtained results can be used for further comparisons with other work.

Making comparisons of the fractal dimensions demands that identical methods and similar scales are used in the estimation process, as described earlier. Such a restriction makes the rules for comparisons of the fractal dimensions from various sources more rigid and meaningful. It can also be extended to the interpretation of the systems dynamics within a system.

The difference of dynamics within a system is not always easy to detect, and alternative approaches have been used. Another means of understanding a system is to extract their multifractal characteristics and the methods for monofractals have been extended to multifractal objects. It is important to separate the observation of discrete fractal elements from truly continuous multidimensionality (Andrle & Abrahams, 1989; Andrle & Abrahams, 1990), since the question of whether a mono- or a multidimensional fractal is the more appropriate model has not been answered in most cases (Klinkenberg, 1994, p.27). The result of any analysis must be carefully examined for evidence of multidimensionality. One way to check for such behaviour is to plot the residuals from the best-fitting line of slope and check for evidence of nonlinearity (Andrle, 1992). A closer examination reveals that the formulation of multifractal dimensions shares the identical implementation methods used in estimating monofractal dimensions. It seems another alternative approach is needed for the exploring of the difference of the sub-systems dynamics.

This thesis offers a conceptually easy alternative to the understanding of sub-systems dynamics of a system: the estimation of the fractal dimension of the sub-systems. A sub-system here means a section of a profile of a system. Because

the estimation method and scale are identical for every sub-system, the comparison of sub-systems dynamics is reliable. The sub-systems dynamics can be identified spatially, unlike the multifractal or the single measure approaches.

3.4.2 On Statistical Analysis

The statistical methods which are used in this thesis are comparatively well-established. Definitions of basic statistics and methods of implementation have been documented and the general characteristics of the sample are revealed once the basic statistics are obtained. This procedure is performed for both the synthetic and natural data sets.

Statistical tests have among other uses the determination of significant differences between two samples. The tests used in this thesis are mainly for comparison between the mean values of raw data and mean values of derived fractal dimensions and for these purposes a normality test has to be performed first for the data to be tested. For parametric tests to be valid, data samples must be normally distributed, that is, with zero mean and unit variance. Because data taken from the natural environment do not usually exhibit normal distribution, more conservative statistical tests known as non-parametric tests are selected for use here.

The choice of the statistical method depends on the nature of the data. Because the raw data and the derived fractal dimensions are of a continuous nature, the one-sample Shapiro and Wilk's W test is used to test the normality of sample. For the same reason, the two-sample t-test and Mann-Whitney U test are chosen for parametric and non-parametric tests, respectively. The t-test is usually used for a

small sample of fewer than thirty data points. Because the sample size of a digital elevation model and fern image is much greater than thirty, the Mann-Whitney U test has been chosen.

The implementation of the box-counting method involves programming with ANSI C and FORTRAN 77 computer languages and the complete listing of the methodology is given in Appendix E; whereas the statistical tools and programmes that are able to modify the data format and make linkage with existing routines are listed in Appendix F.

Part II

Waves, Landforms and Ferns

Chapter 4

Wave Profiles

Figure 4.1: The Teignmouth Estuary in England.
The wave data were collected in 1992 on the beach behind the pier. The pier has been dismantled by the local authority. From Baring-Gould & Hicks (1949, p.204).

4.1 Introduction

This chapter focuses on the study of the relatively homogeneous sea wave system, using both conventional and fractal analyses. This section provides the basics of describing waves, a brief history of wave recording, and the reasoning for the use of pressure transducers as the recording instrument. It is then followed by the description of the natural wave profile data, that were collected on 16th May 1992, at Teignmouth in south-western England; and the synthetic wave, that is generated from a typical wave theory, comprising four sinusoidal waves with different sets of amplitudes, the first angular velocities, and phase lags. This chapter continues with the methods of analysis: the conventional time series analysis includes the qualitative approach of phase portrait reconstruction and the quantitative approach of spectral analysis; while the fractal analysis has been detailed in Chapter Three. Subsequent results are given, followed by discussion and conclusion.

4.1.1 Describing Waves

Hardisty (1990b, p.1) stated that "the more or less regular rise and fall of the sea surface at intervals of up to 20 seconds have been generated since water first liquidified on the earth's crust." It is perhaps surprising that relatively few actual measurements are available of these complex and poorly understood phenomena. The difficulty of understanding waves is largely due to two sets of problems. Firstly, the water level which defines the wave profile is constantly changing so that measurements must be taken at least once a second and often more frequently if fine details are to be discerned. The second problem is of a more theoretical nature

and involves the analysis of the measurements and the formulation of an accurate description of the results which properly encompasses the data set.

Tidal waves and wind waves are two main sources contributing the majority of energy to ocean motions as shown in Figure 4.2. Waves generated by the gravita-

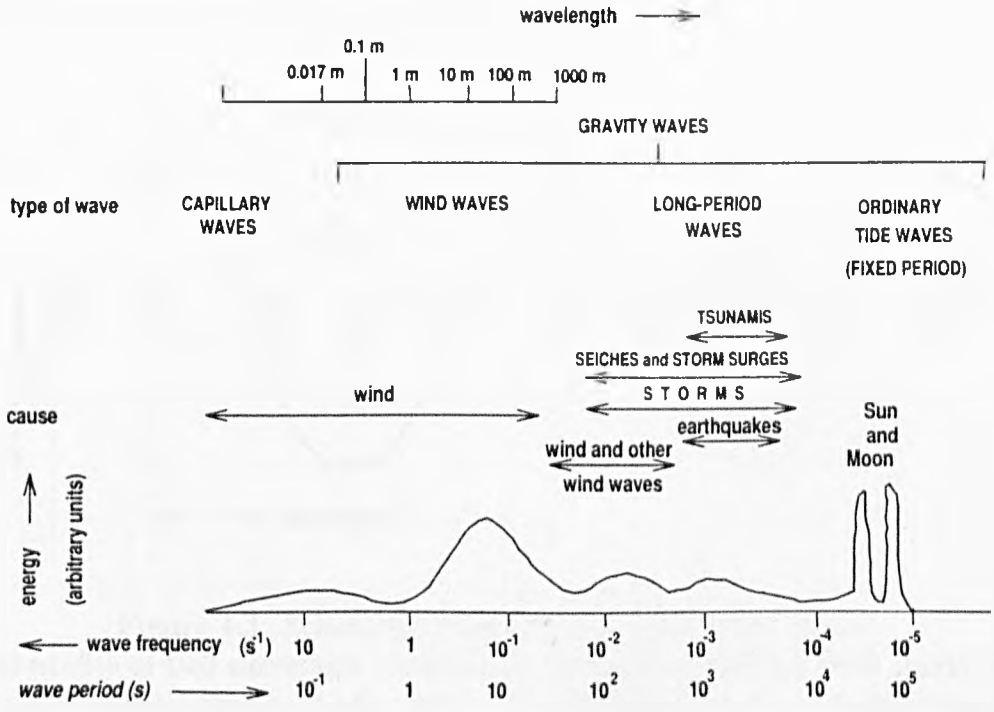

Figure 4.2: Type of Surface Waves.
Here are shown the relationship between wavelength, wave frequency, the nature of the displacing forces, and the relative amounts of energy in each type of wave. Modified from Brown *et al.* (1997, p.10) and Horikawa (1978, p.6).

tional attraction of the sun and the moon are known as "tidal waves" or simply as "tides". "Blowing over the surface of the world ocean, [wind] transfers energy to the water which is manifested as a series of more or less regular crests which develop in lines normal to the wind and travel along the wind direction" (Hardisty, 1990b, p.1). Waves that are generated and developed by such wind action are known as "wind waves". Waves of greatest energy concentration are wind waves and their wave period is normally less than ten to fifteen seconds, while heights of as much as 34 metres have been reported (Horikawa, 1978, p.7). Details of terms such as

Tsunamis and the above schematic diagram of ocean surface waves can be found in, for example, Brown *et al.* (1997, p.10) and Hardisty (1990a, p.49).

There are four important parameters defining a wave: wavelength, wave period, wave height and wave celerity (Hardisty, 1990b), as shown in the schematic diagram of an idealised ocean wave (Figure 4.3) below (Brown *et al.*, 1997).

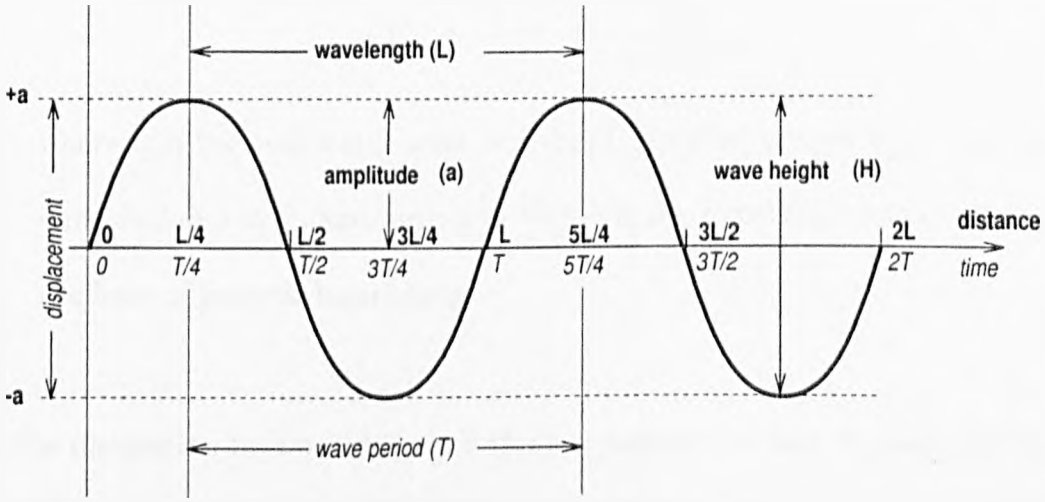

Figure 4.3: Schematic Diagram of An Idealised Wave.
Vertical profile of two successive idealised ocean waves, showing their linear dimensions and sinusoidal shape. It also shows the displacement of an idealised wave at a fixed point, plotted against time. Modified from Brown *et al.* (1997, pp.7,10).

- The **wavelength** L is defined as the horizontal distance between successive crests and has unit metre (m).

- The **wave period** T is defined as the time interval between the occurrence of successive crests at a fixed point and has unit second (s).

- The **wave height** H is defined as the vertical distance between the crest and the trough, which is twice the wave **amplitude** (a), and has unit m.

- The **wave celerity** C is defined as the horizontal distance traversed by the wave crest in one second in a direction normal to the crest line. Such lines

define the path of the wave and are called **wave orthogonal**. The velocity of the wave form is:

$$C = \frac{L}{T}. \tag{4.1}$$

The wave celerity has units m/s and is often referred to as the **wave phase celerity** in order to distinguish it from the **wave group celerity,** C_g,

$$C_g = \frac{1}{2}(1 + \frac{2kh}{sinh(2kh)}), \tag{4.2}$$

where h is the still water level, $k = 2\pi/L$ is called the wave number and has units $radians\ m^{-1}$, and $sinh\ x = \frac{e^x - e^{-x}}{2}$ is the hyperbolic function where e is the base of natural logarithms.

The distinction between deep and shallow waters is in fact "a matter of degree" as Kosko (1993) describes many phenomena. However, some conventions are introduced to describe the water depths. Wavelength with regard to wave period defined by Airy's first order wave theory is as follows (Airy, 1845),

$$L = \frac{gT^2}{2\pi}\ tanh\ (\frac{2\pi h}{L}), \tag{4.3}$$

where $g = 9.81\ m/s^2$ is the gravitational acceleration, h is the still water level, and $tanh\ x = \frac{e^x - e^{-x}}{e^x + e^{-x}}$ is the hyperbolic tangent function. In deep water, $tanh(2\pi h/L)$ approximates to 1. That is, the wavelength in deep water, L_∞, using SI [1] units, becomes

$$L_\infty = \frac{gT^2}{2\pi} = 1.56\ T^2. \tag{4.4}$$

Deep water is defined as $h > L_\infty/4$. Referring to the same hyperbolic function again, in shallow water $tanh(2\pi h/L)$ approximates to $2\pi h/L$, so that, wavelength

[1] SI is a system of metric units (Sinclair, 1994).

in shallow water where water depth is defined as $h < L/20$ becomes,

$$L = T\sqrt{gh}. \tag{4.5}$$

This approximation again applies to within 5% in water depth for which $h < L/20$. The general expression must be used for water in intermediate depths.

In the deep water of the world's oceans, the wave form can travel almost unchanged for very great distances, because there is negligible energy loss as the wave moves forward. Once the wave enters shallower waters, however, the wave is slowed down. Therefore, the wavelength reduces because the wave period remains constant. As a consequence of this foreshortening, the potential energy is squeezed into a shorter distance and there is therefore a corresponding increase in the wave height, until eventually the wave over-steepens and breaks onto the shoreline. These changes are known as **shoaling wave transformations** (Hardisty, 1990b).

The increase in wave height and decrease in wavelength which are predicted by, for example, the first order wave theory have been found to account for the main changes in wave profile (Airy, 1845). Additionally, however, a number of processes which can increase or decrease the wave height are listed below, together with selected references wherein further details can be found (Hardisty, 1990b):

- **Friction.** Sea bed frictional drag reduces the wave height (Nielson, 1982).
- **Percolation.** Wave induced currents within a permeable sea bed which can consume wave energy, and reduce the wave height (Sleath, 1985).
- **Refraction.** Changes in the wave direction during shoaling are known as wave refraction, and converging wave orthogonal will result in wave height increases,

whilst diverging wave orthogonal will result in wave height decreases (Wiegel, 1964).

- **Reflection.** Wave energy is continuously being reflected by the sea bed during the shoaling process and this will steadily reduce the wave height (USACE, 1984).

- **Breaking.** A substantial amount of energy is dissipated in noise and turbulence when the wave finally over-steepens and breaks onto the shoreline (Dyer, 1986).

4.1.2 A Brief History of Wave Recording

Visual observations are the simplest and cheapest method of measuring wave heights and period. However, "observers, particularly in small craft, consistently overestimate wave heights, by a degree which unfortunately varies considerably, and it is better to compare the wave profile with a graduated pole" (Hardisty, 1990b, p.17). Interest and importance in wave research increased rapidly in connection with the amphibious military exercises during the Second World War and resulted in a range of instruments. Some instruments are described by Klebba (1945) for the Woods Hole Oceanographic Institution and Deacon (1946) for the British Admiralty Research Laboratories. The techniques currently available include surface measurements in both deep and shallow water, from above the surface in all water depths, and from below the surface in shallow water.

Ewing (1980) made a review of the developments in the use of wave recording buoys to measure the wave direction in deep water, but all these techniques were

found of little use in coastal geomorphology (Hardisty, 1990b). Possibly the earliest device for measuring the wave surface in shallow water, which received widespread use, was the spark-plug wave recorder. A series of spark plugs, each fixed with the electrode horizontal, was placed with the electrodes a few inches apart in a vertical line, with the idea that as the sea water moved up and down it would short out those plugs which were under water and so yield a wave record (Koontz & Inman, 1967). The signals are usually cabled to a suitable chart recorder or data logger. Williams (1969) gives details of construction, circuit design and calibration of the type of gauge. All these instruments are, however, handicapped by the difficulties connected with the film of water left on the sensor when the water level drops.

Attempts have been made to obtain the wave measurements from above the surface, for example, the recording altimeter, used from flying aircraft; laser instruments, designed originally for precision distance measuring in surveying; using high frequency radio signals to measure sea conditions from space. However, they are "prohibitively expensive if extended records are required" (Hardisty, 1990b).

One of the methods of obtaining wave records from a sea bed instrument is to use an inverted echo-sounder and record the changing distance between it and the water surface. The beam must be fairly narrow and the water depth must be fairly shallow, so that when a crest is over the recorder, a reflection does not come back from the sloping part of water surface (Hardisty, 1990b).

In shallow water most routine wave data collection has been made by transducers mounted on the sea bed. Such devices are inappropriate farther offshore because the pressure effects due to surface waves are attenuated with depth at a rate which

varies with the wave frequency. For this reason the short period waves are filtered out of the record in deep water. A four-second wave, for example, loses more than 90% of its pressure effect at the sea bed in water which is more than 10 metres deep. Hardisty (1990b) concluded that "notwithstanding this problem the vast majority of sea wave recordings have been obtained with pressure transducers." Surface waves induce pressure fluctuations in the entire column of water between the surface and the sea bed. For any given depth of water and wave height the amplitude of these fluctuations depends on the wave period, such that waves of very short period are quickly attenuated. The pressure fluctuations at the bottom are measured by an underwater unit of an electronic transducer. The transducer converts the pressure to an electronic signal which is cabled ashore. A grid of transducers is used to detect the wave direction.

4.1.3 The Use of Pressure Transducers

Although a controversy exists over the adequacy of translating sea bed pressure data to surface wave heights, there is now considerable information affirming that linear wave theory is adequate to compensate pressure data (Esteva & Harris, 1970; Grace, 1978; Forristall, 1982), and that pressure data give reliable estimates of surface wave heights to within five per cent (Bishop & Donelan, 1987). Carson *et al.* (1975) quoted several methods of "avoiding" the dynamic effects of a current while measuring tide by pressure transducers. "Improvements" have been found, for example, in Cavaleri (1980). Grace (1978) concluded that the Gaussian random process model provided a theoretical surface spectrum that corresponded closely to that measured over a reasonable frequency band. His tests were conducted off Hon-

olulu, Hawaii, in 11.3 metres of water and in the Oregon State University, U.S.A., in 2.9 metres and 3.5 metres of water.

However, the linear wave theory was found to be adequate to describe the actual data measured by submerging the pressure transducer in 4.7 metres of water at mean low tide (Esteva & Harris, 1970), in water 11.3 metres deep (Grace, 1978), and even in water 20.7 metres deep (Forristall, 1982), respectively. Laboratory tests (Bishop & Donelan, 1987) conducted to measure wave heights with a capacitance probe as well as pressure transducer in water depths of 90 centimetres and 120 centimetres confirmed that the transducer is adequate to measure the water surface height.

It is relevant to note that continuous measurements are required for environmental monitoring. Hardisty (1993, p.856) concluded that in many geomorphological process applications, two Hz is a reasonable sampling frequency. Although such sampling frequency is reasonable in many geomorphological process applications, this chapter intends to apply it to the geomorphological form study.

4.2 Real Wave Data

Wave profiles were measured by Hardisty & Drumm (1993) in 1992, deploying pressure transducers on the beach of Teignmouth in England. The calibration of the electronic signals was performed on land by computers to obtain the wave profile data. Although there were several days of measurements, the complete data collected in the afternoon of 16th May 1992 were used.

4.2.1 Field Site

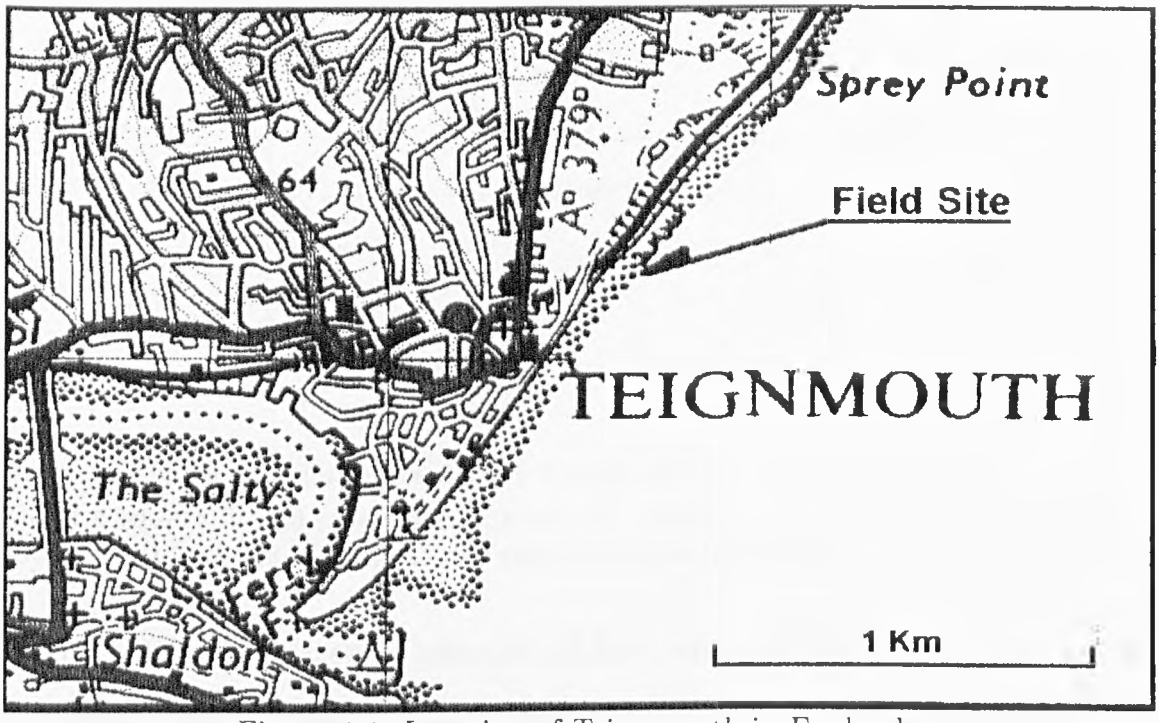

Figure 4.4: Location of Teignmouth in England.

The experiment was carried out by Hardisty & Drumm (1993) at the beach of Teignmouth in England (Figure 4.4). Teignmouth is located at 50°32′40″N/3°29′30″W in the global grid reference system, or *SX* 942 728 in the British National grid reference system by the Ordnance Survey (OS, 1992). The mean spring tidal range at Teignmouth, on the south Devon coast facing the English Channel, is 4.1 metres, whereas, compared with that on the northern Devon coast, which faces the Bristol Channel, it ranges from 7.3 metres at Appledore to 10.3 metres at Watchat (Carr, 1988, p.25). Refer to Appendix G for a brief introduction to Devon.

4.2.2 Data Collection

The data were part of the measurements collected by the third of the three deployments sponsored by the Natural Environmental Research Council (Hardisty &

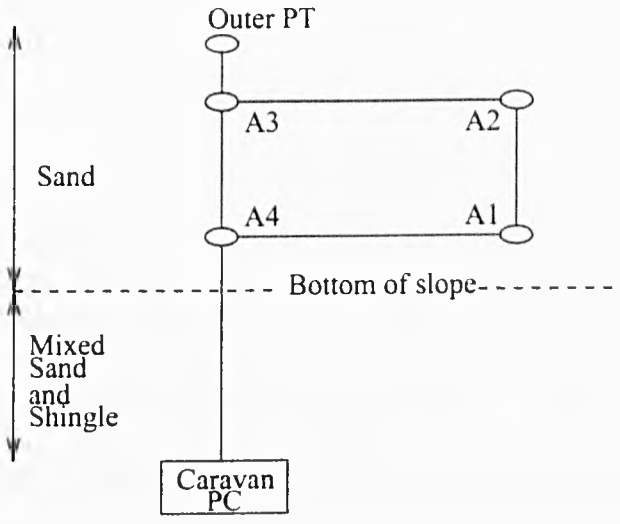

Figure 4.5: The Flux Square Design of Studying Ocean Waves.
The flux square design consisted of pressure transducers and other instruments deployed at A1, A2, A3, A4 and Outer rigs. Modified from Hardisty & Drumm (1993).

Drumm, 1993) and aimed to measure offshore and longshore current speeds, the concentration of the sand in suspension at various heights above the beach surface, and the surface wave profiles. The first two were deployed at Llangenith in West Wales in 1990 and at Spurn Head in East Yorkshire in 1991 and the third was deployed at Teignmouth in Devon in 1992. The deployment consisted of four frames on the inter-tidal beach profile, where the frames were deployed at the corners of a "flux square" (Hardisty & Drumm, 1993) as shown in Figure 4.5. Pressure transducers and other instruments were deployed at each rig (A1 to A4 and Outer), which were all cable-linked to a shore-based power supply, filters and PC logger. Although this flux square was designed with multiple purposes in mind, this study is concerned only with a single wave profile. Therefore, the data measured by the pressure transducer at Outer rig were used.

Signals from sensors were converted, calibrated and logged on microcomputers. The wave recorder and data analysis system used in this study were developed by the Marine Morphodynamics Unit (MMU) at London University, which has now

transferred to the School of Geography & Earth Resources at the University of Hull. The sensing element consists of the LX1601GB gauge type pressure transducer and signal conditioner manufactured by Sensym in the United States and is available from Farnell's in the United Kingdom. The transducer is internally temperature compensated and has an output offset of 7.5 volts (V) with a sensitivity of one volt per PSI[2]. It means that 0.7 metre of water produces a signal of $1V$, providing a very good signal to noise ratio (Hardisty, 1990b, p.26). Only one of these sensors is required for a single wave recorder, but two identical units must be assembled for the directional instrument (Hardisty & Drumm, 1993).

The response of the transducers has been found to be remarkably linear; nevertheless a calibration exercise is useful (Hardisty, 1990b). By lowering the sensor into still water a relationship such as,

$$V_{subm} = (V_{output} - V_{air}) * C_1 * depth, \tag{4.6}$$

can be determined, where V_{subm} is the voltage reading when submerged to a $depth$, V_{output} is the actual signal voltage reading from the transducer, V_{air} is the voltage reading in air, and C_1 is the gradient of the line. According to the manufacturer's specification, V_{air} should be about 30000 volts and C_1 should be about 4000 $metre^{-1}$ (Hardisty, 1990b, p.36).

Raw data were obtained through filtering and smoothing of these signal readings. The signal readings from the transducers were averaged over 0.25-second intervals, and the highest crest and lowest trough were monitored, along with counting the crests and zero crossings over the timed ten-minute interval. The sum of the maxi-

[2] PSI stands for pounds per square inch.

mum crest and trough values were then calculated.

Voltages in raw data were converted to *depth* using proprietary HSDC V.2 (High Speed Data Collection) software (Hardisty & Drumm, 1993). These data were then calibrated using arrays of known instrument sensitivities and instrument offsets. A linear calibration, $y = mx + c$, was performed for each measurement,

$$depth = (V_{subm} * gradient) + offset, \tag{4.7}$$

where the *depth* and the *offset* have the units of m and the *gradient* is derived from *voltage-depth* plot. The depths were then used to construct the wave profile.

The whole sea wave profile consists of many records; and each record was measured at $2Hz$ for 17.07 minutes, totalling 2048 data points per record. The relatively short length was chosen in order to obtain stationary spectral estimates (Hardisty & Drumm, 1993). The full tidal cycle needs around thirty records to cover, depending on the tides and the position of the pressure transducers relative to tide-lines. On the day of measurement, twenty-seven records were obtained, producing a total of 55296 (2048×27) data points for the wave profile. The process that generates the synthetic waves must comply with those numbers, as described below.

4.3 Synthetic Waves

The tidal theory usually starts with the equilibrium tide over the Earth's surface, which contains a constant term for the particular latitude and declination, a diurnal and a semi-diurnal term (Wood, 1969, pp.7-8). Each term of a tidal harmonic analysis may be expressed in the form $A\cos(\omega t - P)$ where A represents amplitude,

ω the angular velocity, t is time, and P the phase lag. As a result, a wave is generally modelled as compound sinusoidal curves (Baldock & Bridgeman, 1981, Ch.1). The simplest form of a wave is a sine wave, $\eta(t) = sin(t)$, where η is height and t is time. A natural wave is typically modelled as a composition of several component sinusoidal waves. See details below and computer programmes in Appendix H.

4.3.1 The Equation

A wave profile can usually be approximated by the following equation, with four component *waves* and an *offset*,

$$\begin{aligned} \eta(t) &= A_1\ sin(\omega_1\ t + P_1) \\ &+ A_2\ sin(\omega_2\ t + P_2) \\ &+ A_3\ sin(\omega_3\ t + P_3) \\ &+ A_4\ sin(\omega_4\ t + P_4) \\ &+ \mathit{offset}, \end{aligned} \tag{4.8}$$

where A is the *amplitude* of waves in *metres*, ω is the *first angular velocity* in *radian*$^{-1}$, t is time in *seconds*, P is the *phase lag* in *radians*, and *offset* is the depth of wave in *metres* that compensates for the possible negative added-up wave heights. The first angular velocity is a function of *period*, T, that is, $\omega = 2\pi/T$; whereas phase lag can be expressed as $P = 2\pi\ lag/T$, where *lag* is the lag time in *seconds*.

The above equation can include any number of waves; however, four waves are proposed. Although some component waves are optional, it is essential to include the tidal wave, for example, *Wave4* with A_4, ω_4 and P_4 in Equation 4.8, which models the natural tidal cycle.

4.3.2 Parameters

Wave	A (m)	T (s)	lag (s)
Wave1	1.0	10	0.0
Wave2	0.5	11	0.1
Wave3	0.25	21	0.2
Wave4	2.0	27648	20736
Offset	4.0		

Table 4.1: Parameters for Generating a Synthetic Wave Profile.
There are three component waves and a tidal wave (*Wave4*). Amplitudes, A, are given in metres, m, while periods (T) and lag time (lag) are indicated in seconds (s). The *offset* cancels out the possible negative heights.

The parameters used to run this synthetic wave model are given in Table 4.1, where A is the *amplitude*, T is the period used to derive the first angular velocity (ω), and lag is the lag time used to derive the phase lag. The first three wave periods can be selected, for example, from either empirical records (Russell & Macmillan, 1952; Horikawa, 1978) or theoretical calculations (Hardisty, 1990a). The amplitude of the tidal wave is set to two metres, relatively smaller than the mean spring tidal range of 4.1 metres (Carr, 1988). Although the principal lunar tidal component repeats itself in a 12.42-hour cycle as described in Table 2.2 and Brown *et al.* (1989, p.57), the synthetic wave profile is modelled according to the actual tidal period in around eight hours, that is, $55296/2Hz = 27648\ seconds = 7.68\ hr$. The lag time for the tidal wave is set at its third quarter of tidal cycle, when the tide is at its lowest level; however, the modelling continues for the full tidal period.

4.3.3 Implementation

Stages of implementing the above equation are introduced as follows, where the corresponding computer programme is given in Appendix H. First of all, the computer

programme needs to calculate the tidal period for the modelling, from the "user-defined" information, for example, numbers of output columns and rows, sampling rate, and the offset. The production of row and column numbers gives the length of the profile; and, when divided by the sampling rate, the "tidal period" is obtained. This tidal period is not necessarily equal to the real one, although the whole wave profile is still maintained (see Figure 4.6).

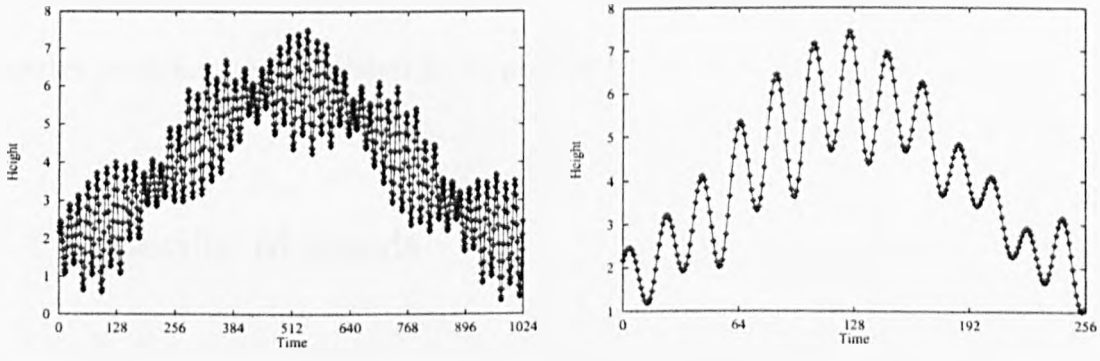

Figure 4.6: Wave Profiles Generated by Various Tidal Periods.
Although the tidal periods may be different, the whole wave profile is maintained.

The second stage is to calculate the first angular velocity, ω, and the phase lag, P, from the wave parameters supplied in Table 4.1. The periods and lags in time units are intrinsic, but the trigonometry calculation demands radian units. Therefore, all those time units are translated into radian units, as described in Section 4.3.1.

The third stage is to sum up the component waves in Equation 4.8. It results in a long list of wave heights against time, which has to be re-organised to comply with the data format needed. In other words, the long list is split into twenty-seven records; and each record contains 2048 data points. Further analyses described in Chapter Three and subsequently can then be applied.

4.4 Analyses

Conventional time series analyses are applied to the sea wave profiles, followed by the fractal and statistical methods described in Chapter Three. Details of the conventional methods are given in this section, including the qualitative approach of the phase portrait reconstructions, and the quantitative approach utilising the spectral methods of the power spectra and auto-correlation coefficients. The corresponding computer programmes are listed in Appendix I.

4.4.1 Specific Methods

A wave profile is an example of time series. A time series is a sequence of measurements x which could be represented in continuous or theoretical function as $x(t)$ where t is the time or, in discrete or sampled function, as $x_i = (x_1, x_2, \cdots, x_N)$ where N is the total number of samples. The discrete function is related to the continuous function as $x_i = x(i\Delta t)$, where Δt is the increment.

The wave profile is continuous in nature. However, the data that represent a wave profile are discrete in reality, because the obtaining of data involves application of the sampling process which discretise the continuous wave profile. Although data used in this study are discrete, methods of analysis are derived for both continuous and discrete data.

Qualitative and quantitative characteristics of a time series can be studied by phase portrait reconstruction and spectral analysis, respectively. The qualitative characteristics of a time series can be revealed by the construction of phase portrait

reconstruction. A phase space is the space where values of variables at a specific time of evolution in a system can be represented by a single point. Sometimes, it is easier to think of phase space as containing all the degrees of freedom of a particular system (Darbyshire & Price, 1991). The technique of phase portrait reconstruction is to reveal the system dynamic in a pseudo-phase space from a single time series measurement (Mullin, 1993b, p.27). The method of optimal delay time is introduced first, followed by the method of singular value decomposition (SVD). Phase portrait reconstruction usually demands a long time series. Therefore, separate records of data are joined together to construct the phase portrait.

The quantitative approach is the power spectrum and its Fourier transformation pair the autocorrelation function (Mullin, 1993b, p.25). The spectrum gives a measure of the amount of power in a given frequency band over a selected frequency range. The autocorrelation function for a periodic signal is itself periodic. This is particularly so when there is a high harmonic content in the signal. Therefore, it provides a useful complementary representation of the data.

The Qualitative Approach: Phase Portrait Reconstructions

The theoretical phase portraits consist of plots of each variable *versus* their derivatives (Mullin, 1993a). Although it is in principle possible to carry out the procedure with experimental data, problems will arise in practice as a result of the presence of noise on the finitely sampled data (Mullin, 1993b, p.32). Therefore, the method of delays, which was first proposed by Packard *et al.* (1980), is a simple and practical alternative to experimental data.

The Method of Optimal Delay Times

The basic idea of the optimal delay time approach is to request an optimal utilisation of the embedding space in order to maximise the distance between trajectories to avoid ambiguity, whereas the original delay time method suffers from the instrumental resolution, the number of data points and the environmental noise (Buzug *et al.*, 1990). The current methods to find the embedding parameters make use of, for example, the autocorrelation function (Schuster, 1988), the mutual information (Fraeser & Swinney, 1986), the generalised correlation integral (Liebert & Schuster, 1989), and trajectory matrices (Broomhead & King, 1986). These mathematical procedures may yield very different values of the delay time, and are often sensitive to noise computing time because of complex sorting or searching procedures. Being aware of their limitations, Buzug *et al.* (1990) developed a method to obtain the best delay time for the reconstruction of the chaotic attractors in phase space. Their method of finding the best delay time and an estimation of the embedding dimension is purely geometrical. The choice of the delay time will not alter the topology of the attractor, although the topology could become completely obscured (Mullin, 1993b, p.32).

The algorithm proposed by Buzug *et al.* (1990) uses the maximisation of the averaged parallelepipeds which are defined by points of the reconstructed attractor. According to Takens' (1981) theorem one can reconstruct the attractor in phase space from a scalar time series $\{\xi(t_k)\}$, where integer $k \in K$ and $K < N$. ξ is the observable and N is the number of data points. Then the state vectors in the

E-dimensional embedding space are, given by Buzug *et al.* (1990),

$$x(t_s) = \begin{bmatrix} \xi(t_s) \\ \xi(t_s + \tau) \\ \xi(t_s + \tau(E - s)) \end{bmatrix}, \tag{4.9}$$

where $t_s = s \cdot T_s$ and $s \in S$, for integral $S = \{0 < s < N - \tau/T_s(E-1)\}$, where τ is the delay time, and with the sampling time T_s.

After the reconstruction of the attractor with state vectors above, one has to choose $(E+1)$ arbitrary indices r_m from the set $S : \{r_m \in S; m = 0, ..., E\}$. Each r_m represents a corner of a parallelepiped. To calculate the vectors spanning the parallelepiped, one may choose r_0 as a reference point. The volume of this parallelepiped, $V_{E,r_0(\tau)}$, is defined by,

$$V_{E,r_0}(\tau) = |\det(M_{E,r_0}(\tau))|, \tag{4.10}$$

where the $(E \times E)$-matrix is defined by the displacement vectors d_n, i.e.,

$$M_{E,r_0}(\tau) = (d_1, ..., d_E), \tag{4.11}$$

and

$$d_n(t_{r_0}) := \begin{bmatrix} \xi(t_{r_0}) - \xi(t_{r_n}) \\ \xi(t_{r_0} + \tau) - \xi(t_{r_n} + \tau) \\ \vdots \\ \xi(t_{r_0} + \tau(E-1)) - \xi(t_{r_n} + \tau(E-1)) \end{bmatrix}, \tag{4.12}$$

where $n = 1, ..., E$. The determinant is calculated using NAG Fortran routine *g03aaf* (Hann & Hounam, 1991).

The measure of the attractor volume, $F_E(\tau)$, is defined, given the volume of the j-th parallelepiped $V_{E,\, r_0(j)}(\tau)$, with j from 1 to a sufficiently large number (N_v) of parallelepipeds,

$$F_E(\tau) = \frac{\frac{1}{N}\sum_{j=1}^{N_v} V_{E,\, r_0(j)}(\tau)}{(\max_{k \in K}\{\xi(t_k)\} - \min_{k \in K}\{\xi(t_k)\})^E}. \tag{4.13}$$

It is convenient to use the logarithm of the above equation, because $F_E(\tau)$ decreases with the power of E when the embedding dimension is increased,

$$f_E(\tau) = \log(F_E(\tau)). \tag{4.14}$$

The maximum of $f_E(\tau)$ in the interval $0 < \tau < 0.5T_c$ provides the best choice of the delay time τ, where T_c is the characteristic recurrence time of the system. Researchers (Buzug *et al.*, 1990, for example) have suggested that one uses the smallest delay time where the $f_E(\tau)$ has its first maximum, for at larger delays coordinates might be uncorrelated in high embedding dimensions. By computing the values of $f_E(\tau)$ with increasing embedding dimension, one recognises the qualitative structure of the attractor. The structure is spaced equidistantly in the logarithmic plot, which means that $f_E(\tau)$ decreases by a constant factor with increasing embedding dimension (Buzug *et al.*, 1990). This effect could be used to estimate the sufficiently large embedding dimension, because no new information of the intrinsic structure of the attractor can be obtained by adding another dimension.

To calculate $f_E(\tau)$, N_v is set to 10% of the number of data points and the initial dimension of $E = 9$. Both are assumed to be large enough to accommodate the system dynamics. After having identified the optimal $f_E(\tau)$ and its related τ, the phase portrait of the attractor can be reconstructed.

Singular Value Decomposition (SVD)

The technique of singular value decomposition was proposed as an alternative of choosing the delay time by Broomhead & King (1986). However, Mullin (1993b) pointed out that it is not possible to construct a meaningful phase portrait from a time series which contains no low-dimensional dynamic structure, even with the

technique of singular value decomposition.

The main practical problem with the standard method of delay is that the phase portrait reconstruction is carried out by projecting the time series onto an arbitrary basis. Thus, no systematic account is taken of the information content of the signal in the reconstruction process, nor are the effects of finite sampling and experimental noise in the time series catered for. The technique of singular value decomposition was proposed as a solution to these difficulties by Broomhead & King (1986). It is used to calculate an optimal basis for the projection of the attractor which is reconstructed from the time series. In addition, the technique was developed to deal with noise and is therefore suited to experimental data.

The object of the singular value decomposition technique is to find the unit vectors which are optimally aligned with the position vectors of the trajectory matrix X. These unit vectors will form the coordinate system onto which the time series will be projected in the phase portrait reconstruction. One may think of this technique as finding the principal moments of an "object" which in this case is the attractor. That is, it is a method of extracting the optimum projection of the phase portrait from the data.

Procedure of SVD

The procedure of the singular value decomposition method is carried out as follows. First of all, a trajectory matrix X is formed, whose rows contain the n-dimensional vectors with the delay time set equal to τ, (sample time). In practice, n is set large enough to capture the lowest frequency component in the signal and n can be selected using the autocorrelation function. This is referred to as the window

length of the trajectory matrix. Each successive row in the matrix is then given by sequential data windows.

The process involves diagonalisation of the covariance matrix $X^T X$ to obtain the set of eigenvectors which are the orthogonal singular vectors. The square roots of the corresponding eigenvalues give the singular values. Thus the singular vectors give the directions for the coordinate axes and the corresponding singular values give the weightings for each. The phase portrait is constructed on this coordinate system and each point on the trajectory is a weighted version of the sampled point in the time series (Mullin, 1993b).

Noise will be present in all the singular values and will appear in the singular value spectrum as a flat noise floor at its upper end. The significant singular values will appear above the noise floor and their numbers give an upper limit on the embedding dimension of the attractor. Thus, this is a way of distinguishing the deterministic part of the signal from the noise. It should be noted that this process does not give the dimension of the attractor directly. However, the scaling of the singular values can be used to give an estimate of the local dimension of an attractor (Broomhead & Jones, 1989).

When using the singular value decomposition technique, its singular spectrum is plotted on a logarithmic scale. If the presence of three significant singular values is seen, for example, it suggests that it is justifiable to plot the phase portrait in three dimensions (Mullin, 1993b).

Some of the limitations of the singular value decomposition techniques were pointed out by Mullin (1993b). For example, it is not possible to construct a

meaningful phase portrait from a time series which contains no low-dimensional dynamical structure. While this may appear to be stating the obvious, he emphasised that these techniques are not filtering processes which in some way reduce the data to a finite-dimensional form. For example, in a phase portrait reconstructed from a time series measured in a distorted fluid flow using the singular value decomposition technique, it was shown that there was no obvious form associated with this phase portrait and the fluid flow motion explores a high-dimensional state space (Mullin, 1993b).

Implementation

The procedure is carried out as follows. First of all, one has to form a trajectory matrix A whose rows contain the E-dimensional vectors used in the method of delays with the delay time set equal to the sampling time T_s. In practice, a large E (512) is arbitrarily set to capture the lowest frequency component in the signal, though E can be selected using the autocorrelation function (Mullin, 1993b, p.34).

The m by n matrix A is factorised as

$$A = QDP^T, \tag{4.15}$$

where

$$\begin{cases} D = \begin{pmatrix} S \\ 0 \end{pmatrix}, & if\ m > n \\ D = S, & if\ m = n \\ D = (S\ 0), & if\ m < n \end{cases} \tag{4.16}$$

where Q is an m by m orthogonal matrix, P is an n by n orthogonal matrix and S is a $\min(m,n)$ by $\min(m,n)$ diagonal matrix with non-negative diagonal elements, $sv_1, sv_2, ..., sv_{\min(m,n)}$, ordered such that $sv_1 \geq sv_2 \geq ... \geq sv_{\min(m,n)} \geq 0$. The first $\min(m,n)$ columns of Q are the left-hand singular vectors of A, the diagonal

elements of S are the singular values of A, and the first $\min(m, n)$ columns of P are the right-hand singular vectors of A.

The routine obtains the singular value decomposition by first reducing A to upper triangular form by means of Householder transformations, from the left when $m \geq n$ and from the right when $m < n$. The upper triangular form is then reduced to bidiagonal form by Givens plane rotations and finally the QR algorithm is used to obtain the singular value decomposition of the bidiagonal form. Refer to $f02wef$ of NAG Fortran Routine (Hann & Hounam, 1991) for details.

This routine produces not only singular values but also singular vectors. Once the vectors are obtained, the phase portrait can be constructed.

The Poincaré Sectioning

An extremely useful way of extracting the vital qualitative characteristics of a phase portrait is to construct its Poincaré map. This can be formed by either stroboscopically sampling the time series at a particular point in a cycle or by forming the intersection of the reconstructed phase portrait with a plane. Consequently, the Poincaré section (map) is used to reduce the dimension of the phase portrait in a meaningful way.

The Poincaré map can be alternatively constructed without using the phase portrait by stroboscopically sampling the data. This is particularly useful for periodically driven systems where the sample point can be set at a particular phase angle of the drive frequency. An example of such a system is provided by the parametrically excited pendulum where a fixed phase in the sinusoidal drive cycle can

be used as the reference (Mullin, 1993b).

The Quantitative Approach: the Spectral Analysis

The most common and useful way of quantifying a time series using linear signal processing techniques is to construct the power spectrum and its Fourier transformation pair, the autocorrelation function. The fundamental assumption of these techniques is that the stationary signal can be decomposed into a series of sines and cosines. The spectrum gives a measure of the amount of power in a given frequency band over a selected frequency range. Example uses of it are given by Mullin (1993b, p.25). If it consists of discrete lines, then the time series is periodic and the spectrum can be used to obtain estimates of the relative power in each frequency component of the time series. On the other hand, irregular, chaotic, and random time series all have continuous lines in their spectra, indicating that the power is spread over a range of frequencies. Therefore, spectral analysis can be used to investigate the transition between discrete and continuous cases, as the controlled parameters in an experiment are varied.

Power Spectra

There are four principal forms of Fourier transformation, each of which has its own variations (Otnes & Enochson, 1972, p.10), see Table 4.2. The differences between the four basic forms are due to the fact that different ranges and domains are employed. In 1965, high speed algorithms that reduce the computational times, the so-called fast Fourier transformation, were developed (Cooley & Tukey, 1965).

The relatively short length of 2048 data points was chosen because it enables

	$X(f)$ or X_k	f or $k\Delta f$	$x(t)$ or x_i	t or $i\Delta t$
I	$\oplus \int_{-\infty}^{\infty} x(t)e^{-j2\pi ft}dt$	$-\infty \leq f \leq \infty$	$\ominus \int_{-\infty}^{\infty} X(f)e^{j2\pi tf}df$	$-\infty \leq t \leq \infty$
II	$\overset{\oplus}{\otimes} \sum_{-\infty}^{\infty} x_i e^{-j\pi i\Delta tf}\Delta t$	$\frac{-1}{2\Delta t} \leq f \leq \frac{1}{2\Delta t}$	$\ominus \int_{\frac{-1}{2\Delta t}}^{\frac{1}{2\Delta t}} X(f)e^{j2\pi fi\Delta t}df$	$-\infty \leq i \leq \infty$
III	$\overset{\ominus}{\otimes} \sum_{i=1}^{N} x_i e^{-j\frac{2\pi ik}{N}}\Delta t$	$0 \leq k \leq N-1$	$\overset{\ominus}{\otimes} \sum_{k=0}^{N-1} X_K e^{j\frac{2\pi ik}{N}}$	$0 \leq i \leq N-1$
IV	$\ominus \int_0^T x(t)e^{-j2\pi tk\Delta f}dt$	$-\infty \leq k \leq \infty$	$\overset{\oplus}{\otimes} \sum_{-\infty}^{\infty} X_k e^{j2\pi k\Delta ft}$	$0 \leq t \leq T$

Table 4.2: Four Basic Forms of Fourier Transformation.
The continuous, discrete and repetitive functions are indicated by $\oplus$, $\ominus$ and $\otimes$, respectively. Modified from Otnes & Enochson (1972), p.10.

the calculation of stationary spectral estimates (Hardisty & Drumm, 1993, p.856). However, it may be necessary to use a trend line to de-mean the signal over such a record length, for otherwise the result can become contaminated by low frequency noise (Clifford, 1993). The record length was carefully chosen (Section 4.2.2) since the modern technique for spectral analysis requires the number of samples to be a power of two in order to reduce the number of computations.

The profile was decomposed into time- and frequency-domain utilising the Fourier transformation, which is one of two principal techniques for the analysis of a time series, the other being the autocorrelation technique. Imagine that the time series, for example, a single record in this case, was plotted in three-dimensional space with coordinates of *amplitude*, *frequency* and *time*. We can visualise the time series in the time-domain, i.e., by generating a heights-time plot, if we look into the time series from the *frequency* coordinate. Similarly, we can obtain the height-frequency plot in the frequency-domain by looking at it from the *time* coordinate. This is a basic technique for understanding the spectral analysis of a time series by visualising it in three-dimensional space (Hardisty, 1993).

A time series can be prescribed either in the physical domain as $x(t)$ or in the frequency domain in terms of the amplitude $X(f)$ where f is the frequency. The quantity $X(f)$ is generally a complex number indicating the phase of the signal. The amplitude in the frequency domain, $X(f)$, is obtained using the Fourier transform of $x(t)$ in the interval $0 < t < T$; it is given by,

$$X(f) = \int_0^T x(t)\, e^{-2\pi j f t} dt, \tag{4.17}$$

where $j = \sqrt{-1}$. The complementary equation relating $x(t)$ to $X(f)$ is the inverse Fourier transform,

$$x(t) = \int_{-\infty}^{\infty} X(f)\, e^{2\pi i f t} df. \tag{4.18}$$

The quantity $|X(f)|^2 df$ is the contributions to the total energy of $x(t)$ from those components with frequencies between f and $f + df$. The vertical bars in $|X|$ refer to the absolute value of the complex quantity. The power is obtained by dividing by T. The power spectral density of $x(t)$ is defined by,

$$S(f) = \frac{1}{T} |X(f)|^2, \tag{4.19}$$

in the limit $T \to \infty$. The product $S(f)df$ is the power in the time series associated with the frequency range between f and $f + df$.

Implementation

The NAG Fortran routine numbered $g13cbf$ is used to calculate the sample spectrum of the time series using spectral smoothing by the trapezium frequency (Daniel) window (Hann & Hounam, 1991). The supplied time series is tapered and smoothed, by mean or trend correction (by least-squares), as well as not smoothed. The logged as well as unlogged spectral estimates are obtained, too.

The tapering factor is those of the split cosine bell:

$$\begin{cases} \frac{1}{2}\left(1-\cos\left(\frac{\pi(t-\frac{1}{2})}{T}\right)\right), & 1 \le t \le T \\ \frac{1}{2}\left(1-\cos\left(\frac{\pi(N-t+\frac{1}{2})}{T}\right)\right), & N+1-T \le t \le N \\ 1. & otherwise \end{cases} \tag{4.20}$$

where $T = \left\lfloor \frac{Np}{2} \right\rfloor$, where p is the tapering proportion and N is the number of data.

The smoothing is defined by a trapezium window whose shape is decided by the tapering proportion, p, being supplied by the user. A value of $p = 0.0$ gives a triangular window, and $p = 1.0$ a rectangular window. The frequency width of the window is fixed as $\frac{2\pi}{M}$, where $M = N/8$ is a user-defined constant, where N is the number of data. In order that the smoothing approximates well to an integration, it is essential that the order of the fast Fourier transformation (FFT), K, be much greater than M, that is, $K \gg M$. A choice of the frequency division, L, greater than M, would normally be required to supply an adequate description of the smoothed spectrum. Here, L must be a factor of K. Typical choices of $L \simeq N$ and $K \simeq 4N$ for usual smoothing situations when $M < N/5$ are applied.

Autocorrelation Function

The autocorrelation function for a periodic signal is itself periodic and can often give a less confusing representation of the data from the power spectrum. This is particularly so when there is a high harmonic content in the signal. It therefore provides a very useful complementary representation of the data. Irregularity in the time series gives rise to a decay in the autocorrelation function and the rate of decaying gives a measure of the degree of irregularity. However, the extracting of quantitative estimates from the autocorrelation function can be problematic and it is usually used as a complement to power spectral analysis.

The autocorrelation function is defined as,

$$R(N\tau_s) = \frac{1}{N-1}\sum_{i=1}^{N} x_i\, x_{i+n\tau_s}, \tag{4.21}$$

where τ_s is the sample time.

Implementation

The implementation algorithm for the autocorrelation coefficient, r, of lag $k = 1, 2, 3, \cdots, K$, where K is a user-specified maximum lag, is defined in NAG Fortran Routine *g13abf* (Hann & Hounam, 1991) as follows,

$$r_k = \frac{\sum_{i=1}^{N-k}(x_i - \bar{x})(x_{i+k} - \bar{x})}{\sum_{i=1}^{N}(x_i - \bar{x})^2}, \tag{4.22}$$

where N is the number of data.

4.4.2 Theme Methods

The box-counting method is used to derive fractal dimensions from the wave profiles. A unique approach is devised to explore the dynamics of sub-systems; that is, the box-counting method is implemented for each record or sub-system of the profile. A more common approach is also implemented; that is, the fractal dimension of the whole profile is calculated. Both approaches utilise the implementation procedures detailed in Chapter Three; and the computer programme listing is available in Appendix E.

Statistical analysis is one of the two theme methods described in Chapter Three, and its computer implementation can be seen in Appendix F. The analysis includes computing the basic statistics and performing one-sample and two-sample statistical

tests. The basic statistics such as minimum, maximum, mean, standard deviation, coefficient of skewness, and coefficient of kurtosis are obtained first for records of both synthetic and natural waves. The mean gives a measure of the central location of the data distribution, and the variance, whose positive square root is standard deviation, gives a measure of the spread about the mean (Eason *et al.*, 1980, p.420). Coefficient of skewness and coefficient of kurtosis are also included. The former measures the skewness of data (Bryman & Cramer, 1990, p.97). The latter is the measure of sharpness of the peak of a frequency-distribution curve (Marsh, 1988; Allen, 1990, p.658).

This is followed by the one-sample normality test such as Shapiro and Wilk's W test (Eason *et al.*, 1980, Ch.24,25); then two-sample statistical tests are performed to test whether the difference between samples is significant. However, the choice of test methods depends on the result of the normality test. In other words, if both samples are normally distributed, a two-sample parametric test is used; otherwise, a non-parametric two-sample test such as the Mann-Whitney U test is more appropriate (Eason *et al.*, 1980, p.487). The process is applied to both raw data and the derived fractal dimension.

4.5 Results

Results from conventional time series analysis are presented first, which include phase portraits and spectral pairs of auto-correlation coefficient and discrete power spectrum; and comparisons are made between the synthetic and natural waves. This is followed by the results from the theme methods, that is, fractal and statistical

analyses; and comparisons are also made between the synthetic and real data.

4.5.1 From Specific Methods

The specific methods used here are the phase portrait reconstruction, which includes the method of delays and the method of singular value decomposition; and the spectral analysis, which is illustrated by the pair of auto-correlation coefficient and discrete power spectrum.

Phase Portrait Reconstruction

In this section, the problem of choosing a proper delay time for Poincaré sectioning in phase portrait is addressed first; then followed by two solutions, that is, method of delays and method of singular value decomposition.

Two methods of reconstructing the temporal dynamics of waves in phase space are presented here, both based on the technique central to the modern non-linear signal processing which is called the "phase portrait". The first involves obtaining the optimal delay time and the embedding dimension from a wave, then reconstructing the wave signals in a phase space of embedding dimensions with optimal delay time. The second utilises the method of delays as well, but instead of the original data, the singular values are used to reconstruct the attractor. That is, if the embedding dimension is three, the first three vectors of the singular value decomposition are used to construct a three-dimensional phase portrait of the attractor.

Phase portrait reconstruction is essentially a qualitative approach to system

dynamic. Although phase portrait is not a new concept, it has been very useful in depicting structure from time series. Poincaré sectioning is a powerful tool used to reveal dynamics by lowering dimensions of phase space. To reduce the dimension one needs to choose a delay time which acts as if it is slicing a "hyper-sheet" through an n-dimensional phase space. The choice of delay time greatly affects the visual presentation of system, although its dynamics remain unchanged.

Choosing a Proper Delay Time

The essential factor in constructing a phase portrait is the choice of delay time. Although poor choice of delay time will not change the topology, the obtained phase portrait will not be comprehensible to human eyes. Using a time series of known characteristics could help the understanding of system dynamics. Therefore, a synthetic wave is generated to illustrate the pros and cons of using phase portrait reconstruction. Fortunately, the computer programme detailed in Section 4.3.1 is implemented in such way that it allows the user to alter the parameters and even the number of waves. In other words, the system is known *a priori*, and its dynamics should be revealed easily.

Figure 4.7 shows some phase portraits reconstructed from the synthetic wave comprising the first three sinusoidal waves in Equation 4.8. In Figure 4.7 (left), 5000 data points are processed initially; however, the number of points plotted in the figure depends on the delay time. Delay times are purposefully chosen. For example, five seconds are half of the period of *Wave1*; ten seconds are the period of *Wave1*; twenty-one seconds are the period of *Wave3*; and 231 seconds are product of periods of *Wave2* and *Wave3*. Refer to Table 4.1.

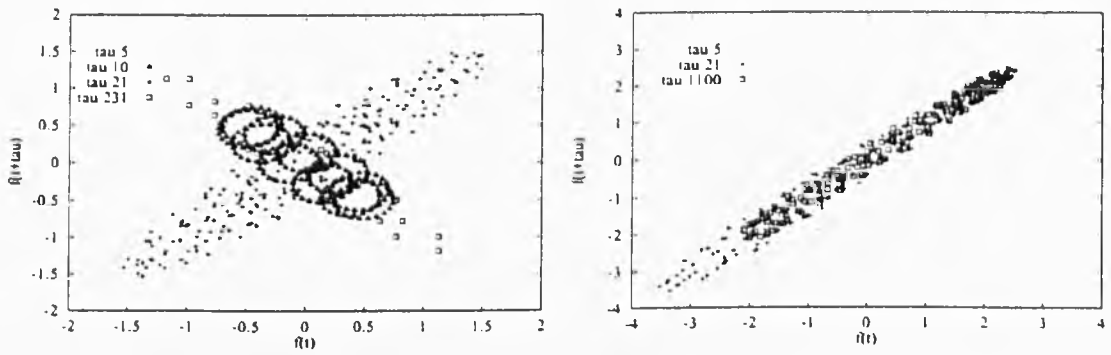

Figure 4.7: Poincaré Sections of Synthetic Waves.
(Left) Poincaré sectioning is produced by plotting value at time, $f(t)$, against value at $t + tau$, $f(t + tau)$, where *tau* is the delay time. There are three component waves involved, that is, all but the tidal waves in Equation 4.8.
(Right) This phase portrait consists of four waves, including the tidal wave. Structures are more difficult to observe simply by "guessing" the delay times.

If a single sinusoidal wave such as *Wave1* is used, a delay time of five seconds corresponding to half its period repeatedly produces four points, that is, (0,1), (1,0), (0,-1) and (-1,0). However, in the composite wave of three waves, this delay time forces the system dynamics to centre around those four points.

A delay time equal to the period of a wave will produce a single point or points closely clustered around origin. For example, the delay time of ten seconds is exactly the period of *Wave1*. The dynamics of *Wave1* disappear into a single point; however, the dynamics of *Wave2* and *Wave3* are easily identified by the two loops they form.

If a delay time is slightly larger than a period or its multitudes, it will produce data clusters along the diagonal direction. The delay time of twenty-one seconds has two effects. Firstly, it is the period of *Wave3*, which reduces itself in a point; and, secondly, it forces the data to cluster along the diagonal direction, because it is too close to the multitudes of *Wave1* and *Wave2*.

The product of two periods can usually bring out the dynamics of the third

wave, in a three-wave system. The delay time of 231 seconds, which is the product of *Wave2* (11) and *Wave3* (21), seems able to reveal the structure of the first wave with a slightly larger delay time than its multitudes, 230.

Figure 4.7 (right) shows the phase portrait reconstruction of the synthetic wave used in this thesis, which has four waves including the tidal wave. Delay times, including an arbitrary large 1100 seconds with 150000 initial data points, have been used to bring out structures from the synthetic wave. None of the delay times seems to show structures as described earlier with three component waves. All data points, no matter what the delay times are, seem to be compressed along [1 1] direction. The most likely explanation would be that, since the comparatively long tidal profile covers only half of the sinusoidal curve, it is expected to observe data clustered along the diagonal direction.

Arbitrary guessing of delay time does not provide rigid support for the method of phase portrait reconstruction. Mathematical approaches are proposed in the following section.

Method of the Optimal Delay Time

The complexity of temporal signals can be reconstructed in phase space by the method of delay (Packard *et al.*, 1980). The choice of delay time has been a problem for the reconstruction and many ways have been developed (Buzug *et al.*, 1990). Here, the optimal delay time approach demands the plotting of the normalised delay time chart, from which phase portraits with delay times are reconstructed.

Synthetic Waves

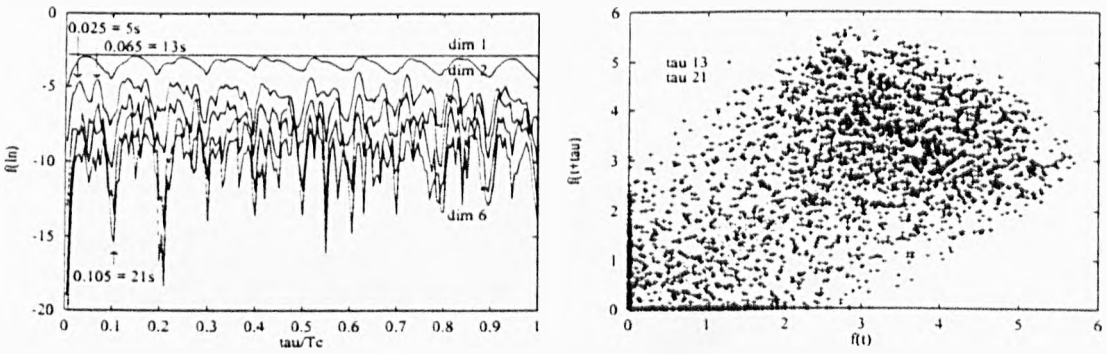

Figure 4.8: Poincaré Sections of the Synthetic Wave Profile.
(Left) The logarithmic fraction of volume utilisation, $f(\ln)$, in dimensions one to six, is plotted against normalised delay time, tau/Tc. Two specific points equivalent to 13 and 21 seconds are selected to reconstruct Poincaré sections below.
(Right) Poincaré sectioning is produced by plotting value at time t, $f(t)$, against value at $t+tau$, $f(t+tau)$, where tau is the delay time. Optimal delay time obtained from the above are used.

Figure 4.8 (left) shows the logarithmic fraction of volume utilisation, in dimensions one to six, being plotted against normalised delay time τ/T_c, where τ is the delay time and T_c is the characteristic recurrence time of the system. Here two types of points are observed. The first type of points are at local optima and the other the local minima of curves. Because higher dimensions do not seem to reveal more information, one of the local optima on the dimension three curve is chosen to bring forward the dynamics clearly. Local optima give a "good" choice of delay times. However, the first minimal delay time common to curves of all dimensions is used to illustrate a "bad" choice of delay time.

The resultant Poincaré sections are shown in Figure 4.8 (right). The delay time of thirteen seconds, that is, $\tau/T_c = 0.065 = 13s$, is used to construct the Poincaré section. Similar structures not shown here can be produced by taking other optimal delay times of dimension three. The delay time of 21 seconds, the bad choice of delay time, packs information along the diagonal direction in the Poincaré section.

The Natural Wave

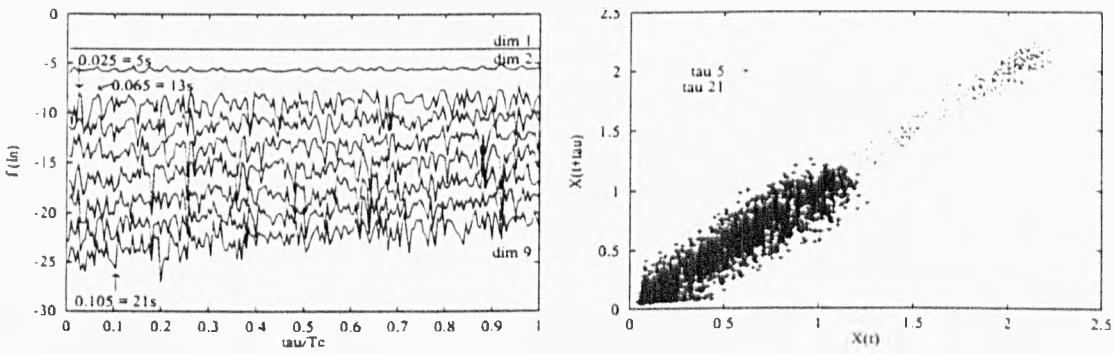

Figure 4.9: Poincaré Sections of the Natural Wave Profile.
(Left) The first three delay times (tau) are identified. Two optima on the top of the graph are so-called "good" choices.
(Right) The Poincaré section of delay time five seconds, which is supposed to reveal structure from the natural wave profile, is found to be concentrated at the bottom left corner; while that of a delay time of twenty-one seconds, which is supposed to hide structure from the phase space, creates a more widespread distribution of data along the diagonal direction.

Figure 4.9 shows the results of phase portrait reconstruction by the method of optimal delay time for the natural wave. The logarithm of the utilised volume, $f(\ln)$, is plotted against the normalised time delay, τ/T_c, for dimensions one to nine, see Figure 4.9 (left). Good delay times are found at the local optima. It has been suggested that the first optima between $0 < \tau < 0.5T_c$ should be used (Buzug *et al.*, 1990). The embedding dimensions are found when no new information on the intrinsic structure of the attractor can be obtained by adding another coordinate. Here, it is seen that the wave can be embedded in the space of low dimension, although one might argue that higher dimensions are possible. The first two possible optimal delays times are five and thirteen seconds. A bad choice of delay time is also presented.

Poincaré sections with good and bad choices of delay time are shown in Figure 4.9 (right). However, even with the good choice of delay time, that is, five seconds,

data points are concentrated at one end of the diagonal direction. In fact, if the delay time of thirteen seconds is used, the structure looks similar to that revealed by a bad choice of delay time.

Comparisons between Synthetic and Natural Waves

Both synthetic and natural waves can be embedded in phase space of low dimensions. The dimension of two is sufficient to reconstruct the wave dynamic in phase space, as suggested by Figures 4.8 (left) and 4.9 (left).

The first few optimal delay times, good or bad, between synthetic and natural waves are all identical. The first two examples of so-called good choices are five and thirteen seconds and the so-called bad choice is twenty-one seconds.

Poincaré sections constructed by those delay times do not appear to be similar between synthetic and natural waves, except that most points concentrate diagonally. Data points in phase portrait of synthetic wave are more dispersed than those of natural wave, except that those data points tend to cluster at the third quadrant of coordinates, if two phase portraits are overlapped.

Method of SVD

Singular values of wave profiles are computed. Here, the phase portraits are constructed from the singular vectors, rather than the profile itself. The results are shown in Figures 4.10 and 4.11.

Synthetic Wave

Singular values and the reconstructed attractor of a synthetic wave profile are

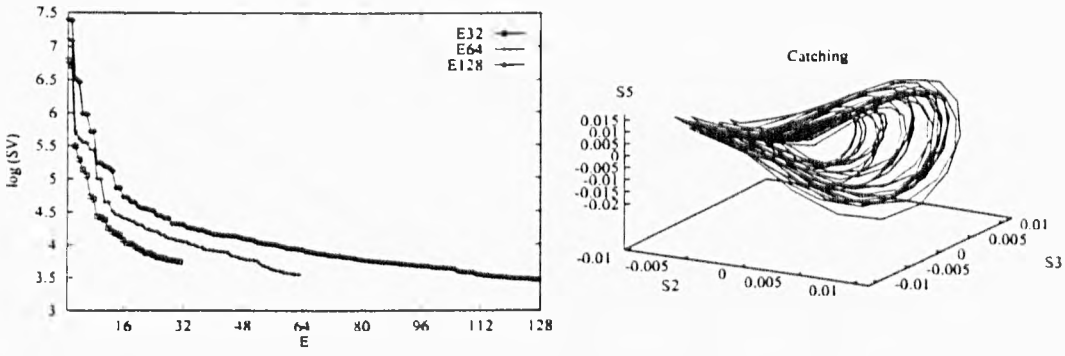

Figure 4.10: The Singular Value Decomposition of a Synthetic Wave Profile. (Left) While the "noise floor" of SV is clearly observed, significant SV cannot be identified clearly, where E is the total number of the singular vectors. (Right) This attractor is reconstructed using the combination of the second (S2), third (S3) and fifth (S5) singular vectors.

shown in Figure 4.10. Three different dimensions enclosing vectors are used to capture the system dynamics. The number of significant singular values and, therefore, the dimensions of phase space, are not easily identifiable. However, the noise floor, as described in Mullin's (1993b, p.37), is quite clear as shown in Figure 4.10 (left).

Phase portraits can be reconstructed by combinations of singular vectors. Some resemble a "comet" and "firework" while the others are more like a "disc". For example, shown in Figure 4.10 (right) and named "catching" is the phase portrait reconstructed by using the second (S2), third (S3) and fifth (S5) singular vectors. Although the attractors can be constructed from various combinations of the singular vectors, their trajectories develop in a confined space (more in Appendix J).

Natural Wave

Singular values and the reconstructed attractor of the wave profile at Teignmouth are shown in Figure 4.11. The number of significant singular values, indicating the dimensions needed to construct the phase portrait, is not clearly observed. Increases of the dimension enclosing vectors do not produce significant values clearly, either.

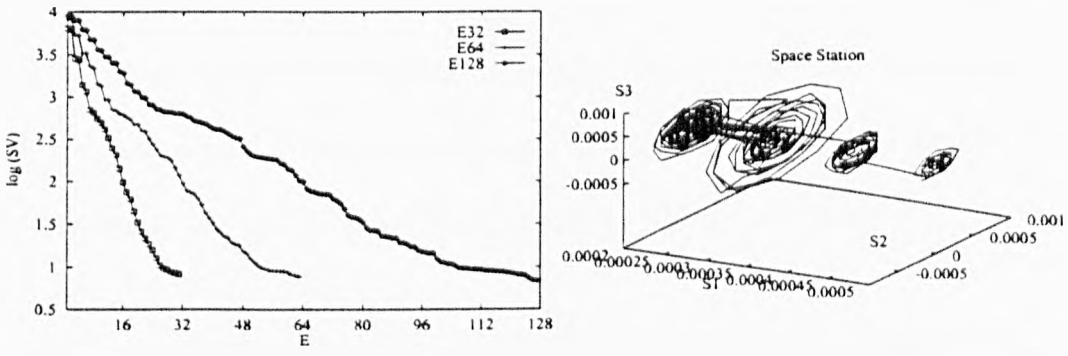

Figure 4.11: The Singular Value Decomposition of the Natural Wave Profile. (Left) Significant singular values, which indicate the dimensions needed to reconstruct phase portrait, cannot be observed clearly. Nor is the "noise floor" clearly observed. E is the total number of singular vectors.
(Right) The first three vectors are used to reconstruct the attractor.

The noise floor cannot be observed clearly.

Figure 4.11 (right) shows the reconstructed structure of the wave profile given by the singular value decomposition method. It is produced by using the first, second, and third singular vectors. The curve starts from the right, to the second right, then left, and ends up at the second left "coil". The second left coil will continue to expand, if longer vectors are given. In fact, unlike the case of the synthetic wave, if the singular vector length is increased, the coordinate ranges change. A long wire-like structure is formed across the phase space. More attractors are constructed and shown in Appendix J.

Comparisons between Synthetic and Natural Waves

The "noise floor" of singular value decomposition is quite clear in the synthetic wave. However, it is not easily seen in the case of the natural wave.

There are a variety of phase portraits reconstructed from singular vectors of both synthetic and natural waves. The range of singular values remains within a

fixed interval for the synthetic wave, if the length of vector changes. However, it is not so, if the length of the singular vectors for the natural wave is changed. Part of some reconstructed attractors becomes relatively insignificant, that is, a dot-like structure, while the rest of it becomes elongated like a wire in space.

Spectral Analysis

In this section, the results of Fourier analysis or harmonic analysis are presented. The discrete power spectrum (DPS) and its Fourier transformation, auto-correlation coefficients (ACC), are a typical pair of the spectral analysis for time series. The discrete power spectrum gives a measure of the amount of power in a given frequency band over a selected frequency range (Mullin, 1993b). In other words, it indicates the number of composite sub-waves in a theoretical wave. The autocorrelation function for a periodic signal is itself periodic and can often give a less confusing representation of the data from the power spectrum. Irregularity in the time series gives rise to a decay in the autocorrelation function and the rate of decaying gives a measure of the degree of irregularity. It is usually accepted that "the spectrum and the autocorrelation function contain the same information, but in some cases one is easier to visually interpret than the other" (Mullin, 1993b, p.27).

Synthetic Waves

A synthetic wave, whose parameters are known *a priori*, provides a basic platform for comparison with a natural wave. For example, peaks of discrete power spectrum values in the synthetic wave can reveal the number of sinusoidal sub-waves embedded, while the auto-correlation coefficient illustrates the periodicity as

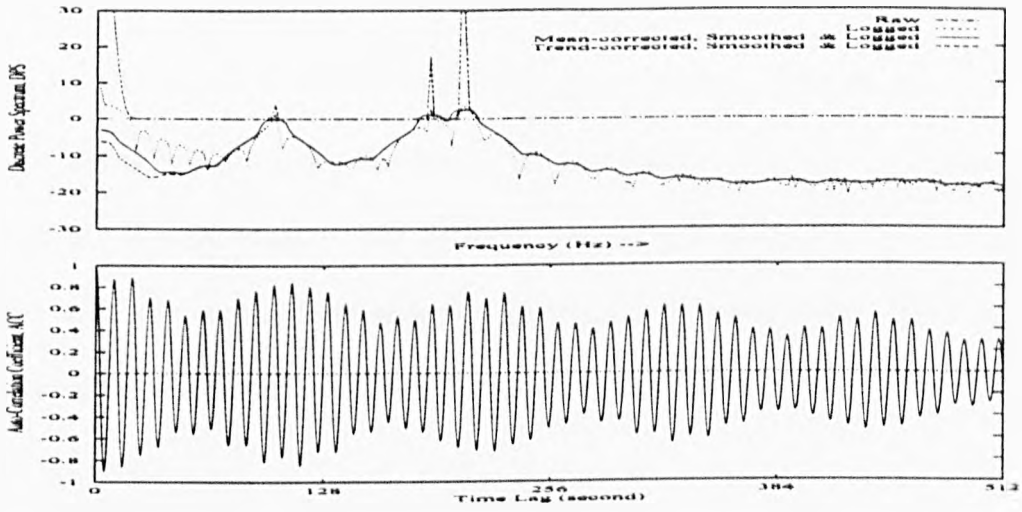

Figure 4.12: Discrete Power Spectra and Auto-correlation Coefficients of a Synthetic Wave.
(Top) Discrete power spectra are given in logarithmic scale as well as raw form. Here, the data are smoothed by the window with the frequency width of $2\pi/256$. *Wave4*, *Wave3*, *Wave2* and *Wave1*, are identified, from left to right, respectively.
(Bottom) The synthetic wave indicates a typical example of a periodic signal. The periodicity is around one hundred seconds.

revealed in Figure 4.12.

By referring to Table 4.1, it is clearly seen that discrete power spectrum gives an excellent indication of the number of component waves. There are four peaks of discrete power spectrum above zero in Figure 4.12 (top), indicated by its raw and logarithmic values. They correspond to the four waves in the equation. Because frequency (Hz) is proportional to $1/T$, four waves are easily identified. They are *Wave4*, *Wave3*, *Wave2* and *Wave1*, from left to right, respectively, because a shorter period has a higher frequency. Peaks in discrete power spectrum values represent the concentrations of power. Tidal influence can be removed by mean- or trend-correction of the raw data, the latter being more effective than the former. After the correction, the other three waves become more dominant than the tide.

The auto-correlation coefficient is typically paired with the discrete power spec-

trum in spectral analysis. Peaks in auto-correlation coefficient values are created by addition or subtraction of phases of the component waves. The distance between dominant peaks indicates the periodicity of the system, that is, the time needed to repeat the system itself. This effect is clearly shown by the synthetic wave in Figure 4.12 (bottom). Note that the patterns of discrete power spectrum and auto-correlation coefficient are identical in all records; that is, there is no difference between records.

The Natural Wave

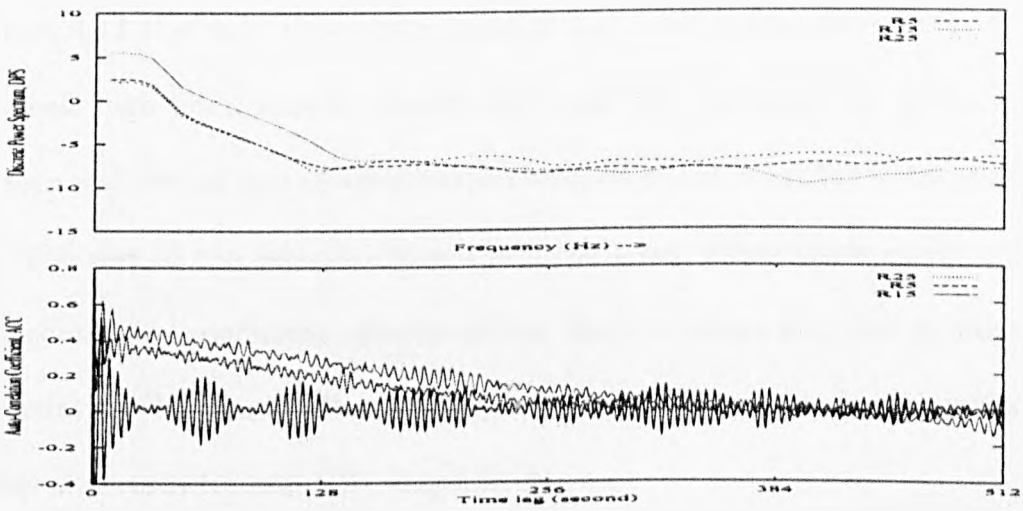

Figure 4.13: Discrete Power Spectra and Auto-Correlation Coefficients of the Natural Wave Profile.
(Top) The strength of dominant power increases before, levels at, then decreases after high tide, indicated by records R5, R15 and R25, respectively. Logarithms of the data are further smoothed by window with the frequency width of $2\pi/256$.
(Bottom) Two types of auto-correlation coefficients are identified: around and outside high tides. The periodicity differs from record to record.

Three records of natural waves are included in Figure 4.13. They are records R15, R5, and R25, which represent dynamics around, before, and after high tide, respectively. The discrete power spectrum raw values in Figure 4.13 (top) indicate that the tide is the dominant force of the natural wave profile. The tidal influence, however, is almost removed by mean- and trend-correction of raw data. On

a logarithmic scale, tidal dominance is visible with or without correction. There is no uniform distribution of discrete power spectrum values between records. Furthermore, the difference of power concentration between each record is clearly seen, especially at lower frequencies. For example, discrete power spectrum values are higher at high tide, that is, record R15. Records approaching high tide, for example, record R5, have relatively high discrete power spectrum values, too. However, discrete power spectrum values are much lower towards either end of the profile, for example, record R25.

Figure 4.13 (bottom) shows two types of auto-correlation coefficients: around and outside high tides, that is, records R15 and R16. At high tide, periodicity is easily seen and the pattern of auto-correlation coefficients is similar to the synthetic wave. The rest of the records shows the other type, where there exists a decay in auto-correlation coefficient, similar to that found in chaos and also to long-term autocorrelation (Mullin, 1993b, pp.27,30). It occurs before and after high tide, for example, at records R5 and R25, respectively.

From the discrete power spectrum, it is certain that the tide is the dominant force in each record. However, the strength differs between records. The auto-correlation coefficients show that periodicity appears in some records while non-periodicity dominates others.

Comparisons between Synthetic and Natural Wave Profiles

Table 4.3 shows the results of one-sample and two-sample statistical tests of discrete power spectrum. Data of normal scores and random numbers from a normal distribution are included for comparison, whose statistics show that they are

Data	N	min	max	$\bar{x}$	std	$Skew$	$Kurt$	W	$c.s.l.$
NS	1024	-3.248	3.248	-0.000	0.999	0.000	-0.044	0.988	0.7666
RN		-2.893	4.114	0.000	0.972	0.185	0.272	0.988	0.7760
Syn.	1024	-19.73	2.586	-16.77	4.072	3.018	8.735	0.510	0.0000*
R5		-12.67	-3.672	-8.086	1.830	-0.229	-12.67	0.955	0.0000*
R15		-14.13	-4.035	-10.03	2.687	0.324	-1.228	0.893	0.0000*
R25		-10.69	-3.699	-7.575	1.583	0.061	-0.784	0.956	0.0000*

Data	Median Test (Me)			Mann-Whitney U Test		
	$Me(X)$	$Me(Y)$	p	U-value	Z-value	p
NS–RN	0.000	-0.019	0.7908	5.3e5	0.297	0.76639
R5–Syn.	-7.847	-18.123	0.000*	9.8e5	34.319	0.0000*
R15–Syn.	-10.453		0.000*	9.6e4	32.826	0.0000*
R25–Syn.	-7.460		0.000*	9.9e5	-34.647	0.0000*
R5–R15	-7.847	-10.453	0.000*	7.5e5	16.866	0.0000*
R5–R25		-7.460	0.003*	4.5e5	-5.679	0.0000*
R15–R25	-10.453		0.000*	2.6e5	-20.063	0.0000*

Table 4.3: Comparison of Discrete Power Spectra between the Synthetic and Natural Waves.
(Top) Basic statistics and one-sample normality test. R5, R15, and R25 denotes records before, around, and after high tide, respectively.
(Bottom) Two-sample non-parametric tests. Me(X) denotes the median of sample X. Median test compares the difference of median between two samples.

normally distributed, as indicated by the calculated significance level. Although the Mann-Whitney U test is a non-parametric test, it produces the expected result ($p = 0.77$). According to the auto-correlation coefficients of the natural wave, three records representing wave dynamics before (R5), around (R15), and after (R25) high tide are selected to compare with the synthetic wave. The table shows that none of the records is normally distributed. Consequently, non-parametric two-sample tests are performed. The Median test ($p = 0.00*$) shows that there is significant difference between medians. The Mann-Whitney U test ($p = 0.00*$) also indicates that there is significant difference between the distribution functions of synthetic and natural waves. Significant difference is detected between records of the natural wave, as shown by both the median and Mann-Whitney U tests.

Tables 4.4 shows results of statistical tests of the auto-correlation coefficient between synthetic and natural waves. Statistics of normal scores and random numbers from normal distribution are not included. The table shows that the auto-correlation

Data	N	min	max	$\bar{x}$	std	$Skew$	$Kurt$	W	$c.s.l$
Syn.	1024	-9.727	-0.066	-1.851	1.307	-1.849	4.798	0.840	0.0000*
R5		-16.658	-0.397	-4.495	2.261	-0.640	0.668	0.941	0.0000*
R15		-18.919	-0.435	-5.081	1.813	-1.414	5.040	0.926	0.0000*
R25		-12.709	-0.282	-3.391	1.798	-1.001	1.456	0.923	0.0000*

	Median Test (Me)			Mann-Whitney U Test		
Data	$Me(X)$	$Me(Y)$	p	U-value	Z-value	p
R5–Syn.	-4.551	-1.482	0.000*	1.4e5	-28.419	0.0000*
R15–Syn.	-4.787		0.000*	6.4e4	-34.425	0.0000*
R25–Syn.	-3.175		0.000*	2.3e5	-22.051	0.0000*
R5–R15	-4.551	-4.787	0.042*	6.1e5	6.348	0.0000*
R5–R25		-3.175	0.000*	3.7e5	-11.788	0.0000*
R15–R25	-4.787		0.000*	2.5e5	-20.447	0.0000*

Table 4.4: Comparison of Auto-Correlation Coefficients between the Synthetic and Natural Waves.
(Top) Basic statistics and one-sample normality test. R5, R15, and R25 denotes records before, around, and after high tide, respectively.
(Bottom) Two-sample non-parametric tests. Me(X) denotes the median of sample X. Median test compares the difference of median between two samples.

coefficients of both synthetic and natural waves are not normally distributed. Standard deviations, skewness and kurtosis coefficients also support the result of the normality test. Consequently, non-parametric tests are conducted between the three records of natural wave and the synthetic wave record. Both median test ($p = 0.00*$) and Mann-Whitney U test ($p = 0.000$) show that the difference between records is significant. The difference between records of the natural wave is significant.

The conventional methods conclude that the difference between the synthetic and real waves is significant. In other words, the natural wave profile is aperiodic of more frequencies than the synthetic wave, as evidenced by Figures 4.8 and 4.9.

Furthermore, the difference between sections of the natural wave profile is also found to be significant. The fractal analysis presents, however, results that differ from those obtained by the conventional methods, as described in the following section.

4.5.2 From Theme Methods

General statistics are summarised for both synthetic and natural waves, including minimum, maximum, mean, standard deviation, coefficient of skewness, and coefficient of kurtosis. Fractal dimensions are presented together with the basic statistics to illustrate the system dynamics not discovered by conventional statistical methods. Comparisons are made between the synthetic and natural wave profiles.

Synthetic Wave

The time series are shown in Figure 4.14 (top), followed by the log-log plots of box counts against sizes for each record in Figure 4.14 (middle). The slopes of the plots, that is, the fractal dimensions, are shown in the diamond line (-◇-) in Figure 4.14 (bottom left). Estimates of fractal dimensions of individual records range from 1.639 to 1.689 and average 1.662; and all the estimates are significant, since their corresponding correlation coefficients ($r > 0.99$) are higher than the critical vaue of 0.632. Furthermore, the differences in the fractal dimensions are not significant between records, because the calculated $t < 1.0$ values are smaller than the critical $t_{.05,18}$ (1.734) value (Appendix K).[3] The fractal dimension of the overall wave is a

[3] The t value for comparing the difference of two regression lines is calculated as $t = \frac{|S_X - S_Y|}{\sqrt{S_X^2 + S_Y^2}}$ and the degree of freedom is $(N_X - 2) + (N_Y - 2)$ (Fowler & Cohen, 1990).

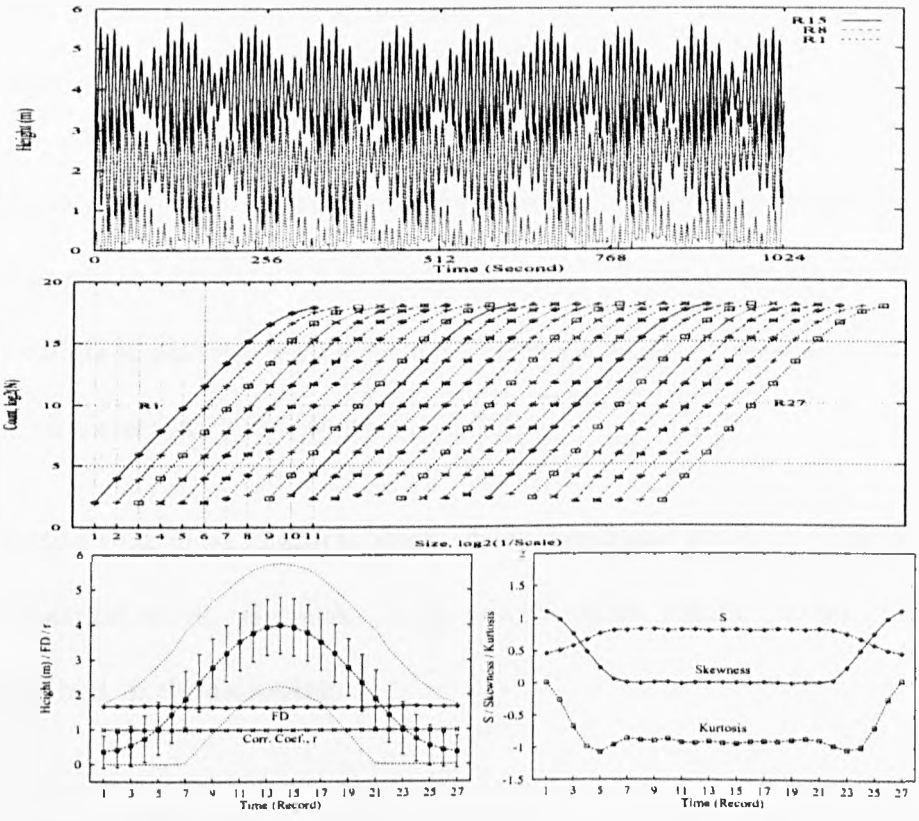

Figure 4.14: Fractal Dimensions of a Synthetic Wave Profile.
(Top) Time series for some records.
(Middle) Log-log plots of box counts against sizes for all records.
(Bottom) Left. Fractal dimensions, i.e., the slope estimates, are significant, for their correlation coefficients ($r > 0.99$) are greater than the critical value of 0.632. Shown also are basic statistics such as the minimum, maximum, mean and the standard deviation (S) of heights. Right. Distributional characteristics of the heights are revealed by S, skewness and kurtosis.

relatively low and meaningless value of 1.386, because its corresponding correlation coefficient ($r = 0.315$) is much lower than the critical value of 0.535.

Figure 4.14 (bottom left) also shows the minimum, maximum, mean, standard deviation and fractal dimension of each record of the synthetic wave. The overall shape of the wave, revealed by average heights, resembles the theoretical sinusoidal wave profile. It shows that the wave gains its height, reaches the high tide, retreats afterwards, then dies down in the end. The mean heights range from 0.4 to 4.0 metres and the overall mean height is 2.1 metres. However, the tidal range is 5.7 metres,

and is slightly higher than the recorded spring tide[4] of 4.1 metres at Teignmouth (Hoskins, 1954, p.17).

The data distribution is measured by the standard deviation, skewness and kurtosis, and is presented in Figure 4.14 (bottom right). Records at either end of the profile show different patterns of distribution from those in the middle, that exhibit some typical characteristics of a synthetic curve.

It is expected that most characteristics of the synthetic wave are different from those of the natural wave. However, there may be some similar patterns between them, as described in the following.

The Natural Wave

Time series of some data record are shown in Figure 4.15 (top). The box-counting method was conducted for each record, and the results are illustrated in the log-log plots of box counts and sizes in Figure 4.15 (middle). The derived fractal dimensions, that is, the slopes, are plotted in Figure 4.15 (bottom left). Estimates of fractal dimension are relatively consistent with each records, ranging from 1.515 to 1.736 and averaging 1.679. their corresponding correlation coefficients ($r > 0.99$) are higher than the critical value of 0.632 thus indicate the estimates are meaningful. The differences in the fractal dimensions are not significant between records, since the calculated $t < 1.0$ values are smaller than the critical $t_{.05,18}$ (1.734) value (Appendix K). The fractal dimension of the overall wave profile (1.144) is a relatively low and

[4] A tidal pattern that occurs twice a month at full and new moon, when the difference in level between high and low tides is greatest (Manser & Thomson, 1997).

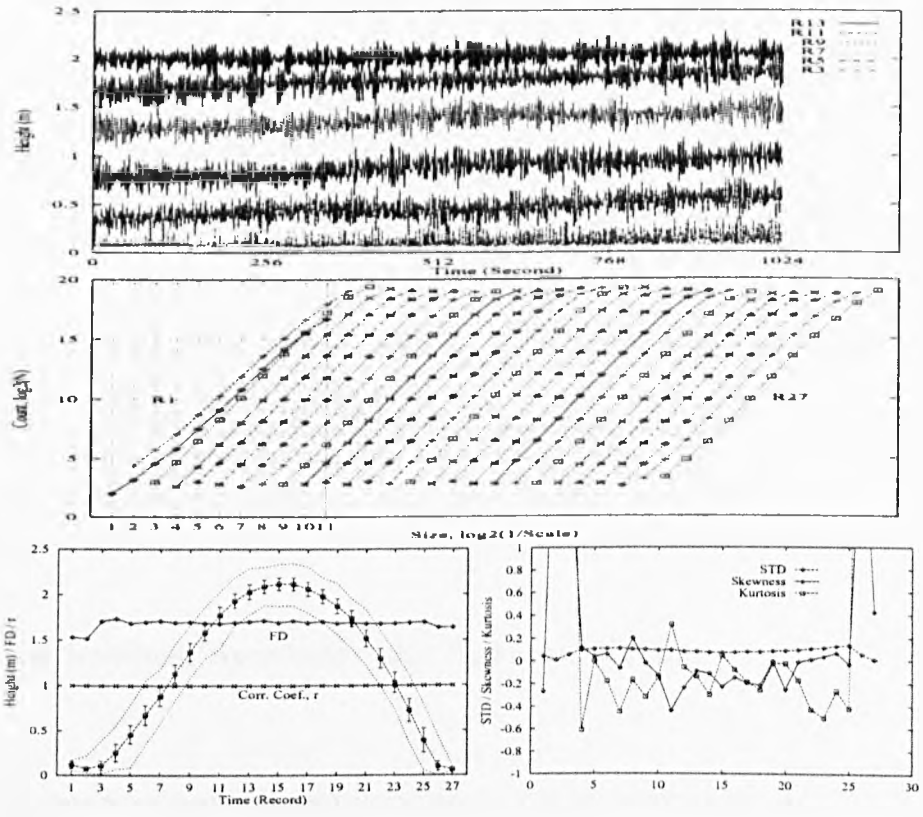

Figure 4.15: Fractal Dimensions of the Natural Wave Profile.
(Top) Time series of some records before high tides.
(Middle) Log-log plots of box counts against sizes for each record.
(Bottom) Left. Fractal dimensions, i.e., the slope estimates, are significant, because their correlation coefficients ($r > 0.99$) are greater than the critical value of 0.632. Shown also are basic statistics such as the minimum, maximum, mean and the standard deviation (S) of heights. Right. Characteristics of the height distribution are revealed by S, skewness and kurtosis.

insignificant value, because its corresponding correlation coefficient ($r = 0.286$) is much lower than the critical value of 0.535.

Figure 4.15 (bottom left) also shows the minimum, maximum, mean, and standard deviation of each record in natural wave. The mean heights, ranging from 0.1 to 2.1 metres, form a sinusoidal curve which completes in about eight hours. The tidal range, read from the minimum and maximum of the heights, is 2.3 metres, a value relatively smaller than the typical spring tide of 4.1 metres recorded at Teignmouth (Hoskins, 1954, p.17).

Figure 4.15 (bottom right) shows the distributional characteristics of the natural wave. Relatively small variations are shown in the records in the middle of the profile; however, sharp coefficients of skewness and kurtosis are observed at either end, indicating highly skewed and peaked distribution of the data.

The similarity and difference of many characteristics of the synthetic and real waves have been revealed graphically. In the following section, however, statistical tests are applied in order to confirm the above observation.

Comparisons between Synthetic and Natural Waves

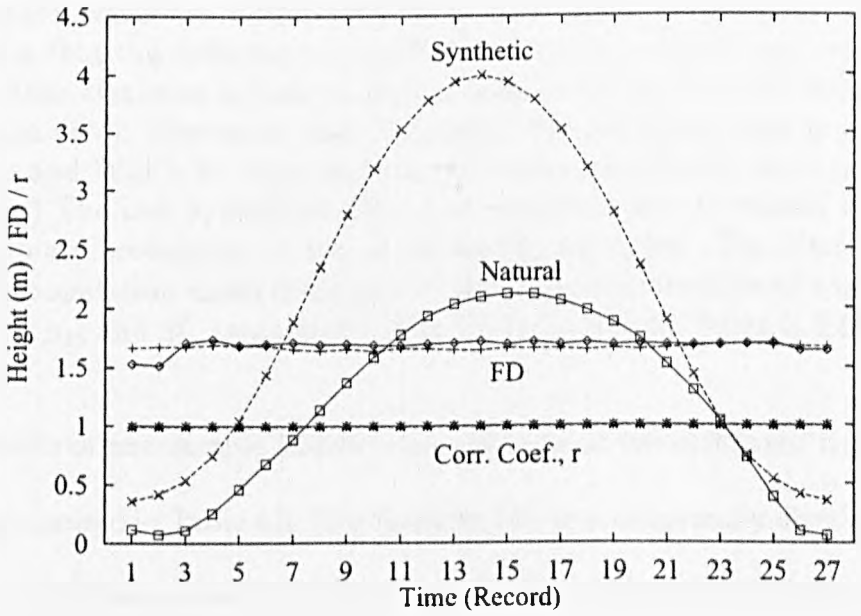

Figure 4.16: Comparison of FDs between the Synthetic and Natural Waves. The estimated fractal dimensions are identical between the natural (—) and synthetic (- -) waves, although the difference in heights is significant.

Comparisons for general statistics and fractal dimensions (FDs) between synthetic and natural wave profiles are presented in Figure 4.16. Both profiles form a sinusoidal curve, while the overall synthetic wave is slightly positively skewed (0.226)

and the overall natural wave is slightly negatively skewed (−0.193). Both profiles are relatively widespread, indicated by coefficients of kurtosis of −1.783 and −1.483 for the synthetic and natural waves, respectively.

Top: One-sample test

Data	n	min	max	$\bar{x}$	std	$Skew$	$Kurt$	W	$c.s.l.$
NS	27	-1.998	1.998	0.000	0.972	0.000	-0.583	0.996	0.9999
RN		-2.265	2.526	0.095	1.141	-0.006	-0.442	0.990	0.9929
Syn	27	1.639	1.689	1.662	0.016	0.240	-1.212	0.927	0.0644
Real		1.515	1.736	1.679	0.049	-2.382	5.002	0.653	0.0000*

Bottom: Two-sample tests

Data	Test	H_0	Statistics	Z	p
NS–RN	t-test ($df = 52$)	$\mu_{NS} = \mu_{RN}$	-0.330		0.7427
Real–Syn	t-test ($df = 52$)	$\mu_{Real} = \mu_{Syn}$	1.677		0.0995
	Mann-Whitney	$F(Real) = F(Syn)$	589	3.876	0.0001*

Table 4.5: Statistical Tests for Fractal Dimensions of Wave Profiles.
"NS" is the normal scores and "RN" is the random numbers of N(0,1). The synthetic and natural waves are indicated by "Syn" and "Real", respectively. The symbol " * " indicates that the difference is significant at the 5% significance level.
(Top) Basic statistics include minimum (min), maximum (max), mean ($\bar{x}$), standard deviation (std), $Skew$ness, and $Kurt$osis. The normality test is indicated by the Shapiro and Wilk's W-value and the calculated significance level ($c.s.l.$).
(Bottom) The null hypothesis (H_0), test statistics and its related Z-value, and the approximate probability of test statistics (p) are given. The distribution function and the population mean of sample x, and degrees of freedom of t-test are indicated by $F(x)$, μ_x, and df, respectively. The critical value for t-test is 2.009.

Results of one-sample and two-sample tests on the estimated fractal dimensions are summarised in Table 4.5, that includes two sets of normally distributed data, that is, the normal scores and random numbers. The Table shows that the synthetic wave has a narrower range of the fractal dimensions than that of the natural wave. Also, the distribution of fractal dimension of a synthetic wave is less skewed and peaked than that of a natural wave. In fact, the Shapiro and Wilk's W test shows that the fractal dimensions of a synthetic wave are of normal distribution ($c.s.l. = 0.064$), while those of a natural wave are not ($c.s.l. = 0.00*$). This leads to difficulty in further comparison between two samples, since one sample is of normal distribution

and the other is not. Therefore, both parametric t-test and non-parametric Mann-Whitney two-sample tests are performed. The result of the former test shows that there is no significant difference ($p = 0.995$) between wave profiles; however, the result of the latter test shows otherwise ($p = 0.00*$). Unfortunately, the statistical tests neither deny nor confirm the difference of the fractal dimensions between the synthetic and real waves as revealed graphically.

Data Length Effect on Estimation of Fractal Dimension

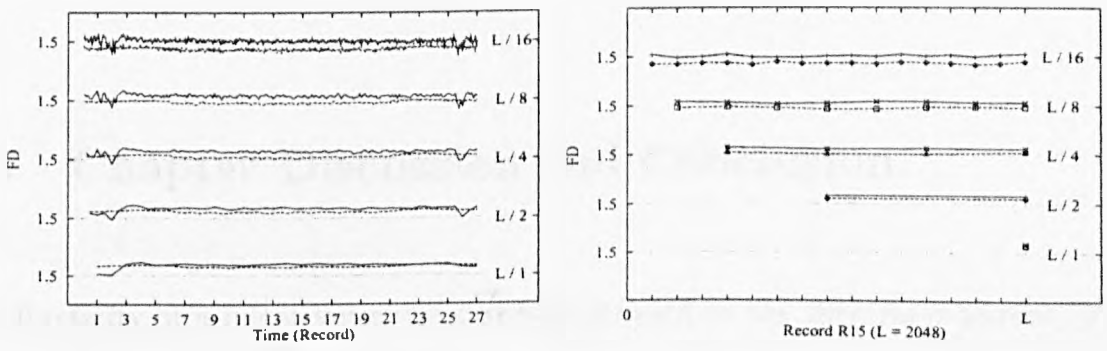

Figure 4.17: Data Length Effect on Estimation of Fractal Dimensions.
(Left) Fractal dimensions are derived from geometrically decreased lengths of data for both the natural (–) and synthetic (- -) wave profiles.
(Right) Fractal dimensions of the record at high tide (R15) are selected to show the effect of record length to the estimation of fractal dimensions.

The effect of reducing record length is illustrated in Figure 4.17, where broken lines represent the synthetic wave and solid lines represent the natural wave. The bottom curves of the Figure 4.17 (left), also seen in Figures 4.15 and 4.14, show the estimated fractal dimensions of the original twenty-seven records. From bottom to top, each record length is further halved, step by step, and the related fractal dimensions are estimated; that is, the upper adjacent curves are composed of fractal dimensions derived from data of exactly half the length of the lower curves.

Several interesting results from such operation are presented in Figure 4.17 (left). First of all, the average of fractal dimensions decreases as the data length decreases. In other words, the shorter record length produces lower estimates of fractal dimension. Secondly, curves of fractal dimensions are rougher at the shorter length of data. Finally, the synthetic wave profile has lower estimates of fractal dimensions than those of natural profile. Similar effects are found in an individual record treated the same way as seen in Figure 4.17 (right). In summary, the effect of reducing the record length is that it lowers the estimates of the fractal dimension and, in general, the curve formed by such estimates becomes rougher as the record length reduces.

4.6 Chapter Discussion and Conclusion

The fractality of a linear structure can be examined by the spectral exponent (β) derived from the log-log plot of the spectral densities (S_f) against frequencies (f), $S_f \propto \frac{1}{f^\beta}$ (Voss, 1988). On the other hand, structures of higher dimensions have to utilise the more fundamental definition of fractals. Structures of fractional dimensions are by definition called fractals (Mandelbrot, 1983) and "fractals [are] everywhere" (Barnsley, 1993), although some researchers (Panico & Sterling, 1995; Kurz *et al.*, 1998, for example) reported that retinal neurons and blood vessels do not exhibit self-similar structures, implying that fractals are not everywhere. Therefore, it is justifiable that almost all natural objects are fractals hence can be measured in terms of fractal dimensions. While the fractal method is aimed to explore the scale-similarity of structures, the conventional approaches usually are utilised to reveal the complexity of structures. Therefore, the conventional methods specific to

time series is reported along with the estimation of fractal dimensions.

Given the reliability of pressure transducers and that the measurements were made in relatively shallow water, the sea wave profile was suitable for study of systems dynamics. Revelation of the simplicity or complexity of the wave, however, depends upon the methods used. The result from the fractal method states that the sub-systems dynamics of the sea wave in shallow water are relatively homogeneous, while the conventional methods reveal complexity.

4.6.1 On Conventional Time Series Analyses

The complexity of wave dynamics can be revealed by the conventional methods: the qualitative approach of the phase portrait constructions and the quantitative approach of the spectral analysis. The advantages of constructing a phase portrait by delay times can be clearly shown in Figure 4.7 using all but the tidal components in Equation 4.8; that is, patterns are revealed by certain delay times. The phase portrait also shows that this method is limited by lack of repetitive dynamics in the system; that is, once the single long tidal wave is involved, the whole system is squeezed along the diagonal direction in the phase portrait. There are alternative means of constructing phase portraits, for example, using the singular vectors. However, they are more suitable for some than for others; that is, dynamics are more easily shown in the synthetic wave than in the natural waves (Figures 4.10 and 4.11).

The spectral analyses also supported that the natural wave is more complex than the synthetic one. The dominant frequencies and the periodicity are clearly

shown by the power spectra and auto-correlation coefficients of the sub-systems in the synthetic wave; that is, the dynamics are actually identical between records (Figure 4.12). In the case of the natural wave profile, dynamics differ from record to record; although distinctly different behaviours can be observed between the high tide records and the rest of the profile (Figure 4.13). The complexity might be attributed to the formulation of near-shore sea waves.

In Chapter Two, it was established that waves in shallow water are formulated as a result of the interference and grouping of component waves that are further modified by local environments. Indeed, such complexity can be revealed by its statistical parameters (Table 4.5) and explored by the conventional methods. However, the fractal approach has produced some interesting results that reveal the simplicity of the waves.

4.6.2 On Fractal Approaches of Time Series

A typical approach to time series analysis was illustrated by Shaw (1993): a plot of measurements as a function of time is plotted, and followed by the calculation of the Fourier transformation. Since the emergence of Chaos Theory and Fractal Geometry, the estimation of the fractal dimension is then added to the time series analysis. The calculation of the fractal dimension is usually made with the construction of a log-log plot, from which the slope is equated to the fractal dimension. At times, other techniques specific to the nature of measurements are employed, such as the calculation of K_2 entropy of an oscillating system (Yamazaki, 1988, for example). Very often, only the log-log plot is presented, from which the fractal dimension is

derived. The subjects under study, however, vary greatly.

The most favourable subjects are systems that produce long-term time series, because the calculation of the fractal dimension demands a large amount of data. Those systems include theoretical models or experimental data on repetitive patterns. For example, Cusumano & Sharkady (1995) studied the system which was parametrically excited through a bifurcation parameter; and the spatial pattern of a trajectory in the phase space drawn by a dynamic system such as a nuclear power plant gives the information (fractal) dimension of the system, and enables the onset of the limit-cycle (or persistent) oscillation to be examined (Suzudo *et al.*, 1997). The following is an ever-growing list of the application of fractal analysis to diverse and complex time series such as flow dynamics (Huber & Alstrom, 1991; Buzug *et al.*, 1992; Hadad *et al.*, 1993; Osborne & Pastorello, 1993; Marvasti & Strahle, 1995; Kozma *et al.*, 1996; Bai *et al.*, 1997), cosmic rays (Aglietta *et al.*, 1993; Bergamasco *et al.*, 1994; Kanetake *et al.*, 1994; Yasue *et al.*, 1996; Kitamura *et al.*, 1997), physiology (Yeragani *et al.*, 1993; Pradhan *et al.*, 1995; Lutzenberger *et al.*, 1995; Wagner & Persson, 1995; Yambe *et al.*, 1995; Vibe & Vesin, 1996; Accardo *et al.*, 1997; Christ *et al.*, 1997; Jartti *et al.*, 1997; Preissl *et al.*, 1997; Yambe *et al.*, 1997; Noguchi *et al.*, 1998), solar study (Polygiannakis & Moussas, 1994; Hirzberger *et al.*, 1997; Zhang, 1997), earthquakes (Frankel, 1991; Volant & Grasso, 1994; Tsai, 1997), and environmental radioactivity (Jaime *et al.*, 1995). Other linear features are also popular subjects, such as fractional Brownian motion (Rani & Mitra, 1995; Tsai, 1997), and protein sequences (Rani & Mitra, 1995; Rani & Mitra, 1996).

The Estimation Method

The estimation of the fractal dimension from time series usually utilises the method of correlation dimension (Theiler, 1991; Anmajunas & Tamasevicius, 1992; Olofsen *et al.*, 1992; Zeng *et al.*, 1992; Bassingthwaighte & Raymond, 1994; Jedynak *et al.*, 1994; Bergmasco *et al.*, 1995; Cusumano & Sharkady, 1995; Heng *et al.*, 1996; Shirer *et al.*, 1997). The correlation dimension based on Grassberger-Procaccia (Grassberger & Procaccia, 1983b; Grassberger & Procaccia, 1983a) algorithms was the most popular method but it was criticised for not being applicable to data of higher dimensions (Jedynak *et al.*, 1994). This might be due to the influence of inhomogeneities in the probability distribution, such as the boundary and the lacunarity effect (Heng *et al.*, 1996), which distinguishes sets that have the same fractal dimension but different textures (Allain & Cloitre, 1991). Since the calculation is time consuming, parallel computation is sometimes employed to calculate the correlation dimension (Corana *et al.*, 1991).

The correlation dimension can also be derived using the re-scale range (R/S) analysis (Feder, 1988, for example), which is "a means of characterising a time series or a one-dimensional spatial signal that provides simultaneously a measure of variance and of the long-term correlation or 'memory' " (Bassingthwaighte & Raymond, 1994). Trend-correction has to be applied to get a closer estimate of the Hurst exponent. Furthermore, this method is confined to one-dimensional features (Karamavruc & Clark, 1997; De la Fuente *et al.*, 1998) and long-term repetitive events such as seasonal floodings in the River Nile (Feder, 1988). The validity of the R/S analysis was questionable; for example, the Hurst exponent of $H > 1$, which is theoretically impossible, has been reported for fractal time series using the

R/S analysis (North & Halliwell, 1994). Given that the wave profile under study was measured in only one tidal cycle, the R/S analysis is unlikely to discern any information from the data. However, data should be collected for days or longer in order to apply the R/S analysis. This is, nevertheless, beyond the scope of this thesis.

Although it is logical to use, for example, the correlation dimension described above and the spectral approaches detailed in Chapter Three for linear features, the use of the box-counting method here is justified as follows. Corresponding to the three types of dynamics revealed in the Mandelbrot set (Chapter Two), the data used in this thesis are of different dimensions. Furthermore, making comparisons demands an identical method and similar scales being used for deriving the fractal dimensions (Chapter Three). While the former requirement is met with the use of the box-counting method, the latter is shown by the data length effect on the estimation of the fractal dimensions.

The Length Effect and Multi-fractality

As with many other methods, the box-counting method yields different estimates if the scale of estimation changes. As revealed by the box-counting method implemented here, fractal dimensions of the sub-sections decrease as lengths of the sub-sections decrease (Figure 4.17). The minimal length is related to the cut-off value of the correlation coefficient in the regression model; that is, thirty-two data with a impossible cut-off of 1.0 are the shortest possible length, according to (Equation 3.7). On the other end of the scale, there is not even a meaningful estimate of the fractal dimension for the whole profile, for the calculated correlation coef-

ficient is much lower than the critical value. Therefore, extreme scales are not advisable for data of limited resolution when calculating the fractal dimension using the box-counting method (Zahn & Zosch, 1997).

An identical result was found in Chan & Page (1997), who studied SEM[5] micrographs of a particle system and found the boundary fractal was "sensitive to magnification with appreciable drops in value at high magnification." Unlike the mathematical object, "the particles studied did not have true fractal boundaries" upon magnification (Chan & Page, 1997). Therefore, the range of scales that are used to derive the fractal dimensions must be specified. Li & Park (1998) calculated a single measure of fractal dimension from each of their model surfaces by fractional Brownian motion and found that the fractal dimension is a function of the observation scale used in the profile measurement. What was demonstrated by Li & Park (1998) is a special case in which multi-fractality is noted by the scaling approach. Other studies would simply ignore such a phenomenon (Tsai, 1997; Stutzki *et al.*, 1998) or adopt the standard multi-fractal approach (Richter & Markewitz, 1995; Veneziano *et al.*, 1995) as mentioned in Appendix D.

The length effect shown here is similar to the findings of Li & Park (1998). Both reveal multi-fractality of a system by means of changing scales, compared to the formal definition of the multi-fractal dimensions, that utilise multiple methods. This subject can be pursued further but it is beyond the interest of this thesis. Further pursuit of the subject can be certainly assumed, although the focus remains on the findings made here.

[5] SEM stands for Scanning Electronic Microscope.

Fractal Characterisation of Sea Waves

The mean fractal dimensions of both the natural and synthetic waves are extremely similar (Figure 4.16), and the difference of the mean fractal dimensions between waves is not significant, as shown by the two-sample t-test result (Table 4.5). For the random water surfaces measured at a fixed point, Stiassnie *et al.* (1991) found that capillary wave solution produced graphs with dimension $1\frac{1}{12}$, whereas the graph for gravity waves had dimension 1.0. Their result is relatively low, compared with the research of Bergmasco *et al.* (1995), who found that, for certain wind-derived surface data measured in Adriatic Sea near Venice, there is a finite value for the correlation dimension similar to 7, said to result from the anomalous statistical behaviour of certain near-Gaussian random processes. An intermediate value was found in the result obtained in this Chapter. Although these examples show that the measurements of water surfaces are of a fractal nature, a comparison of the fractal dimensions cannot actually be made between them: the estimation methods and scales are all different. More importantly, the current implementation method is different from the above authors.

Several estimates of the fractal dimensions are derived from sub-systems or records of the wave system studied here, while only one measure of the fractal dimension was reported from other researchers. The result shows that the fractal dimensions are similar between records, for both the synthetic and natural waves. This approach in the fractal analysis of time series is unusual, although findings in other fields might provide an insight into the current result.

Wilson & Dominic (1998) found that the fractal analysis of topography revealed

no significant variation in the fractal characteristics of topography in the relatively undeformed foreland area. The profiles of the undeformed foreland are very similar to the wave profiles, that are dominated by the long tidal wave. Therefore, sections of the profile should have similar characteristics. This observation was found to be applicable to both the synthetic and natural wave profiles; that is, the difference of mean fractal dimensions between these profiles is not significant. On the other hand, Wilson & Dominic (1998) also found that there is a significant positive correlation between the fractal dimensions of topographic and structural relief along the strike of major folds in the deformed area. However, the investigation of topography itself is provided in the following chapter.

Chapter 5

Landforms

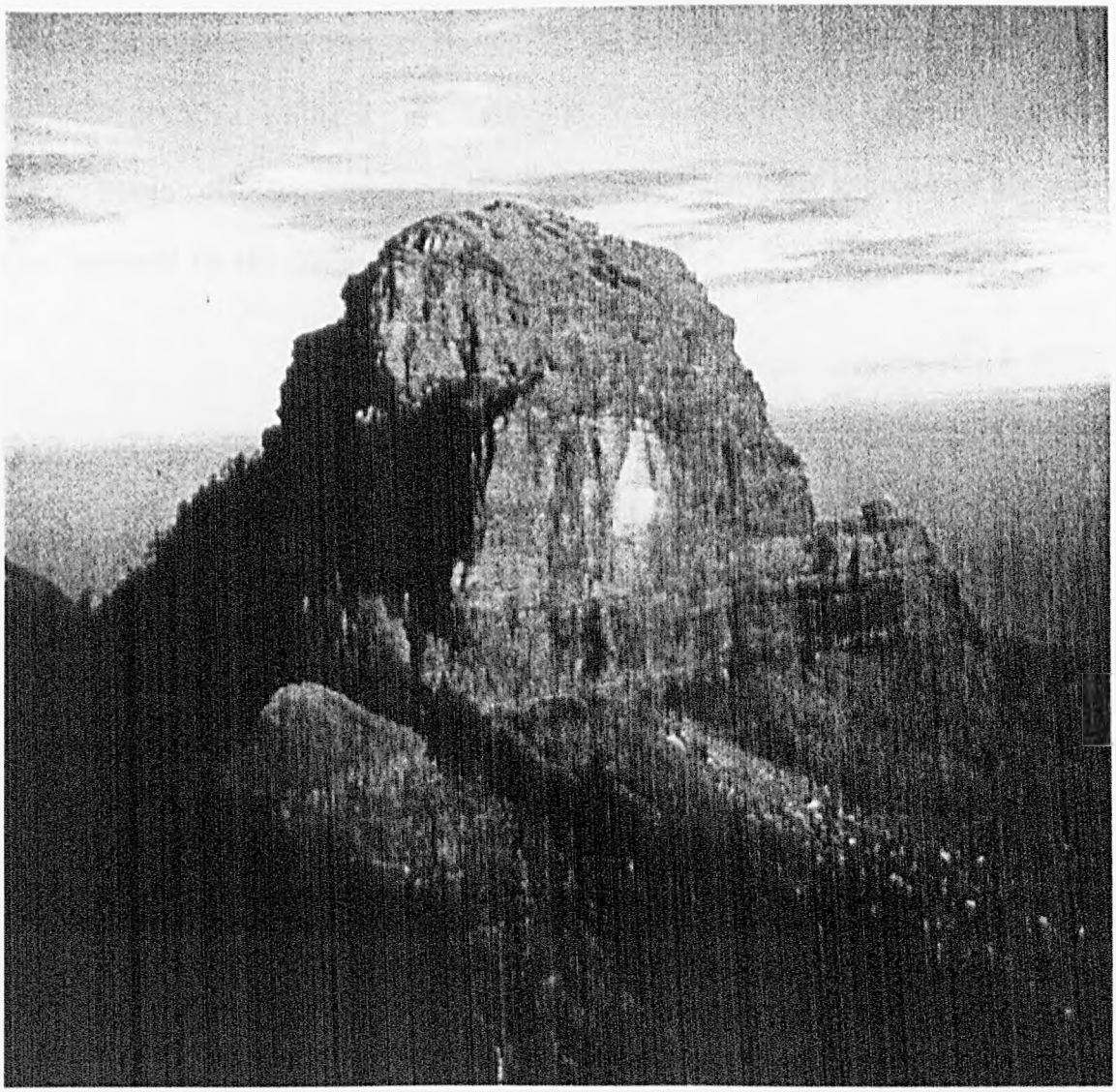

Figure 5.1: The Summit of Shei-pa National Park In Taiwan, R.O.C.
One of the summits that the park is named after, from Tsai & Simpson (1992).

5.1 Introduction

This chapter focuses on the analysis of the topography. The landform especially in the mountainous area of high precipitation is usually comprised of diverse sub-systems. The diversity of the landscape is explored using the conventional and fractal approaches. While the general terrain information can be provided using the conventional methods as described later on, the diversity of the sub-systems is revealed by the fractal method, implemented by applying the box-counting method to each profiles as detailed in Chapter Three. The digital elevation model used here was obtained from the Shei-pa National Park in the northern part of Taiwan, the Republic of China; whilst the synthetic digital elevation models are generated using the mid-point displacement method. The results from both approaches are given, then followed by the discussion and conclusion.

5.2 The Study Area

The study area is located at $24°37'N/121°21'E$, northern part of Taiwan, the Republic of China. It includes most of Shei-pa National Park established in 1992, and its neighbouring area. The digital elevation model covers the area of 41×41 kilometres or 25.5×25.5 miles, which is equivalent to 1681 square kilometres or 649 square miles. Refer to Figure 5.2 for the study area. A brief introduction to Taiwan, the Republic of China, is given in Appendix L, including comparison of the landuse and conservation policies Taiwan, the United Kingdom and the United States.

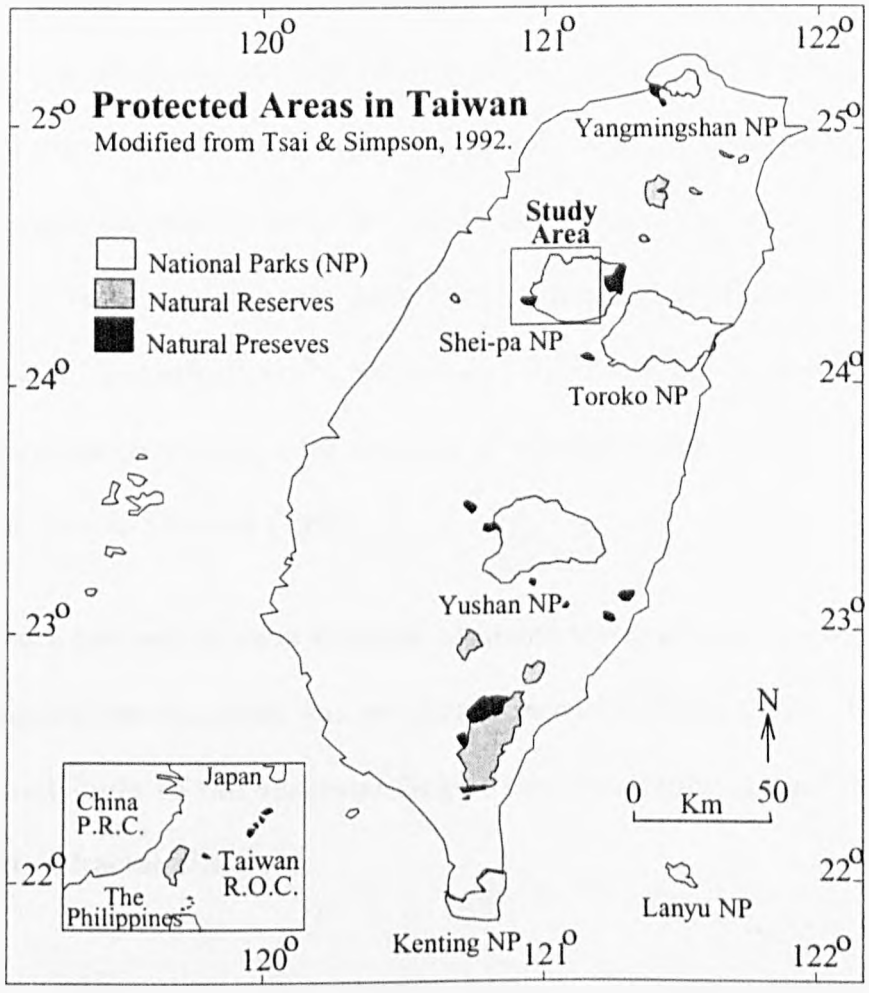

Figure 5.2: Location of the Shei-pa National Park in Taiwan, R.O.C.. Taiwan, the Republic of China, is situated off the south-east coast of mainland China, between Japan and the Philippines (see insert). There are seven National Parks (NP), fifteen Nature Preserves, twenty Nature Reserves, and one Wildlife Sanctuary. The total areas designated for conservation occupy 13% of the total land area. Source: Tsai & Simpson (1992).

Shei-pa National Park falls in IUCN Category II, which defines national parks as "relatively large areas not materially altered by human activity where extractive resource uses are not allowed" (Table L.3 in Appendix L). The Park is one of the seven national parks in Taiwan (refer to Figure 5.2 and Table L.2 in Appendix L), and was established to protect the wilderness mountain area that covers 76850 hectares, and the fauna and flora in it. There are 66 peaks over 1500 metres within the region; seventeen of them are listed in the "Hundred Summits of Taiwan", which details summits 3000 metres or over in height. **Shei-pa** is the combination of

Sheishan and Tapachienshan, where Sheishan, the "Snow Mountain" at 3886 metres above sea level, is the second-highest summit in Taiwan; and Tapachienshan, the "Gigantic Peaks" at 3600 metres above sea level, earns its name by the shape and size of the single 300-metre barrel-like rock formation at the top of the mountain, see Figure 5.1. In fact, the title of the park literally means the "National Park of Snow Mountains and Gigantic Peaks". Surrounded by the tropical lowlands, this Park provides a unique environment for a variety of scientific researches. More details are available in Tsai & Simpson (1992).

Little work has been done in the area, although the application of remote sensing to the geological environment was conducted recently (ERL, 1992). This study is aimed to contribute to the understanding of the topography in that area through the concept of fractal dimension.

5.3 Digital Elevation Models (DEMs)

The digital elevation model of Taiwan was generated from aerial photos by the Remote Sensing Unit of Energy & Resources Laboratories (ERL) in the Industrial Technology Research Institute (ITRI), Taiwan, the Republic of China (ERL, 1992). Figure 5.3 illustrates the digital elevation model plan of Taiwan. The whole area is divided into mosaics of squares. The squares are sequentially numbered. Each square is further divided into four quadrants, labelled I to IV in a clockwise direction, starting from the top-right hand corner of the square. An example is given in square 9519. Each quadrant is approximately 25×27 kilometres or 15.5×16.8 miles in size. Therefore, each square is about 50×54 kilometres or 31.1×33.6 miles. Because

of the persistent clouds in the mountain areas, some mosaics of the Taiwan digital elevation model are still blank, especially in the south-east of Taiwan.

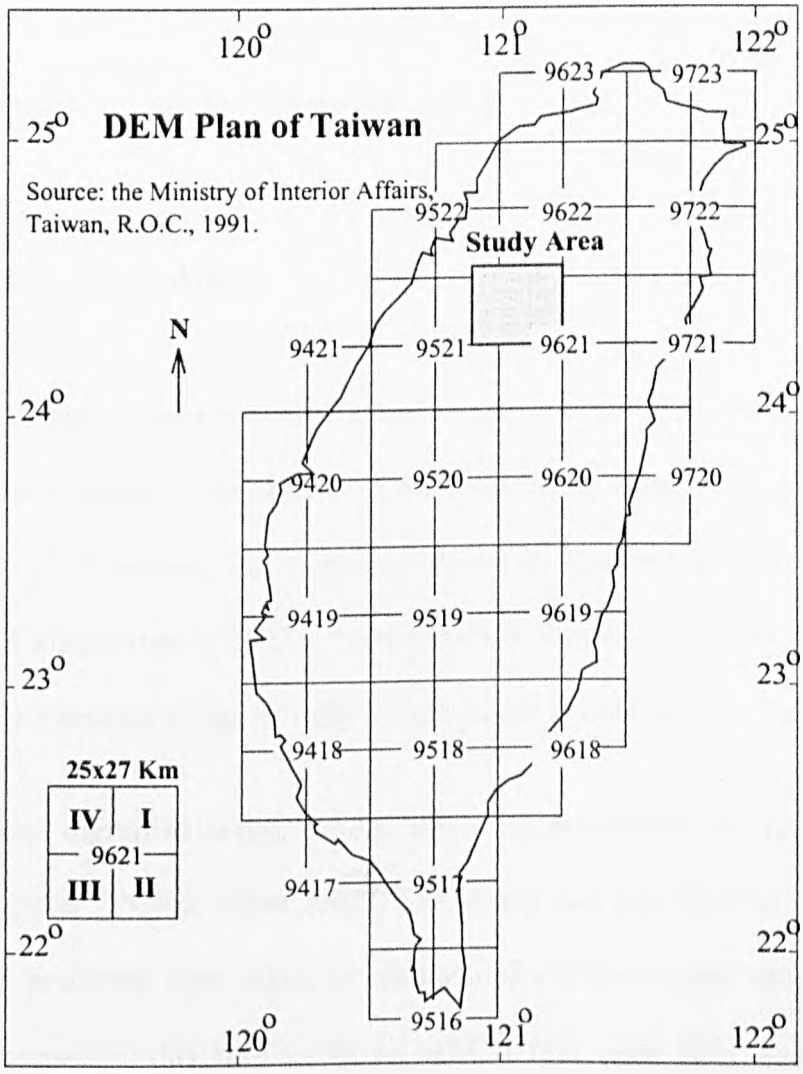

Figure 5.3: Digital Elevation Model Plan of Taiwan.
The island of Taiwan is divided into squares that are labelled with sequential numbers. Each square comprises of four quadrats arranged clockwise from the top-right hand corner, and centred at the sequential number. Each quadrant is about 25×27 kilometres or 15.5×16.8 miles, therefore, a square is about 50×54 kilometres or 31.1×33.6 miles. Islets are also sequenced but not shown here.

The Shei-pa National Park occupies an area of less than two quadrants, that is, 37.5×34.1 kilometres, or 936×853 pixels with 40 metres of resolution (ERL, 1992). Obviously, the size of the image in terms of pixels does not satisfy the requirement of the algorithms described in Chapters Three and Four. The algorithms usually

demand demand a data series of 2^n in length, where n is an integer. Therefore, the neighbouring area to the west of the Park is included to produce the target digital elevation model of 1024×1024 pixels. Refer to the study area in Figure 5.3 and the data decoding process in the following section.

5.3.1 Data Decoding

In the original digital elevation model, each quadrant contains 100 files or 100 unit images, and each image is about 2.5×2.8 kilometres or exactly 63×71 pixels with the resolution of 40 metres. By "stitching" the unit images together, a large image of 50.7×55.3 kilometres or 1267×1383 pixels is formed. Then by "clipping" the large image, the desired image of 1024×1024 pixels is obtained for further analyses.

The original digital elevation model files were generated and recorded by the personal computer (PC) in either ASCII[1] or binary and both formats (ERL, 1992); therefore, pre-processes were taken to render uniform the format used by the computer programmes in this thesis. In an ASCII file, each data point or pixel is represented by a single line containing x, y and z, that is, coordinates and height, respectively. The coordinates x and y are each of eight bytes, that is, seven digits and the appended space, while the height z is of eight or nine bytes. Because the height ranges from 0.0 to 4000.0 metres and recorded to three decimal digits, it is encoded in eight or nine bytes; that is, it includes the eight-byte real numbers and one-byte of "end-of-line" character. Since there are 63 rows and 71 columns of data points in a file, each file amounts to around 104 kilobytes (Kb).

[1] ASCII stands for *American Standard Code for Information Interchange* (Allen, 1990).

The ASCII file can be read by any computer text editor, given that it accommodates a huge quantity of data. Although it takes more than 100 Kb of computer memory to handle a single ASCII file, the ASCII files are comparatively easier to handle than binary ones, which are of 26 Kb in each file.

Each binary file consists of two parts of information, that is, the header and the body of data. The header, the first virtual line in the file, is of 400 bytes in length. However, it is encoded in three different formats; that is, the original programme uses a one-byte character to record the title of the file, a four-byte integer to record the structure of the data, and a blank space to fill the rest of the line. The first sixty bytes of the header, which record the title in a string of single byte, keep track of the organisation of the file names. The following forty-four bytes record eleven essential items of data in four-byte integers; and the items include four corners of the xy coordinates, the resolution, and numbers of rows and columns of the image. The rest of the header consists only of blank space to the end of the 400-byte block. The body of data contains only z values in sequence according to the information given in the header. It starts from the second virtual line of the 400-byte block, and goes on to the end of the file. Each line contains exact number of column data, followed by blank space. The number of lines in the data body is equal to the number of rows. Therefore, each file amounts to around 26 Kb.

It was recommended that the binary files should be decoded by the Fortran 77 program coming with the data files. For some reason, the Fortran 77 compiler on Sun workstation was not compatible with that on PC where the source codes were created. Therefore, the binary data have to be fully decoded as described earlier before any technique of uniformisation could be applied. However, an unexpected

problem was encountered when trying to decode the binary files. The integral and real numbers were unfortunately encoded differently between the PC where the files are stored, and the Unix workstation where the files are processed. A "virtual" mirror has to be used to read the four-byte integer between PC and Unix workstation; that is, the order of four-byte integer on the PC, for example, 1234, has to be mirrored to 4321, in order to be read on the Unix workstation. It was also essential to swap every two bytes in the real number part of the PC file in order that it could be read on the Unix workstation. At last, the structure of both ASCII and binary files were decoded and re-organised, using the computer programme particularly written for decoding and transforming the digital elevation model files into formats applicable to Geographical Information System (GIS) software such as IDRISI[2] (Eastman, 1992a; Eastman, 1992b). Refer to Appendix M for the programme listing.

5.3.2 The Target DEM Obtained

The digital elevation model used by IDRISI is stored in two files; that is, the text document file records the essential information to display the image and the binary file simply contains the heights row by row. However, the real numbers in the binary file have to be truncated to two-byte integers, implying that the range of heights is from 0.0 to 65536 metres. Fortunately, mountain heights in that area are well within the limit. The digital elevation model of the natural landscape is, therefore, obtained for subsequent analyses.

[2] IDRISI is a grid-based geographic information and image processing system developed by the Graduate School of Geography at Clark University, MA, USA.

5.4 Synthetic DEMs

Fractal features are the opposite of smooth curves and surfaces that, in terms of differential geometry, globally may have a very complicated structure but in small neighbourhoods they are narrow straight lines or planes. While the smooth objects yield no greater detail on smaller scales, a fractal possesses infinite detail at all scales, no matter how small they are. It is, therefore, "very suitable to simulate many natural phenomena" and also simple to generate without involving theory such as calculus, necessary for differential geometry (Saupe, 1988a, p.71).

Given that fractals have infinite detail at all scales, it follows that a complete computation of a fractal is impossible. Thus approximations of fractals down to some finite precision have to suffice. The desired level of resolution is naturally limited by constraints such as the numbers of pixels of the available graphics display. Saupe (1988a) proposed algorithms that fall into three categories, that is, the Fourier filtering method, the random cut method, and the midpoint displacement methods. Basically, in the midpoint displacement methods, an approximation of a random fractal with the initial resolution is used as input and the algorithm produces an improved approximation with resolution increased by a certain factor. This process is repeated with outputs used as new inputs until the desired resolution is achieved. The midpoint displacement methods are discussed further by other researchers (Nakagawa & Kobayashi, 1992; Shurtz, 1992; Huang *et al.*, 1992; Polodori & Chorowicz, 1993; Dixon *et al.*, 1994; Stoksik *et al.*, 1995, for example).

5.4.1 Definitions

Brownian motion, also referred to as "brown noise", constitutes the simplest random fractal, and it is the core of the following digital elevation model generations. Small particles of solid matter, for example, pollens, suspended in a liquid can be seen under a microscope to move about in an irregular and erratic way. This was observed by the botanist Brown around 1827, and modelling of this motion has become one of the greatest choices of statistical mechanics (Saupe, 1988a, p.74). In fact, Brownian motion is the special case of *fractional Brownian motion* stated below.

In one dimension, a fractional Brownian motion, $X(t)$, is a single valued function of one variable, usually time, t. Its increments $X(t_2) - X(t_1)$ have a Gaussian distribution with variance,

$$E[|X(t_2) - X(t_1)|^2] \propto |t_2 - t_1|^{2H}, \tag{5.1}$$

where E denotes ensemble averages over many samples $X(t)$ and the parameter H has a value $0 < H < 1$. Although $X(t)$ is continuous, it is nowhere differentiable. Such a function is both stationary and isotropic (Voss, 1988, p.58). Its mean square increments depend only on the time difference $t_2 - t_1$ and all t's are stationary equivalent. The special value $H = \frac{1}{2}$ is the Brownian motion mentioned above.

In higher dimensions, the generalisation of fractional Brownian motion is a multi-dimensional process of $X(t_1, t_2, ..., t_n)$ with two properties. That is, the increments $X(t_1, t_2, ..., t_n) - X(s_1, s_2, ..., s_n)$ are Gaussian with mean zero. Furthermore, the variance of the increments depends only on the distance,

$$\sqrt{\sum_{i=1}^{n}(t_i - s_i)^2}, \tag{5.2}$$

which is proportional to the $2H$-th power of the distance, thus,

$$E[|X(t_1, t_2, ..., t_n) - X(s_1, s_2, ..., s_n)|^2] \propto (\sum_{i=1}^{n}(t_i - s_i)^2)^H, \tag{5.3}$$

where $0 < H < 1$. The function X again has stationary increments and is isotropic, that is, all points and all directions are statistically equivalent (Saupe, 1988a, p.95).

5.4.2 Approximation

In one-dimensional space, Brownian motion can be approximated by random midpoint displacement, proposed by Saupe (1988a, pp.78-80). If the process is to be computed for time, t, between 0 and 1, then one starts by setting $X(0) = 0$ and selecting $X(1)$ as a sample of a Gaussian random variable with mean 0 and variance σ^2. Then $var(X(1) - X(0)) = \sigma^2$ and it is expected such that

$$var(X(t_2) - X(t_1)) = |t_2 - t_1|\sigma^2, \tag{5.4}$$

for $0 \leq t_1 \leq t_2 \leq 1$. $X(\frac{1}{2})$ is set to be the average of $X(0)$ and $X(1)$ plus some Gaussian random offset D_1 with mean 0 and variance Δ_1^2. Then

$$X(\frac{1}{2}) - X(0) = \frac{1}{2}(X(0) + X(1)) + D_1 \tag{5.5}$$

and $X(\frac{1}{2}) - X(0)$ has mean value 0 and the same holds for $X(1) - X(\frac{1}{2})$. Secondly, for Equation 5.4 to be true, it is required that

$$var(X(\frac{1}{2}) - X(0)) = \frac{1}{4}\, var(X(1) - X(0)) + \Delta_1^2 = \frac{1}{2}\, \sigma^2. \tag{5.6}$$

Therefore, $\Delta_1^2 = \frac{1}{4}\sigma^2$.

The next step proceeds in the same way, with setting

$$X(\frac{1}{4}) - X(0) = \frac{1}{2}(X(0) + X(\frac{1}{2})) + D_2 \tag{5.7}$$

and it is observed again that the increments, $X(\frac{1}{2}) - X(\frac{1}{4})$ and $X(\frac{1}{4}) - X(0)$, are Gaussian and have mean 0. So the variance Δ_2^2 of D_2 is chosen such that

$$var(X(\frac{1}{4}) - X(0)) = \frac{1}{4}\, var(X(\frac{1}{2}) - X(0)) + \Delta_2^2 = \frac{1}{4}\,\sigma^2 \tag{5.8}$$

holds, that is, $\Delta_2^2 = \frac{1}{8}\sigma^2$.

Continuing to finer resolution yields

$$\Delta_n^2 = \frac{1}{2^{n+1}}\,\sigma^2 \tag{5.9}$$

as the variance of the displacement D_n. In order to correspond to time differences $\Delta_t = 2^{-n}$, a random element of variance $2^{-(n+1)}\sigma^2$ is added, which is proportional to Δ_t. Figure 5.4 is the graphical presentation of the midpoint displacement method.

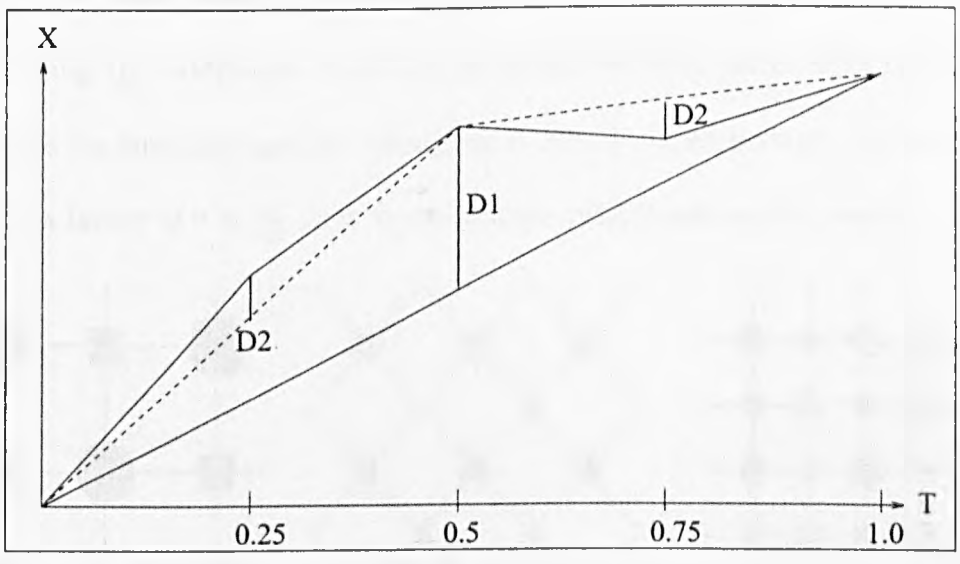

Figure 5.4: One-Dimensional Midpoint Displacement.
The first two stages in the midpoint displacement method.

For the approximation of fractional Brownian motion, the approach taken by the midpoint method can be formally extended to suit parameters $H \neq \frac{1}{2}$ (Saupe, 1988a, pp.84-87). Here the equivalence of Equation 5.4 is:

$$var(X(t_2) - X(t_1)) = |t_2 - t_1|^{2H}\sigma^2. \tag{5.10}$$

Following the same line of thought above, the midpoint displacements D_n is derived, which have variances:

$$\Delta_n^2 = \frac{\sigma^2}{(2^n)^{2H}}(1 - 2^{2H-2}). \tag{5.11}$$

However, it has been shown that the above midpoint displacement technique does not yield true fractional Brownian motion for $H \neq \frac{1}{2}$ (Mandelbrot, 1982). Nevertheless, this is still a useful and popular algorithm for many purposes, since its appearance in Fournier *et al.* (1982a; 1982b).

The midpoint displacement method can work with square lattices of points (Saupe, 1988a, pp.96-105). If the mesh size S denotes the resolution of a grid, another square grid of resolution of $\frac{S}{\sqrt{2}}$ is obtained by adding the midpoints of all squares. The orientation of the new square lattice is now rotated by 45 degrees. Again adding the midpoints of all squares gives the next lattice with the same orientation as the first one and the resolution is now $\frac{S}{2}$. In each stage, the resolution is scaled by a factor of $r = \frac{1}{\sqrt{2}}$, and in accordance with Equation 5.3, random displace-

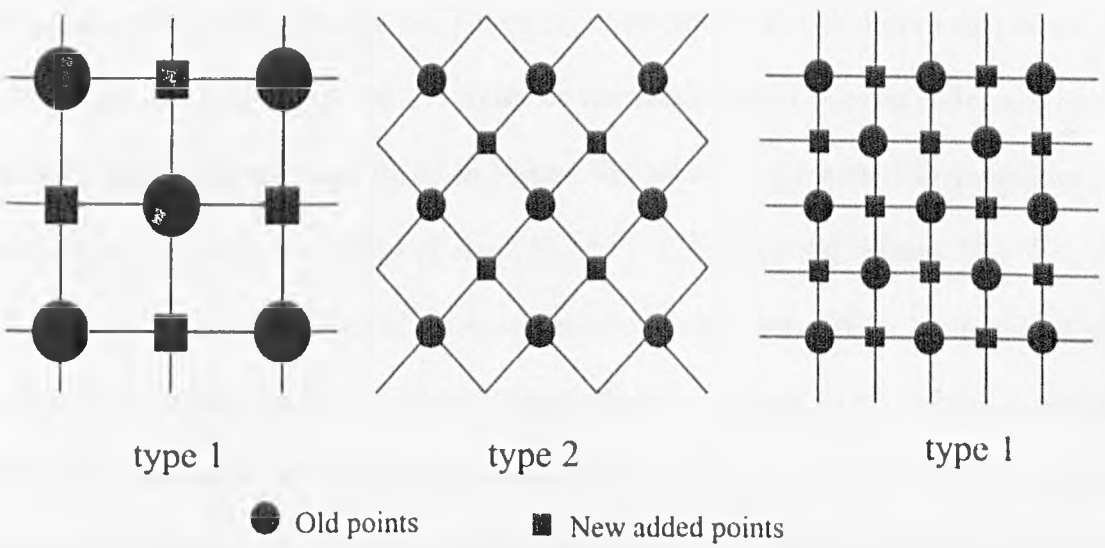

Figure 5.5: Two-Dimensional Midpoint Displacement.
Grid type 1 is given at the beginning from which grid type 2 is generated. The mean size of type 2 is $1/\sqrt{2}$ times the old mesh size. In a similar step a grid type 1 is again obtained. Source: Saupe (1988a, p.96).

ments are added using a variance which is r^{2H} times the variance of the previous stage. If four corner points of the grid are assumed to carry mean square increments of σ^2, then at stage n of the process, a Gaussian random variable of variance $\sigma^2 r^{2Hn} = \sigma^2(\frac{1}{2})^{nH}$ must be added. Refer to Figure 5.5.

For the usual midpoint method, random elements are added to only the new midpoints in each stage, whereas in this random addition method, displacements are added at all points (Saupe, 1988a, p.96). Adding random elements to all points gives more control over the statistical property of the synthetic model. The feasibility of such an algorithm is unique; for example, the random addition is kept permanently applicable in the Fourier filtering method (Saupe, 1988a, p.108). Another advantage of using the algorithm described below is that it unites both methods.

5.4.3 Implementation

The random fractal landscape used here is generated by the midpoint displacement method (Saupe, 1988a, pp.100-1). Refer to the Basic-styled pseudo codes are modified from Saupe (1988a) and listed in Figure 5.6, whereas the actual C programme is detailed in Appendix N. A grid of size $(N+1)^2$, X, is assumed, where $N = 2^{maxlevel}$ and *maxlevel* is the final level of resolution given by the user. Other assigned parameters are the initial standard deviation (*sigma*) which is used as the initial resolution of the grid, parameter H which determines fractal dimension by $D = 3 - H$, boolean parameter *addition* which turns random additions on or off, and *seed* value for random number generator. The function $f3$ is given to interpolate and offset boundary grid points from type 2 to type 1 transformation, whereas function $f4$ is used to

Algorithm: $midFM2D()$	Comments
$f3(S, x0, x1, x2) = (x0 + x1 + x3)/3 + S * Gauss()$	
$f4(S, x0, x1, x2, x3) = (x0 + x1 + x2 + x3)/4 + S * Gauss()$	
$srand(seed)$	Introduces seed value for $rand()$
$addition$	Boolean parameter
$S = sigma$	Variable
$X[i][j] =$ offset	Initialising X with offset value
$X[0\|N][0\|N] = S * Gauss()$	Assigning four corner points of X
$D = N; d = N/2$	Variables
for $level = 1$ to $maxlevel$ do	**Repetition**
$S = S * 0.5^{0.5*H}$	**Going from type 1 to type 2**
for $i = d$ to $N - d$ step D do	*Interpolate and offset points*
for $j = d$ to $N - d$ step D do	
..... $X[i][j] = f4(S, X[i+d][j+d], X[i+d][j-d], X[i-d][j+d], X[i-d][j-d])$	
if $addition$ then	*Random addition*
for $i = 0$ to N step D do	
for $j = d$ to N step D do	
..... $X[i][j] = X[i][j] + S * Gauss()$	
$S = S * 0.5^{0.5*H}$	**Going from type 2 to type 1**
for $i = d$ to $N - d$ step D do	*Interpolate and offset boundary points*
$X[i][0] = f3(S, X[i+d][0], X[i-d][0], X[i][d])$	
$X[i][N] = f3(S, X[i+d][N], X[i-d][N], X[i][N-d])$	
$X[0][i] = f3(S, X[0][i+d], X[0][i-d], X[d][i])$	
..... $X[N][i] = f3(S, X[N][i+d], X[N][i-d], X[N-d][i])$	
for $i = d$ to $N - d$ step D do	*Interpolate and offset interior points*
for $j = D$ to $N - d$ step D do	
$X[i][j] = f4(S, X[i][j+d], X[i][j-d], X[i+d][j], X[i-d][j])$	
for $i = D$ to $N - d$ step D do	
for $j = d$ to $N - d$ step D do	
..... $X[i][j] = f4(S, X[i][j+d], X[i][j-d], X[i+d][j], X[i-d][j])$	
if $addition$ then	*Random addition*
for $i = 0$ to N step D do	
for $j = d$ to N step D do	
$X[i][j] = X[i][j] + S * Gauss()$	
for $i = d$ to $N - d$ step D do	
for $j = d$ to $N - d$ step D do	
..... $X[i][j] = X[i][j] + S * Gauss()$	
$D = D/2; d = d/2$	Reset variables

Figure 5.6: Basic-style Pseudo Codes for Generating Landscapes.
At each level of resolution, data points are added by transformations from type 1 to type 2 then from type 2 to type 1. Repeat the process until it reaches the preset level of resolution. Random addition is performed if it is specified. Modified from Saupe (1988a, pp.100-1).

interpolate and offset interior points, that is, to add new points, from type 1 to type 2 transformation.

The grid X is initially set to an offset value. Four corner points of the grid are initialised by the algorithm, *Gauss()*, that generates Gaussian random numbers with normal distribution, $N(0,1)$. The algorithm assumes that the machine has a pseudo random number generator routine, *rand()*, that returns random numbers uniformly distributed over some interval $[0, A]$, where A is typically $2^{31}-1$ or $2^{15}-1$. Here, the random numbers are generated by the *rand()* routine on the Sun UNIX workstation (Sun4m of SunOS 4.1.3_U1 v.1), where A is $2^{15}-1$. There also exists a routine *srand(seed)*, which introduces a *seed* value for *rand()*. Taking certain linearly scaled averages of the values returned by *rand()* will approximate a Gaussian random variable. Refer to Saupe (1988a, p.77) and pseudo codes in Figure 5.7.

Algorithm: *Gauss*()	Comments
srand(seed)	Introduce seed value for *rand*()
$Nr = 4$	Number of samples of *rand*()
$A = 2^{15} - 1$	Range of *rand*()
$Add = \sqrt{(3 * Nr)}$	Real parameter for linear transformation
$Fac = 2 * Add/(Nr * A)$	Real parameter for linear transformation
$sum = 0$	Variable
for $i = 1$ to Nr do	Calculation
$sum = sum + rand()$	
$Gauss = Fac * sum - Add$	Returned Gaussian random number

Figure 5.7: Basic-style Pseudo Codes for Generating Gaussian Random Number. Modified from Saupe (1988a, p.77).

At resolution level one, new points are added to midpoints of grids going from type 1 to type 2 then from type 2 to type 1 again. Grid transformation from type 1 to type 2 utilises function $f4$, which interpolates and offsets points. If the boolean

parameter *addition* is turned on, random addition is performed. Grid transformation from type 2 to type 1 uses function $f3$, which interpolates and offsets boundary grid points. The interior grid points are calculated by function $f4$. As before, random addition is performed if the boolean parameter *addition* is turned on. The process is repeated until the final level of resolution is reached. At the end of the process, a binary image and, in order to be applicable in IDRISI, a text document file are generated for subsequent analyses. Furthermore, various digital elevation models can be obtained by altering the parameters of the computer programme. Details of the above C programmes are listed in Appendix N.

5.5 Analysis

Conventional methods are used to extract terrain information such as aspects, slopes and elevations, then followed by the fractal analysis that calculates the fractal dimensions from both the synthetic and natural digital elevation models. Statistical techniques are also used to compare the results obtained.

5.5.1 General Terrain Information

General terrain information depicted here includes aspects and slopes. The slope at any pixel of the raster image is determined by comparing the height to that of each of its neighbouring pixels. It is determined by calculating the maximum slope around each pixel from the local slopes in X and Y. Only the neighbours above, below, and to either side of the pixel were accounted for in this procedure. Slopes

are expressed either in decimal degrees or percentages. Essentially, creating a slope map requires that the spacing of contours be evaluated over the whole map. These neighbour relations are then used to determine the context elements such as the direction that the slope is facing, known as the *aspect*, and the manner in which sunlight would illuminate at that point given a particular sun position, known as *analytical hill-shading*. Aspects were indicated in decimal degrees, using standard azimuth designations, 0 to 360, clockwise from north.

Implementation of the above is relatively simple, since there is much Geographical Information System (GIS) software available that provides such standard functions. Here, the package called IDRISI is used to derive the slope and aspect maps and the statistics associated with the maps.

5.5.2 The Fractal Analysis

A statistically self-similar fractal is by definition isotropic. A formal definition of a self-similar fractal in a two-dimensional xy-space is that $f(rx, ry)$ is statistically similar to $f(x, y)$ where r is a scaling factor (Turcotte, 1992, p.74). It satisfies Equation 3.1 in Chapter Three and has the form of

$$N = \frac{C}{r^D}, \tag{5.12}$$

where C is a constant. Here, the number of boxes with dimensions (x_1, y_1) required to cover. For example, a rocky coastline is N_1, and the number of boxes with dimensions $(x_2 = rx_1, y_2 = ry_1)$ required to cover a rocky coastline is N_2. If the coastline is a self-similar fractal, the fractal dimension is derived from $N_2/N_1 = r^{-D}$ (see also Equation 3.2 in page 63).

A statistically self-affine fractal is not isotropic. A formal definition of a self-affine fractal in a two-dimensional xy-space is that $f(rx, r^H y)$ is statistically similar to $f(x, y)$ where H is known as the Hurst measure. The Hurst measure is related to fractal dimension, D, topological dimension, D_T, and Euclidean space, D_E, as follows (Mandelbrot, 1983, pp.15 & 249):

$$H = D_E - D \quad or \quad H = D - D_T, \tag{5.13}$$

because $D_T \leq D \leq D_E$ and $0 < H < 1$.

The box-counting method can be used to determine the Hurst measure hence fractal dimension of an elevation. However, the box size must be scaled using the Hurst measure. If N_1 is the number of boxes with dimensions (x_1, y_1) required to cover the elevation and N_2 is the number of boxes with dimensions $(x_2 = rx_1, y_2 = r^H y_1)$, then the elevation is a self-affine fractal if $N_2/N_1 = r^{-D}$. Several other aspects of self-affine fractals need to be considered. However, Turcotte (1992, p.74) has proved that a random walk in two-dimensional space satisfies

$$H = 2 - D. \tag{5.14}$$

A discussion on estimation of fractal dimension has been given in Chapter Three; and a practical derivation of the fractal dimension of a self-affine linear feature is given here by Turcotte (1992, p.76). Firstly, a rectangular reference "box" is taken with a width T and height $\sigma_T = \sigma(T)$. Note that since the units of the signal hence the units of standard deviation can differ from the unit of time, the aspect ratio (width/height) of the box can have arbitrary units.

Secondly, the time interval T is divided into n smaller time intervals with the length $T_n = T/n$. Therefore, scaled smaller boxes of width, T_n, and height, $\sigma_n =$

σ_T/n, are introduced. These boxes have the same aspect ratio as the reference box. However, the standard deviation associated with the interval T_n, $\sigma_{T_n} = \sigma(T_n) = \sigma(T/n)$, is not equal to σ_n. Then numbers of scaled smaller boxes of size $T_n \times \sigma_n$, N_n, that are required to cover the area of width T and height σ_{T_n}, are determined. This is given by

$$N_n = \frac{T\sigma_{T_n}}{T_n\sigma_n} = n^2\frac{\sigma_{T_n}}{\sigma_T}. \tag{5.15}$$

Since $\sigma(T) \sim T^H$ (Voss, 1988; Turcotte, 1992), the relation below holds,

$$\frac{\sigma_{T_n}}{\sigma_T} = \frac{\sigma(T/n)}{\sigma(T)} = \left(\frac{T/n}{T}\right)^H = \frac{1}{n^H}. \tag{5.16}$$

The above two equations combine to give

$$N_n = n^{2-H} = \left(\frac{T}{T_n}\right)^{2-H}. \tag{5.17}$$

This is basically a fractal relation if T_n is associated with r_n. The relation $2-H = D$ is obtained, if the above is compared with the definition of fractal dimension in Equation 5.12.

In order to examine the diversity of the system, the box-counting method is applied to latitudinal and longitudinal profiles, regarded here as sub-systems. This unique approach is aimed to reveal the systems dynamics in a very different way from the "single measure" approach and the "dimension map" approach, as described earlier in Chapter Two. The box-counting method is implemented with the core routine that was detailed in Chapter Three and used for the sea waves in Chapter Four, and supporting routines that are mainly used to organise the data.

Implementation

The algorithm $DemFD()$ is the main programme for calculating fractal dimensions from profiles of a digital elevation model (Figure 5.8). It includes the sub-routine, $BoxFD()$, which returns the fractal dimension of a time series. Refer to the Basic-style pseudo code of $BoxFD()$ in Figure 3.4 and its C programme listing in Appendix E. The main programme reads image into array, extracts horizontal or vertical

Algorithm: *DemFD(InImage,width,length,H/V)*	
$w = width$;	Variable
$h = height$	Variable
$ReadImage(InImage, XY, w, h)$	Reads image into array XY[w][h]
if H do	Horizontal profiles are chosen
for $i = 1$ to h do	Obtains horizontal profile
$ExtArray(X, XY, w, h, i, H)$	Extract i-th H profile from XY
$Stats1(X, w, S)$	Calculates standard deviation, S
$Dh[i] = BoxFD(X, w, S)$	Calculates D
$Ouput(Dh, h)$	Prints out $Dh[h]$
if V do	Vertical profiles are chosen
for $i = 1$ to W do	
$ExtArray(X, XY, w, h, i, V)$	
$Stats1(X, h, S)$	
$Dv[i] = BoxFD(X, h, S)$	
$Ouput(Dv, w)$	
Sub-Routine: ReadImage(Image,XY,m,n)	Reads image into array XY[m][n]
Sub-Routine: ExtArray(X,XY,m,n,i,H/V)	Extract H/V profile, X
Sub-Routine: Stats1(X,n,S)	Returns standard deviation from X
Sub-Routine: BoxFD(X,n,S)	Returns D. See Figure 3.4
Sub-Routine: Output(D)	Prints out D

Figure 5.8: Basic-style Pseudo Codes for Estimating Fractal Dimension from DEM. This routine reads in the input image, then extracts profiles upon which the procedure of estimating fractal dimension is performed.

profiles from the array, calls sub-routine $BoxFD()$ to obtain the fractal dimension, and prints out the resultant fractal dimensions. Refer to the Basic-style pseudo codes for estimating fractal dimensions from digital elevation models in Figure 5.8 and the complete C programme listing in Appendix O.

Before the routine starts, the user needs to supply the title of the input image and its dimensions, *width* and *height*, and decide whether to calculate fractal dimensions from horizontal or vertical profiles. First of all, the input image is read into an array, because it takes a much shorter time for the computer to deal with an array than with an image file and/or its related document.

Assume that horizontal profiles are selected. The sub-routine $ExtArray()$ will extract a single profile from the array obtained above, according to the parameters given. The standard deviation of this profile, which is the height of the reference box in box-counting method, is calculated using the sub-routine $Stats1()$. The sub-routine $BoxFD()$ detailed earlier is called to perform the estimation of fractal dimension. The above procedure is repeated for each profile. The sub-routine $Ouput()$ is called to print out the results of calculated fractal dimensions. Similarly, the main routine will skip to another set of parameters, if calculation of vertical profiles is selected.

5.5.3 Making Comparisons

The statistical test procedure was explained in Chapter Three, and is repeated briefly as follows. The Shapiro and Wilk's W test is performed to test whether the data distribution is normal; then it is followed by the non-parametric two-sample Mann-Whitney U test, because, most likely, the data are not normally distributed. Two sets of samples with known statistical parameters are also included to help interpret the test results.

5.6 Results

General terrain information such as the aspect, slope and elevation is presented; then followed by the fractal dimensions of the digital elevation models. Comparisons are subsequently made between the synthetic and natural landforms.

5.6.1 The Natural Landform

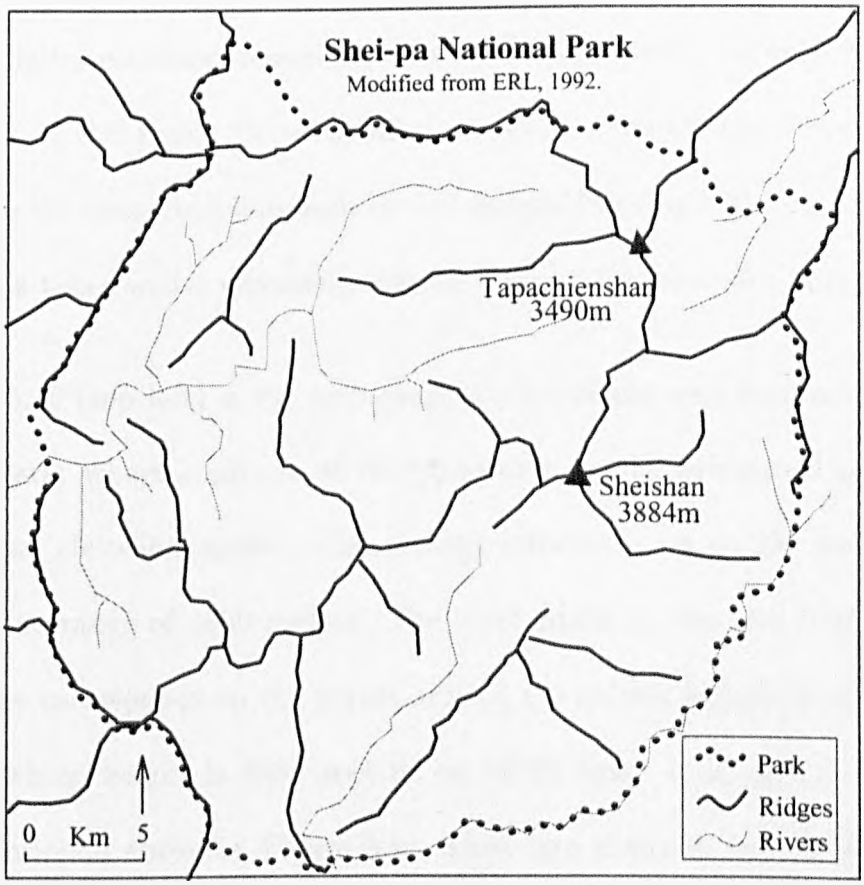

Figure 5.9: The Ridges and Rivers of the Shei-pa National Park.
The Park obtains its name from the summits of **Shei**shan (the Snow Mountain) and **Tapa**chienshan (Gigantic Peaks). Modified from ERL (1992)

Figure 5.9 shows the rugged mountains that dominate the Shei-pa National Park area. The western part of the area, which descends to the plain along the west coast, appears to be smoother than that in the east. The ridges run along the direction

from north-east to south-west. In fact, these ridges are the northern part of the Central Ridges. Rivers begin their flow among the peaks in the Park area. Because of the formation of the ridges, some of the rivers merge with the Taiwan Strait to the west, while others join the Pacific Ocean to the east coast of the island (Figure 5.2). There are 76850 hectares of complex ridges and rivers in the Park. For example, mountaineers cannot reach the summit of Tapachienshan without rock-climbing skills, because the iron ladder and chains built during the Japanese occupation of Taiwan were dismantled immediately after the Park was established in 1992. However, the digital elevation model used in this study covers the neighbouring area to the west of the Park. Some missing mosaics are inevitable, since this digital elevation model comprises hundreds of unit images (Section 5.3) formed from aerial photographs taken under genuinely tropical and marine weather (Appendix L).

Figure 5.10 (top left) is the orthographic view of the area surrounding Shei-pa National Park, where contours of the same area are superimposed onto the top of the digital elevation model. The contour interval is set to 250 metres, or 820 feet, with the range of 4000 metres. The black patch at the east (top right) edge of the figure corresponds to the region around the second highest peak of Taiwan, Sheishan, whose height is 3883 metres, or 12739 feet. It is part of the Central Ridges mentioned above in Figure 5.9. There are rivers in the valleys alongside the ridges. To the west, they join the flat plain which is very close to the sea. The histogram of height, not shown here, indicates that, under 2250 metres, there are two concentrated frequencies between 500 and 750, and between 1750 and 2000 metres. However, the percentages, ranging from 7.7% to 9.8%, are relatively similar between these two intervals. The area higher than 2250 metres occupies almost

one-fifth (19.7%) of the image. The overall average height is 1446 metres.

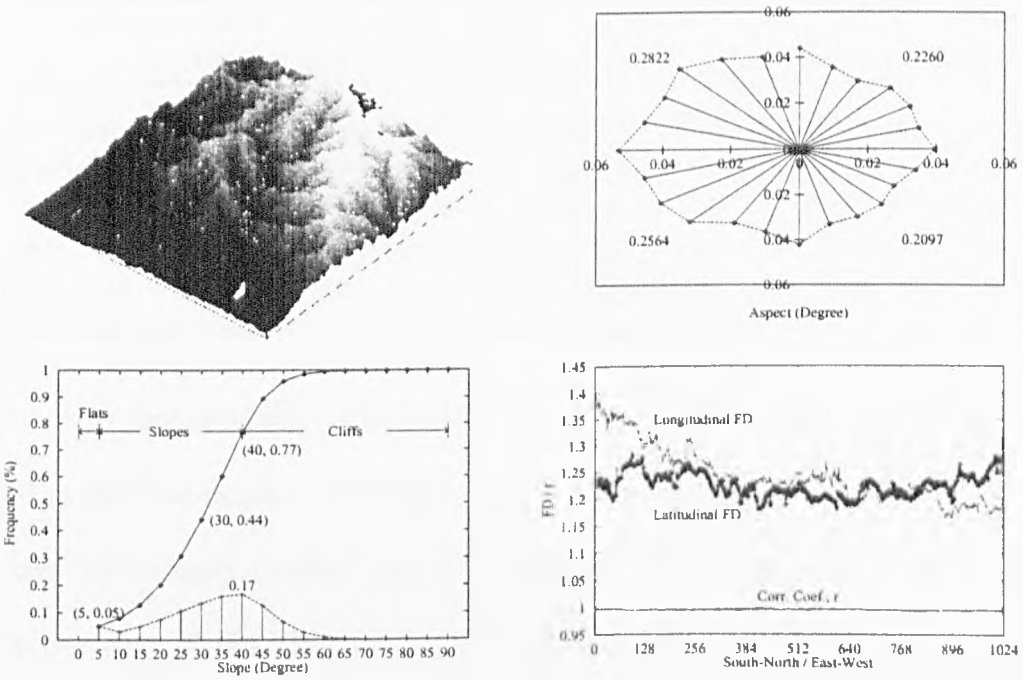

Figure 5.10: Terrain Information and Fractal Dimensions of Shei-pa National Park. Aspects and slopes are measured in degrees but displayed in polar and Euclidean coordinates, respectively. Fractal dimensions of longitudinal and latitudinal profiles are meaningful, for the correlation coefficients are high ($r > 0.99$).

The complexity of the area can be revealed by its aspects and slopes. Figure 5.10 (top right) shows the aspects of the region. The aspect is the direction the maximum slope faces, ranging from 0 to 360 degrees, clockwise from north. Therefore, it is best presented with polar coordinates. In this figure, each direction is equally spaced by 15 degrees. The sub-total of each quadrant is also given. However, this figure does not include the totally flat area which has no aspect reading. It shows that there are slightly more north-facing ($0.226 + 0.2822 = 50.82\%$) than south-facing ($0.2097 + 0.3564 = 46.61\%$) slopes. Also, there are more west-facing ($0.2822 + 0.2564 = 53.86\%$) than east-facing ($0.2260 + 0.2097 = 43.57\%$) slopes. Note that it does not include 2.57% of the totally flat area.

Data	n	min	max	$\bar{x}$	std	$Skew$	$Kurt$	W	$c.s.l$
NS	1024	-3.248	3.248	0.000	0.999	0.000	-0.044	0.988	0.7667
RN		-2.893	4.114	0.000	0.972	0.185	0.272	0.988	0.7760
Lat.	1024	1.180	1.696	1.226	0.027	5.294	85.230	0.827	0.0000*
Long.		1.164	1.401	1.243	0.053	0.993	0.185	0.886	0.0000*

Table 5.1: Comparison of Fractal Dimensions between Profiles of Natural Landform. Normality test (W) is performed against 5% significance level. If it is not normally distributed, indicated by low *c.s.l.*, it is marked by " * ". "NS" is the normal scores and "RN" is the random numbers from $N(0.0, 1.0)$. The Mann-Whitney U test shows that $U = 4.6e5$ and $z = -4.405$. Therefore, the difference between latitudinal and longitudinal profiles is significant ($p = 0.00*$).

Figure 5.10 (bottom left) is the histogram of slopes of the study area. Slopes are indicated in decimal degrees, ranging from 0 to 90 degrees. The flat area is defined as the area with slopes smaller than five degrees (Rice, 1988, p.137) and occupies only five per cent of the total area. According to the theoretical slope profile of Dalrymple *et al.* (1968, p.62), also cited in Summerfield (1991, p.181), landforms between 26 and 35 degrees are called transportational mid-slope. However, from the point of view of Rice (1988, p.137), 72 per cent of the area is comprised of slopes of between five and 40 degrees. Landforms steeper than that are called fall face (Summerfield, 1991) or cliffs (Rice, 1988). More than one-fifth (23%) of the area falls into that category. That is, material in this 23% area tends to roll or slide further downhill. In summary, the "flat" area occupies only 5% of the area, 72% is "slope", and more than one-fifth, 23% is "cliff" or "fall face".

Fractal dimensions are displayed in Figure 5.10 (bottom right) and the related statistics are summarised in Table 5.1. The average fractal dimensions are 1.23 and 1.24 for latitudinal and longitudinal profiles, respectively. The corresponding correlation coefficients ($r = 0.99$) are much higher than the critical value of 0.67, thus confirm that the derived fractal dimensions are meaningful. The distribution of fractal dimensions from latitudinal profiles is more wide-ranged, skewed and peaked

than that from longitudinal profiles. The one-sample normality test (W) shows that neither is normally distributed, and the two-sample Mann-Whitney U test shows that the difference of distributions of fractal dimensions between the two sets of profiles is significant.

The fractal dimensions of profiles actually reflect the ground truth, given the figure 5.10 and Table 5.1. For the longitudinal profiles, the number of high fractal dimensions in the mountainous areas in the east is balanced out by the number of low fractal dimensions in the rolling plain in the west. On the other hand, the fractal dimensions estimated from latitudinal profiles are highly concentrated at a certain value; and relatively few high and low dimensions indicate that most latitudinal profiles are similar in some way. The orthographic view of the area gives a visual impression of the difference in the profiles. Although the mean fractal dimensions of both sets of profiles are very close, it is obvious that they cannot solely be used to interpret the landform.

5.6.2 Synthetic Landforms

Some synthetic landform examples are presented in Figure 5.11 and more are given in Appendix P. The contours are generated by the UN-supervised contour plotting technique, one of the built-in functions of the *gnuplot* plotting programme UNIX version 3.2. Five levels of contours are generated for landform of a lower H value, while ten levels are assigned to that of a higher H value. In order to have a clear illustration, the resolution of each landform is reduced to 32×32 pixels; however, all subsequent analyses are based on the normal size of 1024×1024 pixels.

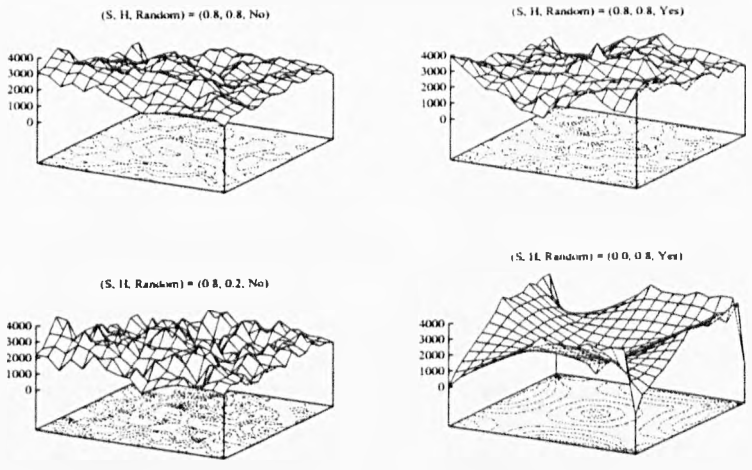

Figure 5.11: Some Synthetic Landforms.
Parameters controlling the simulation include the initial variation of landform, S, the Hurst exponent, H, and the random addition switch. While the randomness adds complexity to the landforms of the same H value, the complex of landforms is mainly controlled by the H values. However, both parameters have no impact on the flat initial surface ($S = 0.0$).

There are three main parameters that control the synthetic process, that is, initial variation of landform (S), the Hurst exponent (H) and the random addition switch. The complexity of the landforms is mainly controlled by the H values; that is, the lower H values produce landforms of higher complexity. The randomness adds complexity to the landforms of the same H value; and it is arguable that it gives a more natural appearance to the generated landforms. Comparatively little difference on the generated landforms is introduced by various initial surfaces, although a flat initial surface ($S = 0.0$) produces the uniform landscape that cannot be altered by the other two parameters.

Figure 5.12 presents some results from the analysis of the example landforms in Figure 5.11. The histogram of heights in metres shows that landforms of lower H values tend to concentrate in narrower range of heights. The odd landform with a flat initial variation of land, $S = 0.0$, shows two frequency peaks of heights. Aspects

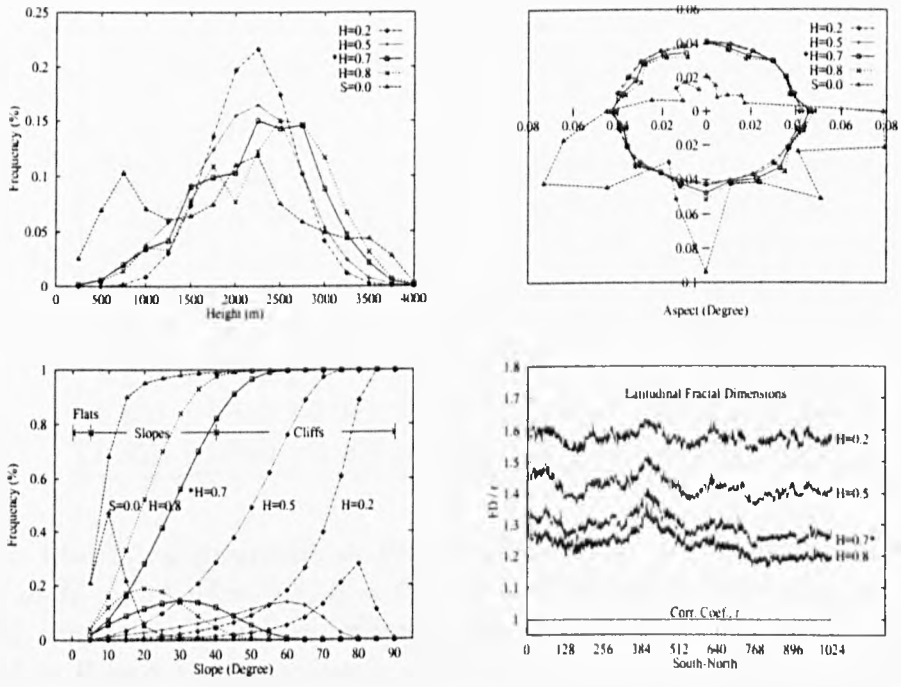

Figure 5.12: Terrain Information and Fractal Dimensions of Synthetic Landforms. General terrain information such as heights, aspects and slopes are presented. The fractal dimensions of latitudinal profiles are also given.

are equally distributed for every landforms except the one with flat intimal surface. The slope measurements for various H values are given in degrees. The percentages of flats, slopes and cliffs can be seen by the cumulative frequency of slopes. A low H value has a high percentage of steep slopes. As the H value increases, the concentration of measurements tends to shift towards less steep slopes. A fair amount of gentle slopes is found in landform of $H = 0.8$. The landform generated with $S = 0.0$ is rather different from others, where flats and slow slopes occupy most of the area. All the estimated fractal dimensions are meaningful, given the high correlation coefficients ($r > 0.99$).

The results of one-sample statistical tests are given in Table 5.2. All the fractal estimates of both latitudinal and longitudinal profiles are statistically meaningful, given the high correlation coefficients ($r > 0.99$). The average fractal dimensions

Data	n	min	max	$\bar{x}$	std	$Skew$	$Kurt$	W	$c.s.l$
H2.H	1024	1.520	2.336	1.576	0.032	12.943	302.813	0.621	0.0000*
H2.V		1.503	1.665	1.563	0.022	-0.045	-0.073	0.986	0.2904
H5.H		1.357	2.105	1.423	0.038	5.924	98.978	0.805	0.0000*
H5.V		1.318	1.672	1.390	0.037	0.758	2.682	0.951	0.0000*
H7.H		1.221	1.934	1.296	0.041	4.037	55.060	0.862	0.0000*
H7.V		1.168	1.708	1.248	0.048	1.441	8.987	0.917	0.0000*
H8.H		1.159	1.857	1.235	0.042	3.490	45.792	0.879	0.0000*
H8.V		1.095	1.719	1.179	0.050	2.093	13.952	0.895	0.0000*
S0.H		0.951	1.399	0.986	0.021	9.442	160.098	0.546	0.0000*
S0.V		0.925	1.260	0.964	0.024	3.512	29.280	0.801	0.0000*

Table 5.2: Statistical Summary of Fractal Dimensions of Synthetic Landforms. Landforms of $H = 0.2$, $H = 0.5$, $H = 0.7$, $H = 0.8$ and $S = 0.0$ are denoted as H2, H5, H7, H8, and S0, respectively, whereas the latitudinal and longitudinal profiles are denoted as H and V, respectively.

of latitudinal profiles from landforms of $H = 0.2$, $H = 0.5$, $H = 0.8$ and $S = 0.0$ are 1.576, 1.423, 1.235 and 0.986, respectively. Although the distribution of fractal dimensions for each landform is not greatly dispersed, it is rather skewed and peaked. The normality W test indicates that none of them is normally distributed. The average fractal dimensions of longitudinal profiles from landforms of $H = 0.2$, $H = 0.5$, $H = 0.8$ and $S = 0.0$ are 1.563, 1.390, 1.179 and 0.964, respectively. Apart from landform of $H = 0.2$ whose fractal dimensions are normally distributed, the others are not normally distributed. In general, the skewness and kurtosis values are comparatively smaller than those of latitudinal profiles.

Landform with $S = 0.0$ is a special case among others, for its average fractal dimensions are very close to a line which has a fractal dimension of 1.0. This implies that the profiles of such a landform are as smooth as a straight line. Refer to Figure 5.11 (bottom right) for its geomorphology.

The theoretical fractal dimensions for landforms of $H = 0.2$, $H = 0.5$, and

Theoretical Dimensions	Calculated Dimensions
$H = 0.2$ / $D = 1.8$	$D \approx 1.6$ (1.50, 1.66)
$H = 0.5$ / $D = 1.5$	$D \approx 1.4$ (1.35, 1.67)
$H = 0.7$ / $D = 1.3$	$D \approx 1.3$ (1.22, 1.70)
$H = 0.8$ / $D = 1.2$	$D \approx 1.2$ (1.16, 1.72)

Table 5.3: The Theoretical and Calculated Fractal Dimensions of Synthetic DEMs.

$H = 0.8$ are 1.8, 1.5, and 1.2, respectively. In general, the calculated dimensions are reasonably close to the theoretical values, especially at the higher H values (Table 5.3). The most accurate calculated dimension is from the landform of $H = 0.7$. Furthermore, having compared it with Figure 5.10, the synthetic landform of $H = 0.7$ was found to be similar to the natural counterpart in many respects; for example, the distribution of aspects, slopes and the measurements of the fractal dimensions are all similar between them. Therefore, the specific landform of $H = 0.7$ is isolated

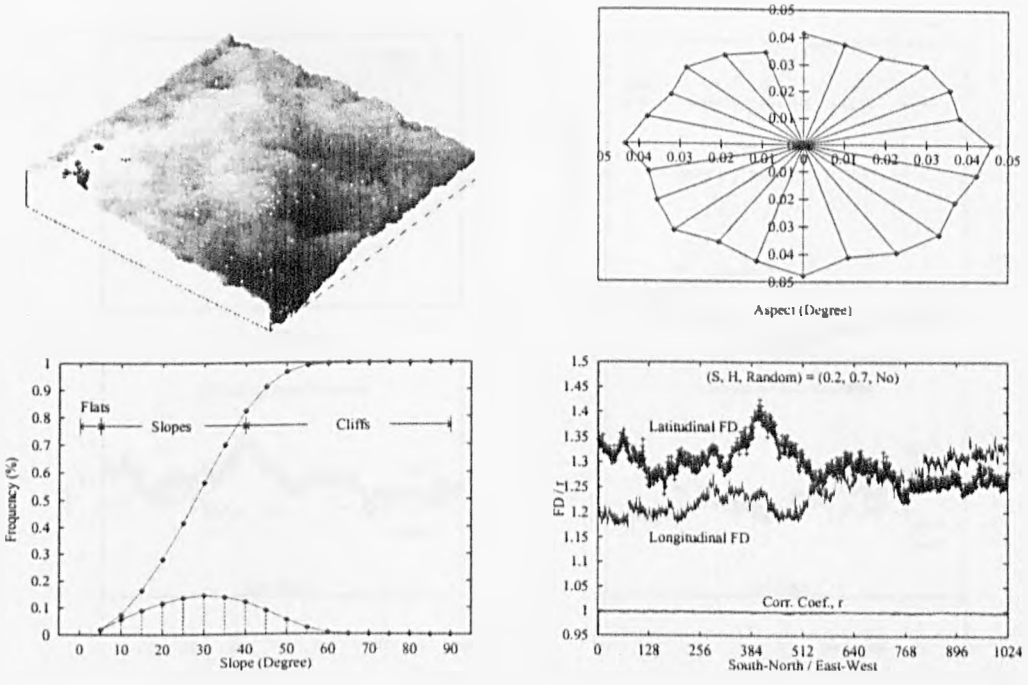

Figure 5.13: Terrain Information and Fractal Dimensions of the Landform $H = 0.7$. Aspects and slopes are measured in degrees but displayed in polar and Euclidean coordinates, respectively. The fractal dimensions of latitudinal and longitudinal profiles are meaningful, for the correlation coefficients are high ($r > 0.99$).

here for further analysis.

Figure 5.13 shows the orthography, aspects, slopes and fractal dimensions of landforms with $S = 0.2$ and $H = 0.7$. The orthography is produced by superimposing a map of sixteen contours of 250-metre resolutions on top the original image. The aspect chart reveals that there are slightly more slopes facing east than west. There are around 80% of slopes and 20% of cliffs on the synthetic landform. The fractal dimensions are of an average of 1.296 and 1.248 for latitudinal and longitudinal profiles, respectively, and the corresponding correlation coefficients are high ($r > 0.99$). The result from the Mann-Whitney U test ($p = 0.00*$; Table 5.4) indicates that there is significant difference in the distribution of the fractal dimensions between latitudinal and longitudinal profiles. The estimated fractal dimensions are shown to be very close to theoretical values of 1.3, and, indeed, the natural landform.

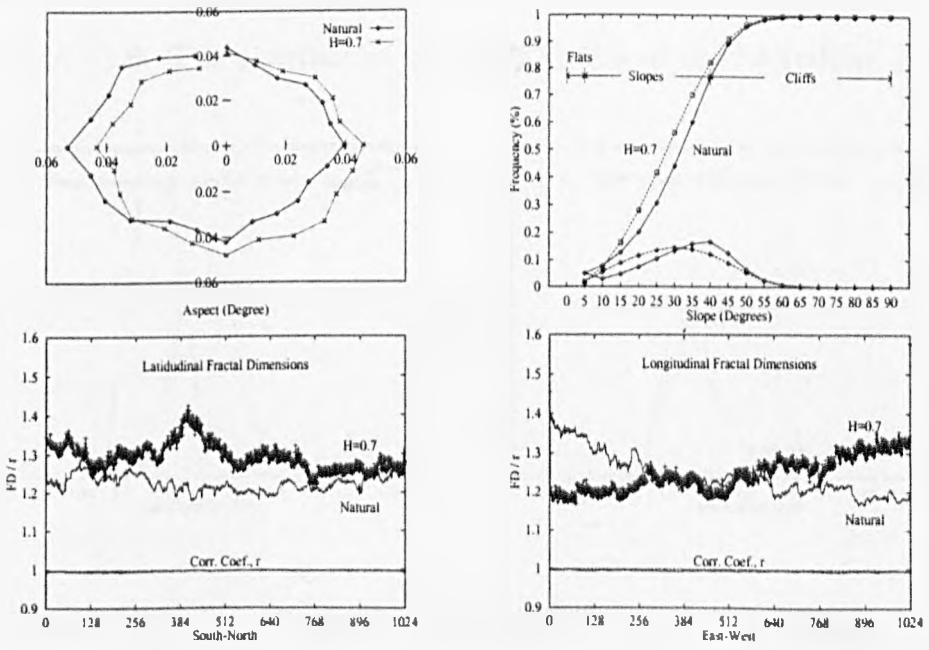

Figure 5.14: Comparisons between the Synthetic and Natural Landforms. Aspects are measured in degrees, while slopes are measured in percentage. All fractal dimensions are meaningful, for the correlation coefficients are high ($r > 0.99$).

5.6.3 Comparisons Between Landforms

The aspects, slopes, and fractal dimensions of the natural landform and the synthetic landform of $H = 0.7$ are compared in Figure 5.14. The landforms seem similar graphically, although the synthetic landform appears to have more uniform distribution of aspects and slopes. In other words, there are more steep than gentle slopes and more slopes are facing west than east in the natural landform; whereas slopes of the synthetic landform are more equally distributed in terms of aspects and frequencies. The distribution of the fractal dimensions appears more rugged in the synthetic than in the natural landform as shown here and in the statistics of Tables 5.1 and 5.2.

The alternative presentation of the distribution of the fractal dimensions is shown in the frequency distribution histogram (Figure 5.15), that has sixteen class intervals between 1.0 and 1.6. The distribution of the estimates of the latitudinal profiles is

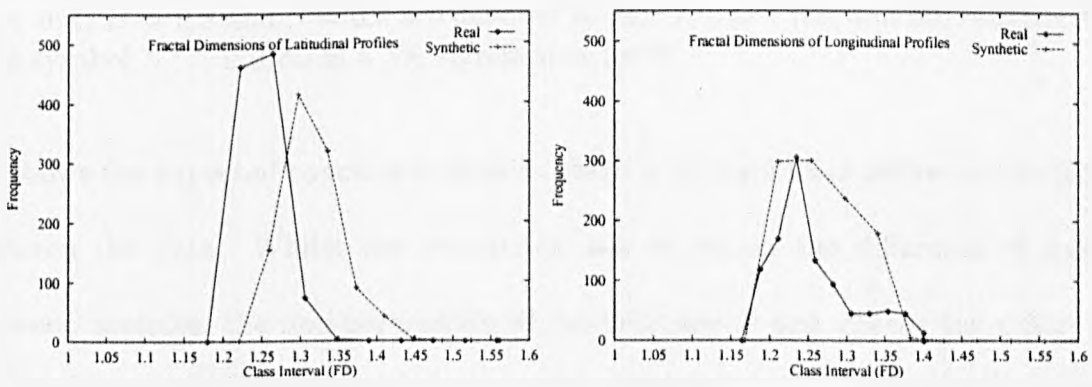

Figure 5.15: The Histogram of the DEM Fractal Dimensions.

highly skewed and peaked in both the synthetic and natural digital elevation models; and the modes are also relatively close to the means in both models. Similarly, in the fractal dimensions of the longitudinal profiles, the distribution is slightly skewed

and peaked; and the modes are close to the means. Further tests are performed to examine the difference in the statistics.

Table 5.4 shows the results of some two-sample tests for the natural and some synthetic landforms. The parametric test between data of normal distribution is provided as a guidance for interpretation of the rest of comparisons. The test statis-

Profile	Landform	U-value	Z-value	P
	N.Scores-R.Numbers	-0.003	(df = 2046)	0.99794
Latitudinal v. Longitudinal	Natural	4.7e5	-4.405	0.00001*
	H2	6.7e5	11.086	0.00000*
	H5	7.8e5	19.124	0.00000*
	H7	8.3e5	22.498	0.00000*
	H8	8.6e5	25.329	0.00000*
	S0	8.8e5	26.709	0.00000*
Latitudinal	Natural–H7	4.3e4	-35.951	0.00000*
Longitudinal	Natural–H7	4.8e5	-3.628	0.00028*

Table 5.4: Statistical Tests of Fractal Dimensions between Landforms. Whilst the two-sample parametric test is conducted for the normal scores (N.Scores) and random numbers (R.Numbers), the non-parametric Mann-Whitney U test is performed for the rest of data. Natural landform is the digital elevation model of Shei-pa National Park, whereas the synthetic landforms of $H = 0.2$, $H = 0.5$, $H = 0,7$, $H = 0.8$ and $S = 0.0$ are denoted by H2, H5, H7, H8, and S0, respectively. The symbol " * " indicates a 5% significance level.

tic shows the expected conclusion; that is, there is no significant difference of means between the data. Whilst the parametric test examines the difference of means between samples, the non-parametric Mann-Whitney U test checks the difference of distribution between samples. Since none of the landforms is found to possess a normal distribution of fractal dimensions (Table 5.2), the non-parametric Mann-Whitney U test is conducted. The natural and several synthetic landforms are tested for the difference of the distributions of the fractal dimensions between latitudinal and longitudinal profiles. The results show that there is a significant difference of the

distribution of the fractal dimensions between profiles of different directions for the natural and all synthetic landforms. Further comparisons are conducted between the natural landform and the landform of $H = 0.7$, because they appear to have similar characteristics as described earlier.

The non-parametric two-sample Mann-Whitney U test was conducted, although mean fractal dimensions are similar (Table 5.2). The difference of the distribution of the fractal dimensions is significant between the natural and the specific landforms for both the latitudinal and longitudinal profiles. As a result, the fractal dimensions between landforms are different in terms of statistics.

5.7 Chapter Discussion and Conclusion

In this Chapter, results from some conventional methods and the fractal analysis are presented. As discussed in Chapter Two, landform is a complex system comprising inhomogeneous sub-systems such as rocks, soils and vegetation. In other words, landform sub-systems, the key players in landform processes and forms, evolve or erode in various time scales; those sub-systems maintain their own paces of evolution, unlike component waves that merge to form relatively homogeneous group waves, as described in Chapter Four. The resultant geomorphology is therefore inhomogeneous and some methods are more suitable than others for revealing such diversity.

The combined use of the conventional and fractal methods reveals the ground truth rather well, as seen in the calculated terrain information and the fractal dimensions of the natural landform in Figure 5.10. There is high proportion of west-facing

slopes and high proportion of cliffs. Where those slopes and cliffs are located is not clear until the fractal dimensions of the longitudinal profiles are examined. It shows that the slopes are concentrated in the west and the cliffs in the east. Used together, the findings explain well the heavy impact of monsoons on the river networks in the area. In addition to the cyclones that occur irregularly with unpredictable frequency and force, the south-westerly winds bring, in sumer, constant rainstorms and downpours, that greatly erode then deposit materials on the west sides of slopes. This combined impact seem to be the major influence that makes the rivers run westwards; however, tectonic movement is as important. The whole area is actually subject to the majestic power of the Eurasian plate's being crushed by the Pacific plate (Rice, 1988, Ch.3), that created the Marianas Trench and Ryuku Arc along the east of Taiwan (Rice, 1988; Summerfield, 1991). The uplifting force created summits, while the advancing momentum squeezed the mountains from the east, hence left behind more steep east-facing cliffs in the east and relatively gentle west-facing slopes further west. As a result, slopes are distributed in the current pattern.

Although the ground truth cannot be verified, the above approach is still applicable to the synthetic landforms (Figure 5.12). The distributions of aspects remain relatively similar for all landforms except the one with a flat initial surface; and higher portion of steep slopes are observed in landforms of lower Hurst exponents, that is, higher fractal dimensions. The fractal dimensions of the latitudinal profiles indicate that the irregularity is higher in the south than in the north, yet this cannot be shown by conventional methods. Wilson & Dominic (1998) also found that there is a significant positive correlation between the fractal dimensions of topographic and structural relief along the strikes of major folds in the deformed area

of Appalachian Mountains. It could not have been perceived through the single measure approach (Liu, 1992) or the dimension map approach (Müssigmann, 1992). With the unique approach used here, the diversity of the landform system is easily identified.

The comparison between the natural landform and the landform with the Hurst exponent of 0.7 is shown in Figure 5.14. Both landforms appear similar when subjected to conventional methods; however, the fractal dimensions indicate that there is a great degree of diversity between different landforms and also within the same landform. Despite the fact that the approximation of the Brownian motion is intensively extended to model the natural phenomena (Voss, 1988; Saupe, 1988a), the current results suggest that the algorithm might need to be investigated further.

The above conclusion confirms that landform is a system of heterogeneity and that diversity can be detected by estimating the fractal dimensions of its profiles. Following the theme of this thesis, the focus moves now to the spectral imagery containing both homogeneous and heterogeneous systems, in the following chapter.

Chapter 6

Plants

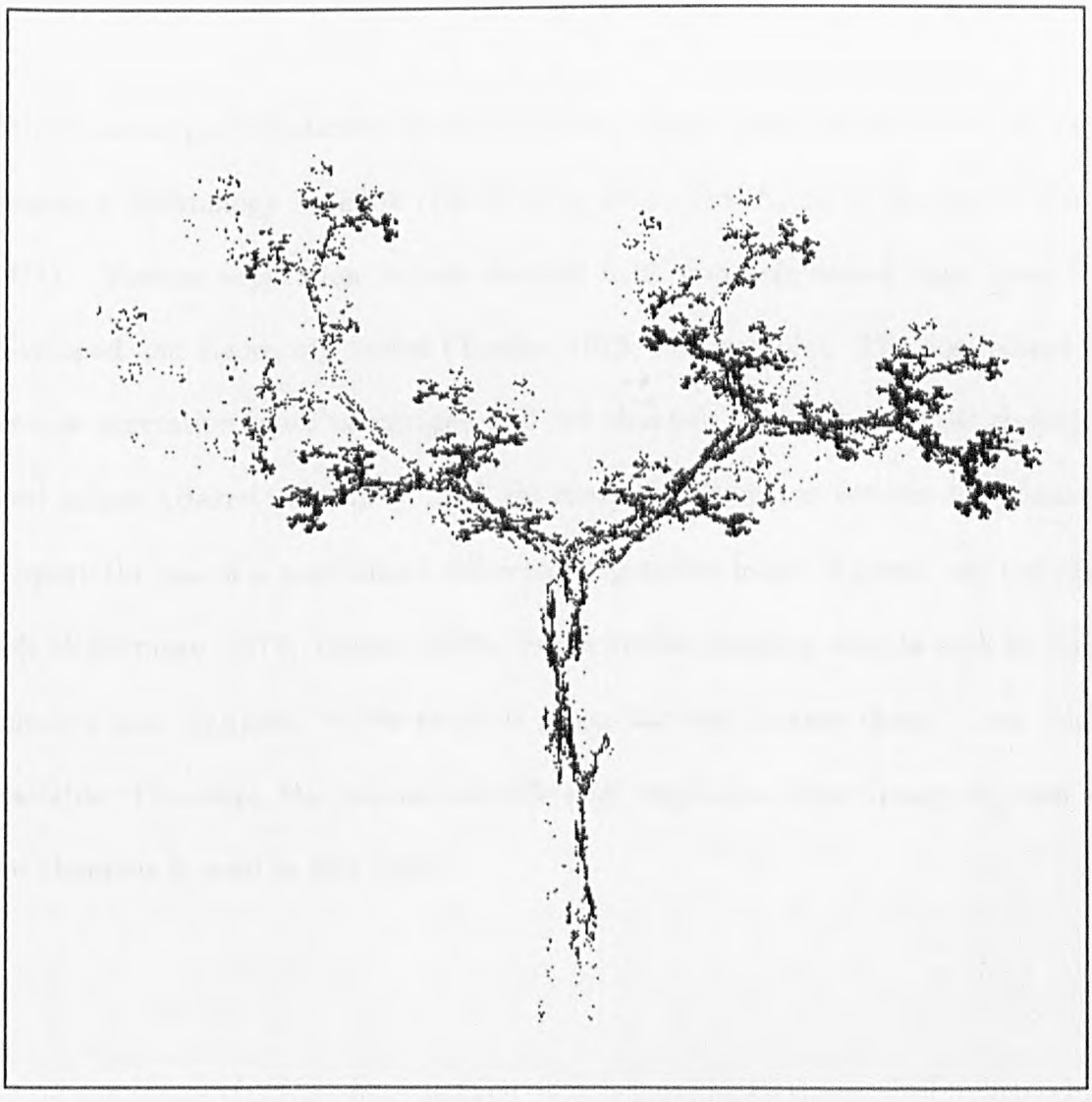

Figure 6.1: An IFS Tree.
The IFS code is in Table 6.1 and the computer programme is in Appendix S.

6.1 Introduction

This Chapter introduces the formation of a normalised difference vegetation index image from remotely-sensed data of natural plant, followed by the simulation of synthetic ferns. The estimation of the fractal dimensions is the key analysis of the spectral image that consisted of both heterogeneous leaf and homogeneous background sub-systems, using the algorithms detailed in Chapter Five.

6.2 The Natural Fern

Remote sensing of vegetation has become very popular since the launch of the Earth Resource Technology Satellite (ERTS-1) in 1972 (NASA, 1972; Barrett & Curtis, 1974). Various vegetation indices derived from remotely-sensed data have been developed and rigorously tested (Tucker, 1979, for example). The normalised difference vegetation index of infrared and red channels is one of the most commonly used indices (Barrett & Curtis, 1992, for example). However, articles were found to support the use of a normalised difference vegetation index of green and red channels (Kanemasu, 1974; Tucker, 1979). Furthermore, imaging devices such as digital cameras and scanners, which produce green and red images cheaply, are widely available. Therefore, the normalised difference vegetation index image of green and red channels is used in this thesis.

6.2.1 Remote Sensing of Vegetation

The early images of the earth's surface were aerial photographs taken mainly from aircraft and have been applied to land uses, geographical and geological mapping, agriculture, forestry, water resource, wildlife conservation, ecology, and archaeology (Cracknell & Hayes, 1991; Barrett & Curtis, 1992; Lillesand & Kiefer, 1994, for example). The Department of Industry of United Kingdom published a list of UK groups and individuals engaged in remote sensing with a brief account of their activities and facilities (DOI, 1979). However, the study of vegetation by its spectral characteristics was not reported until relatively late. Thomas *et al.* (1966) found a coefficient of determination (r^2) of 0.75 and 0.49 between the optical density of false colour film and the yield of cotton and wheat, respectively. Others (Steen *et al.*, 1969; Stoner *et al.*, 1972, for example) also reported a high correlation between multi-spectral reflectance and plant growth parameters. Linear combinations of spectral channels did not become popular until the launch of earth resource satellites. The technical details regarding remote sensing platforms are given in Appendix Q.

Vegetation Index

Vegetation indices are the linear combinations of spectral channels such as infrared (IR) and red (R) channels, for example, the vegetation index, $VI = \frac{IR}{R}$, the normalised difference vegetation index, $NDVI = \frac{IR-R}{IR+R}$, and the transformed vegetation index, $TVI = \sqrt{\frac{IR-R}{IR+R} + 0.5}$, among others. Many researchers have contributed to the development and application of vegetation indices (Richard & Wiegand, 1977; Tucker, 1977; Tucker, 1979; Curran, 1981; Satterwhite, 1984; Satterwhite & Henley,

1987; Gardner *et al.*, 1985; Choudhury & Tucker, 1987; Gallo & Daughtry, 1987; Huete & Jackson, 1987; Tucker & Choudhury, 1987; Rees, 1990; Barrett & Curtis, 1992; Lillesand & Kiefer, 1994, for example). The vegetation indices used in studies of vegetation and land use are extensively discussed in Curran (1980). Various plant growth parameters are found to be related to the vegetation indices include cover, leaf area, leaf water content, chlorophyll content, productivity, and biomass (Agazzi & Franzetti, 1975; Tucker, 1977; Tucker, 1979; Holben *et al.*, 1980; Curran, 1981; Asrar *et al.*, 1985; Best & Harlan, 1985; Elvidge & Lyon, 1985, for example).

NDVI of Green and Red Channels

The majority work on the IR and red linear combination has used satellite (Landsat) data (Tucker, 1979, p.129). However, Kanemasu (1974) reported on a ground-based reflectance study of crop types where various ratios were investigated and concluded that the green/red ratio closely followed crop growth and development; although Tucker (1979, p.127) stated that the red and IR linear combinations had a 7% and 14% greater regression significance than the green (G) and red (R) linear combinations for the June and September sampling periods, respectively. Tucker (1979) further verified that the normalised difference vegetation index of green and red channels, that is, $\frac{G-R}{G+R}$, is highly correlated with the total wet biomass, leaf water content, and dry green biomass of the Blue Grama Grass sampled in summer, because the coefficients of determination are greater than 0.80. The normalised difference vegetation index of the green and red channels is, therefore, suitable for studying vegetation particularly on a relatively small scale.

Satellite images are usually of relatively low resolution, compared with the com-

plexity of an individual plant stand. Whilst a patch of meadow in England might contain tens of vascular species, the best satellite image so far is the panchromatic image of SPOT, with ten-metre spatial resolution (Price, 1987) and the SPOT-5 image of five-metre resolution scheduled in 1999 (Dagras *et al.*, 1995). For a detailed study of woodland ecology, for example, aerial photographs might be more feasible (Barrett & Curtis, 1992, Part Two). Although IR filming facilities such as filters and cameras are available, they are generally expensive and too sophisticated to operate (Curran, 1981). The use of ordinary imaging instruments is, therefore, theoretically applicable in practice. The latest development in scanning and imaging hardware also facilitates the detailed study of individual plants as well as the small scale study of vegetation. Therefore, it was decided that the normalised difference vegetation index obtained by the green and red channels of a scanner be used for the study of a plant.

6.2.2 NDVI Image of the Natural Fern

A fresh fern leaf was sampled and immediately scanned as a digital colour image by a colour scanner connected to a personal computer. Refer to Appendix R for a brief introduction to the natural history of ferns. The scanner used here is named CLC10 manufactured by Canon Europa NV and the software which comes with the scanner is called PhotoShop (Canon, 1992). The image was carefully adjusted to include the fern with the final size of 1024×1024 pixels, the size of a digital elevation model used in Chapter Five. The colour image was then split into three spectral channels, that is, blue, green, and red. The green and red images created by the scanners were transferred to geographic information system software such as IDRISI (Eastman,

1992a; Eastman, 1992b), where the normalised difference vegetation index of the fern is calculated. The final image contains two major systems, that is, the leafy and background areas.

6.3 Synthetic Ferns

There have been attempts to define the shapes of plant leaves in algebraic terms (Thomas, 1942), but this has met with no long-lasting success (Campbell, 1996). Extensive quantitative analysis of leaf shape has depended on methods either like Fourier analysis (Dickinson *et al.*, 1987) or by sampling landmarks on leaves and treating the geometric relations between these special points (Jehnsen, 1990; Ray, 1992; Jones, 1993). None of these approaches seems suitable to dealing with the highly dissected shapes of many ferns (Campbell, 1996).

Fractal Geometry involves only relationships between parts, not the shapes of parts themselves (Campbell, 1996). Methods of fractal dimension have been sued to draw fern-like shapes (Barnsley *et al.*, 1987; Prusinkiewicz & Lindenmayer, 1990). Campbell (1996) proposed four fractal methods in generating a spectrum of forms displayed by different species of ferns; and the methods, including two Iterated Function System (IFS) methods, produce fractal structures. The synthetic ferns are generated by the IFS method, utilising the IFS code and the collage theorem (Barnsley, 1993). The strengths and weaknesses of the method were noted by Campbell (1996); that is, the strengths include that the computation of these figures is rapid and simple and a variety of classes of real ferns can be approximated, whilst the weaknesses include that the method cannot produce forms that are not perfectly

self-similar. for example, the forms in which there is only a finite level of branching.

6.3.1 The Construction of Fractals

The metric space where fractals "reside" is detailed in Chapter Two. This section describes the affine transformations and the contraction mapping, followed by the introduction to the Iterated Function System (IFS). Then the design of the Iterated Function System, the Collage Theorem, is detailed.

The Affine Transformation and the Contracting Mapping

Fractal Geometry details complicated subsets of geometrically simple spaces such as the real number (R), the Euclidean space (R^2), the complex plane (C), and the Rieman sphere ($\hat{C}$). In deterministic fractal geometry the focus is on those subsets of a space that are generated by, or possess invariance properties under, simple geometrical transformations of the space into itself. A simple geometrical transformation is one that is easily conveyed or explained to someone else. Usually it can be completely specified by a small set of parameters. Examples include affine transformations in R^2, which are expressed using 2×2 matrices and 2-vectors, and rational transformations on the Riemann Sphere, which require the specification of the coefficients in a pair of polynomials. In order to work in Fractal Geometry one needs to be familiar with the basic families of transformations in R, R^2, C, and $\hat{C}$, and to know well the relationship between "formulas" for transformations and the geometric changes, stretching, twisting, foldings, and skewing of the underlying fabric, the metric space upon which they act. However, the discussion below is

based in the Euclidean plane. More details on the transformations are given by, for example, Barnsley (1993).

The Affine Transformation

An affine transformation on the Euclidean plane is defined by Barnsley (1993, p.49) as follows. A transformation $w : R^2 \mapsto R^2$ of the form $w(x_1, x_2) = (ax_1 + bx_2 + e,\ cx_1 + dx_2 + f)$, where a, b, c, d, e and f are real numbers, is called a (two-dimensional) affine transformation. It is often denoted as,

$$w(x) = w\begin{pmatrix} x_1 \\ x_2 \end{pmatrix} = \begin{pmatrix} a & b \\ c & d \end{pmatrix}\begin{pmatrix} x_1 \\ x_2 \end{pmatrix} + \begin{pmatrix} e \\ f \end{pmatrix} = Ax + t. \tag{6.1}$$

Here $A = \begin{pmatrix} a & b \\ c & d \end{pmatrix}$ is a two-dimensional, 2×2 matrix and t is the column vector $\begin{pmatrix} e \\ f \end{pmatrix}$, which is not distinguished from the coordinate pair $(e, f) \in R^2$.

The matrix A can always be written in the form,

$$\begin{pmatrix} a & b \\ c & d \end{pmatrix} = \begin{pmatrix} r_1 \cos\theta_1 & -r_2 \sin\theta_2 \\ r_1 \sin\theta_1 & r_2 \cos\theta_2 \end{pmatrix}, \tag{6.2}$$

where (r_1, θ_1) are the polar coordinates of the point (a, c) and $(r_2, (\theta_2 + \pi/2))$ are the polar coordinates of the point (b, d). This general affine transformation $w(x) = Ax + t$ in R^2 consists of a linear transformation, A, which deforms space relative to the origin by *rotating* and *scaling* specified by the angle θ and the scale factor r, respectively, followed by a *translation* or *shift* specified by the vector t.

Contraction Mapping

Contraction mapping is formally defined by Barnsley (1993, p.74) as follows. A transformation $f : X \mapsto X$ on a metric space (X, d) is called *contractive* or *a contraction mapping*, if there is a constant $0 \leq s < 1$ such that,

$$d(f(x), f(y)) \leq s \cdot d(x, y), \tag{6.3}$$

where $\forall x, y \in X$. Any such number s is called a *contractivity factor* for f, where $d(x, y)$ is the distance between x and y. The transformation f possesses exactly one fixed point $x_f \in X$ and moreover for any point $x \in X$ in the space, the sequence $\{f^{\circ n}(x) : n = 0, 1, 2, ...\}$ converges to x_f. Refer to Chapter III of Barnsley (1993) for the formal mathematical proof.

The Iterated Function System (IFS)

After having proven that a contraction mapping of the metric space is *continuous*, Barnsley (1993, p.80) at last reached the definition of the iterated function system; that is, "a hyperbolic *iterated function system* consists of a complete metric space (X, d) together with a finite set of contraction mappings $w_n : X \mapsto X$, with respective contractivity factors s_n, for $n = 1, 2, ..., N$." The abbreviation "IFS" is used for "Iterated Function System." The word "hyperbolic" is sometimes dropped in practice; furthermore, Barnsley (1993) proved that there is a unique fixed point in the space, where this fixed point is called the *attractor* of the IFS.

The Design of IFS: The Collage Theorem

The Collage Theorem is central to the design of IFS's whose attractors are close to given sets (Barnsley *et al.*, 1985). The Theorem states that in order to find an IFS whose attractor is "close to" or "looks like" a given set, one must find a set of transformations — contraction mappings on a suitable space within which the given set lies — such that the union, or collage, of the images of the given set under the transformations is near to the given set, where nearness is measured using the

Hausdorff metric. The proof of the Collage Theorem can be found in the last section of Chapter III in Barnsley (1993).

6.3.2 The Simulation

The IFS code needed to record a fern leaf is relatively concise, compared with methods such as the digital scanning technique (Peitgen *et al.*, 1992, p.258). The implementation of the code varies; here, two types of methods are presented: the deterministic and the random algorithms.

The IFS Code

The primary component in generating scenes with an Iterated Function System is the affine transformation, which is a rotation, translation, and scaling of the coordinates of a point (x, y) to a new position (x_n, y_n). The transformation is performed according to Equation 6.1, where the parameters a, b, c and d perform a rotation, and their magnitudes result in the scaling; and the parameters e and f cause a linear translation of the point being operated upon (Stevens, 1989, p.385). Barnsley (1988) referred those parameters as IFS codes. The IFS codes used in this thesis are given in Table 6.1.

Table 6.1 also provides numbers p_i associated with each transformations w_i for $i = 1, 2, ..., N$. Their values can be approximated (Barnsley, 1993),

$$p_i \approx \frac{|\det C_i|}{\sum_{i=1}^{N} |\det C_i|} = \frac{|a_i d_i - b_i c_i|}{\sum_{i=1}^{N} |a_i d_i - b_i c_i|}, \tag{6.4}$$

where $i = 1, 2, ..., N$. If, for some i, $|\det C_i| = 0$, then p_i should be assigned a small

a	b	c	d	e	f	p
Fern No.1 (Peitgen *et al.*, 1992)						
0.849	0.037	-0.037	0.849	0.075	0.183	0.85 T
0.197	-0.226	0.226	0.197	0.4	0.049	0.07 L
-0.15	0.283	0.26	0.237	0.575	-0.84	0.07 R
0.0	0.0	0.0	0.16	0.5	0.0	0.01 S
Fern No.2 (Barnsley, 1993)						
0.0	0.0	0.0	0.16	0.0	0.0	0.01
0.85	0.04	-0.04	0.85	0.0	1.6	0.85
0.2	-0.26	0.23	0.22	0.0	1.6	0.07
-0.15	0.28	0.26	0.24	0.0	0.44	0.07
Tree No.1 (Peitgen *et al.*, 1992)						
0.195	-0.488	0.344	0.443	0.4431	0.2452	0.049
0.462	0.414	-0.252	0.361	0.2511	0.5692	0.6
-0.058	-0.07	0.453	-0.111	0.5976	0.0969	0.05
-0.035	0.07	-0.469	-0.022	0.4884	0.5069	0.01
-0.637	0.0	0.0	0.501	0.8562	0.2513	0.3
Tree No.2 (Barnsley, 1993)						
0.0	0.0	0.0	0.5	0.0	0.0	0.05
0.1	0.0	0.0	0.1	0.0	0.2	0.4
0.42	-0.42	0.42	0.42	0.0	0.2	0.4
-0.42	0.42	-0.42	0.42	0.0	0.2	0.15

Table 6.1: IFS Codes of Some Plants.
The refined codes by Peitgen *et al.* are designed to work on the $[0,1]\times[0,1]$ plane. The four transformations, i.e., top, left, right and stem, are denoted by T, L, R and S, respectively. The original codes used by Barnsley (1993) are also given.

positive number, such as $\sigma = 0.001$. Other situations should be treated empirically. The procedure of choosing the probabilities may be summarised by the formula (Peitgen *et al.*, 1992),

$$p_i = \frac{\max(\sigma,\ |\det C_i|)}{\sum_{k=1}^{N} \max(\sigma,\ |\det C_k|)}, \tag{6.5}$$

where $i = 1, 2, ..., N$. The IFS code can be altered to display the same object. For example, the fern generated by the code of Peitgen *et al.* (1992) is confined to the range between real numbers 0.0 and 1.0; whilst that generated by Barnsley's code (1993) has a range of between -100.0 and +200.0 (Stevens, 1989).

The associated probabilities, p_i, which obey $\sum_{i=1}^{N} p_i = 1$, play an important role

in the computation of images of the attractor of an IFS using the Random Iteration Algorithm; however, they play no role in the Deterministic Algorithm (Peitgen *et al.*, 1992, p.328). More details are given in the following section.

The Algorithms

There are two types of algorithms to generate a synthetic fern. The Deterministic Algorithm is based on the idea of directly computing a sequence of sets $\{A_n = W^{\circ n}(A)\}$ starting from an initial set A_0 (Barnsley, 1993). The Random Iteration Algorithm is founded in ergodic theory and also called the "Chaos Game" (Stevens, 1989; Peitgen *et al.*, 1992; Barnsley, 1993).

The Deterministic Algorithm

When using the deterministic method, one takes each point in the initial set and applies to it each of the affine transformations that make up the IFS code for the fern (Stevens, 1989, p.386). The new points are plotted, then the same process is applied again as many times as necessary to obtain a final result. However, no probability is involved in this process.

Barnsley (1993, p.85) defined the deterministic algorithm as follows. Let $\{X; w_1, w_2, \cdots, w_N\}$ be a hyperbolic IFS. Choose a compact set $A_0 \subset r^2$. Then compute successively $A_n = W^{\circ n}(A)$ according to,

$$A_{n+1} = \cup_{j=1}^{n} w_j(A_n), \tag{6.6}$$

for $n = 1, 2, 3, \cdots$. Thus one constructs a sequence $\{A_n : n = 0, 1, 2, 3 \cdots\}$ converging to the attractor of the IFS in the Hausdorff metric.

The Random Iteration Algorithm

The computer programme for the random iteration algorithm is fairly straightforward (Stevens, 1989, p.394). The programme works by selecting one of the affine transformations at random with some probability that approximately represents the percentage of the picture that will be illustrated by that transformation, where the sum of the probabilities is equal to one. After having repeated the operation a certain number of times, one should have generated a fern on the computer monitor.

The following is a formal definition of the random iteration algorithm given by Barnsley (1993, p.88). Let$\{X; w_1, w_2, \cdots, w_N\}$ be a hyperbolic IFS, where probability $p_i > 0$ has been assigned to (the affine transformation) w_i for $i = 1, 2, \cdots, N$, where $\sum_{i=1}^{n} p_i = 1$. Choose $x_0 \in X$ and then choose recursively, independently,

$$x_n \in \{w_1(x_{n-1}), w_2(x_{n-1}), \cdots, w_N(x_{n-1})\}, \tag{6.7}$$

for $n = 1, 2$ and 3. where the probability of the event $x_n = w_i(x_{n-1})$ is p_i. Thus construct a sequence $\{x_n : \ n = 0, 1, 2, 3, \cdots\} \subset X$.

The Implementation

There are computer programs available for implementing the algorithms (Stevens, 1989; Peitgen *et al.*, 1992; Barnsley, 1993, for example). Each has its own limitations as well as advantages in relation to the computer language or the displaying device used. Here, the IFS code and the pseudo codes found in Peitgen *et al.* (1992) are modified to generate the synhteic ferns; whilst the corresponding complete listing of the computer programme is given in Appendix S.

The Deterministic Iteration Model

PARAMETER

- N, user defined number of iterations.
- IFS, the IFS code, which includes transformations, w_j, without probability p, where $j = 0, 1, 2$ and 3.. Refer to Table 6.1.
- x_0, the initial set.

TRANSFORM (Sub-routine, to be called by MAIN)

- Start from level L
- Calculate new points $x_{i+1} = x_i \times w_j$. Refer to Equation 6.1
- $L = L - 1$
- IF $L > 0$
- TRANSFORM(x_{i+1}, L)

MAIN (Main routine)

- TRANSFORM(x_0, L)

Figure 6.2: The Pseudo Code for Generating the Fern by Deterministic Algorithm. Modified from Peitgen *et al.* (1992, p.294).

The pseudo code for implementing the deterministic algorithm is given in Figure 6.2. Firstly, we define the level of iteration, the IFS code of the fern and the initial set that must be a non-empty set. Then, the main routine (MAIN) is called, upon which the sub-routine (TRANSFORM) is called iteratively. The sub-routine needs two input parameters, that is, the x- or y-coordinate (x_i) and the level of iteration (L), which are supplied by the MAIN. It generates from the previous point the new points according to Equation 6.1. Meanwhile, the level of iteration is reduced by one. If the level of iteration is larger than zero, it will call upon itself once again. The repetition will continue for each point until the level reaches zero.

The resultant image was confined in $[0, 1] \times [0, 1]$ real plane, refer to refined IFS

code in Table 6.1. The image can easily be displayed onto a graphic device using a variety of graphical display utilities such as *gnuplot* available on Unix. In other words, all it requires from the programme is to produce the data format recognisable to the graphic routine.

There is a serious problem associated with the use of the deterministic algorithm; that is, one has to be very careful about the range which the transformations might generate. Stevens (1989) suggested that, in order to get a whole fern leaf, one has to specify the x coordinate to the range from -100 to $+200$, using the Fern No.2 code in Table 6.1. On the other hand, there is no such problem when using the code given by Peitgen *et al.* (1992). Another drawback of the deterministic algorithm is the slowness of the drawing process for certain pictures; however, this is can be improved by using, for example, a recursive structure proposed by Peitgen *et al.* (1992). Furthermore, there is no simple way to determine *a priori* how many iterations will be needed to produce a picture of adequate quality. The user has to experiment with various combinations of parameters in order to obtain the desired image.

The Random Iteration Model

The computer code for generating a fern using a random iteration algorithm is relatively simpler than that using a deterministic algorithm, refer to Figure 6.3. In the random model, the user has to supply the number of iterations, the IFS code with probability to represent each transformation, and the initial set which is a single point. Then one runs a random number generator to the probability of the run between 0.0 and 1.0. Although most generators give integral numbers, there

PARAMETER

- L, user defined level of iteration.
- IFS, the IFS code, which includes transformation, w_j,s with probability p_j, where $j = 0, 1, 2$ and 3. Refer to Table 6.1.
- x_0, the initial set.
- n, iteration indicator.
- p, probability given by a random number generator

MAIN

- FOR $n < N$ DO
- p, given by a random number generator
- IF $p < p_0$ DO $x_{i+1} = x_i \times w_0$
- IF $p > p_0$ DO $x_{i+1} = x_i \times w_1$
- IF $p > (p_0 + p_1)$ FO $x_{i+1} = x_i \times w_2$
- IF $p > (p_0 + p_1 + p_2)$ DO $x_{i+1} = x_i \times w_3$
- $n = n + 1$

Figure 6.3: The Pseudo Code for Generating the Fern by Random Algorithm. Modified from Peitgen *et al.* (1992, p.394).

are a few that give real numbers exactly between 0.0 and 1.0, such as the linear congruential pseudo-random number generator `r_lcrans()` available on UNIX and used here. According to the probability, the corresponding transformation is chosen; hence, a new point is obtained. This "game" is repeated a pre-defined number of times and the final image is obtained.

Three-Dimensional Images

Although the final image is displayed in two-dimensional space, it actually contains heights created as a result of the discretisation process. The continuous plane of 1.0×1.0 is divided into 1024 pixels. Data points within a fixed range of a pixel

are grouped and plotted at that specific position; that is, the number of visits is recorded as the height. Therefore, a three-dimensional image is constructed.

6.4 Analyses

The fractal dimensions are estimated for the profiles of the image, the outline of the fern and the three-dimensional display of the image, using the same box counting approach. The estimation of the profile fractal dimensions was detailed in Chapter Five which is based on the method of Chapter Four, as briefly reviewed here. In Chapter Four, rectangular boxes of size $S_n = (\frac{S_x}{n} \times \frac{\sigma_y}{n})$ are applied in order to cover a time series, where S_x is the length of x-coordinate and σ_y is the standard deviation of the y-coordinate, and n is the geometric scaling factor; then the number of boxes (N_n) needed to cover the time series is counted. The slope of the log-log plot of $1/S_n$ against N_n is the fractal dimension. In Chapter Five, profiles of the digital elevation model are extracted and followed by the application of the method used in Chapter Four. Since the spectral image of the fern is similar to the digital elevation model, the method used in Chapter Five is applicable in this chapter.

The estimation of the fern's outline utilises the square box that covers the self-similar horizontal coordinates; that is, the box size is $S_n = (\frac{S_x}{n} \times \frac{S_y}{n})$, where S_x and S_y are the lengths of the xy-coordinates and n is the geometric scaling factor. The box of size S_n is run across the image one length at a time; and the corresponding number (N_n) of boxes that include both the background and leafy areas is counted. The slope of the log-log plot of $1/S_n$ against N_n is the fractal dimension.

The fractal dimension of the three-dimensional image is estimated using the hyper cubes of $S_n = (\frac{S_x}{n} \times \frac{S_y}{n} \times \frac{\sigma_z}{n})$ that cover the self-affine surface, where S_x and S_y are the lengths of the xy-coordinates, σ_z is the standard deviation of the z-coordinate and n is the geometric scaling factor. The number of the hyper cubes of size S_n that cover the image is counted as follows. The hyper cube is moved along the xy-coordinates one length at a time so the range of z values in that area can be identified; then the corresponding box count (N_n) is equal to the difference between the "ceiling" of the maximum z value divided by size σ_z and the "floor" of of the minimum z value divided by the size σ_z. Similarly to the above, the fractal dimension is equated to the slope of the log-log plot of $1/S_n$ against N_n. The complete computer programme of this section is listed in Appendix T, while the results are given in the following section.

6.5 Results

The estimated profile fractal dimensions of both the natural and synthetic ferns are presented here, followed by the results of the corresponding statistical tests. The fractal dimensions of the fern in higher dimensions are also given.

6.5.1 The Natural Fern

Figure 6.4 is the normalised difference vegetation index image of the fern. The normalised difference vegetation index, ranging from -1.0 to 1.0, corresponds to the plant growth rigour. The highest values are found in the leaflets where most growth

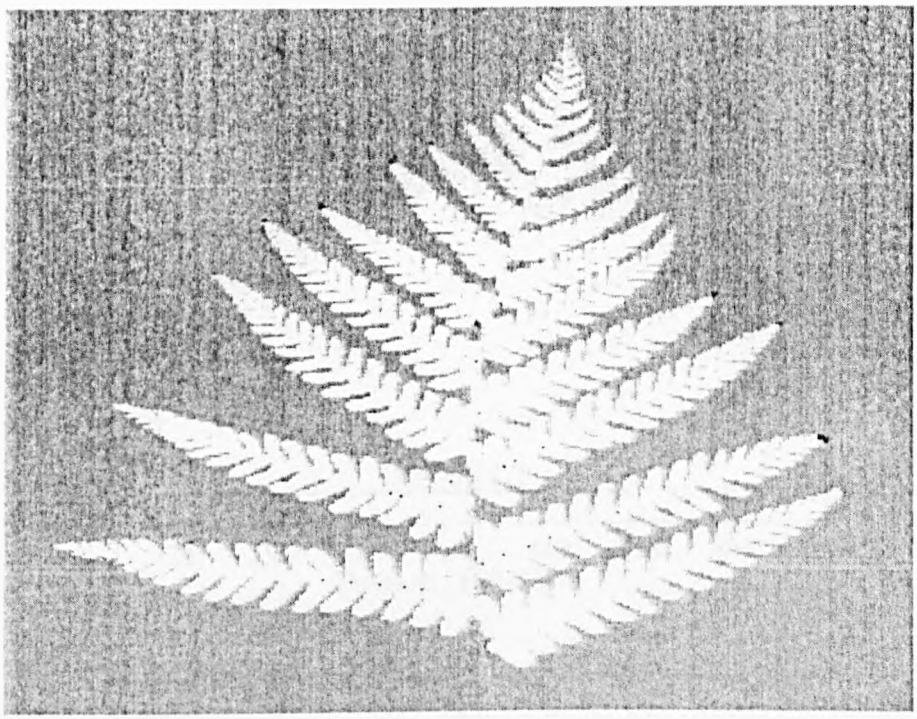

Figure 6.4: The NDVI Image of the Natural Fern.
Brighter colour reflects higher growth rigour in the plant. Background occupies 74.4% of total pixels.

activity takes place; and comparatively lower values are located in the main stem that is responsible for transporting nutrients and fluids to the leaflets. The leafy area occupies around 25.6% of the total pixels, while the rest is taken up by the grey-board with much lower reflectance than any part of the leaf.

Fractal Dimensions

Figure 6.5 shows the profile fractal dimensions of the fern image and Table 6.2 gives statistics of the fractal dimensions derived. All the estimated fractal dimensions are meaningul as indicated by their corresponding correlation coefficients ($r > 0.99$). The fractal dimensions of the profiles in both directions appear higher in the middle, where they reach the maximum, than near the edge, which approach 1.0. The

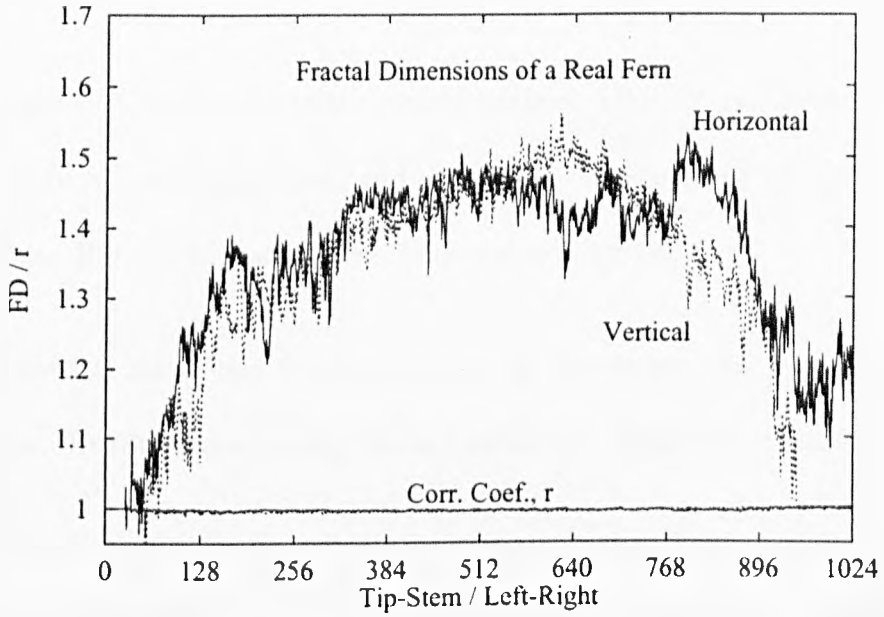

Figure 6.5: Fractal Dimensions of the Natural Fern.
The fractal dimensions are meaningful, indicated by the correlation coefficients.

normality tests indicate that the estimated fractal dimensions are not normally distributed in both directions ($p = 0.00*$). The subsequent two-sample Mann-Whitney U test shows that the difference of the distribution of the fractal dimensions is significant ($U = 5.8e5$ and $p = 0.00*$).

Data	n	min	max	$\bar{x}$	std	$Skew$	$Kurt$	W	$c.s.l$
NS	1024	-3.248	3.248	0.000	0.999	0.000	-0.044	0.988	0.7667
RN		-2.893	4.114	0.000	0.972	0.185	0.272	0.988	0.7760
H	1024	1.000	1.549	1.345	0.131	-1.100	0.309	0.854	0.0000*
V		1.000	1.564	1.309	0.166	-0.767	-0.721	0.852	0.0000*

Table 6.2: Statistics of Fractal Dimensions of the Natural Fern.
Statistics are given to fractal dimensions of horizontal (H) and vertical (V) profiles. "NS" is the normal scores and "RN" is the random numbers from $N(0.0, 1.0)$. The Shapiro and Wilk's normality test (W) is performed at 5% significance level. If it is not normally distributed, it is marked by " * ".

6.5.2 Synthetic Ferns

Two types of synthtetic ferns are presented here. The first synthetic fern is generated by the deterministic algorithm, and the second one is created by the random iterated algorithm. Results of fractal dimension estimation are given.

Figure 6.6 shows the ferns generated by the deterministic and the random algorithms. In the case of using the deterministic algorithm, transformations in the

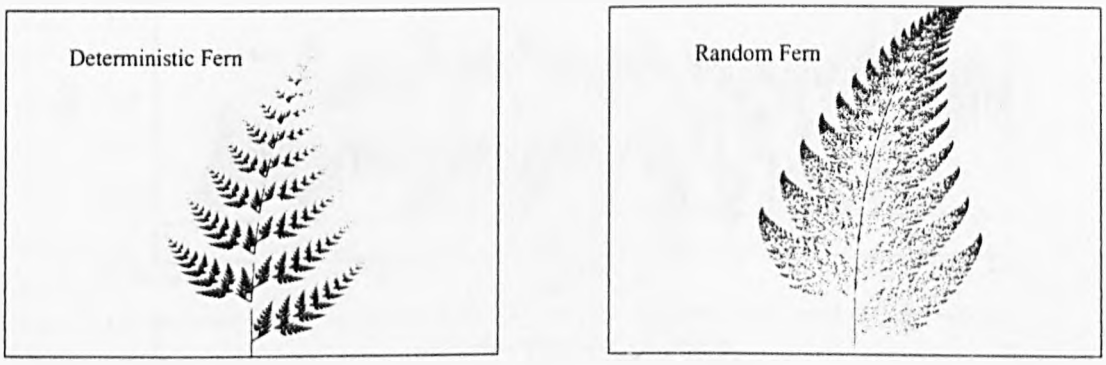

Figure 6.6: Synthetic Ferns by the Deterministic and Random Algorithms.

IFS codes (Table 6.1) are used to generate new output points which then become input points. The transformations, that is, top, left, right, and stem, are applied in sequence. In other words, the image is generated by starting from an arbitrary point which is transformed according to the sequence of the IFS codes, then ending at the given level of iteration. The probability of using any one of the transformations is not considered. The resultant image is better produced if the starting point falls within the final image. However, the outline is more like a bracken than a fern.

Similarly to the deterministic fern, a random fern is generated using the transformations in Table 6.1. However, the sequence of applying the transformations depends upon the associated probabilities. Starting from an artbitrary point that

is preferably located within the finished image, the generation process stops at the given number of iterations. This is a more realistic simulation of a natural fern.

Fractal Dimensions

Figure 6.7 shows the fractal dimensions of horizontal and vertical profiles of the synthetic ferns generated by the deterministic and random algorithms. Table 6.3 is

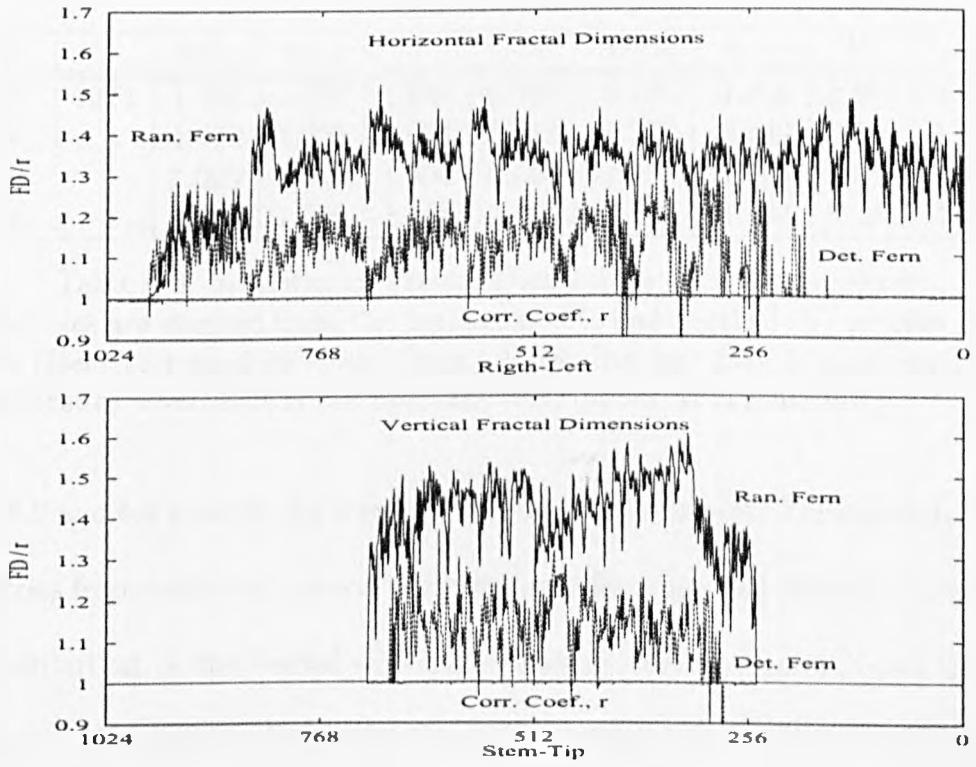

Figure 6.7: Fractal Dimensions of Synthetic Ferns.
Fractal dimensions are estimated for horizontal (H) and vertical (V) profiles form ferns by deterministic (Det) and random (Ran) iterated algorithms. The corresponding correlation coefficients (r) are also given.

the summary of statistics and statistical tests of fractal dimensions. The estimated fractal dimensions are meaningful for deterministic and random ferns because of high values of correlation coefficients ($r > 0.99$). The distribution of the fractal dimensions is not normal for both directions of deterministic and random ferns.

The average fractal dimensions of the horizontal profiles of deterministic and random ferns are 1.054 and 1.186, respectively. The difference of distribution of the fractal dimensions between the two types of ferns is significant ($p = 0.00*$). The difference of distribution of the fractal dimensions between both synthetic ferns is also significant ($p = 0.00*$) for the vertical profiles.

6.5.3 Comparisons

Data	n	min	max	$\bar{x}$	std	$Skew$	$Kurt$	W	$c.s.l$
Det.H	1024	1.000	1.357	1.095	0.082	0.294	-1.026	0.888	0.0000*
Det.V		1.000	1.395	1.054	0.082	1.276	0.449	0.688	0.0000*
Ran.H		1.000	1.520	1.304	0.106	-1.387	1.704	0.851	0.0000*
Ran.V		1.000	1.606	1.186	0.213	0.402	-1.624	0.728	0.0000*

Table 6.3: Statistics of Fractal Dimensions of Synthetic Ferns.
The statistics are derived from the horizontal (H) and vertical (V) profiles of deterministic (Det) and random (Ran) ferns. Normality test (W) is performed against 5% significance level. If it is not normally distributed, it is marked by " * ".

Tables 6.2 and 6.3 provide the results from the normality test. The estimated fractal dimensions from both the natural and synthetic ferns are not normally distributed. The distribution of the fractal dimensions can be further shown in the frequency distribution histogram in Figure 6.8, that has sixteen class intervals between 1.0 and 1.6. For the horizontal profiles, low estimates with a distinct amount of background profiles are observed in the deterministic fern; whilst most estimates are higher than the mean fractal dimensions in the natural and random ferns. The mode of the fractal dimensions is higher in the natural fern than in the random fern. For the vertical profiles, a distinct portion of background profiles and a skewed and flat distribution of the fractal dimensions is observed for all the three ferns. The modes are higher than the means of the estimates for both the random and natural ferns.

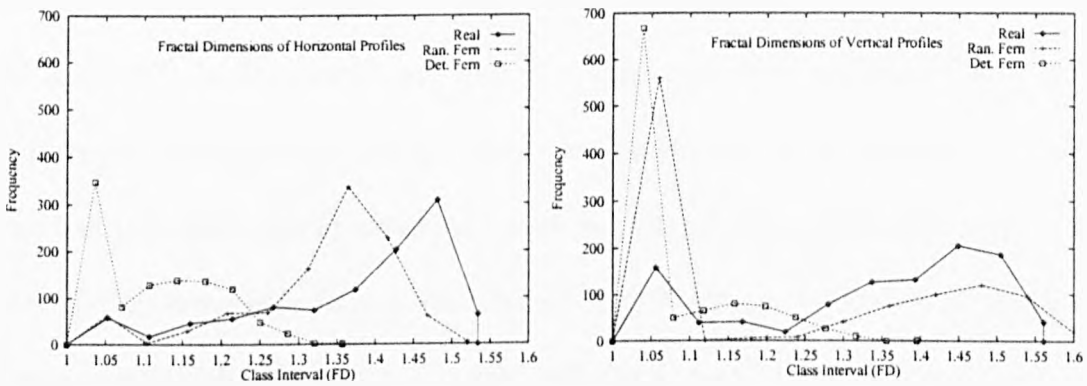

Figure 6.8: The Histogram of the Fern Fractal Dimensions.

Results of the two-sample tests on the fractal dimensions of synthetic and natural ferns are given in Table 6.4. The parametric two-sample t-test is used only for the test between the normal scores and random numbers, whereas the other tests employ the non-parametric two-sample Mann-Whitney U test. Comparisons of the fractal dimensions are conducted between profiles within the same fern, and between ferns of the same direction of profiles.

Profile	Fern Types	U-value	Z-value	P
	NS-RN	-0.003	(2046)	0.99794
Horizontal v. Vertical	Natural	5.8e5	3.845	0.00001*
	Deterministic	6.9e5	12.789	0.00000*
	Random	6.6e5	10.394	0.00000*
Horizontal	Natural–Deterministic	9.6e5	32.991	0.00000*
	Natural–Random	6.9e5	12.177	0.00000*
	Deterministic–Random	8.1e4	-33.235	0.00000*
Vertical	Natural–Deterministic	9.2e5	30.661	0.00000*
	Natural–Random	6.9e4	12.845	0.00000*
	Deterministic–Random	3.9e5	-10.912	0.00000*

Table 6.4: Two-Sample Statistics Tests of Fractal Dimensions between Ferns. The difference is significant at 5% of significance level for all comparisons except the paired normal scores (NS) and random numbers (RN).

The comparison of fractal dimensions between profiles within the same fern is given in the second block of Table 6.4. It shows that the difference of the distribution of the fractal dimensions between profiles of the natural fern is significant statisti-

cally ($p = 0.00*$); although the average fractal dimensions are quite similar, that is, 1.345 and 1.309 for horizontal and vertical profiles, respectively (Table 6.2). Similar comparisons are conducted for the other two synthetic ferns. Again, the results show that the difference of distribution of the fractal dimensions between profiles within the deterministic fern is statistically significant ($p. = 0.00*$); although the means are relatively close, that is, 1.095 and 1.054, respectively, for horizontal and vertical profiles. Furthermore, the difference of distribution of the fractal dimensions between profiles within the random fern is statistically significant ($p = 0.00*$); whereas the means are slightly different from each other, that is, 1.304 and 1.186 for horizontal and vertical profiles, respectively.

Three different comparisons are performed within the same direction of either the horizontal or vertical profiles, that is, comparisons between natural and deterministic, between natural and random, and between deterministic and random ferns. However, none of the six combinations of tests shows any similarity for the specific comparison. All the differences of means under test are statistically significant ($p = 0.00*$).

6.5.4 The Fractal Dimensions of Other Features

Other applications of the box-counting method include the estimation of the fractal dimension from the outline of the fern and the shape of the fern in three dimensions. Figure 6.9 shows the fractal dimensions of the ferns' shapes in two- and three-dimensional spaces. The fractal dimensions of the two-dimensional shape of ferns are very similar to each other between synthetic and natural ferns, whereas those of

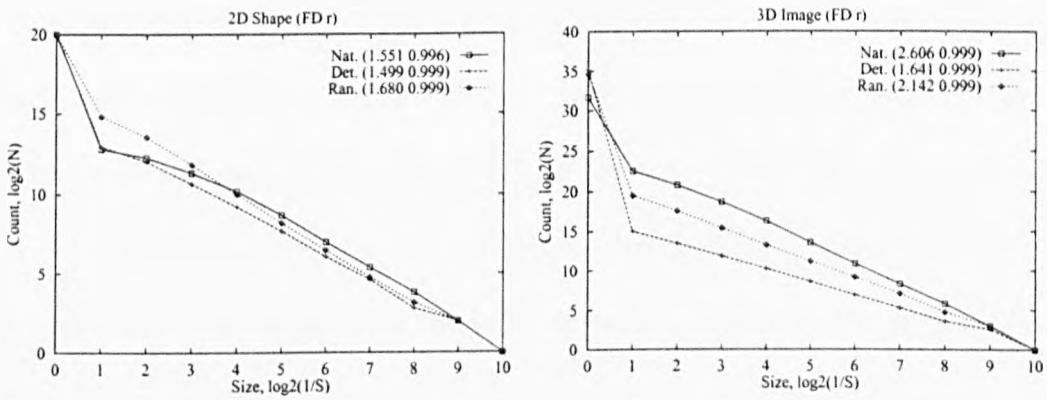

Figure 6.9: Log-Log Plots for the 2D Shape and the 3D Image of Ferns.

three-dimensional ferns vary to some extent. Nevertheless, all of their corresponding correlation coefficients are significant ($r > 0.99$).

6.6 Chapter Discussion and Conclusion

Although the vegetation index is usually utilised to relate vegetation parameters, this study focuses on the morphology of normalised difference vegetation index images. A normalised difference vegetation index image can be equated to a digital elevation model in that the normalised difference vegetation index values are analogous to the heights of a digital elevation model; and greater resemblance between them is found in terms of systems dynamics. Therefore, the fractal analysis for a digital elevation model can be easily applied to the analysis of the normalised difference vegetation index image. It has been proved that vegetation growth parameters can be related with the normalised difference vegetation index; that is, the normalised difference vegetation index is an indicator of plant systems dynamics. Depending on the resolution of the spectrometer or scanner, each pixel on the normalised difference vegetation index image represents the collective dynamics of

a certain number of sub-systems such as chlorophyll, carotene, and xanthophyll; similarly, each pixel on the digital elevation model represents the height formulated by various soil and rock types (Chapter Two). However, the spectral image is comprised of homogeneous background and heterogeneous leafy areas. Some interesting systems dynamics are revealed by the same approach applied to the digital elevation model.

There are two major findings that deserve special attention. The first is the confirmation of using the analytical approach to explore the dynamics of landforms in Chapter Five; and the second is the feasibility and future use of IFS codes on modelling the spectral characteristics of plants. The difference in the composition of sub-systems is easily visualised by the spectral images (Figures 6.4 and 6.6) and clearly illustrated by the estimated fractal dimensions (Figure 6.5 and 6.7). While the fractal dimensions of the empty space approach 1.0, high fractal dimensions are found in the middle part of both the natural and synthetic ferns where more leaflets are concentrated. In other words, fractal dimensions reflect the dynamics of photosynthesis, or the systems dynamics in terms of the normalised difference vegetation index. No scientific article was found to describe a fern in this way, as far as the search result from the Bath Information Database Service (BIDS) is concerned. However, further work is needed to establish the link between the normalised difference vegetation index and the fractal dimension, hence the use of the fractal dimension as an indicator of vegetation growth.

The simulation method using the IFS code has shown its power in generating a natural object. The two-dimensional outline of a synthetic fern is very similar to that of a natural fern in terms of the fractal dimension; although the deterministic

fern is visually more like a bracken which has triangular blades of bi- to tripinnate pinnules, and the random fern is like a Lady Fern which has blades of bi- to tripinnate leaves with alternate leaflets (Toman & Felix, 1990, pp.89 & 91). Whereas Fractal Geometry treats forms as relationships between parts rather than as areas in general (Campbell, 1996), various algorithms might contribute further to the difference in appearance. Alternative measures such as the "lacunarity" can thus be used to distinguish the difference of "voidness" between them (Mandelbrot, 1983, Ch.34). Although it is a possible subject to pursue further, this chapter is more closely concerned about other aspects of using the IFS code.

The fractal dimensions of the three-dimensional synthetic ferns are less close to that of the natural fern. One of the possible problems might be the discretisation process that generates the image. In the domain of real numbers, the distance between nearby points could be so indefinitely far that each point corresponds to only one pair of coordinates; that is, a virtually flat leaf image of uniform height and indefinite details is almost certain. Unfortunately, techniques used to produce the three-dimensional image lead to discretisation of data. The discretisation process affects the computation of fractal dimensions in two opposite ways: it enables the calculation of the fractal dimension for a three-dimensional image at the expense of the accuracy of presenting the data. In other words, the fractal dimension cannot be calculated from a totally flat image; and some points might be shifted to the coordinates to which they do not belong. This effect seemingly contributes to the low fractal estimate of the deterministic fern.

The diversity of the sub-systems is modelled closely by the algorithms. Although the seeming randomness seen in the distribution of the fractal dimensions derived

from the one-dimensional profiles could not be interpreted easily, it is evident that the fractal dimension of the empty background is distinctly different from that of other areas. In conclusion, the use of fractal dimensions derived from the approach designed in this thesis has successfully identified the difference of dynamics between the homogeneous and the heterogeneous sub-systems.

Part III

Discussion and Conclusion

Chapter 7

Condensed Discussion

The scientist does not study nature because it is useful; he studies it because he delights in it, and he delights in it because it is beautiful. If nature were not beautiful, it would not be worth knowing, and if nature were not worth knowing, life would not be worth living. Henri Poincaré, circa 1900s.

In *Chaos and Fractals* (Peitgen *et al.*, 1992, p.15).

7.1 Introduction

This chapter presents a discussion of wider aspects, with the focus on the results obtained in the previous three chapters. It is generally accepted that the contemporary methodology in science is rooted in the inductive-deductive procedure attributed as far back as to the Greek philosopher Aristotle (384-322 BC.) and the hypotheses-experiments method of the French philosopher and mathematician René Descartes (1596-1650); and fortified with the falsificationism (TSP, 1996) of the Austrian philosopher of science Karl Popper (1902-1994). This thesis utilises this possibly standard approach in science to study three natural systems and their corresponding mathematical models (Figure 2.2). Those natural systems were not arbitrarily chosen but carefully selected according to the three types of systems dynamics revealed in the Mandelbrot set (Chapter Two). Subsequent analyses utilise the conventional methods, followed by the box-counting method, that is implemented for each sub-system within the system (Chapter Three), where a sub-system can be a section of the sea wave profile (Chapter Four) or a profile of the digital elevation model (Chapter Five) and the spectral image of a fern (Chapter Six). The results obtained here have arguably proven that the fractal dimensions derived by this approach can be used to interpret various types of systems dynamics reasonably well. The following literature provides a furhter insight into the work accomplished in this thesis.

7.2 Rendered Results

This chapter firstly re-organises the results from the previous three chapters, although the study of those three natural systems is united under the single box-counting method that is applied to the derivation of fractal dimensions for all the systems. Whilst such an approach would not have been new to Renaissance Man ("the complete human being") between the fourteenth and seventeenth centuries (Hellemans & Bunch, 1988), it is certainly a unfamiliar scientific methodology characterised by the Linnaean classification scheme devised by the Swedish botanist Carolus Linnaeus (1707–1778) (TSP, 1996), until the development of, for example, Fractal Geometry (Mandelbrot, 1983). Although three systems were presented in three chapters, it would be more appropriate to summarise the results for further discussion. Figure 7.1 shows the summary of fractal dimensions obtained for waves, landforms and plants in Chapters Four, Five and Six, respectively; whilst Tables 7.1 and 7.2 extract some essentials of the basic statistics and statistical test results, respectively.

FRACTAL DIMENSIONS OF SEA WAVE PROFILES. The estimated fractal dimensions of each of 27 records are meaningful ($r > 0.99$) and relatively consistent for both natural and synhteic waves (Figure 4.16); whereas the fractal dimension of the overall wave is not statistically meaningful for the natural ($r = 0.286$) and synthetic ($r = 0.315$) waves. The average heights and standard deviations are very different between both waves (Table 4.5); however, the difference of mean fractal dimensions is arguably significant, depending on the statistical results referred. The two-sample t-test shows that the difference is not significant, although the Mann-Whitney U concludes otherwise (Table 4.5).

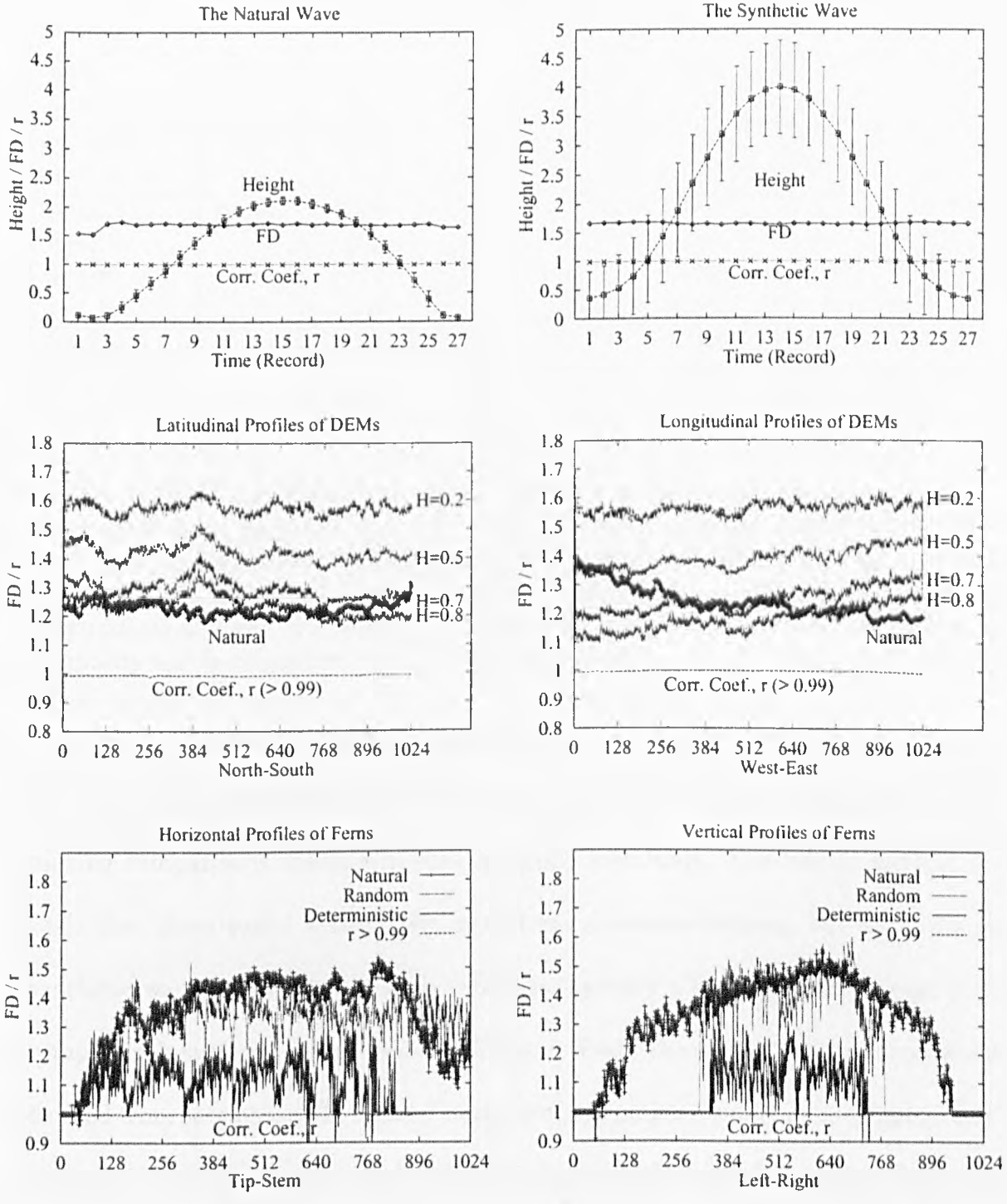

Figure 7.1: Summarised Fractal Dimensions of the Synthetic and Natural Systems. The fractal dimensions (FD) and their corresponding correlation coefficients (r) are summarised for the sea wave profiles, where the wave profile is modelled by multi-frequency sinusoids and each record is of 1024 seconds; digital elevation models, where the synthetic landforms of various Hurst exponents are generated by the mid-point displacement method; and fern images, where the synthetic ferns are produced using the IFS code implemented with the deterministic and random algorithms.

Data	n	$\bar{x}$	std	$Skew$	$Kurt$	W	$c.s.l.$
N.Scores	27	0.000	0.972	0.000	-0.583	0.996	0.9999
R.Number		0.095	1.141	-0.006	-0.442	0.990	0.9929
Real	Waves	1.679	0.049	-2.382	5.002	0.653	0.0000*
Syn.		1.662	0.016	0.240	-1.121	0.927	0.0644
N.Scores	1024	0.000	0.999	0.000	-0.044	0.988	0.7667
R.Number		0.000	0.972	0.185	0.272	0.988	0.7760
Real.H	DEMs	1.226	0.027	5.294	85.23	0.827	0.0000*
Real.V		1.243	0.053	0.993	0.185	0.886	0.0000*
Syn.H		1.296	0.041	4.037	55.060	0.862	0.0000*
Syn.V		1.248	0.048	1.441	8.987	0.917	0.0000*
Real.H	Ferns	1.345	0.131	-1.100	0.309	0.854	0.0000*
Real.V		1.309	0.166	-0.767	-0.721	0.852	0.0000*
Syn.H		1.304	0.106	-1.387	1.704	0.851	0.0000*
Syn.V		1.186	0.213	0.402	-1.624	0.728	0.0000*

Table 7.1: Basic Statistics and Results of the Normality Test.
"N.Scores" is the normal scores. "R.Number" is the random numbers. For the natural (Real) and synthetic (Syn) systems, the latitudinal profiles of a digital elevation model (DEM)) and the horizontal profiles of a fern are indicated as "H"; and the longitudinal and vertical profiles are marked with "V". The Shapiro and Wilk's W normality test is conducted at 5% significance level.

While a comparative study using the fractal dimensions derived from different sources can be restricted by the estimation and scales employed (Chapter Three), making comparisons within a system is totally justifiable. The fractal method reveals that there exists a similarity in systems dynamics between the natural and synthetic waves. The natural wave profile is arguably a homogeneous system with complex sub-systems, as described in Chapter Two. The similar fractal dimensions derived from sections of the system have provided positive evidence to support that argument. A simple mathematical model of a natural wave also reaches the same conclusion, although a totally different distribution of data is observed. Such a high degree of agreement between the natural and synthetic wave systems confirms that the measurement of the fractal dimension is a reasonable quantitative indicator of systems dynamics. Meanwhile, the conventional methods show that the difference between systems is significant; for example, the spectral analysis revealed

Data	n	$U-value$	$Z-value$	p
Artificial	27	-0.330		0.7427
Waves		589		0.0001*
		1.677	(t-test)	0.0995
Artificial	1024	-0.003		0.9979
DEM.Latitudal		4.3e4	-35.951	0.0000*
DEM.Longitudal		4.8e5	-3.628	0.0000*
Fern.Horizontal		6.9e5	12.177	0.0000*
Fern.Vertical		6.9e4	12.845	0.0003*

Data	n	$Me.R$	$Me.S$	$< Me.R$	$< Me.S$	$c.s.l.$
Artificial	27	0.000	-0.97	12	14	0.7853
Waves		1.321	1.387	25	0	0.0000*
Artificial	1024	0.000	-0.019	508	515	0.7909
DEM.Latitudal		1.775	1.749	380	634	0.0000*
DEM.Longitudal		1.771	1.813	735	287	0.0000*
Fern.Horizontal		1.626	0.000	224	804	0.0000*
Fern.Vertical		1.607	1.666	649	379	0.0000*

Table 7.2: Summary of Two-Sample Tests of Fractal Dimensions.
Two-sample Mann-Whitney U and median (Me) tests are conducted for the fractal dimensions derived from the real (R) and synthetic (S) sea waves, landforms (DEM), ferns, and the artificial data that include normal scores and random numbers. All tests are conducted at 5% significance level.

that there is no single dominant component frequency in the natural wave, unlike in the synthetic wave. The fractal method has apparently explored one of the aspects unrevealed by the conventional methods. This approach is extended to examine the heterogeneous systems such as landforms.

FRACTAL DIMENSIONS OF DEM PROFILES. The mean fractal dimensions of latitudinal and longitudinal profiles of the digital elevation model of Shei-pa National Park are similar (Table 5.1); however, the fractal dimensions are significantly different in terms of distribution (Table 5.4). The fractal dimensions estimated from synthetic DEMs of various Hurst (H) exponents generally agree with the theoretical values (Figure 5.12 and Table 5.3); furthermore, the difference of the fractal dimensions between profiles of different directions is significant for each synthetic DEM (Table 5.1). The particular DEM of $H = 0.7$ was used in further comparison with

the natural landform, because its estimated dimension fits best with the theoretical value and appears similar to that of the real landform (Chapter Five).

The measurement of fractal dimension has further supported the observation on landform as described in Chapter Two. Unlike a wave that has similar sub-systems (sections), the complexity of a landform system can be shown by the different fractal dimensions derived from the sub-systems or profiles; similarly, the complexity of an individual profile is created by the mostly unknown sub-systems within that profile, each having maintained its own characteristics. Since possible discrepency in comparative studies using fractal dimensions is usually caused by the different methods and scales employed (Chapter Three), the approach used here provides a simple way of exploring the complexity of landforms. In terms of digital images, a spectral image is similar to a digital elevation model in many ways; the only difference is that a spectral image contains information of inert or homogeneous as well as leafy or heterogeneous areas. Therefore, the methods used to analyse the landform are transferable to such an image.

FRACTAL DIMENSIONS OF THE NDVI IMAGE OF PLANTS. For a natural fern, the mean fractal dimensions of horizontal and vertical profiles are similar graphically (Figure 6.5) and different statistically (Table 6.4); futhermore, the distribution patterns between profiles are also significantly different (Table 6.4). For the synthetic ferns, the mean fractal dimensions as well as the distribution of the fractal dimensions between profiles are significantly different (Tables 6.3 and 6.4). In general, the distribution of the fractal dimensions of different profiles is smoother in the natural than in the synthetic ferns.

The approach for landforms has produced successful comparisons between the natural and simulated ferns; that is, the measurement of the fractal dimension is especially useful in distinguishing the inert from leafy areas. The distribution of the fractal dimensions of profiles leads to the conclusion that the IFS code is not used to simulate spectral characteristics; whereas the fractal dimensions of the shape reveals that such a code is aimed at modelling the fern's outline (Figure 6.9).

In summary, the results obtained in this thesis have provided many forms of support for the use of the fractal dimension as an indicator and a tool for comparing systems dynamics between natural systems and their corresponding mathematical models. The following section focuses on the discussion based on the current results and the results reported in other work.

7.3 Summarised Discussion

While it seems rather straightforward that Fractal Geometry is applicable to analysing irregular objects, there are some essential issues regarding the application of the fractal concept. These issues are mainly concerned with whether the application of fractal analysis requires an object to be fractal; whether it is necessary to identify noise prior the estimation of fractal dimension; and whether the same estimates represent objects of the same complexity.

The first issue is concerning the requirement of an object's being fractal for the estimation of fractal dimension, that is not tautologically trivial but logically true by definition. The classic definition of a "fractal" is given by Mandelbrot (1983) as

"a set for which the Hausdorff-Bescovitch dimension strictly exceeds the topological dimensions." The structure of fractals, as Feder (1988) defined it, is "a shape made of parts that are similar to the whole in some way." With regard to the process that creates such structure, *The Hutchinson Softback Encyclopedia* (TSP, 1996), refers a fractal to "an irregular shape or surface produced by a procedure of repeated subdivision." The quantification of such an object using fractional dimension is totally new as far as the Euclidean geometry is concerned. For example, a Cantor set is a fractal because its fractal dimension is $D = \log 2/\log 3 \sim 0.6309$, while its Euclidean dimension is $D_E = 1$ and topological dimension is $D_T = 0$; the original Koch curve is a fractal with $D = \log 4/\log 3 \sim 1.2618 > 1$, while $D_E = 2$ and $D_T = 1$; and the trail of Brownian motion is a fractal with $D = 2$ and $D_T = 1$. Therefore, the fractal dimension may be an integer, that is, not greater than D_E but strictly greater than D_T (Mandelbrot, 1983, p.15; Chs. 6, 8 & 25). Euclidean objects such as straight lines, rectangles and cubes are thus not fractals by definition, although the dimension of Euclidean objects is calculable with the estimation method used in fractal science. In other words, the fractal dimensions can be used to identify fractals from Euclidean objects.

The second issue concerns whether it is necessary to identify noise or randomness from a system before the calculation of the fractal dimension commences. In the light of Chaos Theory and Fractal Geometry, the quantitative study of time series is mainly characterised by the calculation of Lyapunov exponents and the estimation of fractal dimensions from the reconstructed attractor (Brown *et al.*, 1991; Rowlands & Sprott, 1992; Zeng *et al.*, 1992; Mukesh, 1993; Bergmasco *et al.*, 1995; Murphy *et al.*, 1996; Chandra, 1997; Zhang, 1997). Chaotic systems have the appearance

of unpredictability but are sensitive to the initial condition while determined by precise deterministic laws (Crilly *et al.*, 1991); whilst the Lyapunov exponent is used to characterise the exponential divergence of neighbouring trajectories induced by the system's sensitivity of initial conditions (Mullin, 1993b, p.42). In brief, the sum of all the exponents will be negative if there is an attractor and there will be at least one positive exponent if the attractor is strange; whereas the geometrical characterisation of a reconstructed attractor is to calculate its fractal dimension, which measures the self-similarity and self-affinity of a system that is implied by the embedded deterministic laws. However, the attractor might resemble that of noisy data, Malinetskii *et al.* (1993) warned; and the Lyapunov exponent and the fractal dimension are inseparable and always used together to assure that the use of the latter is valid following the calculation of the former (Brown *et al.*, 1991; Prichard & Price, 1992; Rowlands & Sprott, 1992; Mukesh, 1993; Wagner *et al.*, 1995; Murphy *et al.*, 1996). Indeed, the use of the fractal dimension as an indicator of chaos is widely suggested; for example, it is quite common to have statements such as "a low and fractal dimension shows chaotic dynamics [of atmospheric pollen counts]" (Bianchi *et al.*, 1992) or "the fractal dimension of the attractor...[indicates] chaotic behavior [in off-Bragg photorefractive four-wave mixing time series]" (Shaw, 1993). It is also true that noisy and chaotic signals in time series could be separated by the combined use of Lyapunov exponents and fractal dimensions (Bianchi *et al.*, 1992; Bauer *et al.*, 1993; Shaw, 1993; Serio, 1994; Arizmendi *et al.*, 1995; Gopinathan, 1997). In general, the fractal dimension is popularly used to characterise the attractor which represents the characteristics of chaotic systems such as a time series. However, such an estimation is unlikely to be applicable to structures embedded in higher dimensions, unless they can be expressed in terms of time series.

The methods for estimating fractal dimensions vary greatly according to the subjects under study. The researchers on time series try to justify the view that the use of fractal dimension should follow the identification of chaos by the calculation of Lyapunov exponents and noise is either un-attended or "corrected". On the other hand, others would just use fractal dimension to identify randomness; for example, De Vries *et al.* (1994) found that the α exponent is 0.45 for the model of river network of $D = 1.8$, using the relationship of $\alpha = 1 - 1/D$, where α is the measure of the integrated mean annual discharge and D is the topological dimension. Furthermore, De Vries *et al.* (1994) also obtained an exponent of 1/2 for the random model, implying that a random river network is plane-filling and has dimension of 2.0. Although such a river network means an unrealistic surface covered with a layer of water, the measure of fractal dimension was found to reflect randomness.

Randomness actually plays an important role in creating deterministic and/or irregular shapes (Peitgen *et al.*, 1992, Chs.6 & 9). Barnsley (1988; 1993) used the "chaos game" to generate life-like fern leaves as well as self-similar or exact fractal objects such as the Sierpinski gasket. The chaos game works because every point it produces falls in the attractor, i.e., the fern or the gasket (Peitgen *et al.*, 1992, p.305). Since there exists the invariant measure in the IFS transformations (Peitgen *et al.*, 1992, p.330), it is absolutely possible to quantify the object by the measure of fractal dimension (Peitgen *et al.*, 1992, p.469). Furthermore, irregular shapes ranging from the fragmentation of atomic nuclei to the formation of clusters of galaxies can be simulated by percolation models (Lidar *et al.*, 1997; Jan & Stauffer, 1998), based on the fractional Brownian motion, the generalisation of Brownian motion (Peitgen *et al.*, 1992; Stutzki *et al.*, 1998, p.458). In other words, such systems

possess the properties decipherable by means of approximating Brownian motion of particles, which underlines the scaling laws from which fractal dimension is derived (Peitgen *et al.*, 1992, p.458). Indeed, Sommerer (1994) has proved that there is a firm quantitative connection between the dimension of an experimentally observed fractal spatial pattern and the process producing it. In this thesis, randomness is actually utilised to generate landforms and ferns.

The third issue is about whether the same fractal dimension represents objects of the same complexity (Müssigmann, 1992). It is quite possible that objects of different textures would yield similar fractal dimensions. This was observed by Mandelbrot (1983, Chs. 34 & 35), who proposed an alternative measure called "lacunarity", which is from *lacuna*, Latin for *gap*. Lacunarity measures difference in texture in terms of gap composition (Allain & Cloitre, 1991). Since it was designed for spatial phenomena, it is unlikely to be applicable to time series analysis without the time series being transformed into phase portraits; this might introduce further complication through the transformation process (Heng *et al.*, 1996; Shirer *et al.*, 1997). Comparison of objects with the same fractal dimension is more feasible in theory than in reality (Mandelbrot, 1983, Ch. 34); while this is an area worthy of future research.

Having discerned the three issues regarding the application of the fractal concept, this chapter continues on the major discussion in the following three sub-sections. The immediate sub-section illustrates issues on the fractal characterisations of the natural systems, and includes the discussion on the technical consideration of using estimation methods, which leads to the exploration of multi-fractals. It is followed by the discussion on the unique approach of this thesis, that enables comparisons

of sub-systems within a system and presents a different way of illustrating multi-fractality from other existing methods. The last sub-section is the main discussion based on the comparison with published work.

7.3.1 Fractal Characterisation of Nature

Many mathematical structures such as the Mandelbrot set are self-similar fractals, that are of geometric invariance under certain transformations (Mandelbrot, 1983). In other words, magnified subsets of an object are identical to the whole and to each other (Mandelbrot, 1988, p.22). Beyond the mathematical structures, most geographic phenomena behave like fractals only statistically, hence are called the self-affine fractals (Mandelbrot, 1983). In contrast to self-similar fractals, self-affine fractals are anisotropic, thus appear to be the same if the length along different directions is scaled down or up by various factors (Voss, 1985b; Mandelbrot, 1986).

The fractal study of geographical features includes the measuring of linear features (Mandelbrot, 1977; Goodchild, 1980; Hjelmfelt, 1988; La Barbera & Rosso, 1989; Nikora, 1991; Breyer & Snow, 1992, for example); describing, characterising and delineating landforms (Fox & Hayes, 1985; Roy *et al.*, 1987; Klinenberg, 1988; Huang & Turcotte, 1989; Piech & Piech, 1990; Xia, 1993, for example); and simulating realistic-looking terrains (Fournier *et al.*, 1982c; Goodchild, 1982; Voss, 1985b; Miller, 1986; Goodchild & Mark, 1987; Klinenberg, 1988; Mandelbrot, 1988; Voss, 1988; Mareschal, 1989; Clarke, 1993, for example). The subjects under study are mostly either linear features including coastlines, shorelines, river channels, boundaries of drainage basins and terrain profiles (Mandelbrot, 1967; Kent &

Wong, 1982; Qiu, 1988; Phillips, 1986; Culling & Datko, 1987; La Barbera & Rosso, 1989; Phillips, 1989; Robert & Roy, 1990; Philippe, 1993; Seyb, 1994, for example); or the areal features such as topographic surfaces or sea floors (Goodchild, 1982; Mark & Aronson, 1984; Brown & Scholz, 1985; Power *et al.*, 1987; Klinenberg, 1988; Robert, 1988; Andrle & Abrahams, 1989; Gilbert, 1989; Huang & Turcotte, 1989; Norton & Sorenson, 1989; Milne, 1990; Rex & Malason, 1990; Turner, 1990; Chase, 1992; Klinkenberg, 1992; Burrough, 1993; Olsen *et al.*, 1993; Xia, 1993, for instance). Although some geographic features do behave as fractals at all scales, these features are the exception rather than the norm (Gao & Xia, 1996). Furthermore, it is more likely that fractals occur for certain types of features, along certain directions or at limited scales (Bradbury *et al.*, 1984; Mark & Aronson, 1984; Goodchild & Mark, 1987; Xia, 1993).

The fractal characterisation of such objects usually utilises the measure of the fractal dimension. A number of methods have been proposed to determine the fractal dimension of linear and areal features, as shown in Tables 3.1 and 3.2. The statistical regression model is applied in most methods to the log-log plots, first proposed in conjunction with the divider method for complex curves by Richardson (1961); although Leohle & Li (1996) argued that approaches using regression models to estimate fractal dimensions of spatial patterns are statistically invalid. The advantages and disadvantages of various methods are discussed below; where the central issue is on the scales of estimation, that lead to the exploration of multi-fractals.

The Estimation of Fractal Dimensions

Central to the understanding of fractals is the property of scale independence, which can be quantified by the measurement of fractal dimension, a real number that measures the degree of an entity's irregularity (Gao & Xia, 1996). A popular method for determining the fractal dimension of the linear features is the divider method, employed by Mandelbrot (1967) to measure the dimension of the British coastline. In this method, a table is built up on the relationship between the scales of the divider and the corresponded counts; then, a statistical regression model is used to derive the fractal dimension from the slope of the Richardson or log-log plot. Other methods for areal or higher dimensional features were founded upon Richardson's method; that is, the use of the regression model on the log-log plot is basically the same. Here, the fundamental problems regarding the derivation of the fractal dimension are closely related with the remainder length and scales used to construct the log-log plot and the linearity of the plot.

The divider method involves measuring the length of a curve using a ruler or divider of variable lengths decreasing geometrically. A common problem with the divider method is that the results are sensitive to the treatment of the remainder length (Aviles *et al.*, 1987; Klinkenberg & Goodchild, 1992; Andrle, 1992). Whilst Andrle (1992) and Klinkenberg (1994) provided some in-depth discussions on the divider method, Beauvais & Montgomery (1996) reported three ways proposed by Aviles *et al.* (1987) to treat the remainder problem, that is, add the remainder length to the estimated length of the curve; neglect the remainder length; and round the counted steps to the nearest whole number. The remainder problem is nevertheless common to other methods, including the box-counting method. The most viable

solution, as seen here, is to collect the sample of suitable length.

The second concern is the scale problem, more significant in experimental measurements than in theoretical objects. For a theoretically generated structure, there is virtually no limitation on the range of scale. For naturally occurring objects, the divider method applies only over a limited range of scales, and misapplication can lead to inconsistent results (Goodchild, 1980; Beauvais & Montgomery, 1996). The plateau at extreme resolutions in the log-log plot is inevitable (Peitgen *et al.*, 1992, p.722). The log-log plots also can exhibit deviations from simple power law scaling, as revealed by systematic curvature of the structure of the standard residuals (Andrle & Abrahams, 1989; Andrle, 1992; Klinkenberg & Goodchild, 1992). Therefore, the final concern of deriving the fractal dimensions is on the linearity of the plot.

The linearity of the log-log plot could be examined by many ways. For example, whether the fractal dimension is scale-independent can be tested using the method of Andrle (1992), that examines the curvature in the log-log plots for deviation from strict self-similarity using the standardised residuals from least squares linear regression model (Andrle & Abrahams, 1989; Beauvais & Montgomery, 1996). In other words, if there is no structure to the regression residuals, then a single fractal dimension is estimated using least squares linear regression of data between the smaller length scale cut-off and the upper limit; whereas the plots exhibiting systematic structure to regression residuals are examined for distinct linear trends and new regressions are performed. The identification of multi-linearity leads to the distinguishing of mono- and multi-fractals, especially in geomorphology.

Mono- and Multi-fractals

In order to accomplish a perfect fit between the fractal model and the real terrain data, two line segments (Culling & Datko, 1987) or even more lines (Mark & Aronson, 1984; Norton & Sorenson, 1989) are usually required in the log-log plot. These phenomena are thus multi-fractals, although the derivation of the fractal dimensions is different from the formal definition of multi-fractal dimensions as given in Appendix D. For example, Sengupta *et al.* (1990) reported on cumulus cloud scales and processes that the break in two power laws is at the size where clouds begin to modify their environment; whereas Packepsky (1996) also found two distinct intervals of fractal dimensions in the range of soil pore radii from 4 nm to 1 μm. Changing the scale of observation also enables in identifying multiple segments in the log-log plots. Campbell & Shepard (1996) measured the lava surface roughness using radar observations at 5.7, 24 and 68 cm (C, L and P band) wavelengths; and they concluded that the roughness at the two large scales is well described by a single fractal dimension, but the texture at very small scale is not. Chan & Page (1997) captured boundary images at a range of magnification and found that the estimated fractal dimensions vary with magnifications.

Multifractal terrains may be attributed to the processes responsible for the formation of the landscape (Kent & Wong, 1982). For example, Armstrong (1986) found that the fractal dimension in the range 1-10 cm represented animal-treading effects while those over the range 10-100 cm were caused by geomorphological effects; and Chase (1992) speculated that the evolution of a landscape at different stages or the changes in climate and tectonic activities were the causes of multifractal topography. In addition, the changed relative importance of diffusional and erosional

processes shaping the landscape may also facilitate the formation of multifractal landforms (Gao & Xia, 1996).

Multifractal geographic surfaces are actually much more common than their fractal counterparts (Mark & Aronson, 1984; Chase, 1992). Considering that most geographic entities are statistical fractals, many of them are multifractal and their fractal nature is scale dependent (Gao & Xia, 1996). The multifractal nature of geographic entities is not limited to topographic surfaces alone. Many linear features such as channel networks are multifractals as well (Burrough, 1981; Kent & Wong, 1982; Tarboton *et al.*, 1988; Elliot, 1989; Snow, 1989). Whereas some features are mono-fractals or multi-fractals, some others are not fractals at all, in terms of being scalable at all scales (Klinenberg, 1988, for example). The concept of multi-fractal is used to model landforms quite successfully and efforts have been made to explain the reasons for multi-fractal geographic phenomena and the significance of scaling (Gao & Xia, 1996).

According to Berntson & Stoll (1997), methods of estimating the fractal dimension have often been applied in an uncritical manner, "violating assumptions about the nature of fractal structure." The most common error involves ignoring the fact that ideal, i.e., indefinitely nested, fractal structures exhibit self-similarity over any range of scales; whereas the real world structures exhibit self-similarity only over a finite range of scales. Using the multi-scaling idea of Coniglio & Zannetti (1989a; 1989b), Mann & Jan (1991) calculated the fractal dimension of the percolation clusters from the density profile and reported that they did not find any evidence of multifractal or multi-scaling behaviour; however, other studies on percolation (Loehle & Li, 1996; Bershadskii, 1997) using the similar method (Na-

gatani & Stanley, 1991) reached the opposite conclusion. Whilst researchers such as Claps & Oliveto (1996, p.3123) simply regarded the multifractal phenomena as self-affine objects which present "self-similar behavior only in a defined range of scales"; Berntson & Stoll (1997) devised a new technique, which utilises a combination of curve fitting and tests of curvilinearity of residuals to identify the largest range of contiguous scales that exhibit statistical self-similarity.

The multi-fractality explained above is totally different from the formal definition of the multi-fractal dimensions, as given in Appendix D. Since "the idea of self-similarity is readily extended from [mono-fractal] sets to [multi-fractal] measure" (Evertsz & Mandelbrot, 1992), the calculation of the multi-fractal dimensions, based on the identical estimation method, also suffers from the same scale problem stated above. Researchers on fractals are usually interested in comparing the estimated fractal dimensions between systems, hence, encountered with the problems on the methods and scales used, as described earlier. An alternative is to localise the sub-system dynamics within a system so that comparisons can be made with the identical method and scales between the sub-systems within the system. The complexity within the system can therefore be understood, provided that the linearity in the log-log plots is statistically significant.

7.3.2 The Unique Contribution of This Thesis

The above observation leads to the development of the approach of this thesis, that is to calculate the fractal dimension of sub-systems using box-counting method (Chapter Three). This approach is unique in three aspects; the approach utilises the basic

estimation method of the mono-fractal dimension; the calculation of the fractal dimensions from sub-systems enables the comparison of systems dynamics within a system; and the box-counting method is applicable to objects embedded in higher dimensional systems.

The use of the monofractal method is fundamental, as long as there exists a single line segment and its linearity is statistically significant in the log-log plot. The concern over multi-fractality arises from either the existence of multiple line segments in the log-log plots or the algorithms (Appendix D), that might be questionable if there are multiple segments, because "the program [for the mono-fractals]...has been carried out and runs (*sic*) under the theme *multifractals*" (Peitgen *et al.*, 1992, p.216). With an alternative implementation approach, the complexity of a system can be shown using the basic estimation method.

The fractal dimensions estimated from sub-systems can reflect the systems dynamics within a system better than the more common single measurement approach; that is, the sub-systems dynamics can be physically located within the system and the comparison between sub-systems dynamics is under the identical method and scales. In other words, the sub-systems and their dynamics can be clearly located in the wave profiles, digital elevation models and the plant images; and subsequent comparisons can be made with the identical criteria. This approach as well as other methods is subject to the linearity of the log-log plots, quantifiable by the correlation coefficients of the linear regression model; however, the relatively high correlation coefficients indicate that the linearity is significant. Since the data selected are of various dimensions, a feasible estimation method has to be found.

The box-counting method is subsequently chosen, because it is more feasible than other methods in deriving fractal dimensions from systems of higher dimensions. In other words, the counting unit can be easily changed to any dimensions. Since temporal, spatial and tempospatial data may be collected on the same study area, the use of the box-counting method will minimise the inherited difference between methods and allow meaningful comparisons to be made.

Therefore, the contribution of this thesis is twofolds: the methodology and the results. The advantages of using this approach have been illustrated in Chapters Two and Three and above. Whilst a moderate discussion on the findings from the sea wave profiles, digital elevation models and plant images was given respectively in Chapters Four, Five and Six; the major discussion is given in the following section.

7.3.3 Comparisons with Other Results

This section compares the current findings with the results of others. The basic requirements for making a meaningful comparison is explained in Chapter Three; that is, the comparison must be based on the identical method and the range of scales. Whilst relatively few examples are available for perfect comparison under such restraints, comparisons on a loose basis are nevertheless valuable.

The following three sub-sections contribute to the comparisons with others. Each section starts with a discussion of broader areas such as time series, landforms and plants; followed by a discussion on similar subjects such as waves, digital elevation models and NDVI images; and finally, comparisons are made with the two fundamental requirements met as closely as possible.

Temporal Systems and Sea Wave Profiles

A typical approach to time series is to construct a plot of measurements against time, to calculate the Fourier transformation, and to estimate the fractal dimension using the linear regression model on the log-log plot (Shaw, 1993). One of the most favourable subjects is long-term time series produced by, for example, a wide range of systems listed in Section 4.6.2 and described below.

Time series are suitable subjects for distinguishing noise from chaos (Serio, 1994; Arizmendi *et al.*, 1995; Vibe & Vesin, 1996; Gopinathan, 1997), that is arguably more common in nature. The scenarios from the rotational Taylor-Couette flow were used to show a variety of routes to chaos (Buzug *et al.*, 1992); while the white and/or "coloured random noise" could be examined by means of multifractals (Osborne & Pastorello, 1993; Bergamasco *et al.*, 1994). Using the definition of the singularity spectrum of the time series, researchers explored the multifractal characteristics of turbulent flows (Hadad *et al.*, 1993), and the seismicity of the Himalayan region (Teotia *et al.*, 1997). The fractal analysis also contributes to the understanding of human physiology; for example, the arterial pressure and renal blood flow are in fact "nonlinear dynamic (chaotic) processes" (Wagner & Persson, 1995; Christ *et al.*, 1997; Yambe *et al.*, 1995; Yambe *et al.*, 1997); and the sleep stages were significantly different (Pradhan *et al.*, 1995; Noguchi *et al.*, 1998) in the electroencephalogram (EEG) (Accardo *et al.*, 1997). Bianchi *et al.* (1992) detected the existence of chaos from a time series of atmospheric pollen counts, suggesting that the current models applying aerobiological knowledge to medical or agricultural practices should include chaotic elements.

That randomness plays a significant role in modelling is supported by the results obtained in this thesis as well as in published work (Voss, 1988; Barnsley, 1993, for example). The synthetic wave profile was modelled by multi-frequency sinusoids, that do not contain a single random element; therefore, the distribution in heights is less realistic than the natural wave. Although both synthetic landforms resemble the natural landscape, the synthetic landform with randomness is statistically more robust than the one without. Furthermore, the difference in appearance between the deterministic and random ferns is distinct both visually and statistically. The measure of the fractal dimension is an alternative in making comparisons.

The more significant implication on the use of the fractal dimensions can be illustrated here. Eghball & Power (1995) used a semi-variogram to calculate the fractal dimensions for the average yields of nine grain crops along with fibre yield of cotton from 1930 to 1990 in the U.S.A.; where a small fractal dimension (near 1) indicates the dominance of long-term variation, while a large fractal dimension (near 2) indicates the dominance of short-term variation and non-dominance or lack of long-term variation or trend. This effect is demonstrated by the fractal dimensions of 1.20 for the relatively stable rice production and 1.47 for the soybean rich in protein and susceptible to insect invasion. Haastrup & Funtowicz (1992) applied fractal techniques to accident time series and suggested that accidents occur in a structured way. An attempt was made to detect the machinery faults from time series vibration signals (Logan & Mathew, 1996). The fractal analysis can be used in conjunction with the conventional signal analysis especially if non-stationary and non-Gaussian features of the signal become important (Sakuma *et al.*, 1996); whilst some researchers even devised a "dimensiometer" (Anmajunas & Tamasevicius, 1992) or a diagnostic tool

(Chandra, 1997) for time series.

The discussion so far has been on the widest possible range of subjects. The following sub-section will concentrate on the fractals found in geographical time series, followed by the discussion on the sea waves.

Fractals in Geophysical Time series

Fractal analysis has been applied to geophysical time series such as soil temperature (Outcalt *et al.*, 1992; Hinkel & Outcalt, 1995; Outcalt & Hinkel, 1996), earth climate (Gober *et al.*, 1992; Bitouk, 1994), atmosphere (Gober *et al.*, 1992; Islam *et al.*, 1993; Sahay & Sreenivasan, 1996; Shirer *et al.*, 1997), sea level (Triantafyllou *et al.*, 1995), seismicity (Costain & Bollinger, 1996; Teotia *et al.*, 1997), and earthquakes (Volant & Grasso, 1994; Tsai, 1997; Wang, 1997).

Fractal dimensions were found to be related to various geophysical factors and parameters. In the air, the dynamics in the atmosphere are complicated (Islam *et al.*, 1993); the temperature variation is generally characterised as having high dimensionality (Gober *et al.*, 1992; Sahay & Sreenivasan, 1996; Shirer *et al.*, 1997); and the horizontal component of wind speed time series were said to have a fractal dimension of 1.60 (Syu & Kirchhoff, 1993). On the ground, Outcalt *et al.* (1992) reported that the fractal dimension decreased with depth in the frozen regime of the re-freezing layer in northern Alaska; whilst Hinkel & Outcalt (1995) found the relationship between the fractal dimension and Hurst exponent is not linear from the data collected in central Alaska. In the water, the dynamics of the sea level are "a rather nonuniform chaotic one" (Triantafyllou *et al.*, 1995); furthermore, Costain & Bollinger (1996) suggested that climate plays a key role in triggering the intraplate

seismicity in the eastern United states, because the fractal dimension determined from downward-continued streamflow is approximately the same as the fractal dimension of intraplate seismicity. In space, the deterministic and chaotic dynamics were thought to exist in the solar wind turbulence (Polygiannakis & Moussas, 1994).

Since the methods and scales are different in the above researches, the corresponding results are not suitable for further comparison with the current findings. The focus of discussion is, therefore, on the fractals in sea wave dynamics.

Fractals in Sea Wave Profiles

As far as this thesis can determine, very few articles have been published on the fractal characteristics of sea water waves. Nevertheless, a severe issue has emerged to challenge one of the traditional assumptions regarding sea waves; that is, the statistics of the sea surface displacement produced by waves are Gaussian, or equivalently, the statistics of the wave amplitudes are Rayleigh (West, 1996). In other words, the randomness in surface waves was assumed .

Bergamasco *et al.* (1995) found not only a finite value for the correlation dimension similar to 7 but also a positive value for the Lyapunov exponent, which indicates the possibility of chaotic behaviour; that is, the wave data were essentially stochastic and the correlation dimension and Lyapunov exponent resulted from the anomalous statistical behaviour of certain near-Gaussian (or near-bell-shaped) random process. Others tended to abandon utterly the traditional assumption regarding sea waves; for example, West (1996) proposed that the statistical properties of sea waves are of "the visibly random behaviour", which result in the stochastic forces that load off-shore structures and ships. Shaw & Churnside (1997) also concluded that the

glint count histogram widths of ocean surface did not follow Gaussian statistics, and histogram shapes were approximately log normal. The presumption of sea waves being seemingly random was further examined by others; for example, based on an analysis of airborne visible and near-infrared imagery of the ocean surface under a limited range of wind speed and fetch, Kerman & Bernier (1994) showed that the lower-intensity reflective areas follow a Rayleigh probability distribution, while the higher-intensity pixels associated with the scattered light from foam and breaking waves demonstrated scaling characteristics in both the optical spectra and the cumulative probability distributions. In other words, the scaling characteristics imply the estimation of the fractal dimension is possible.

Despite the poor understanding of the fractal nature of waves, few authors have estimated the fractal dimensions from different wave data; and most seem to liken relating the fractal characteristics with the forces that generate the waves. Shen & Mei (1993) used Fractal Geometry to model the intermittency of energy input from wind to wave components and proved that "the classical frequency spectral exponent 4 must be replaced by $4 + (2 - D)$, where D [~ 1.88] is the informational entropy dimension of the support subset, upon which energy input from the wind to the gravity waves in the equilibrium range [of spectra] is considered." In the experiment measuring laser glint counts from the ocean surface by Shaw & Churnside (1997), spectral density peaks were found to exist at frequencies corresponding to swell and long-wind waves, which implied that the glint count process contains information related to long-wave modulation of surface roughness.

The obvious discrepancy in interpreting the characteristic forces that generate waves might be due to what were measured. For example, Bergamasco *et al.* (1995)

measured the time series of the surface wave displacement driven mainly by gravity (as discussed in Chapter Four), while Shaw & Churnside (1997) focused on the surface glint counts induced by wind. Furthermore, the spectral density peaks do not exist in the offshore wave profiles it would in the open sea waves. While only the tidal dominance is observed in the current study of the natural wave (Chapter Four), the tidal waves measured twenty kilometres from land can be easily decomposed into component waves (Shaw & Churnside, 1997). Such dominant force might be attributed to the current findings.

Since no article using similar approach to the study is available, a self-reflection on the current findings is given. The major findings include, firstly, the fractal dimension of one section is similar to that of another, and secondly, the first finding holds for both synthetic and natural wave profiles. As stated in Chapter Two, the individual waves afar have interfered to become grouped waves that have the characteristics of a single wave; therefore, the first result is reached for the natural wave profile. The effect of the tidal force has become clear with the synthetic wave, that has distinct frequency peaks including the tide. The sections of the profile are actually parts of the tidal cycle; therefore, the fractal dimensions are consistent between sections. Such homogeneity in the sea wave profile was questioned in Chapter Two and finally proved in Chapter Four.

Systems of Higher Dimensions and Landforms

The method used in the analysis of sea wave profiles can be readily extended to the analysis of heterogeneity in landforms. It is becoming popular to construct a two-dimensional map of surface roughness by laser (Vandenberg & Osborne, 1992;

Aggarwal & Kalra, 1994; Bergmasco *et al.*, 1995; Parkin & Calkin, 1995) or radar (Dellepiane *et al.*, 1991; Blacknell & Oliver, 1994; Lin *et al.*, 1996; Lin *et al.*, 1997; Mather *et al.*, 1998) imagers. Such map is actually a composition of profiles of information collected by a linearly scanning device such as a laser. The above examples demonstrate both the formulation of a surface image and the applicability of the same method for both the sea waves and landforms.

Applications of fractal measurements to systems of higher dimensions are found in, for example, solar studies (Balke *et al.*, 1993; NesmeRibes *et al.*, 1996; Stark *et al.*, 1997), percolation (Schmittbuhl *et al.*, 1992; Balke *et al.*, 1993; Kolb & Rosso, 1993; Muller *et al.*, 1995; Jan & Stauffer, 1998), physiology (Genny *et al.*, 1991; Caruthers & Harris, 1994; Volant & Grasso, 1994; Arsos & Dimitriu, 1995), plant root development (Chikushi & Hirota, 1998), morphology (Karam & Tonyan, 1993), image analysis in molecular clouds (Hetem & Lepine, 1993; Stutzki *et al.*, 1998), nuclear magnetic resonance (NMR) (Muller *et al.*, 1995), and surface scanning (Li & Park, 1998). The range of use of the fractal dimension in systems of higher dimension is enormous. Sommerer (1994) used the fractal dimension of a tracer distribution as a potential diagnostic for the dynamics of the underlying surface flow. Tian & Yao (1998) suggested that the fractal dimension can be regarded as a useful parameter in evaluating the sweep efficiency and oil recovery. Shcherbakov *et al.* (1995) used the fractal dimension to represent the soil pore space. Lipiec *et al.* (1998) used the fractal dimension to quantify soil pore distribution patterns and found that the more compact the soil is, the smaller the fractal dimension.

The fractal dimension could be a useful tool for the texture analysis. A useful technique of pattern recognition of textual image is to convert the grey level into

a third coordinate, providing a "terrain" of unit density. An alternative method of calculating fractal dimension from virtual terrains was derived using this technique (Sarkar & Chaudhuri, 1992); although Critten (1996) noted that techniques by which shade is converted into shape are inherently unreliable. However, Huang *et al.* (1994) suggested that "one should not place too much reliance in the absolute value of a fractal estimate, but that the estimates [resulting from the rounding of sampled values, for example, do vary monotonically with (fractal dimension) D and might be useful descriptors in tasks such as image segmentation and description."

The fractal analysis of some systems of higher dimensions is concerned with the measurement of the "toughness" of materials. Carpinteri (1994) studied the size effects on tensile strength and fracture energy of brittle and disordered materials such as rocks and reported that "variations in the fractal dimension of fracture surfaces produce variations in the physical domain of toughness, and not...only in the measure of toughness." Shek *et al.* (1998) determined the fractal dimensions of the fracture profiles by the perpendicular sectioning method and also suggested that, under the brittle fracture conditions of an alloy, the fracture toughness was approximately a linear function of fractal dimension. However, an earlier report concluded that "no quantitative relationship between fractal dimension and toughness was found" on the fracture surfaces of glass and some porcelain (Baran *et al.*, 1992).

The fractal analysis should, therefore, be applied with caution. Using the variation method to estimate the fractal dimensions of some microscopic surfaces of particles, Li & Park (1998) found that, while some surfaces have consistent fractal dimensions under all scales, others vary according to the scale of scanning; and the implied multi-fractal features and the scale-dependency of fractal dimension could

result from "the artificial processes controlling the surface morphology." Souriau (1994) showed that, for instances ranging from 100 metres to 100 kilometres, the elevation statistical distribution is well approximated by a standard Brownian surface with a fractal dimension of 2.5; however, when dealing with continental wide hydrographic basins, the large scale elevation beyond a threshold around 150 kilometres follows a logarithmic trend constrained by two boundary conditions, that is, the sea level and the tectonic ridge.

This section is now focusing on the geophysical features, in the following two sub-sections. The immediate sub-section gives a detailed discussion on the fractal analysis of landforms as characterised by drainage network. The discussion on the fractal analysis of the digital elevation models then follows.

Fractals in Drainage Networks

Most published work on the fractal dimension of landforms focuses on river channels or drainage networks (Nikora & Sapozhnikov, 1993; De Vries *et al.*, 1994); whilst relatively few contribute to the study of transects (Sornette & Zhang, 1993) or areal features (Fox, 1996). Gao & Xia (1996) made an intensive review of the application of the fractal concept to physical geography, as summarised in the following. Most determination methods require one or more straight line segments to fit the log-log plot (Chapter Three). Although fractal analysis has been successfully used to measure and characterise irregular linear features such as coastline (Mandelbrot, 1967), to describe and characterise landforms (Milne, 1990), and to delineate landform regions statistically (Klinenberg, 1988); it also shows that some topographic features are fractal at limited scales (Mark & Aronson, 1984). Despite the fact

that the multifractal nature of some geographical phenomena has been explored in great depth, it is not completely understood why some terrains are better modelled with Fractal Geometry than others (Gao & Xia, 1996). However, the estimated fractal dimensions are generally used to describe the branching patterns of the river channels (Feder, 1988; Tarboton *et al.*, 1988; La Barbera & Rosso, 1989; Nikora & Sapozhnikov, 1993; Beauvais & Montgomery, 1996; Wilson & Strom, 1993; De Jong & Burrough, 1995; Claps & Oliveto, 1996), the processes that create the landform (Hatano *et al.*, 1992; Liu, 1992; Beauvais & Montgomery, 1996) and the transects (Sornette & Zhang, 1993; Gallant *et al.*, 1994; Pachepsky *et al.*, 1997).

There are several common methods of calculating the fractal dimension from the branching patterns of a drainage network. One is based on Hack's (1957) law, which explores the relationship between main stream length and basin area (Beauvais & Montgomery, 1996); whilst the other relies on the statistical properties of branching networks known as Horton's (1945) and Strahler's (1952) laws (Feder, 1988; Tarboton *et al.*, 1988; La Barbera & Rosso, 1989; Beauvais & Montgomery, 1996; Claps & Oliveto, 1996, for example). Nikora & Sapozhnikov (1993) provide a detailed review of those two methods; and show that the river network is a fractal object with self-affine properties, where the fractal dimension and Hurst exponent are 1.52 and 1.0 for the river network simulation of small scale, 1.71 and 0.58 for that of large scale, and 1.87 and 0.73 for natural networks. Fractal dimensions estimated by Wilson & Strom (1993) used the divider method and a relationship based on Horton's bifurcation and length ratios. In contrast to Nikora & Sapozhnikov (1993), the small scale fractal dimensions in their study are generally in good agreement with reported values for large-scale river systems. De Jong & Burrough (1995) proposed

a three-dimensional version of the "walking divider" method, that was claimed to be able to distinguish rangeland, marquis and chosen garrique, and to a lesser extent agricultural regions on the Landsat Thematic Mapper image of southern France.

Other studies attempted to link fractal dimensions with the underlying geomorphic processes. Fractal dimensions were used to describe rivers flowing through different types of valleys by Beauvais & Montgomeny (1996); where the results showed that scaling properties of river platforms are related to the geomorphological processes governing the valley floor morphology, and none of the valley types related differences in form, that is, the fractal dimension, to differences in process, in part because estimates of the fractal dimension using Hortonian or allometric relation provide unreliable fractal dimensions. Other researchers such as Liu (1992, p.2981) had a similar concern; he stated that "the fractal structure and properties of stream networks as a distorted system have been poorly understood", and also implied that there is a link between hydrology and the fractal dimensions of stream networks. The link between the fractal dimension and the underlying process is clearly shown at macroscale by Hatano *et al.* (1992), who used fractal dimensions of methylene blue staining patterns in five undisturbed soil columns to explain solute transport in five soils and found that the fractal dimension of the internal structure of staining patterns decreased with an increase in soil depth.

Although a great majority of study in geomorphology focuses on processes, the characterisation of geomorphologic forms remains fundamentally important in landform studies; for example, the existing form is not necessarily shaped by the current processes or the processes occurring nearby (Gregory & Walling, 1973). A full understanding of forms would certainly facilitate the study of form-process relation-

ships. Rhea (1993) suggested that the difference of the fractal dimensions and other parameters in river profiles led to the tectonic interpretations that "the central western Coast Range is the locus of synclinal tilting and that the entire Oregon coast is experiencing landward tilting and uplift." Upon re-examining the determination of the fractal dimension of river networks, however, Claps & Oliveto (1996) argued that "natural networks tend to have the same fractal dimensions [no matter what the underlying processes may be]."

The fractal dimensions of landforms can be estimated either for the whole area or for the boundaries or profiles within that area. Fox (1996) developed a two-dimensional spectral model of bathymetry; where parameters of his model clearly defined the contrast between the constructional volcanic terrain (rough, isotropic, with a high fractal dimension) and the tectonic extensional terrain (smoother, anisotropic, with a low fractal dimension). Thibert & Tawashi (1991) used the estimate of fractal dimension to show that a significant difference was observed in the boundary variation of the calcium oxalate stone fragments treated by shock wave and ultrasound. The semi-variogram, roughness-length, and two spectral methods were compared, by Gallant *et al.* (1994), using synthetic 1024-point profiles generated by two methods, and using two profiles derived from a gridded digital elevation model and two profiles from a laser-scanned soil surface; the estimation methods were found to be quite consistent for the Hurst exponent near 0.5, but vary at other values. Using a laser altimeter, Pachepsky *et al.* (1997) found that the root-mean-square roughness data had two intervals of self-affine fractal scaling on grass transects and four such intervals on shrub transects.

The issue of noise and randomness is important in landform process, that can

be explored using the spectral approach in particular. Spectral studies by Sornette & Zhang (1993) have shown vertical transect profiles of landscapes and mountains to be self-affine fractals. Using the generalisation of the deterministic Culling's linear equation (Culling, 1960; Culling, 1963), Sornette & Zhang (1993) showed that the self-affine rough landscapes are created by the interplay of non-linearity, coming from the requirement that erosion is proportional to the exposed area of the landscape, and noise, accounting for the fact that erosion is locally irregular as a result of the heterogeneity of soils and distribution of storms. Robert & Roy (1993) reviewed the application of fractals to the spatial variability of different phenomena; and proposed that fractal surfaces could be used as a null hypothesis and initial surface for the study of geomorphic processes, and the fractal dimension be used for the characterisation of surface roughness. The synthetic landforms generated by the random algorithms are not only statistically sound but also visually realistic.

The fractal dimension is, therefore, generally accepted as an indicator of landform complexity; however, making a comparison of the derived fractal dimensions must be carried out with caution. The main concerns are on the scales and methods used to derive the fractal dimensions, as described in Chapter Three. Very few articles are, therefore, available for further comparisons under such considerations.

Digital Elevation Models

This sub-section aims to compare the current results with other work that applies the box-counting method to estimate the fractal dimensions from profiles of digital elevation models. A "profile" in the current study is referred to as the linear features taken along meridian lines; whereas other authors may refer a profile to a fractured

face (Carpinteri, 1994; Shek *et al.*, 1998) or a river profile (Rhea, 1993). Since the profile in the current study comprises a mixture of features created by various processes, the dynamics are expected to be different from, for example, a river profile shaped by the river it contains.

Two almost identical cases are presented here. Pardini & Gallart (1998) measured surface roughness with a laser metre and estimated the fractal dimension of the profile by linear regression; their results revealed distinct micro- and macrotopographic variations of artificially weathered surface samples. As noticed by Liao (1995), "the fractal analysis of profiles is limited by the traced length at larger scales and the measuring method at smaller scales." Although the fractal dimensions are estimated from profiles, both cases are more concerned with the difference induced by scales than by profiles. Whilst both cases have revealed the diversity of the landform under different scales; the current results explore the complexity by showing the difference of the fractal dimensions between profiles. In other words, the current approach implies a new direction of research, one that deserves further investigation.

Ecological Systems and Ferns

Whilst (geo)morphologists are trying to reason the use of the fractal dimensions, other applied scientists such as ecologists have already accredited fractal analysis. Leohle & Li (1996) proposed a sampling theory for studies of fractals; that is, for nonisotropic media (or maps), random placement of transects is shown to give an unrealistic estimate of pattern, whilst for transects taken perpendicular to a directional pattern (i.e., strata), it is shown that the mean of multiple estimates of the multi-scale fractal dimensional profile does converge to the true value. Others

(Raulier & Ung, 1997) have claimed to link the fractal dimension with faunal, floral and environmental parameters.

The fractal dimension of natural habitats may influence both numbers and body size distribution of fauna (Gunnarsson, 1992). An important feature of a fractal curve is that its length or area becomes disproportionately large as the unit of measurement is decreased (Sugihara & May, 1990); therefore, for woody plant surfaces, there should be more usable space for smaller animals (a small unit of measurement) than for larger ones. Whilst Shorrocks *et al.* (1991) showed that the body-size distribution of the small arthropods found on lichens can similarly be predicted from the fractal dimension; Laussen *et al.* (1997) also suggested that vegetation cover affects the sinuosity of turtle trails. However, Stork & Blackburn (1993) suggested that the fractal nature of surfaces is less important in determining arthropod assemblages than it has previously been considered, using the samples collected in the lowland rain forest in Seram, Indonesia. Not only the static distribution but also the dynamic movement of individuals could be quantified by fractal dimensions. The expansion of a plant disease from a single focus was simulated by Shaw (1995), who concluded that the distribution of individuals produced is approximately self-similar across a wide range of scales, and the fractal dimension changes systematically with scale in a way which may be characteristic of the dispersal distribution.

Some studies on plants and vegetation contribute to the relationship between the fractal dimensions and canopies and stems; whilst the majority focuses on the root system. Patterns of crown fractal dimension were related to the self-thinning exponent in four tree species by Osawa (1995). Smith *et al.* (1995) concluded that the fractal dimensions of canopy profiles have value for predicting the physiognomy

of Alpine vegetation from the microenvironment. Esco *et al.* (1995) found that the box-counting fractal dimension of branch architecture of green peppers (*Capsicum annum*) declined under stress infection. However, Zeide (1991) argued that "not all tree variables are fractals"; for example, stem surface is fractal but volume is not, implying that volume as well as tree height should be calculated using the methods of classical geometry.

Fitter & Stickland (1992) carried out extensive research into the fractal characterisation of root system architecture, using the divider method; the main findings included those that fractal dimensions are mostly below 1.5, differ significantly between species and increase with age. Eghball *et al.* (1993) showed that the fractal dimension of corn (*Zea mays* L.) root systems was "significantly smaller for zero N[itrogen]...[than]...applied N levels." Lynch & Vanbeem (1993) observed that significant genetic differences were related to the root fractal dimension. A peanut root system inoculated with a wild type strain of *Agrobacterium rhizogenes* was shown to have a high fractal dimension compared to the control (Akasaka *et al.*, 1998). Ohdan *et al.* (1995) conducted an experiment on the allelopathic effect of aqueous extracts of six Crotalania species on wheat root growth. Although Ohdan *et al.* (1995) were reluctant to relate the application of the extract with fractal dimensions, significant suppression of root lengths as related to the variation in fractal dimensions of profiles of root systems was observed. However, whether the root system in three-dimensional space is a fractal object was a topic not addressed until relatively recently. Nielsen *et al.* (1997) found that the three-dimensional fractal dimension differs from a corresponding projected fractal dimension, suggesting that the analysis of roots grown in a narrow space or excavated and flattened prior

to analysis is problematic; however, a log-linear relationship was found between the fractal dimension of roots and spatial dimension, suggesting that the three-dimensional fractal dimension of root systems may be accurately estimated from excavations and a tracing of root intersections on exposed planes. Eshel (1998) concluded that the root system has the characteristics of a fractal object, using an empirically derived root system in three dimensions.

The difference of species is also detectable through applying fractal dimensions. The discrimination between plant and weed species is possible by the use of their fractal dimensions (Critten, 1997). Corbit & Garbary (1995) compared three species of brown algae and found no difference in fractal dimension among mature fronds, but the fractal dimension was highly correlated with both developmental algae and structural complexity. Izumi *et al.* (1995) also suggested the possibility for characterising the root system morphology of rice cultivars, *Taichung Native 1* (TN-1, *indica* type) and *Yukara* (*japonica* type), through the fractal dimension. Kubler & Dudgeon (1996) studied the temperature dependent change in the form complexity of fronds of *Chondrus crispus*, a perennial red seaweed, and found that the growth of morphologically more complex thalli at the higher temperature resulted in a significantly higher fractal dimension than that at a lower temperature.

Detection of a difference between species might, however, require more than merely the measure of the fractal dimension. Critten (1996) noted that different patterns may have similar dimensions, and suggested that other measures such as "lacunarity" should be used as well. Berntson & Stoll (1997) developed a technique that combines curve fitting and tests of curvilinearity of residuals, and claimed that it reduces significantly variations in estimated fractal dimensions arising from

variations in the method of preparing digital images of the rhizome systems of golden rod (*Solidago altissima*).

The Spectra of Plants

Very few published works have been devoted to the spectral characteristics of plant and vegetation using the fractal concept; although Bedford (1993) established the relationship between the fractal dimension and the roughness parameter in radiative transfer models of surface reflection. Also, Knyazikhin *et al.* (1998) showed that both the radiation regime and the photosynthesis depend on the fractal dimension of the plant stand at a scale at which Beer's law loses its validity. The closest example to this current study was reported by Vedyushkin (1994), who concluded that "the fractal method can be used for discrimination of remotely sensed data but further investigations, including detailed comparison of fractal characteristics of remotely sensed forest images with results of on-site field studies are necessary to validate them." Although the normalised difference vegetation index image was similar to that used in the current study, further comparison is prevented due to the difference in the scales and method. A comparison of the fractal dimension derived from the outline of ferns is also prohibited; for example, even the fractal dimension of the first-ever virtual fern was not mentioned by the author (Barnsley, 1993). An interpretation might be given by McLellan & Endler (1998), "fractal dimension is highly related with the ratio of perimeter to area (dissection index) and reveals little additional information about shape [of maple leaves]." Although the current results (Chapter Six) have identified the distinct difference between the inert and leafy areas using the fractal dimensions, the relationship between the fractal dimension and spectral characteristics is actually unclear and deserves further investigation.

7.4 Future Work

Some further improvements can be performed, based on the findings from the current study and other work as deduced from the above discussion. Since the mono-fractal dimension is estimated here, the possible multi-linearity in the log-log plot should be treated carefully by means of the corresponding correlation coefficient or other methods (Andrle, 1992, for example). The measure of lacunarity can be used to distinguish systems of different textures with the same fractal dimension (Allain & Cloitre, 1991); therefore, it can be further applied to the analysis of the sea wave profile that exhibits similar fractal dimensions between sections of the wave profile. Furthermore, the systematic estimation of the fractal dimensions from meridian profiles of a digital elevation model enables direct understanding of the system compexity within a system; therefore, an in-depth evaluation of this approach is suggested. The study on the relationship between the spectral characteristics and fractal dimensions has become fundamentally important in terms of applying the fractal concept to the remotely-sensed data; and deserves further contribution.

Chapter 8

Conclusion

As far as the laws of mathematics refer to the reality, they are not certain. And so far as they are certain, they do not refer to reality.

Albert Einstein (1879-1955).

In *Fuzzy Thinking* (Kosko, 1993, p.3).

The two main objectives of the thesis were defined in Chapter One as

1. the determination of the fractal dimensions of three natural systems, and
2. the comparison of these results with corresponding analyses of mathematical models of the same three systems.

These objectives have been achieved and this thesis has also affirmed the method of fractal dimension. The proceeding chapter has also examined possible future work.

The approach of the current study has followed the inductive-deductive procedures, the hypotheses testing and the falsificationism, as explained in Chapter Two. The chapter also brought out the theoretical development of Chaos Theory and Fractal Geometry, from which the concept of fractal dimension is derived. The three types of dynamics revealed in the Mandelbrot set were identified; and three corresponding natural systems were also located and detailed, that is, the sea waves, landforms and spectral images.

The methodology was detailed in Chapter Three, which included the estimation of fractal dimension, and a description of the statistical methods. Whilst the fractal dimension quantifies the dynamics of three natural systems and their corresponding mathematical models, statistical techniques were used to give a general description of the data, and to examine the difference between natural data and synthetic models. The basic requirements for comparing fractal dimensions were also derived: the comparison must be based on the identical method and a similar range of scales.

The main work was completed in Chapters Four, Five and Six, appended with the discussion based on the findings corresponding to the specific type of systems; the condensed discussion followed in Chapter Seven. The specific methods were deduced for the waves, landforms, and fern images and the mathematical models corresponding to those natural systems were also induced. The fractal dimensions of the natural and synthetic systems were estimated and compared. The method of fractal dimension was proved to be scientific as a result.

The analysis of the natural and synthetic wave forms was given in Chapter Four. The fractal dimensions were found to be similar between records, for both the natural and synthetic waves. Statistical tests suggested that there is no significant difference of the estimates between waves. The systems dynamics were found to be homogeneous for the sea wave profiles.

The results derived from the digital elevation models were presented in Chapter Five. Whilst a range of fractal dimensions was derived from the profiles of a digital elevation model, the significant difference was between profiles and between the natural and synthetic landforms. In other words, the systems dynamics were found to be heterogeneous for the digital elevation models.

The spectral images of ferns were analysed in Chapter Six. Similarly to the digital elevation model, a range of fractal dimensions was found, and the difference of fractal dimensions was significant between profiles and images. Furthermore, the difference between background and leafy areas was easily identified by the fractal dimensions, supporting the observation that the fractal dimensions can be used to

identify a system mixed with the inert and active sub-systems.

The current results and the summarised discussion in Chapter Seven revealed that a simple fractal method, with proper implementation, can be used to describe the complexity of a system.

In conclusion, through the unique approach devised in the current thesis, the similarities and differences of the estimated fractal dimensions of three natural and synthetic systems have been fully explored in the context of system evolution introduced by the Mandelbrot set.

Bibliography

ABP. 1997. *Tide Tables 1998: Hull, Immingham, Grimsby, Goole, Keadby.* Associated British Ports (ABP), Hull, England.

Accardo, A., Affinito, M., Carrozzi, M., & Bouquet, F. 1997. Use of the fractal dimension for the analysis of electroencephalographi time series. *Biol. Cybernetics*, **77**(5), 339–50.

Adam, C., & Tannery, P. (ed.). 1964-76. *Oeuvres de Descartes.* Rev. edn. Paris: Vrin/CNRS. 12 Volumes. Cited in: (Cottingham, 1988).

Agazzi, A., & Franzetti, G. 1975. Effects of rice biomass and yield on reflectance in the Landsat channels. *Agreste Project Objective*, **2.53.0(15)**, 2.6–2.10. Cited in (Curran, 1981).

Aggarwal, P.K., & Kalra, N. 1994. Analyzing the limitations set by climatic factors, genotype, and water and nitrogen availability on productivity of wheat .2. Climatically potential yields and management strategies. *Field Crops Resear.*, **38**(2), 93–103.

Aglietta, M., Alessandro, B., Arneodo, F., Bergamasco, L., Fauth, A.C., Castagnoli, C., Castellina, A., Cattadori, C., Chiavassa, A., Cini, G., Piazzoli, B.D., Fulgione, W., Galeotti, P., Chia, P.L., Mannocchi, G., Morello, C., Navarra, G., Osborne, A.R., Riccati, L., Saavedra, O., Serio, M., Trinchero, G.C., Vallania, P., & Vernetto, S. 1993. Fractal behavior of cosmic ray time series–chaos or stochasticity. *J. Phys. Resear.–Space Phys.*, **98**(A9), 15241–54.

Airy, G.B. 1845. Tides and waves. *In:* (Hardisty, 1990b), 241–396.

Akasaka, Y., Mii, M., & Daimon, H. 1998. Morphological alterations and root module formation in *Agrobacterium rhizogenas* mediated transgenic hairy root of peanut (*Arachis hypoganea* L.). *Annals of Botany*, **81**(2), 355–62.

Allain, C., & Cloitre, M. 1991. Characterizing the lacunarity of random and deterministic fractal sets. *Phys. Review A*, **44**(6), 3552–58.

Allen, R.E. (ed.). 1990. *The Concise Oxford Dictionary of Current English.* Oxford: Clarendon Press.

Amos, E.M., Blakeway, D., & Warren, C.D. 1986. Remote sensing techniques in civil engineering surveys. *Quart. J. Engine. Geol.*, **19**(3), 313.

ANDRLE, R. 1992. Estimating fractal dimension with the divider method in geomorphology. *Geomorphology*, **5**, 131–41.

ANDRLE, R. 1996. Complexity and scale in geomorphology-statistical similarity vs characteristic scales. *Math. Geology*, **28**(3), 275–93.

ANDRLE, R., & ABRAHAMS, A.D. 1989. Fractal techniques and surface roughness of Talus slopes. *Earth Surf. Proc. Landforms*, **14**, 197–209.

ANDRLE, R., & ABRAHAMS, A.D. 1990. Fractal techniques and surface roughness of Talus slopes: Reply. *Earth Surf. Proc. Landforms*, **15**, 287–90.

ANMAJUNAS, A., & TAMASEVICIUS, A. 1992. A technique for measuring fractal dimensions from time series on a real time scale. *Physica D*, **58**(1-4), 482–88.

ARIZMENDI, C.M., SANCHEZ, J.R., & FOTI, M.A. 1995. Randomness in airborne pollen–chaos or noise. *Fractals–An Interdisciplinary J. Complex Geom. Nature*, **3**(1), 155–60.

ARMSTRONG, A.C. 1986. On the fractal dimensions of some transient soil properties. *J. Soil Sciences*, **37**, 641–52.

ARSOS, G.A., & DIMITRIU, P.P. 1995. A fractal characterization of the type-II fiber distribution in the extensor digitorum longus and soleus muscles of the adult rat. *Muscle & Nerve*, **18**(9), 961–68.

ASRAR, G., KANEMASU, E.T., JACKSON, R.D., & PINTER, P.J., JR. 1985. Estimation of total above-ground phytomass production using remotely sensed data. *Remote Sens. Env.*, **17**, 211–20.

AVILES, C.A., SCHOLZ, C.H., & BOATWRIGHT, J. 1987. Fractal analysis applied to characteristic segments of the San Andreas fault. *J. Geophys. Res.*, **92**(B1), 331–44. Cited in (Beauvais & Montgomery, 1996).

BAI, D., SHIBUYA, E., NAKAGAWA, N., & KATO, K. 1997. Fractal characteristics of gas solids flow in a circulating fluidized bed. *Powder Technol.*, **90**(3), 205–12.

BALDOCK, G.R., & BRIDGEMAN, T. 1981. *Mathematical Theory of Wave Motion.* John Wiley & Sons.

BALKE, A.C., SCHRIJVER, C.J., ZWAAN, C., & TARBELL, T.D. 1993. Percolation theory and the geometry of photospheric magnetic flux concentrations. *Solar Phys.*, **143**(2), 215–27.

BARABÁSI, A.-L., & STANLEY, H.E. 1995. *Fractal Concepts in Surface Growth.* Cambridge University Press.

BARAN, G.R., ROQUESCARMES, C., WEHBI, D., & DEGRANGE, M. 1992. Fractal characteristics of fracture surfaces. *J. Am. Ceramic Soc.*, **75**(10), 2687–91.

BARING-GOULD, S., & HICKS, H.R. 1949. *Devonshire.* 10th edn. London: Methuen.

BARNSLEY, M. F. 1988. *Fractals Everywhere.* Academic Press Inc.

BARNSLEY, M. F. 1993. *Fractals Everywhere (2nd ed.).* Academic Press Inc.

BARNSLEY, M.F., ERVIN, V., HARDIN, D., & LANCASTER, J. 1985. Solution of an inverse problem for fractals and other sets. *Proc. Natl. Acad. Sci.*, **83**, 1975–77.

BARNSLEY, M.F., MASSOPUST, P., STRICKLAND, H., & SLOAN, A.D. 1987. Fractal modeling of biological structures. *Ann. N.Y. Acad. Sci.*, **504**, 179–94. Cited in (Campbell, 1996).

BARRETT, E.C., & CURTIS, L.F. 1974. Introduction. *Chap. 1 of:* BARRETT, E.C., & CURTIS, L.F. (eds), *Environmental Remote Sensing: Applications and Achievements.* Edward Arnold.

BARRETT, E.C., & CURTIS, L.F. 1992. *Introduction to Environmental Remoet Sensing.* 3rd. edn. Chapman & Hall.

BASSINGTHWAIGHTE, J.B., & RAYMOND, G.M. 1994. Evaluating rescaled range analysis for time series. *Annals Biomed. Engin.*, **22**(4), 432–44.

BAUER, M., HENG, H., & MARTINESSEN, W. 1993. Characterization of spatiotemporal chaos from time series. *Phys. Review Lett.*, **71**(4), 521–24.

BEAUVAIS, A.A., & MONTGOMERY, D.R. 1996. Influence of valley type on the scaling properties of river planforms. *Water Resources Resear.*, **32**(5), 1441–48.

BEFORD, N.D. 1993. Scattering laws for reflected solar radiation and the characterization of terrain roughness. *International J. Remote Sens.*, **14**(6), 1055–80.

BELLEHUMEUR, C., & LEGENDRE, P. 1998. Multiscale sources of variation in ecological variables: modeling spatial dispersion, elaborating sampling designs. *Landscape Ecol.*, **13**(1), 15–25.

BERGAMASCO, L., SERIO, M., & OSBORNE, A.R. 1994. The impact of background noise on the determination of the fractal and statistical properties of cosmic ray time series. *J. Geophys. Resear.-Space Physics*, **99**(A3), 4235–52.

BERGMASCO, L., SERIO, M., & OSBORNE, A.R. 1995. Finite correlation dimension and positive Lyapunov exponents for surface wave data in the Adriatic Sea near Venice. *Fractals-An Interdisciplinary J. on the Complex Geometry of Nature*, **3**(1), 55–78.

BERNTSON, G.M. 1997. Topological scaling and plant root system architecture: developmental and functional hierarchies. *New Phytol.*, **135**, 621–34.

BERNTSON, G.M., & STOLL, P. 1997. Correcting for finite spatial scales of self-similarity when calculating the fractal dimensions of real-world structures. *Proc. Roy. Soc. Lond. B-Biol. Sci.*, **264**(1387), 1531–37.

BERSHADSKII, A. 1997. Generalized scaling and multifractal phase transition in some physical and astrophysical processes. *Phys. Lett. A*, **227**(5-6), 287–90.

BEST, R.G., & HARLAN, J.C. 1985. Spectral estimation of green leaf area index of oats. *Remote Sens. Env.*, **17**, 27–36.

BIANCHI, M.M., ARIZMENDI, C.M., & SANCHEZ, J.R. 1992. Detection of chaos–new approach to atmospheric pollen time series analysis. *Int. J. Biometeo.*, **36**(3), 172–75.

BISHOP, C.T., & DONELAN, M.A. 1987. Measuring waves with pressure transducers. *Coastal Eng.*, **11**, 309–28.

BITOUK, D.R. 1994. Dynamics of Earth climate evolution. *ACTA Physica Polonica A*, **85**(SS), S7–S12.

BLACHER, S., BROUERS, F., & VAN DYCK, R. 1993. On the use of fractal concept in image analysis. *Physica A*, **197**, 516–27.

BLACKNELL, D., & OLIVER, C.J. 1994. Recognizing chaos in radar images. *J. Phys. D–Appl. Phys.*, **27**(8), 1608–18.

BLAND, A.S., & ROWLANDS, G. 1986. Calculation of transport coefficients in chaotic systems. *In:* SARKAR, S. (ed), *Nonlinear Phenomena and Chaos.* Bristol Boston: Adam Hilger Ltd.

BOHIGAS, O., & WEIDENMULLER, H.A. 1988. Aspects of chaos in nuclear physics. *Ann. Rev. Nuclear Particle Sci.*, **38**, 421–53.

BORGANI, S., PLIONIS, M., & VALDARNINI, R. 1993. Multifractal analysis of cluster distribution in two dimensions. *Astrophysical J.*, **401**(1.1), 21–37.

BOUMAN, B.A.M. 1992. Linking physical remote-sensing models with crop growth simulation-models, applied for sugar-beet. *Intl. J. Remote Sens.*, **13**(4), 2565–81.

BOUMAN, B.A.M. 1995. Crop modeling and remote-sensing for yield prediction. *Netherlands J. Agrl. Sci.*, **43**(2), 143–61.

BRADBURY, R.J., REICHELT, R.E., & GREEN, D.G. 1984. Fractals in ecology: methods and interpretation. *Marine Ecology Progress Series*, **14**, 295–96.

BREYER, S., & SNOW, S. 1992. Drainage basin perimeters: A fractal significance. *Geomorphology*, **5**, 143–57.

BROOMHEAD, D.S., & JONES, R. 1989. Time-series analysis. *Proc. R. Soc. Lond. A*, **423**, 103–121.

BROOMHEAD, D.S., & KING, G.P. 1986. Extracting qualitative dynamics from experimental data. *Physica D*, **20**, 217–236.

BROWN, J., COLLING, A., PARK, D., PHILIPS, J., ROTHERY, D., & WRIGHT, J. 1989. *Waves, Tides and Shallow-water Processes.* The Open University.

BROWN, J., COLLING, A., PARK, D., PHILIPS, J., ROTHERY, D., & WRIGHT, J. 1997. *Waves, Tide and Shallow-water Processes.* The Open University.

BROWN, R., BRYAN, P., & ABARBANEL, H.D.I. 1991. Computing the Lyapunov spectrum of a dynamic system from an observed time-series. *Phys. Rev. A*, **A43**(6), 2787–06.

BROWN, S.R., & SCHOLZ, C.H. 1985. Broad bandwidth study of the topology of natural rock surfaces. *J. Geophys. Res.*, **90**, 12575–82.

BRUNO, B., TAYLOR, G., ROWLAND, S., LUCEY, P., & SELF, S. 1992. Lava flows are fractals. *Geophys. Res. Lett.*, **19**, 305–08.

BRYAN, R.B. 1968. The development, use and efficiency of indices of soil erodibility. *Geoderma*, **2**(1), 5–25. cited in (Gregory & Walling, 1973).

BRYMAN, A., & CRAMER, D. 1990. *Quantitative Data Analysis for Social Sientists.* Rev. edn. London: Routledge.

BRYMAN, A., & CRAMER, D. 1994. *Quantitative Data Analysis for Social Scientists.* Revised edn. Routledge.

BURROUGH, P.A. 1981. Fractal dimensions of landscape and other environmental data. *Nature*, **294**, 240–42.

BURROUGH, P.A. 1984. The application of fractal ideas to geophysical phenomena. *Inst. Math. App. Bull.*, **20**, 36–42.

BURROUGH, P.A. 1993. Fractals and geostatistical methods in landscape studies. *In:* LAM, N.S., & COLA, L. DE (eds), *Fractals in Geography.* Prentice-Hall.

BUZUG, T., VONSTAMM, J., & PFISTER, G. 1992. Fractal dimensions of strange attractors obtained from the Taylor-Couette experiment. *Physica A*, **191**(1-4), 559–63.

BUZUG, T.H., REIMERS, T., & PFISTER, G. 1990. Optimal reconstruction of strange attractors from purely geometrical arguments. *Europhys. Lett.*, **13**(7), 605–610.

CAMPBELL, B.A., & SHEPARD, M.K. 1996. Lava flow surface roughness and depolarized radar scattering. *J. Geophys. Resear.-Planets*, **101**(E8), 18941–51.

CAMPBELL, R.D. 1996. Describing the shapes of fern leaves: a fractal geometrical approach. *Acta Biotheoretica*, **44**(2), 119–42.

CANON. 1992. *CLC10 PC IPU Kit: Operator's Manual.* Canon Europa NV.

CARPINTERI, A. 1994. Fractal nature of material microstructure and size effects on apparent mechanical properties. *Mech. of Matrials*, **18**(2), 89–101.

CARR, A. 1988. The implications of the tidal range. *Pages 25–31 of:* STARKEY, D.J. (ed), *Devon's Coastline and Coastal Waters.* Exeter University Publications.

CARR, J.R., & MELA, K. 1998. Visual basic programs for one, two or three-dimensional geostatistical analysis. *Comp. Geosci.*, **24**(6), 531–38.

CARSON, R.M., LAWFORD, V.A., RINA, M., & GWILLIAM, T.J.P. 1975 (Sept.). A pressure sensor probe which is insensitive to velocity, primarily designed for tide-gauge use. *Pages 23–27 of: Proc. of IERE Conf. on "Instrumentation in Oceanography".*

CARUTHERS, S.D., & HARRIS, T.R. 1994. Effects of pulmonary blood flow on the fractal nature of flow heterogeneity in sheep lungs. *J. Appl. Physiol.*, 3, 1474–79.

CAVALERI, L. 1980. Wave measurement using pressure transducer. *Oceanologica Acta*, **3**(3), 339–46.

CHAN, L.C.Y., & PAGE, N.W. 1997. boundary fractal dimensions from sections of a particle profile. *Particel & Particle Systems Character.*, **14**(2), 67–72.

CHANDRA, S. 1997. A tutorial and diagnostic tool for chaotic oscillators and time series. *Comp. Graph.*, **21**(2), 253–62.

CHASE, C.G. 1992. Fluvial landsculpting and the fractal dimension of topography. *Geomorphology*, **1/2**, 39–57.

CHATFIELD, C. 1988. *Problem Solving: A Statistician's Guide.* London: Chapman and Hall.

CHIKUSHI, J., & HIROTA, O. 1998. Simulation of root development based on the dielectric breakdown model. *Hydol. Sci. J.-Journal de Sciences Hydrologiques*, **43**(4), 549–60.

CHOUDHURY, B.J., & TUCKER, C.J. 1987. Satellite observed seasonal and inter-annual variation of vegetation over the Kalahari, the Great Victoria Desert, and the Great Sandy Desert: 1979–1984. *Remote Sens. Env.*, **23**, 233–41.

CHRIST, F., ABICHT, J.M., ATHELOGOU, M., BASCHNEGGER, H., NIKLAS, M., PETER, K., & MESSMER, K. 1997. Cardiovascular monitoring of elective aortic aneursm repair using methods of chaos analysis. *Int. J. Microcirculation-Clinical and Experimental*, **17**(6), 374–84.

CIA. 1996. *The 1996 World Factbook.* Compiled by the Central Intelligence Agent (CIA) of USA. Available at World Wide Web (WWW) site: http://www.odci.gov/cia/publications.

CLAPS, P., & OLIVETO, G. 1996. Reexamining the determination of the fractal dimension of river networks. *Water Resources Resear.*, **32**(10), 3123–35.

CLARKE, K.C. 1993. One thousand Mount Everests? *In:* N.S., LAM, & DE COLA, L. (eds), *Fractals in Geography.* Prentice-Hall.

CLAUSSEN, D.L., FINKLER, M.S., & SMITH, M.M. 1997. Thread trailing of turtles: methods for evaluating spatial movements and pathway structure. *Canad. J. Zool.-Revue Candienne de Zoologie*, **75**(12), 2120–28.

CLIFFORD, N.T. 1993. The analysis of turbulence time series: Statistical and correlation approaches using the Minitab package. *Earth Surface Processes and Landforms*, **18**, 845–54.

COLES, P. 1998. An unpredictable universe? *Nature*, **391**(6663), 120–21.

COLWELL, R.N. 1956. Determining the prevalence of certain cereal crop disease by means of aerial photography. *Hilgardia*, **26**(5), 223–86. Cited in: (Curran, 1985).

CONIGLIO, A., & ZANNETTI, M. 1989a. Multiscaling and multifractality. *Physica D*, **38**(1-3), 37–40.

CONIGLIO, A., & ZANNETTI, M. 1989b. Multiscaling in growth kinetics. *Europhys. Lett.*, **10**(6), 575–80.

CONOVER, W.J. 1980. *Practical Nonparametric Statistics*. 2nd edn. John Wiley and Sons. Cited in (Norušis, 1993).

COOLEY, J.W., & TUKEY, J.W. 1965. An algorithm for the machine calculation of complex Fourier series. *Math. Compt.*, **19**, 297.

CORANA, A., CASALEGGIO, A., ROLANDO, C., & RIDELLA, S. 1991. Efficient computation of the correlation dimension from a time series on a LIW omputer. *Parallel Computing*, **17**(6-7), 809–20.

CORBIT, J.D., & GARBARY, D.J. 1995. Fractal dimension as a quatitative measure of complexity in plant development. *Proc. Roy. Soc. Lond. B-Biol. Sci.*, **262**(1363), 1–6.

COSTAIN, K., & BOLLINGER, G.A. 1996. Climatic changes, streamflow, and long-term forecasting of intraplate seismicity. *J. Geodynamics*, **22**(1-2), 97–117.

COTTINGHAM, J. 1988. *The Rationalists*. Oxford: Oxford University Press.

COTTINGHAM, J., STOOTHOFF, R., & MARDOCH, D. (TR.). 1985-91. *The Philosophical Writings of Descartes*. Cambridge: Cambridge University Press. Three Volumes.

CRACKNELL, A., & HAYES, L. 1991. *Introduction to Remote Sensing*. London New York Philadelphia: Taylor & Francis.

CRILLY, A.J., EARNSHAW, R.A., & JONES, H. 1991. *Fractals and Chaos*. Springer-Verlag.

CRILLY, T. 1991. The roots of chaos–A brief guide. *In:* CRILLY, A.J., EARHSHAW, R.A., & JONES, H. (eds), *Fractals and Chaos*. Springer-Verlag.

CRITTEN, D.L. 1996. Fourier based techniques for the identification of plants and weeds. *J. Agric. Engineer. Resear.*, **64**(2), 149–54.

CRITTEN, D.L. 1997. Fractal dimension relationships and values associated with certain plant canopies. *J. Agric. Engineer. Resear.*, **67**(1), 61–72.

CRUTCHFIELD, J.P., FARMER, J.D., PACKARD, N.H., & SHAW, R.S. 1986. Chaos. *Sci. Am.*, **255**, 38–49.

CRYER, J.D. 1986. *Time Series Analysis.* Boston (Mass.): Duxbury Press.

CULLING, W.E.H. 1960. Analytical theory of erosion. *J. Geol.*, **68**, 336–44. Cited in (Sornette & Zhang, 1993).

CULLING, W.E.H. 1963. soil creep and the development of hillside slopes. *J. Geol.*, **71**, 127–61. Cited in (Sornette & Zhang, 1993).

CULLING, W.E.H. 1986. Highly erratic spatial variability of soil-pH on Iping Common, West Sussex. *Catena*, **13**, 81–89.

CULLING, W.E.H., & DATKO, M. 1987. The fractal geometry of the soil-covered landscape. *Earth Surf. Proc. Landforms*, **12**, 369–85.

CURRAN, P.J. 1980. Multispectral remote sensing of vegetation amount. *Progress in Physical Geography*, **4**, 315–41.

CURRAN, P.J. 1981. *Remote Sensing: the Role of Small Format Light Aircraft Photography.* Geographical papers 75. Department of Geography, University of Reading.

CURRAN, P.J. 1985. *Principles of Remote Sensing.* London New York: Longman.

CUSUMANO, J.P., & SHARKADY, M.T. 1995. An experimental study of bifurcation, chaos, and dimensionality in a system forced through a bifurcation parameter. *Nonlinear Dynamics*, **8**(4), 467–89.

DAGRAS, C.H., DURAN, M., ZARROUATI, O., & FRATTER, C. 1995. The SPOT-5 mission. *Acta Astronautica*, **35**(9-11), 651–60.

DALRYMPLE, J.B., BLONG, R.J., & CONACHER, A.J. 1968. A hypothetical nine-unit landsurface model. *Zeitschrift für Geomorphologie*, **12**, 60–76. Cited in (Summerfield, 1991).

DANCER, E.N. 1988. *Bifurcation and Chaos.* An Inaugural Public Lecture delivered in Armidale, New South Wales, on 15 August 1988.

DARBYSHIRE, A.G., & PRICE, T.J. 1991. Phase portrait from chaotic time series. *In:* CRILLY, A.J., EARNSHAW, R.A., & JONES, H. (eds), *Fractals and Chaos.* Springer-Verlag.

DAROS, D., & BORGA, M. 1997. Use of digital elevation model data for the derivation of the geomorphological instaneous unit hydrograph. *Hydrological Processes*, **11**(1), 13–33.

DAS, D.K., MISHRA, K.K., & KALRA, N. 1993. Assessing growth and yield of wheat using remotely-sensed canopy temperature and spectral indices. *Int. J. Remote Sens.*, **14**(17), 3081–3092.

DAVIS, P.A., BREED, C.S., MCCAULEY, J.F., & SCHABER, G.G. 1993. Surficial geology of the Safsaf region, south-central Egypt, derived from remote sensing and field data. *Remote. Sens. Env.*, **46**(2), 183–203.

DE JONG, S.M., & BURROUGH, P.A. 1995. A fractal approach to the classification of Mediterranean vegetation types in remotely-sensed images. *Photogram. Engineer. Remote Sens.*, **61**(8), 1041–53.

DE LA FUENTE, I.M., MARTINEZ, L., AGUIRREGABIRIA, J.M., & VEGUILLAS, J. 1998. R/S analysis in strange attractors. *Fractals–An Interdisciplinary J. Compex Geom.*, **6**(2), 95–100.

DE VRIES, H., BECKER, T., & ECKHARDT, B. 1994. Power law distribution of discharge in ideal networks. *Water Resource Resear.*, **30**(12), 3541–43.

DEACON, G.E.R. 1946. Ocean wave and swell. *Oceanogr. Pap. 'Challenger' Soc.*, **1**, 1–13. Cited in J. Hardisty.

DELLEPIANE, S., GIUSTO, D.D., SERPICO, S.B., & VERNAZZA, G. 1991. SAR image recognition by integration of intensity and textual information. *Int. J. Remote Sens.*, **12**(9), 1915–32.

DEVARA, P.C.S., PANDITHURAL, G., RAI, P.E., MAHESKUMAR, R.S., & DANI, K.K. 1998. Atmospheric aerosol-cloud stability relationship as observed with optical and radio remote sensing techniques. *Atmospheric Resear.*, **49**(1), 65–76.

DICKINSON, T.A., PARKRE, W.H., & STRAUSS, R.E. 1987. Another approach to leaf shape comparisons. *Taxon.*, **36**, 1–20. Cited in (Campbell, 1996).

DIXON, A.R., KIRBY, G.H., & WILLS, D.P.M. 1994. A data structure for artificial terrain generation. *Computer Graphics Forum*, **13**(1), 37–47.

DIXON, R. 1987. *Mathographics.* Oxford: Basil Blackwell.

DOI. 1979. *Remote Sensing of Earth Resources.* Department of Industry (DOI) of UK.

DOODSON, A.T., & WARBURG, H.D. 1941. *Admiralty Manual of Tides.* London: His Majesty's Stationery Office.

DUBUC, B., QUINIOU, J.F., ROQUES-CARMES, C., TRICOT, C., & ZUCKER, S.W. 1989. Evaluating the fractal dimension of profiles. *Phys. Rev. A*, **39**(3), 1500–12.

DUOADY, A. 1986. Julia sets and the Mandelbrot set. *In:* PEITGEN, H.-O., & RICHTER, P.H. (eds), *The Beauty of Fractals.* Berlin: Springer-Verlag.

DUONG, N.D., & TAKEUCHI, S. 1997. WinASEAN for remote sensing data analysis. *ISPRS J. Photogram. Remote Sens.*, **52**(6), 253–60.

DYER, K.R. 1986. *Coastal and Estuarine Sediment Dynamics.* Chichester New York Brisbane Toronto Singapore: Wiley & Sons.

EASON, G., COLES, C.W., & GETTINBY, G. 1980. *Mathematics and Statistics for the Bio-Sciences.* Ellis Horwood.

EASTMAN, J.R. 1992a. *IDRISI Technical Reference: Version 4.0.* Graduate School of Geography, Clark University, Massachusetts, 01610, USA.

EASTMAN, J.R. 1992b. *IDRISI User's Guide: Version 4.0.* Graduate School of Geography, Clark University, Massachusetts, 01610, USA.

EFETOV, K. 1995. Suppersymmetry in quantum chaos and mesocopic physics. *Physica D*, **83**(1-2), 151–62.

EGHBALL, B., & POWER, J.F. 1995. Fractal description of temporal yield variability of 10 crops in the U.S. *Agron. J.*, **87**(2), 152–56.

EGHBALL, B., STTIMI, J.R., MARANVILLE, J.W., & PARKHURST, A.M. 1993. Fractal analysis for morphological description of corn roots under nitrogen stress. *Agron. J.*, **85**(2), 287–89.

ELLIOT, J.K. 1989. An investigation of the change in surface roughness through time on the foreland of Austre Okstindbreen, north Norway. *Computers and Geoscience*, **15**, 209–17.

ELNASCHIE, M.S. 1996. Chaos, information and diffusion in quantum physics – introduction. *Chaos Solitons & Fractals*, **7**(5), R7–R10.

ELVIDGE, C.D., & LYON, R.J.P. 1985. Influence of rock-soil spectral variation on the assessment of green biomass. *Remote Sens. Env.*, **17**, 265–79.

ENGBERT, R., & DREPPER, F.R. 1994. Chance and chaos in population biology–models of recurrent epidemics and food-chain dynamics. *Chaos Solitons & Fractals*, **4**(7), 1147–69.

EPPLEY, R.W. 1992. Chlorophyll, photosynthesis and new production in the southern California Bight. *Progress Oceanog.*, **30**(1-4), 117–50.

ERL. 1992. *Application of Remote Sensing to the Geological Environment in High Mountain Areas of Taiwan: Hsuehshan-Tabachienshan Area (1).* Tech. rept. Energy & Resources Laboratories (ERL), Industrial Technology Research Institute, Taiwan, R.O.C.

ESCHER, M.C. 1967. *The Graphic Work of M.C. Escher.* MacDonald.

ESCO, J.M., ALADOS, C.L., & EMLEN, J.M. 1995. Fractal structures and fractal functions as disease indicators. *Oikos*, **74**(2), 310–14.

ESHEL, A. 1998. On the fractal dimension of a root system. *Plant Cell Environ.*, **21**(2), 247–51.

ESTEVA, D., & HARRIS, L. 1970. Comparison of pressure and staff wave gage records. *Pages 101–16 of: Proc. 12th Coastal Eng. Conf.*, vol. 1.

EVANS, J.L. 1964. *The Foundations of Empiricism: An Inaugural Lecture Delivered at University College, Cardiff 11th May, 1964.* University of Wales Press Cardiff.

EVERTSZ, C.J.G., & MANDELBROT, B.B. 1992. Multifractal measures. *In:* PEITGEN, H-O, JÜRGEN, H., & SAUPE, D. (eds), *Chaos and Fractals: New Frontiers of Science.* Springer-Verlag.

EWING. 1980. Presentation and interpretation of directional wave data. *Underwater Technology*, **2**, 17–23. Cited in J. Hardisty.

EXNER, P., & NEIDHARDT, H. (eds). 1990. *Order, Disorder and Chaos in Quantum Systems.* Basel Boston Berlin: Birkhäuser Verlag. Proceedings of a Conference held at Dubna, USSR on October 17-21, 1990.

FATOU, P. 1919. Sur les équations fonctionnelles. *Bull. Soc. Math. Fr.*, 161–271. Cited in: (Peitgen *et al.*, 1992).

FEDER, J. 1988. *Fractals.* New York London: Plenum Press.

FEIGENBAUM, M.J. 1979. Qualitative universality for a class of nonlinear transformations. *J. Statist. Phys.*, **19**, 25. Cited in: (Holton & May, 1993).

FEIGENBAUM, M.J. 1980. Universal behavior in nonlinear systems. *Los Alamos Sci.*, **1**, 4–27. Cited in: (Scott, 1991).

FEIGENBAUM, M.J. 1992. Forward. *In:* PEITGEN, H-O, JÜRGEN, H., & SAUPE, D. (eds), *Chaos and Fractals: New Frontiers of Science.* Springer-Verlag.

FIELD, M., & GOLUBITSKY, M. 1992. *Symmetry in Chaos: A Search for Pattern in Mathematics, Art and Nature.* Oxford: Oxford University Press.

FIELD, R.J., & GYÖRGYI, L. 1993. *Chaos in Chemistry and Biochemistry.* Singapore: World Scientific.

FISCHER, W.A. 1975. History of Remote Sensing. *Pages 27–50 of:* REEVES, R.G. (ed), *Manual of Remote Sensing.* Falls Church, Virginia: American Society of Photogrammetry. Cited in (Curran, 1985).

FITTER, A.H., & STICKLAND, T.R. 1992. Fractal characterization of root system architecture. *Functional Ecol.*, **6**(6), 632–35.

FLORINSKY, I.V. 1998. Combined analysis of digital elevation models and remotely sensed data in landscape investigations. *Progress Phys. Geog.*, **22**(1), 33–60.

FOLLAND, G.B. 1992. *Fourier Analysis and Its Applications.* Pacific Grove, Calif.: Wadsworth & Brooks/Cole Advanced Books & Software.

FORRISTALL, G.Z. 1982. Subsurface wave-measuring systems. *Pages 194–209 of: Measuring Ocean Waves.* Washington, D.C.: National Academic Press.

FOURNIER, A., FUSSELL, D., & CARPENTER, L. 1982a. Computer rendering of fractal stochastic models - reply. *Comm. of the ACM*, **25**(8), 583–84. Also in (Saupe, 1988a).

FOURNIER, A., FUSSELL, D., & CARPENTER, L. 1982b. Computer rendering of stochastic models. *Comm. of the ACM*, **25**(6), 371–84. Also in (Saupe, 1988a).

FOURNIER, A., FUSSEL, D., & CARPENTER, L. 1982c. Computer rendering of stochastic models. *Communications of the ACM*, **25**, 371–84.

FOWLER, J., & COHEN, L. 1990. *Practical Statistics for Field Biology.* Chichester New York: John Wiley & Sons.

FOX, C., & HAYES, D.E. 1985. Quantitative methods for analyzing the roughness of the seafloor. *Rev. Geophys.*, **23**, 1–48.

FOX, C.G. 1996. Objective classification of oceanic ridge-crest terrains using 2-dimensional spectral models of bathymetry-application to the Juan de Fuca Ridge. *Marine Geomorphology Resear.*, **18**(6), 707–28.

FRACTAL, & CHARACTERIZATION OF DIAMOND WHEEL PROFILES, DDS. 1995. T.W. Liao. *J. Material Process. Technol.*, **53**(3-4), 567–81.

FRAESER, A.M., & SWINNEY, H.L. 1986. Independent coordinates for strange attractor from mutual information. *Phys. Rev. A.*, **33**(2), 1134–40.

FRANKEL, A. 1991. High frequency spectral falloff of earthquakes, fractal dimension of complex rupture, b-value, and the scaling of strength of faults. *J. Geophys. Resear.-Solid Earth and Planets*, **96**(B4), 6291–302.

GAFFNEY, D.A. 1993. Dune scarp exhibits bifurcation sequence. *J. Coastal Res.*, **9**(1), 279–81.

GALLANT, J.C., MOORE, I.D., HUTCHINSON, M.F., & GESSLER, P. 1994. Estimating fractal dimension of profiles–A comparison of methods. *Math. Geology*, **26**(4), 455–81.

GALLO, K.P., & DAUGHTRY, C.S.T. 1987. Differences in vegetation indices for simulated Landsat-5 MSS and TM, NOAA-9 AVHRR, and SPOT-1 sensor systems. *Remote Sens. Env.*, **23**, 439–52.

GAO, J., & XIA, Z.G. 1996. Fractals in physical geography. *Progress in Phys. Geog.*, **20**(2), 178–91.

GARDNER, B.R., BLAD, B.L., THOMPSON, D.R., & HENDERSON, K.E. 1985. Evaluation and interpretation of Thematic Mapper ratios in equations for estimating corn growth parameters. *Remote Sens. Env.*, **18**, 225–34.

GAUSMAN, H.W. 1974. Leaf reflectance of near infrared. *Photogram. Engine. Remote Sens.*, **40**, 183–91. Cited in (Curran, 1985).

GENNY, R.W., ROBERTSON, H.T., YAMASHIRO, S., & BASSINGTHWAIGHTE, J.B. 1991. Applications of fractal analysis to physiology. *J. Appl. Physiol.*, **70**(6), 2351–67.

GIBBS, G. 1998. As darkest hour looms, solar fans look west. *The Guardian*, Aug.8, p.10.

GILBERT, L.E. 1989. Are topographic data sets fractal? *Pure Appl. Geophys.*, **131**, 241–54.

GLEICK, J. 1987. *Chaos: Making a New Science.* Abacus.

GOBER, M., HERZEL, H., & GRAF, H.F. 1992. Dimension analysis of *El Niño*/southern oscillation time series. *Annales Geophysicae–Atmos. Hydyospheres and Space Sci.*, **10**(10), 729–34.

GOODCHILD, M.F. 1980. Fractals and the accuracy of geographical measures. *Math. Geology*, **20**, 615–20.

GOODCHILD, M.F. 1982. The fractional Brownian process as a terrain simulation model. *Modelling Simulation*, **13**, 1133–37.

GOODCHILD, M.F., & MARK, D.M. 1987. The fractal nature of geographic phenomena. *Annals of the Assoc. Am. Geographers*, **77**, 265–78.

GOPINATHAN, M.S. 1997. Detection of deterministic and randomness in time series: A method based on phase space overlap of attractor. *Pramana–J. Phys.*, **49**(6), 581–90.

GRACE, R.A. 1978. Surface wave heights from pressure records. *Coastal Eng.*, **2**, 55–67.

GRASSBERGER, P., & PROCACCIA, I. 1983a. Characterization of strange attractors. *Phys. Rev. Lett.*, **50**, 346–49.

GRASSBERGER, P., & PROCACCIA, I. 1983b. Measuring the strangeness of strange attractors. *Physica D*, **9**, 189–208.

GREENSIDE, H.S., WOLF, A., SWIFT, J., & PIGNATARO, T. 1982. Impracticality of a box-counting algorithm for calculating the dimensionality of strange attractors. *Phys. Rev. A.*, **25**(6), 3453–56.

GREGORY, K.J., & WALLING, D.E. 1973. *Drainage Basin Form and Process.* Edward Arnold.

GUNNARSSON, B. 1992. Fractal dimension of plants and body size distribution in spiders. *Functional Ecol.*, **6**(6), 634–41.

GUTIERREZ, J.M., IGLESIAS, A., & RODRGUEZ, M.A. 1996. A multifractal analysis of IFSP invariant measures with application to fractal image generation. *Fractals–An Interdiscip. J. Complex Geom. Nature*, **4**(1), 17–27.

GUZZO, L. 1997. Is the universe homogeneous? (On large scales). *New Astron.*, **2**(6), 517–32.

GYÖRGYI, L., & FIELD, R.J. 1993. Modelling and interpretation of chaos in the Belousov-Zhabotinskyreaction. *In:* FIELD, R.J., & GYÖRGYI, L. (eds), *Chaos in Chemistry and Biochemistry.* Singapore: World Scientific.

HAASTRUP, P., & FUNTOWICZ, S. 1992. Accident generating sysstems and chaos – A dynamic study of accident time series. *Relaibility Engin. & System Safety*, **35**(1), 31–37.

HACK, J.T. 1957. Studies of longitudinal stream profiles in Virginia and Maryland. *U.S. Geol. Surv. Prof. Pap.*, **194-B**, 45–94. Cited in (Beauvais & Montgomery, 1996).

HADAD, A., STIASSNIE, M., POREH, M., & CERMAK, J.E. 1993. Fractal aspects of integrated concentration fluctuations. *Boundary Layer Meteor.*, **62**(1-4), 291–302.

HALSEY, T., JENSEN, M.H., KADANOFF, L.P., PROCACCIA, I., & SHRAIMAN, B.I. 1986. Fractal measures and their singularities: the characterization of strange sets. *Phys. Rev. A*, **33**(2), 1141–51.

HAMILTON, J.D. 1994. *Time Series Analysis.* Princeton, N.J.: Princeton University Press.

HANN, R., & HOUNAM, I. 1991. *NAG Fortran Library, Mark 15.* Numerical Algorithms Group Ltd.

HAO, B-L. 1984. *Chaos.* Singapore: World Scientific. Cited in: (Gleick, 1987).

HARDISTY, J. 1990a. *Beaches, Form and Process: numerical experiments with monochromatic waves on the orthogonal profile.* London Boston Sydney Wellington: Unwin Hyman.

HARDISTY, J. 1990b. *An Introduction to Wave Recording: with special reference to pressure transducers and geomorphological applications.* Technical Report. British Geomorphological Society.

HARDISTY, J. 1993. Time series analysis using spectral techniques: Oscillatory currents. *Earth Surface Processes and Landforms*, **18**, 855–62.

HARDISTY, J., & DRUMM, I. 1993. *B-Band Data Summary.* SGER Working Paper 999. The School of Geography & Earth Resources, The University of Hull, HU6 7RX, UK.

HARDISTY, J., TAYLOR, D.M., & METCALFE, S.E. 1993. *Computerised Environmental Modelling.* John Wiley & Sons.

HARVEY, P. 1990. *An Introduction to Buddhism: Teachings, history and practices.* Cambridge University Press.

HASTINGS, H.M., & SUGIHARA, G. 1993. *Fractals: A User's Guide for the Natural Sciences.* Oxford New York Tokyo: Oxford University Press.

HATANO, R., KAWAMURA, N., IKEDA, J., & SAKUMA, T. 1992. Evaluation of the effect of morphological features of flow paths on solute transport by using fractal dimensions of methylene blue staining pattern. *Geoderma*, **53**(1-2), 31–44.

HAUSMAN, D.M., & MCPHERSON, M.S. 1990. Agricultural economics and the chaos of economic methodology. *J. Agri. Economics Resear.*, **42**(2), 3–4.

HELD, R.J., & ILLANGASEKARE, T.H. 1995. Fingering of dense nonaqueous phase liquids in porous media .2. Analysis and classification. *Water Resour. Resear.*, **31**(5), 1223–31.

HELLEMANS, A., & BUNCH, B. 1988. *The Timetables of Science. A Chronology of the Most Important People and Events in the History of Science.* New York London Toronto Sydney Tokyo: Simon and Schuster.

HELMLINGER, K.R., KUMAR, P., & FOUFOULA-GEORGIOU, E. 1993. On the use of digital elevation model data for Hortonian and fractal analyses of channel networks. *Water Resource Resear.*, **29**(8), 2599–13.

HENG, H., BAUER, M., & MARTIENSSEN, W. 1996. Correlation integrals for inhomogeneously distributed random data. *Chaos Solitons & Fractals*, **7**(2), 197–203.

HENTSCHEL, H.G.E., & PROCACCIA, I. 1983. The infinite number of generalized dimensions of fractals and strange attractors. *Physica D*, **8**, 435–444.

HETEM, A., & LEPINE, J.R.D. 1993. Fractal 3D simulations of molecular clouds. *Astron. Astrophys.*, **270**(1-2), 451–61.

HINKEL, K.M., & OUTCALT, S.I. 1995. Detection of heat mass transfer regime transitions in the active layer using fractal geometric parameters. *Cold Regions Sci. Tech.*, **23**(4), 293–304.

HIRABAYASHI, T., ITO, K., & YOSHI, T. 1992. Multifractal analysis of earthquakes. *Pure Appl. Geophys.*, **138**(4), 591–610.

HIRZBERGER, J., VAZQUEZ, M., BONET, J.A., HANSLMERIER, A., & SOBOTKA, M. 1997. Time series of solar granulation images. 1. Differences between small and large granules in quiet regions. *Astrophys. J.*, **480**(1.1), 406–19.

HJELMFELT, A.T., JR. 1988. Fractals and river-length catchment-area ratio. *Water Resources Bull.*, **24**, 455–59.

HOLBEN, B.N., TUCKER, C.J., & FAN, C.J. 1980. Spectral assessment of soybean leaf area and leaf biomass. *Photogramm. Engin. Remote Sens.*, **46**, 651–56.

HOLMGREN, P., & THURESSON, T. 1998. Satellite remote sensing for forestry planning–a review. *Scand. J. Forest Resear.*, **13**(1), 90–110.

HOLTON, D., & MAY, R.M. 1993. Chaos and one-dimensional maps. *In:* MULLIN, T. (ed), *the Nature of Chaos.* Clarendon Press.

HORIKAWA, K. 1978. *Coastal Engineering: An Introduction to Ocean Engineering.* University of Tokyo Press.

HORTON, R.E. 1932. Drainage basin characterisitcs. *Trans. Am. Geophys. Union*, **13**, 350–61. Cited in (Gregory & Walling, 1973).

HORTON, R.E. 1945. Erosional development of streams and their drainage basins: Hydrological approach to quantitative morphology. *Geol. Soc. Am. Bull.*, **56**, 275–370. Cited in (Gregory & Walling, 1973; Beauvais & Montgomery, 1996).

HOSKINS, W.G. 1954. *Devon.* London: Collins.

HUANG, J., & TURCOTTE, D.L. 1989. Fractal mapping of digitized images: application to the topography of Arizona and comparisons with synthetic images. *J. Geophy. Resear.*, **94**, 7491–95.

HUANG, Q., LORCH, J.R., & DUBES, R.C. 1994. Can the fractal dimension of images be measured? *Pattern Recognition*, **27**(3), 339–49.

HUANG, S.L., OELFKE, S.M., & SPECK, R.C. 1992. Applicability of fractal characterization and modeling to rock joint profiles. *Intl. J. Rock Mechanics and Mining Sci.*, **29**(2), 89–98.

HUBER, G., & ALSTROM, P. 1991. The dimension of turbelence. *J. Phys. A – Math. General*, **24**(18), L1105–10.

HUETE, A.R., & JACKSON, R.D. 1987. Suitability of spectral indices for evaluating vegetation characteristics on arid rangelands. *Remote Sens. Env.*, **23**, 213–32.

HUTCHINSON, J.E. 1981. Fractals and self-similarity. *Indiana University Mathematics J.*, **30**, 713–47.

ISLAM, S., BRAS, R.L., & RODRIGUEZITURBE, I. 1993. A possible explanation for low correlation dimension esimates for the atmosphere. *J. Appl. Meteorol.*, **32**(2), 203–08.

IUCN. 1994. *Guidelines for Protected Area Management Categories.* The World Conservation Union.

IZUMI, Y., KONO, Y., YAMAUCHI, A., & IIJIMA, M. 1995. Analysis of timecourse changes in root system morphology of rice in excised root culture. *Jp. J. Crop Sci.*, **64**(3), 636–43.

JAIME, B., UGO, F., ELIO, G., & STEFANO, M. 1995. Low dimensional chaos is present in Radon time variations. *J. Envl. Radioactivity*, **28**(1), 73–89.

JAN, N., & STAUFFER, D. 1998. Random site percolation in three dimensions. *Int. J. Modern Phhys.*, **9**(2), 341–47.

JARTTI, T.T., KUUSELA, T.A., KAILA, T.J., TAHVANAINEN, K.U.O., & VALIMAKI, I.A.T. 1997. The dose response effects of terbutaline on the variability, approximate entropy and fractal dimension of heart rate and blood pressure. *Br. J. Clinical Pharmacol.*, **45**(3), 277–85.

JEDYNAK, A., BACH, M., & TIMMER, J. 1994. Failure of dimension analysis in a simple 5-dimensional system. *Phys. Review E*, **50**(3), 1770–80.

JEHNSEN, R. 1990. Detecting shape variation in oak leaf morphology: a comparison of rotational-fit methods. *Am. J. Bot.*, **77**, 1279–93. Cited in (Campbell, 1996).

JENSEN, M.H., KADANOFF, L.P., LIBCHABER, A., PROCACCIA, I., & STAVANS, J. 1985. Global universality at the onset of chaos: Results of a forced Rayleigh-Bénard experiment. *Phys. Rev. Lett.*, **55**(25), 2798–2801.

JENSEN, R.V. 1987. Classical chaos. *Am. Scientist*. Cited in: (Gleick, 1987).

JENSEN, R.V. 1995. Quantum physics–the signature of chaos. *Nature*, **373**(6509), 16.

JONES, C.S. 1993. Heterochrony and heteroblastic leaf development in two subspecies of *Cucurbita argyrosperma* (Cucurbitaceae). *Am. J. Bot.*, **80**, 778–95. Cited in (Campbell, 1996).

JONES, H. 1991. Fractals before Mandelbrot. *In:* CRILLY, A.J., EARNSHAW, R.A., & JONES, H (eds), *Fractals and Chaos*. Berlin: Springer-Verlag.

JULIA, G. 1918. Mémoire sur l'iteration des fonctions rationnelles. *Journal de Maath. Pure et Appl.*, **8**, 47–245. Cited in: (Peitgen *et al.*, 1992).

KAANDORP, J.A. 1994. *Fractal Modelling Growth and Form in Biology*. Berlin Heidlberg New York London Paris Tokyo Hong Kong Barcelona Budapest: Springer-Verlag.

KANEMASU, E.T. 1974. Seasonal canopy reflectance patterns of wheat, sorghum and soybean. *Remote Sens. Env.*, **3**, 43–47.

KANETAKE, R., TAKEUTI, M., TAKESHIMA, T., & MAKISHIMA, K. 1994. Fractal analysis of X-ray emission from Centaurus X-3 observed by Ginga. *Publications of Astron. Soc. Japan*, **46**(3), 235–41.

KARAM, G.N., & TONYAN, T.D. 1993. Fractal morphology of cement foams. *Materials Lett.*, **16**(5), 278–80.

KARAMAVRUC, A.I., & CLARK, N.N. 1997. A fractal approach for interpretation of local instaneous temperature signals around a horizontal heat transfer tube in a bubbling fluidized bed. *Powder Technol.*, **90**(3), 235–44.

KELLER, J.M., CHEN, S., & CROWNOVER, R.M. 1989. Texture description and segementation through fractal geometry. *Computer Vision and Image Processing*, **45**, 150–66.

KENT, C., & WONG, J. 1982. An index of Littoral zone complexity and its measurement. *Ca. J. Fisheries Aquatic Sci.*, **39**, 847–53.

KERMAN, B.R., & BERNIER, L. 1994. Multifractal representation of breaking waves on the ocean surface. *J. Geophys. Resear.–Oceans*, **99**(C8), 16179–96.

KIDWELL, K.B. 1981. *NOAA Polar Orbiter User's Guide*. National Oceanic and Atmospheric Administration, Washington, DC, USA. Cited in (Price, 1987).

KIRBY, M. 1999. Models to address some scale issues in forecasting soil erosion risk. *In:* TURNOCK, D. (ed), *Geographies of the Future: RGS-IBG Annual Conference (4-7th 1999)*. The Royal Geographical Society with the Institute of British Geographers, Univesity of Leicester, England. Conference Handbook.

KITAMURA, T., OHARA, S., KONISHI, T., TSUJI, K., CHIKAWA, M., UNNO, W., MASAKI, I., URATA, K., & KATO, Y. 1997. Chaos in cosmic ray air showers. *Astroparticle Phys.*, **6**(3-4), 279–91.

KLEBBA, A. 1945. *A summary of shore recording meters*. Prel. Rpt. Woods Hole Oceanogr. Inst.

KLINENBERG, B. 1988. *Tests of a Fractal Model of Topography*. Ph.D. thesis, University of Eastern Ontario. Cited in (Gao & Xia, 1996).

KLINKENBERG, B. 1992. Fractal and morphometric measures: is there a relationship? *Geomorphology*, **5**, 5–20.

KLINKENBERG, B. 1994. A review of methods used to determine the fractal dimensions of linear features. *Mathematical Geology*, **26**(1), 23–46.

KLINKENBERG, B., & GOODCHILD, M.F. 1992. The fractal properties of topography: A comparison of methods. *Earth Surf. Proc. Landforms*, **17**, 217–34.

KNAPP, B. 1984. *Dartmoor and South Devon*. London Boston Sydney: George Allen and Unwin.

KNYAZIKHIN, Y., KRANIGK, J., MYNENI, R.B., PANFYOROV, O., & GRAVENHORST, G. 1998. Influence of small-scale structure on radiative transfer and photosynthesis in vegetation canopies. *J. Geophys. Resear.–Atmosphere*, **103**(P6), 6133–44.

KOLB, M., & ROSSO, M. 1993. Loop structure of percolation hulls. *Phys. Review E*, **47**(5), 3081–86.

KOONTZ, P.D., & INMAN, D.L. 1967. *A multipurpose data acquisition system for field and laboratory instrumentation of the nearshore environment*. Tech. Memo. 21. U.S. Army Coastal Engineering Research Centre.

KOSKO, B. 1993. *Fuzzy Thinking: the new science of Fuzzy logic*. Flamingo.

KOZMA, R., KOK, H., SAKUMA, M., DJAINAL, D.D., & KITAMURA, M. 1996. Characterization of two-phase flows using fractal analysis of local temperature fluctuations. *Int. J. Multiphase Flow*, **22**(5), 953–68.

KRASNOSEL'SKIĬ, M.A. 1946. *Topological Methods in the Theory of Nonlinear Integral Equations.* Pergamon. Cited in: (Dancer, 1988).

KUBLER, J.E., & DUDGEON, S.R. 1996. Temperature dependent change in the complexity of form of *Chondrus crispus* fronds. *J. Experimental Marine Biol.*, **207**(1-2), 15–24.

KULATILAKE, P.H.S.W., UM, J., & PAN, G. 1998. Requirements for accurate quantification of self-affine roughness using the variogram method. *Int. J. Solids Struct.*, **35**(31-32), 4167–89.

KURZ, H., WILTING, J., SANDAU, K., & CHRIST, R. 1998. Automated evaluation of angiogenic effects mediated by VEGF and PIGF homo- and heterodimers. *Microvascular Resear.*, **55**, 92–102.

KYRIAZIS, M. 1991. Applications of chaos theory to the molecular-biology of aging. *Experimental Gerontology*, **26**(6), 569–72.

LA BARBERA, P., & ROSSO, R. 1989. On the fractal dimension of stream networks. *Warer Resources Resear.*, **25**, 735–41.

LABINI, F.S., MONTUORI, M., & PIETRONERO, L. 1996. Statistical analysis of the Perseus Pisces redshift survey–spatial and luminosity properties. *Physica A*, **230**(3-4), 336–58.

LABINI, F.S., MONTUORI, M., & PIETRONERO, L. 1998. Scale invariance of galaxy clustering. *Phys. Rep.–Review Sect. Phys. Lett.*, **293**(2-4), 62–226.

LAND, S.N., & RICHARDS, K.S. 1997. Linking river channel form and process: time space and causality revisited. *Earth Surface Processes and Landforms*, **22**(3), 249–60.

LANSDOWN, J. 1991. Chaos, design and creativity. *In:* CRILLY, A.J., EARNSHAW, R.A., & JONES, H. (eds), *Fractals and Chaos.* Springer-Verlag.

LAUTERBORN, W., & PARLITZ, U. 1988. Methods of chaos physics and their application to acoustics. *J. Acoustical Soc. Am.*, **84**(6), 1975–93.

LAUWERIER, H. 1991. *Fractals: Endlessly Repeated Geometrical Figures.* Princeton University Press. Translated by Gill-Hoffstädt, S.

LAUWERIER, H.A., & KAANDORP, J.A. 1987. *Tutorial: Fractals (Mathematics, Programming and Applications).* Nyon, Switzerland: Eurographics, Amsterdam.

LAVERTY, M. 1987. Fractals in Karst. *Earth Surf. Proc. Landforms*, **12**, 475–80.

LEBARON, B. 1994. Chaos and nonlinear forecastability in economics and finance. *Phil. Trans. Roy. soc. London Series A*, **348**(1688), 397–404.

LEE, J., SCHWARZER, S., CONIGLIO, A., & STANLEY, H.E. 1993. Localisation of growth sites in diffusion-limited-aggregation clusters: Multifractality and multiscaling. *Phys. Rev. E*, **E48**(2), 1305–1315.

LEGGE, J. 1990. *The I Ching.* Scotland: Tyron Press.

LEHMANN, A., & LACHAVANNE, J.B. 1997. Geographic information systems and remote sensing in aquatic botany. *Aquatic Botany*, **58**(3-4), 195–207.

LI, T.L., & PARK, K. 1998. Fractal analysis of pharmaceutical particles by atomic force microscopy. *Pharmaceutical Resear.*, **15**(8), 1222–32.

LIDAR, D.A., BIHAM, O., & AVNIR, D. 1997. Limited range fractality of randomly absorbed rods. *J. Chem. Phys.*, **106**(24), 10359–67.

LIEBERT, W., & SCHUSTER, H.G. 1989. Proper choice of the time-delay for the analysis of chaotic time series. *Phys. Lett. A.*, **142**(2-3), 107–11. *Cited in:* (Buzug *et al.*, 1990).

LIEBOVITCH, L., & TOTH, T. 1989. A fast algorithm to determine fractal dimensions by box counting. *Phys. Lett. A*, **141**, 386–90.

LILLESAND, T.M., & KIEFER, R.W. 1994. *Remote Sensing and Image Interpretation.* John Wiley & Sons, Inc.

LIN, C.P., SANO, M., & SEKINE, M. 1996. Detection of targets embedded in sea ice clutter by means of MMW radar based on fractal dimensions, wavelets, and neural classifiers. *IEICE Trans. Communications*, **E79B**(12), 1818–26.

LIN, C.P., SANO, M., & SEKINE, M. 1997. Detection of radar targets by means of fractal error. *IEICE Trans. Communications*, **E80B**(11), 1741–48.

LINNETT, L.M. 1991. *Multi-texture Image Segementation.* Ph.D. thesis, Heriot-Watt University, U.K.

LIPIEC, J., HATANO, R., & SLOWINSKAJURKIEWICZ, A. 1998. The fractal dimension of pore distribution patterns in variously-compacted soil. *Soil & Tillage Resear.*, **47**(1-2), 61–66.

LIU, T.Z. 1992. Fractal structure and properties of stream networks. *Water Resources Research*, **28**(11), 2981–88.

LLOYD, A.L., & LLOYD, D. 1995. Chaos-its significance and detection in biology. *Biol. Rhythms Research*, **26**(2), 233–52.

LOBO, A., MOLONEY, K., CHIC, O., & CHIARIELLO, N. 1998. Analysis of fine-scale spatial pattern of a grassland from remotely-sensed imagery and field collected data. *Landscape Ecol.*, **13**(2), 111–31.

LOEHLE, C., & LI, B.L. 1996. Statistical properties of ecological and geologic fractals. *Ecol. Modelling*, **85**(2-3), 271–84.

LOGAN, D., & MATHEW, J. 1996. Using correlation dimension for vibration fault diagnosis of rolling element bearings. 1. Basic concepts. *Mechanical Systems and Signal Processing*, **10**(3), 241–50.

LORENZ, E. N. 1993. *The Essence of Chaos.* UCL Press.

LORENZ, E.N. 1963. Deterministic non-periodic flow. *J. Atmos. Sci.*, **20**, 130–141.

LOSEE, J. 1980. *A Historical Introduction to the Philosophy of Science*. 2nd edn. Oxford University Press.

LOVEJOY, S., & SCHERTZER, D. 1986. Scale invariance, symmetries, fractals, and stochastic simulations of atmospheric phenomena. *Bull. Am. Meteorol. Soc.*, **67**, 21–32.

LUTZENBERGER, W., PREISSEL, H., & PULVERMULLER, F. 1995. Fractal dimension of electroencephalographic time series and underlying brain processes. *Biol. Cybernetics*, **73**(5), 477–82.

LYNCH, J., & VANBEEM, J.J. 1993. Growth and architecture of seedling roots of common bean genotypes. *Crop Sci.*, **33**(6), 1253–57.

MALANSON, G.P., BUTLER, D.R., & GEORGAKAKOS. 1992. Nonequilibrium geomorphic processes and deterministic chaos. *Geomorphology*, **5**(3-5), 311–22.

MALINETSKII, G.G., POTAPOV, A.B., RAKHMANOV, A.I., & RODICHEV, E.B. 1993. Limitations of delay reconstruction for chaotic systems with a broad spectrum. *Phys. Lett. A*, **179**(1), 15–22.

MANDELBROT, B.B. 1967. How long is the coastline of Britain? Statistical self-similarity and fractal dimension. *Science*, **56**, 636–38.

MANDELBROT, B.B. 1974a. Intermittent turbulence in self-similar cascades: divergence of high moments and dimension of the carrier. *J. Fluid Mech.*, **62**, 331. Cited in (Evertsz & Mandelbrot, 1992).

MANDELBROT, B.B. 1974b. Multiplications aléatoires itérées et distributions invariantes par moyenne pondérée aléatoire, I & II. *Comptes Rendus (Paris)*, **278A**, 289–92 & 355–58. Cited in (Evertsz & Mandelbrot, 1992).

MANDELBROT, B.B. 1977. *Fractals: Form, Chance and Dimension*. San Francisco: W.H. Freeman & Co. Cited in (Mandelbrot, 1983).

MANDELBROT, B.B. 1982. Computer rendering of fractal stochastic models-comment. *Comm. of the ACM*, **25**(8), 581–83. Also in (Saupe, 1988a).

MANDELBROT, B.B. 1983. *Fractal Geometry of Nature*. New York: W.H. Freeman and Company.

MANDELBROT, B.B. 1985. Self-affine fractals and fractal dimension. *Physica Scripta*, **32**, 257–60.

MANDELBROT, B.B. 1986. Self-affine fractal sets I: the basic dimension. *Pages 3–15 of:* PIETRONERO, L., & TOSATTI, E. (eds), *Fractals in Geophysics*. North Holland Physics Publishing. Cited in (Gao & Xia, 1996).

MANDELBROT, B.B. 1988. People and events behind the "science of fractal images". *Chap. Forward of:* PEITGEN, H-O, & SAUPE, D. (eds), *The Science of Fractal Images.* Springer-Verlag.

MANDELBROT, B.B. 1989. Multifractal measures, especially for the geophysicist. *PAGEOPH*, **131**(1/2), 5–42.

MANDELBROT, B.B., PASSOJA, D., & PAULLAY, A. 1984. Fractal character of fracture surfaces of metal. *Nature*, **308**, 721–22.

MANN, S.S., & JAN, N. 1991. Growth probability distribution in percolation. *J. Phys. A–Math. General*, **24**(7), 1593–601.

MANSER, M., & THOMSON, M. 1997. *Chambers Combined Dictionary Thesaurus.* Chambers.

MARESCHAL, J-C. 1989. Fractal reconstruction of sea-floor topology. *PAGEOPH*, **131**(1/2), 197–210.

MARK, D.M., & ARONSON, P.B. 1984. Scale-dependent fractal dimensions of topographic surfaces: an empirical investigation with applications in geomorphology and computer mapping. *Math. Geology*, **16**, 671–83.

MARSH, C. 1988. *Exploring Data: An Introduction to Data Analysis for Social Scientists.* Cambridge: Polity Press.

MARVASTI, M.A., & STRAHLE, W.C. 1995. Fractal Geometry analysis of turbulent data. *Signal Process.*, **41**(2), 191–201.

MATHER, P.M. 1987. *Computer Processing of Remotely Sensed Images: An Introduction.* John Wiley & Sons.

MATHER, P.M., TSO, N., & KOCH, M. 1998. An evaluation of Landsat TM spectral data and SAR-derived textual information for lithological discrimination in the Red Sea Hills, Sudan. *Int. J. Remote Sens.*, **19**(4), 587–604.

MATSUSHITA, M., & OUCHI, S. 1989. On the self-affinity of various curves. *Physica D*, **38**, 246–51.

MATSUSHITA, M., OUCHI, S., & HONDA, K. 1991. On the fractal structure and statistics of contour lines on a self-affine surface. *J. Phys. Soc. Jpn.*, **60**, 2109–12.

MAY, R. 1974. Biological populations with nonoverlapping generations: Stable points, stable cycles, and chaos. *Science*, **186**, 645–47.

MAY, R. 1976. Simple mathematical models with very complicated dynamics. *Nature*, **261**, 459–67.

MAY, R. 1992. The chaotic rhythms of life. *In:* HALL, N. (ed), *The* New Scientist *Guide to Chaos.* Penguin Books.

MAY, R.M. 1989. Does God play dice? *Nature*, **338**(6217), 686.

McHenry, T.J.P., & Lin, Y-Y. 1984. Taiwan's first national parks. *Parks*, **9**(3/4), 113–16.

McLellan, T., & Endler, J.A. 1998. The relative success of some methods for measuring and describing the shape of complex objects. *Systematic Biol.*, **47**(2), 264–81.

Merttes, L.A.K., Hickman, M., Waltenberger, B., Bortman, A.L., Inlander, E., McKenzie, C., & Dvorsky, J. 1998. Synoptic views of sediment plumes and coastal geomorphology of the Santa Barbara Channel, California. *Hydrol. Process.*, **12**(6), 967–9.

Miller, G. S. P. 1986. The Definition and Rendering of Terrain Maps. *Computer Graphics*, **20**(4), 39–48.

Milne, B.T. 1990. Lessons from applying fractal models to landscape patterns. *In:* Turner, G., & Gardner, R.H. (eds), *Quantitative Methods in Landscape Ecology*. Springer-Verlag.

Milton, L.E. 1966. The geomorphic irrelevance of some drainage net laws. *Australian Geographical Studies*, **4**, 89–95. Cited in (Gregory & Walling, 1973).

Monteiro, T.S. 1994. Chaos in atomic physics. *Contemporary Phys.*, **35**(5), 311–27.

Morse, D., Lawton, J., Dodson, M., & Williamson, M. 1985. Fractal dimension of vegetation and the distribution of arthropod body lengths. *Nature*, **314**, 731–33.

Mukesh, O. 1993. Modeling of Belousov-Zhabotinskii reaction on a surface. *Chaos Solitons & Fractals*, **3**(3), 285–93.

Muller, H.P., Weis, J., & Kimmich, R. 1995. Computer simulation and 6-dimensional spin density and velocity NMR microimaging of lacunar systems–A comparative analyis of percolation properties. *Phys. Review E*, **52**(5.B), 5195–204.

Müller, J.-C. 1986. Fractal dimension and inconsistencies in cartographic line representations. *Cartograph. J.*, **23**, 123–30.

Müller, J.-C. 1987. Fractal and automated line generalization. *Cartograph. J.*, **24**.

Mullin, T. 1993a. Chaos and its application to physical systems. *In:* Mullin, T. (ed), *The Nature of Chaos*. Clarendon Press.

Mullin, T. 1993b. A dynamical systems approach to time series analysis. *In:* Mullin, T. (ed), *The Nature of Chaos*. Oxford: Clarendon Press.

Mullin, T. 1993c. *The Nature of Chaos*. Oxford: Clarendon Press.

MURPHY, K.D., VIRGIN, L.N., & RIZZI, S.A. 1996. Characterizing the dynamic response of a thermally loaded, acoustically excited plate. *J. Sound and Vibration.* **196**(5), 635–58.

MÜSSIGMANN, U. 1989. Texture analysis, fractals and scale-space filtering. *In: Proc. 6th Scand. Conf. on Image Ana.* SCIA'89, vol. II.

MÜSSIGMANN, U. 1990. Homogeneous fractals and their application in texture analysis. *In:* PEITGEN, H-O., HENIQUE, J.M., & PENEDO, L.F. (eds), *Fractals in the Fundamental and Application Science.* Elserier Sci. Pub. B.V. (North-Holland).

MÜSSIGMANN, U. 1992. Texture analysis using fractal dimensions. *In:* AO, J.L. ENCARNAC PEITGEN, H-O, SAKAS, G., & ENGLERT, J.L. (eds), *Fractal Geometry and Computer Graphics.* Springer-Verlag.

MYRBERG, P.J. 1958. *Ann. Akad. Sc. Fennicae.* A,I, No.259. Cited in: (Holton & May, 1993).

NAGATANI, T. 1993. Scaling and multifractality in a river network model with flow-dependent meandering. *J. Phys.*, **A26**, 4273–79.

NAGATANI, T., & STANLEY, H.E. 1991. Diffusion limited aggregation on percolating cluster crossover and multifractal structure. *J. Phys. Soc. JP.*, **60**(4), 1217–25.

NAKAGAWA, M., & KOBAYASHI, K. 1992. A diffusion-limited aggregation model with a fractional Browian motion. *J. Phys. Soc.*, **60**(10), 3386–91.

NASA. 1972. *ERTS Document No. 71SD4249.* Goddard Space Flight Center, Greenbelt MD, USA: National Aeronautic and Space Administration. Cited in (Price, 1987).

NESMERIBES, E., MEUNIER, N., & COLLIN, B. 1996. Fractal analysis of magnetic patterns from Meudon spectroheliograms. *Astron. Astrophys.*, **308**(1), 213–28.

NICHOLIS, C., & NICHOLIS, G. 1995. Chaos in dissipative systems–understanding atmospheric physics. *Advances che. Phys.*, **91**, 511–70.

NIELSEN, KL., LYNCH, J.P., & WEISS, H.N. 1997. Fractal Geometry of bean root systems: correlatins between spatial and fractal dimension. *Am. J. Botany*, **84**(1), 26–33.

NIELSON, P. 1982. Explicit formulae for practical wave calculations. *In:* (Hardisty, 1990b), 389–98.

NIKORA, V.I. 1991. Fractal structure of river plan forms. *Water Resources Resear.*, **100**, 433–39.

NIKORA, V.I., & SAPOZHNIKOV, V.B. 1993. River network Fractal Geometry and its computer simulation. *Water Resources Resear.*, **29**(10), 3569–75.

NOGUCHI, T., YAMADA, N., SADAMATSU, M., & KATO, N. 1998. Evaluation of self-similar features in time series of serum growth hormone and prolactin levels by fractal analysis: Effect of delayed sleep and complexity of diurnal variation. *J. Biomedi. Sci.*, **5**(3), 221–25.

NORTH, C.P., & HALLIWELL, D.I. 1994. Bias in estimating fractal dimension with the rescaled-range (R/S) technique. *Math. Geol.*, **26**(5), 531–555.

NORTON, D., & SORENSON, S. 1989. Variation in geometric measures of topographic surface underlain by fractured granitic plutons. *Pure and Applied Geophys.*, **131**, 77–97.

NORUŠIS, M.J. 1993. *SPSS for Windows: Base System User's Guide.* SPSS Inc. Release 6.0.

NORWAY, A.H. 1898. *Highways and Byways in Devon and Cornwall.* London: MacMillan and Co., Limited.

OHDAN, H., DAIMON, H., & MIMOTO, H. 1995. Evaluation of allelopathy in Crotalaria by using a seed pack growth pouch. *Jp. J. Crop Sci.*, **64**(3), 644–49.

OLOFSEN, E., DEGOEDE, J., & HEIJUNGS, R. 1992. A maximum likelihood approach to correlation dimension and entropy estimation. *Bull. Math. Biol.*, **54**(1), 45–58.

OLSEN, E.R., RAMSEY, R.D., & WINN, D.S. 1993. A modified fractal dimension as a measure of landscape diversity. *Photogramm. Engin. Remote Sens.*, **59**, 1517–20.

OS. 1992. *Ordnance Survey: Exeter & Sidmouth.* 1:50 000 Landranger Series. Sheet 192. OS stands for "Ordnance Survey".

OSAWA, A. 1995. Inverse relationship of crown fractal dimension to self-thinning exponent of tree populations–a hypothesis. *Canadian J. Forest Research–Revue Canadienne de Recherche Forestiere*, **25**(10), 1608–17.

OSBORNE, A.R., & PASTORELLO, A. 1993. Simultaneous occurrence of low-dimensional chaos and colored random noise in nonlinear physical systems. *Phys. Lett. A*, **181**(2), 159–71.

OTNES, R. K., & ENOCHSON, L. 1972. *Digital Time Series Analysis.* New York London Sydney Toronto: John Wiley & Sons.

OTTL, H. 1997. The SIR–C/X–SAR mission – overview and some results. *ACTA Astronautica*, **41**(3), 155–63.

OUCHI, S., & MATSUSHITA, M. 1991. Measurement of self-affinity on surfaces as a trial application of fractal geometry to landform analysis. *Geomorphology*, **5**, 115–30.

OUTCALT, S.I., & HINKEL, K.M. 1996. The response of near-surface permafrost to seasonal regime transitions in tundra terrain. *Arctic and Alpine Resear.*, **28**(3), 274–83.

OUTCALT, S.I., HINKEL, K.M., & NELSON, F.E. 1992. Spectral signature of coupled flow in the refreezing active layer, northern Alaska. *Phys. Geog.*, **13**(3), 273–84.

PACHEPSKY, Y.A., RITCHIE, J.C., & GIMENEZ, D. 1997. Fractal modeling of airborne laser altimetry data. *Remote Sens. Environ.*, **61**(1), 150–61.

PACKARD, N.H., CRUTCHFIELD, J.P., FARMER, J.D., & SHAW, R.S. 1980. Geometry from a time series. *Phys. Rev. Lett.*, **45**, 712–716.

PACKEPSKY, Y.A., KORSUNSKAIA, L.P., & HAJONOS, M. 1996. Fractal parameters of soil pore surface area under a developing crop. *Fractal–An Interdispl. J. Complex Geom. Nature*, **4**(1), 97–104.

PANICO, J., & STERLING, P. 1995. Retinal neurons and vessels are not fractal but space filling. *J. Comp. Neurol.*, **361**, 479–90. Cited in (Kurz *et al.*, 1998).

PARDINI, G., & GALLART, F. 1998. A combination of laser technology and fractals to analyse soil surface roughness. *Europ. J. Soil Sci.*, **49**(2), 197–202.

PARKIN, R.M., & CALKIN, D.W. 1995. Intelligent optomechatronic instrumentation for online inspection of crushed rock aggregates. *Minerals Engin.*, **8**(10), 1143–50.

PEITGEN, H.-O., & RICHTER, P.H. 1986. *The Beauty of Fractals.* Berlin: Springer-Verlag.

PEITGEN, H-O, & SAUPE, D. 1988. *The Science of Fractal Images.* Springer-Verlag.

PEITGEN, H-O, JÜRGEN, H., & SAUPE, D. 1992. *Chaos and Fractals: New Frontiers of Science.* Springer-Verlag.

PENTLAND, A.P. 1984. Fractal-based description of natural scenes. *IEEE Trans. Pattern analysis Machine Intell.*, **PAMI-6**(6), 661–74.

PERCIVAL, I. 1992. Chaos: a science for the real world. *In:* HALL, N. (ed), *The New Scientist Guide to Chaos.* Penguin Books.

PHILIPPE, P. 1993. Chaos, population biology, and epidemiology–some research implications. *Human Biol.*, **65**(4), 525–46.

PHILLIPS, J.D. 1986. Spatial analysis of shoreline erosion, Delaware Bay, New Jersey. *Annals of the Association of Am. Geographers*, **76**, 50–62.

PHILLIPS, J.D. 1989. Erosion and platform irregularity of an estuarine shoreline. *Zeitschrift für Geomorphologie Supplement*, **73**, 59–71. Cited in (Gao & Xia, 1996).

PHILLIPS, J.D. 1994. Deterministic uncertainty in landscape. *Earth Surface Processes and Landforms*, **19**(5), 389–401.

PHILLIPS, J.D. 1995. Self-organization and landscape evolution. *Prog. Phys. Geog.*, **19**(3), 309–21.

PICKOVER, C.A. 1986. Biomorphs: Computer displays of biological forms generated from mathematical feedback loop. *Comput. Graph. Forum*, **5**, 313–16.

PIECH, M.A., & PIECH, K.R. 1990. Fingerprints and fractal terrain. *Math. Geology*, **22**, 457–85.

PLATT, D.E., & FAMILY, F. 1993. Consistent scaling of multifractal measures: multifractal spatial correlations. *Phys. Rev.*, **E47**(4), 2281–88.

POINCARÉ, H. 1899. *Les methods nouvelles de la mechanique celeste.* Paris: Gauthier-Villars. Cited in: (Holton & May, 1993).

POLODORI, L., & CHOROWICZ, J. 1993. Comparison of bilinear and Brownian interpolation for digital models. *ISPRS J. Photogram. Remote Sens.*, **48**(2), 18–23.

POLYGIANNAKIS, J.M., & MOUSSAS, X. 1994. Fractal properties of the interplanetary magnetic field fluctuations–indications of chaotic dynamics. *Astron. Astrophys.*, **283**(3), 990–96.

POON, C.Y., SAYLES, R.S., & JONES, T.A. 1992. Surface measurement and fractal characterisation of naturally fractured rocks. *J. Phys.*, **D25**, 1269–75.

POWER, W., TULLIS, T., BROWN, S., BOITNOTT, G., & SCHOLZ, C. 1987. Roughness of natural fault surfaces. *J. Geophys. Res.*, **14**, 29–32.

PRADHAN, N., SADASIVAN, P.K., CHATTERJI, S., & NARAYANA, D. 1995. Patterns of attractor dimensionns of sleep EEG. *Computers in Biol. and Medicine*, **25**(5), 455–62.

PREISSL, H., LUTZENBERGER, W., PULVERMULLER, F., & BIRBAUMER, N. 1997. Fractal dimension of short EEG time series in humans. *Neurosci. Lett.*, **225**(2), 77–80.

PRICE, J.C. 1987. Calibration of satellite radiometers and the comparison of vegetation indices. *Remote Sens. Env.*, **1**, 15–27.

PRICHARD, D., & PRICE, C.P. 1992. Spurious dimension estimates from time series of geomagnetic indexes. *Geophys. Resear. Lett.*, **19**(15), 1623–26.

PRIEST, S. 1990. *The British Empiricists.* Penguin Books.

PROFETI, G., & MACINTOSH, H. 1997. Flood management through Landsat TM and ERS SAR data: A case study. *Hydrol. Process.*, **11**(10), 1397–408.

PRUSINKIEWICZ, P., & LINDENMAYER, A. 1990. *The Algorithmic Beauty of Plants.* New York Berlin Heidelberg London Paris Tokyo Hong Kong Barcelona Budapest: springer-Verlag.

QIU, H. 1988. *Measuring the Louisiana coastline–an application of fractals.* The Assoc. of Am. Geographers Cartography Specialty Group Occasional Paper 1. Cartography Specialty Group of the Assoc. of Am. Geographers, Washington, DC. Cited in (Gao & Xia, 1996).

RADONS, G. 1993. A new transition for projections of multifractal measures and random maps. *J. Stat. Phys.*, **72**(1/2), 227–39.

RANI, M., & MITRA, C.K. 1995. Correlation analysis of frequency distributions of residues in proteins. *J. Biosci.*, **20**(1), 7–16.

RANI, M., & MITRA, C.K. 1996. Pair-preferences: A quantitative measure of regularities in protein sequences. *J. Biomole. Structure Dynam.*, **13**(6), 935–44.

RAULIER, F., & UNG, C.H. 1997. Influence of shading on the relationship between leaf area and crown surface area in sugar maple stands. *Ecol. Model.*, **104**(1), 51–69.

RAY, T.S. 1992. Landmark eigenshape analysis: homologous contours: leaf shape in syngonium (Araceae). *Am. J. Bot.*, **79**, 69–76. Cited in (Campbell, 1996).

REAMS, M. 1992. Fractal dimensions of sinkholes. *Geomorphology*, **5**, 159–65.

REES, W. 1992. Measurement of the fractal dimension of icesheet surfaces using Landsat data. *Int. J. Remote Sens.*, **13**, 663–71.

REES, W.G. 1990. *Physical Principles of Remote Sensing.* Cambridge University Press. Reprinted in 1993.

REEVE, D.E. 1991. Mandelbrot, Julia sets and nonlinear mappings. *In:* CRILLY, A.J., EARNSHAW, R.A., & JONES, H. (eds), *Fractals and Chaos.* Berlin: Springer-Verlag.

REX, K.D., & MALASON, G.P. 1990. The fractal shape of riparian forest patches. *Landscape Ecology*, **4**, 249–58.

RHEA, S. 1993. Geomorphic observations of rivers in the Oregon Coast Range from a regional reconnaissance perspective. *Geomorph.*, **6**(2), 135–50.

RICE, R.J. 1988. *Fundamentals of Geomorphology.* 2nd edn. Longman Scientific & Technical.

RICHARD, A.J., & WIEGAND, C.L. 1977. Distinguishing vegetation from the soil background information. *Photogramm. Engin. Remote Sens.*, **43**, 1541–52.

RICHARDSON, L.F. 1961. The problem of contiguity: an appendix of statistics of deadly quarrels. *General Systems Yearbook*, **6**, 139–187. *Cited in* (Mandelbrot, 1983; Beauvais & Montgomery, 1996, for example).

RICHTER, D.D., & MARKEWITZ, D. 1995. Carbon changes during the growth of loblolly pine on formerly cultivated soil. *Pages 397–409 of:* POWLSON, D.S., SMITH, P., & SMITH, JU. (eds), *Evaluation of Soil Organic Matter Models Using Long-term Datasets.* Springer-Verlag.

ROBERT, A. 1988. Spatial properties of sediment bed profiles in alluvial channels. *Math. Geology*, **20**, 205–25.

ROBERT, A., & ROY, A. 1990. On the fractal interpretation of the mainstream length drainage area relationship. *Water Resources Resear.*, **26**, 839–42.

ROBERT, ANDRÉ, & ROY, ANDRÉ G. 1993. La modélisation fractale et la variabilité spatiale des phénoménes naturels (Fractal modeling and spatial variability of natural phenomena). *Géographie Physique et Quaternaire*, **47**(1), 3–19.

ROGERS, T.D. 1981. Chaos in systems in population biology. *Progress Theoret. Biol.*, **6**, 91–146.

ROUX, J.-C. 1993. Dynamical systems theory illustrated: chaotic behavior in the Belousov-Zhabotinsky reaction. *In:* FIELD, R.J., & GYÖRGYI, L. (eds), *Chaos in Chemistry and Biochemistry.* Singapore: World Scientific.

ROWLANDS, G., & SPROTT, J.C. 1992. Extraction of dynamic equations from chaotic data. *Physica D*, **58**(1-4), 251–59.

ROY, A., GRAVEL, G., & GAUTHIER, C. 1987. Measuring the dimension of surfaces: a review and appraisal of different methods. *In: AutoCarto 8 Proceedings.* Cited in (Gao & Xia, 1996).

RUELLE, D., & TAKENS, F. 1971. On the nature of turbulence. *Commun. Math. Phys.*, **20**, 167. Cited in: (Holton & May, 1993).

RUSSELL, R.C.H., & MACMILLAN, D.H. 1952. *Waves and Tides.* London: Hutchinson's Scientific and Technical Publications.

SAHAY, A., & SREENIVASAN, K.R. 1996. The search for a low-dimensional characterization of a local climate system. *Phil. Trans. Royal Soc. Lond. A -Math. Phys. Engin. Sci.*, **354**(1713), 1715–50.

SAKUMA, M., KOZMA, R., & KITAMURA, M. 1996. Characterization of anomalies by applying methods of fractal analysis. *Nuclear Technology*, **113**(1), 86–99.

SANTILLANA, G. DE, & ZILSEL, E. 1941. *The Development of Rationalism and Empiricism.* The University of Chicago Press.

SARKAR, N., & CHAUDHURI, B.B. 1992. An efficient approach to estimate fractal dimensions of textural images. *Pattern Recognition*, **25**(9), 1035–41.

SATTERWHITE, M.B. 1984. MSS and Thematic Mapper bands and band ratios. *Proc. Am. Soc. Photogramm.*, **2**, 479–90. Cited in (Satterwhite & Henley, 1987).

SATTERWHITE, M.B., & HENLEY, J.P. 1987. Spectral characteristics of selected soils and vegetation in northern Nevada and their discrimination using band ratio techniques. *Remote Sens. Env.*, **23**. 155–75.

SAUPE, D. 1988a. Algorithms for random fractals. *In:* PEITGEN, H-O, & SAUPE, D. (eds), *The Science of Fractal Images.* Springer-Verlag.

SAUPE, D. 1988b. A unified approach to fractal curves and plants. *In:* PEITGEN, H.-O., & SAUPE, D. (eds), *The Science of Fractal Images.* Springer-Verlag.

SCHATTSCHNEIDER, D. 1990. *Visions of Symmetry: Notebooks, Periodic Drawings and Related Work of M.C. Escher.* W.H. Freeman and Company.

SCHECK, F. 1990. *Mechanics: From Newton's Law to Deterministic Chaos.* Springer-Verlag.

SCHEIDEGGER, A.E. 1966. Stochastic branching processes and the law of stream orders. *Water Resour. Resear.*, **2**, 199–203. Cited in (Gregory & Walling, 1973).

SCHMITTBUHL, J., OLIVIER, G., & ROUX, S. 1992. Multifractality of the current distribution in directed percolation. *J. Physcs A–Math. General*, **25**(8), 2119–25.

SCHUMM, S.A. 1956. The evolution of drainage systems and slopes in badlands at Perth Amboy, New Jersey. *Geol. Soc. Am. Bull.*, **67**, 597–646. Cited in (Gregory & Walling, 1973).

SCHUSTER, H.G. 1988. *Deterministic Chaos.* VCH-Verlag. *Cited in:* (Buzug *et al.*, 1990).

SCHWABE, C. 1990. Evolution and chaos – the genomic potential hypothesis and phase-state mathematics. *Comp. Math. Appl.*, **20**(4-6), 287–301.

SCOTT, S.K. 1991. *Chemical Chaos.* Oxford: Clarendon Press.

SCOTT, S.K. 1994. *Oscillations, Waves, and Chaos in Chemical Kinetics.* Oxford: Oxford University Press.

SENGUPTA, S.K., WELCH, R.M., NAVAR, M.S., ERENDES, T.A., & CHEN, D.W. 1990. Cumulus cloud field morphology and spatial patterns derived from high spatial resolution Landsat imagery. *J. Appl. Meteo.*, **29**(12), 1245–67.

SERIO, C. 1994. Detecting chaos in time series. *IFIP Trans. A–Computer Sci. Technol.*, **41**, 371–83.

SEYB, A. 1994. *Drainage Network Nanlysis Using Fractal Geometry.* Cited in (Gao & Xia, 1996).

SHAW, J.A., & CHURNSIDE, J.H. 1997. Fractal laser glints from the ocean surface. *J. Optical Soc. Am. A: Optics Image Sci. Vision*, **14**(5), 1144–50.

SHAW, K.D. 1993. Observation of chaos in off-Bragg photorefractive 4-wave mixing. *Optics Communications*, **97**(1-2), 148–56.

SHAW, M.W. 1995. Simulation of population exponent and spatial pattern when individual dispersal distributions do not decline exponentially with distance. *Proc. Roy. Soc. Lond. B-Biol. Sci.*, **259**(13156), 243–48.

SHAW, R. 1981. Modeling chaotic systems. *In:* HAKEN, H. (ed), *Chaos and Order in Nature.* Proc. of the Intl. Symp. on Synergetics at Schloß Elman, Bavaria, April 27–May 2, 1981.

SHCHERBAKOV, R.A., KORSUNSKAYA, L.P., & PACHEPSKIY, Y.A. 1995. A stochastic model of the soil pore space. *Eurasian Soil Sci.*, **27**(2), 93–100.

SHEK, C.H., LIN, G.M., LEE, K.L., & LAI, J.K.L. 1998. Fractal fracture of amorphous $Fe_{46}Ni_{32}V_2Si_{14}B_6$ alloy. *J. Non-Crystalline Solids*, **224**(3), 244–48.

SHEN, Z., & MEI, L.M. 1993. Equilibrium spectra of water waves forced by intermittent wind turbulence. *J. Phys. Oceanography*, **23**(9), 2019–26.

SHIRER, H.N., FOSMIRE, C.J., WELLS, R., & SUCIU, L. 1997. Estimating the correlation dimension of atmospheric time series. *J. Atomos. Sci.*, **54**(1), 211–29.

SHOOK, K., GRAY, D.M., & POMEROY, J.W. 1993. Temporal variation in snow-cover area during melt in prairie and Alpine environment. *Nordic Hydrology*, **24**(2-3), 183–98.

SHORROCKS, B., MARSTERS, J., WARD, I., & EVENNETT, P.J. 1991. The fractal dimension of the distribution of arthropod body lengths. *Functional Ecology*, **5**(4), 457–60.

SHREVE, R.L. 1966. Statistical law of stream numbers. *J. Geol.*, **74**, 17–37. Cited in (Gregory & Walling, 1973).

SHURTZ, R.F. 1992. Pseudo-fractal interpolation for risk analysis. *Math. Geology*, **24**(1), 99–128.

SINCLAIR, JOHN. 1994. *Collins Cobuild English Language Dictionary.* London: Harper Collins Publishers.

SINGAL, S.P., GERA, B.S., & PAHWA, D.R. 1994. Application of Sodar to air pollution meteorology. *Int. J. Remote Sens.*, **15**(2), 427–41.

SLATER, P.N. 1980. *Remote Sensing: Optics and Optical Systems.* Addison-Wesley Publishing Company.

SLEATH, J.F.A. 1985. *Sea Bed Mechanics.* New York: Wiley.

SMALE, S. 1967. Differentiable dynamical systems. *Bull. Am. Math. Soc.*, **73**, 747–17. Cited in: (Dancer, 1988; Holton & May, 1993).

SMART, J.S. 1969. Topographical properties of channel networks. *Geol. Soc. Am. Bull.*, **80**, 1757–74. Cited in (Gregory & Walling, 1973).

SMITH, B., MARK, A.F., & WILSON, J.B. 1995. A fractal analysis of New Zealand Alpine vegetation in canopy roughness and functional diversity in response to an experimental wind barrier. *Functional Ecol.*, **9**(6), 904–12.

SNOW, R.S. 1989. Fractal sinuosity of stream channels. *Pure and applied Geophysics*, **131**, 99–109.

SOMMERER, J.C. 1994. Fractal tracer distributions in complicated surface flow–An application of random maps to fluid dynamics. *Physica D*, **76**(1-3), 85–98.

SORNETTE, D., & ZHANG, Y.C. 1993. Nonlinear Langevin model of geomorphic erosion processes. *Geophys. J. International*, **113**(2), 382–86.

SOURIAU, M. 1994. Scaling and physical threshold–the case of continental topography. *Int. J. Remote Sens.*, **15**(12), 2403–08.

SPAROW, C. 1982. *The Lorenz Equations: Bifurcations, Chaos, and Strange Attractors.* New York Berlin: Springer-Verlag. Cited in: (Crilly, 1991).

STARK, B., ADAMS, M., HATHAWAY, D.H., & HAGYARD, M.J. 1997. Evaluation of two fractal methods for magnetogram image analysis. *Solar Phys.*, **174**(1-2), 297–309.

STEEN, D.M. VON, LEAMER, R.W., & GERBERMANN, A.H. 1969. Relationship of optical density to yield indicators. *Pages 1115–22 of: Proc. 6th Intl. Symp. Remote Sens. of Env.* Cited in (Curran, 1980).

STEVENS, R. T. 1989. *Fractal Programming in C.* Redwood City, California: M&T Books, M&T Publishing Inc.

STEWART, H.B. 1984. The geometry of chaos. *In: The Unity of Science.* 209. Brookhaven Lecture Series. Cited in: (Gleick, 1987).

STIASSNIE, M., AGNON, Y., & SHEMER, L. 1991. Fractal dimensions of random water surfaces. *Physica D*, **47**(3), 341–52.

STOKSIK, M.A., LANE, R.G., & NGUYEN, D.T. 1995. Practical synthesis of accurate fractal images. *Graph. Models and Image Processing*, **57**(3), 206–19.

STONER, E.R., BAUMGARDNER, M.F., & CIPRA, J.E. 1972. *Determining density of maize canopy. II airbourne multispectral scanner data.* Laboratory of Applications in Remote Sensing, Purdue Univeristy, Purdue University, West Lafayette, Indiana 111272. Cited in (Curran, 1980).

STORK, N.E., & BLACKBURN, T.M. 1993. Abundance, body size and biomass of arthropods in tropical forest. *Oikos*, **67**(3), 483–89.

STRAHLER, A.N. 1952. Hypsometric (area-altitude) analysis of erosional topography. *Bull. Geol. Soc. Am.*, **63**, 1117–42. Cited in (Claps & Oliveto, 1996).

STUTZKI, J., BENSCH, F., HEITHAUSEN, A., OSSENKOPF, V., & ZIELINSKY, M. 1998. On the fractal structure of molecular clouds. *Astron. Astrophys.*, **336**(2), 697–720.

SUGIHARA, G., & MAY, R.M. 1990. Nonlinear forecasting as a way of distinguishing chaos from measurement error in time series. *Nature*, **344**, 734–741.

SUMMERFIELD, M.A. 1991. *Global Geomorphology: an Introduction to the Study of Landform.* Longman Scientific & Technical.

SUZUDO, T., TURKCAN, E.. & VERHOEF, H. 1997. Monitoring and analysis of nuclear power plant signals based on nonlinear dynamical methodology. *J. Nuclear Sci. Techno.*, **34**(3), 240–47.

SYU, C.Y., & KIRCHHOFF, R.H. 1993. The fractal dimension of the wind. *J. Solar Energy Engin.–Trans. ASME*, **115**(3), 151–54.

TAKENS, F. 1981. Detecting strange attractors in turbulence. *Pages 366–381 of:* RAND, D.A., & YOUNG, L.S. (eds), *Dynamical Systems and Turbulence.* Berlin: Springer.

TARBOTON, D.G., BRAS, R.L., & RODRIGUEZ-ITURBE, I. 1988. The fractal nature of river networks. *Water Resour. Res.*, **24**, 1317.

TATE, N.J. 1996. Estimating the fractal dimensions of synthetic topographic surfaces. *Pages 794–808 of: Proceedings of 1st International Conference on GeoComputation.*

TATE, N.J. 1998. Estimating the fractal dimension of synthetic topographic surfaces. *Comp. Geosci.*, **24**(4), 325.

TAUBES, G. 1984. The mathematics of chaos. *Discover*, **5**(9), 30.

TCHEOU, J.M., & BRACHET, M.E. 1996. Multifractal scaling of probability density function–a tool for turbulent data analysis. *J. de Physique II*, **6**(6), 937–43.

TEITSWORTH, S.W. 1989. The physics of space-charge instability and temporal chaos in extrinsic photoconductors. *Appl. Phys. A*, **48**(2), 127–36.

TEOTIA, S.S., KHATTRI, K.N., & ROY, P.K. 1997. Multifractal analysis of seismicity of the Himalayan region. *Current Sci.*, **73**(4), 359–66.

TESSIER, Y., LOVEJOY, S., SCHERTZER, D., LAVALLÉÉ, D., & KERMAN, B. 1993a. Universal multifractal indices for the ocean surface at far red wavelengths. *Geophys. Res. Lett.*, **20**(12), 1167–70.

TESSIER, Y., LOVEJOY, S., & SCHERTZER, D. 1993b. Universal multifractals: Theory and observations for rain and clouds. *J. Appl. Meteo.*, **32**(2), 223–50.

THEILER, J. 1991. Some comments on the correlation dimension of $1/f^{-\alpha}$ noise. *Physics Lett. A*, **155**(8-9), 480–93.

THIBERT, R., & TAWASHI, R. 1991. The study of the surface geometry of Renal stone fragments after shock wave and ultrsound disintegration. *Scanning Microscopy*, **5**(2), 549–54.

THOMAS, D.W. 1942. *On Growth and Form.* 2nd edn. Cambridge University Press. Cited in (Campbell, 1996).

THOMAS, J.R., MYERS, V.I., HEILMAN, M.D., & WIEGLAND, C.L. 1966. Factors effecting light reflectance in cotton. *Pages 305–12 of: Proc. 4th Intl. Symp. on Remote Sens. of Env.* Cited in (Curran, 1980).

TIAN, J.P., & YAO, K.L. 1998. Fractal structure of viscous fingering in random Sierpinski carpet. *Chinese Phys. Lett.*, **15**(7), 507–09.

TOMAN, J., & FELIX, J. 1990. *A Field Guide in Colour to Plants and Animals.* Chancellor Press.

TRAVIS, J.F. 1993. *The Rise of the Devon Seaside Resorts 1750-1990.* University of Exeter Press.

TRIANTAFYLLOU, G.N., ELSNER, J.B., LASXARATOS, A., KOUTITAS, C., & TSONIS, A.A. 1995. Structure and properties of the attractor of a marine dynamical system. *Math. Computer Modell.*, **21**(6), 73–86.

TSAI, C.C.P. 1997. Slip, stress drop and ground motion of earthquakes: A view from the perspective of fractional Brownian motion. *Pure Appl. Geophys.*, **149**(4), 689–706.

TSAI, H-M, & SIMPSON, S. 1992. *Island of Diversity – Nature Conservation in Taiwan, R.O.C.* Council of Agriculture, Executive Yuan and Department of National Parks, Construction and Planning Administration, Ministry of Interior, Taiwan, R.O.C.

TSONIS, P.A., & TSONIS, A.A. 1989. Chaos-principles and implications in biology. *Computer Appl. Biosci.*, **5**(1), 27–32.

TSP. 1996. *The Hutchinson Softback Encyclopedia.* 3rd edn. Australia: Helicon Publishing Ltd. TSP stands for "The Softback Preview".

TUCKER, C.J. 1977. *Use of Near Infrared/red Radiance for Estimating Vegetation Biomass and Physiological Status.* Report X-923-77-183. NASA/GSFC. Cited in (Curran, 1981).

TUCKER, C.J. 1979. Red and photographic infrared linear combinations for monitoring vegetation. *Remote Sens. Env.*, **8**, 127–50.

TUCKER, C.J., & CHOUDHURY, B.J. 1987. Satellite remote sensing of drought conditions. *Remote Sens. Env.*, **23**, 243–51.

TURCOTTE, D.L. 1992. *Fractals and Chaos in Geology and Geophysics.* Cambridge University Press.

TURNER, M.G. 1990. Spatial and temporal analysis of landscape patterns. *Landscape Ecology*, **4**, 21–30.

USACE. 1984. *Shore Protection Manual.* U.S. Army Corps of Engineers, Coastal Engineering Research Centre, Washington. Cited in J. Hardisty.

ŠARKOVSKII, A.N. 1964. Coexistence of cycles of a continuous map of a line into itself. *Ukr. Mat. Z.*, **16**, 61. Cited in: (Holton & May, 1993).

VANDENBERG, S., & OSBORNE, C.F. 1992. Digital image processing techniques, fractal dimensionality and scale-space applied to surface roughness. *Wear*, **159**(1), 17–30.

VAUS, D.A. DE. 1993. *Surveys in Social Research.* 3rd edn. UCL Press.

VEDYUSHKIN, M.A. 1994. Fractal properties of forest spatial structure. *Vegetatio*, **113**(1), 65–70.

VELANOVICH, V. 1994. Chaos Theory and fractal analysis–theoretical considerations and a practical example–reductionism in biology and medicine–the implications of fractal and chaos theory. *Theoretical Surgery*, 9(2), 104–07.

VENEZIANO, D., MOGLEN, G.E., & BRAS, R.L. 1995. Multifractal analysis–pitfalls of standard procedures and alternatives. *Phsy. Review E*, **52**(2), 1387–98.

VIBE, K., & VESIN, J.M. 1996. On chaos detection methods. *Int. J. Bifurcation and Chaos*, **6**(3), 529–43.

VIDAL, C. 1981. Dynamic instabilities observed in the Belousov-Zhabotinsky system. *In:* HAKEN, H. (ed), *Chaos and Order in Nature.*

VIGNES-ADLER, M., & LE PAGE, A. 1991. Fractal analysis of fracturing in two African regions, from satellite imagery to ground scale. *Tectonophysics*, **196**, 69–86.

VOLANT, P., & GRASSO, J.R. 1994. The finite extension of fractal geometry and power law distribution of shallow earthquakes – A geomechanical effect. *J. Geophys. Resear.–Solid Earth*, **99**(B11), 21879–89.

VOSS, R.F. 1985a. Random fractal forgeries. *In:* (Turcotte, 1992).

VOSS, R.F. 1985b. Random fractal forgeries. *In:* EARNSHAW, R.A. (ed), *Fundamental Algorithms for Computer Graphics.* Springer-Verlag.

VOSS, R.F. 1985c. Random fractals: characterization and measurement. *In:* (Turcotte, 1992).

VOSS, R.F. 1988. Fractals in nature: From characterization to simulation. *Pages 21–70 of:* PEITGEN, H-O, & SAUPE, D. (eds), *The Science of Fractal Images.* New York: Springer-Verlag.

WAGNER, C.D., & PERSSON, P.B. 1995. Nonlinear chaotic dynamics of arterial blood pressure and renal blood flow. *Am. J. Physiol.–Heart Circulatory Physiol.*, **37**(2), H621–H627.

WAGNER, C.D., MROWKWA, R., NAFZ, B., & PERSSON, P.B. 1995. Complexity and chaos in blood pressure after baroreceptor denervation of conscious dogs. *Am. J. Physiol.–Hart and Circulatory*, **38**(5), H1760–66.

WALTER, K. 1994. *Tao of Chaos.* Element.

WANG, J.H. 1997. On the frequency distribution of rupture lengths of earthquakes synthesized from a one dimensional dynamic lattice model. *J. Phys. Earth*, **45**(5), 363–81.

WCMC. 1994. *1993 United Nations List of National Parks and Protected Areas.* Cambridge: World Conservation Monitoring Centre and the IUCN Commission on National Parks and Protected Areas.

WEST, B.J. 1996. Extrema of fractal random water waves. *Int. J. Modern Phys. B*, **10**(1), 67–132.

WHITTINGHAM, C.P. 1974. *The Mechanics of Photosynthesis.* London: Edward Arnold. Cited in (Curran, 1985).

WIEGEL, R.L. 1964. *Oceanographical Engineering.* Englewood Cliffs, N.J.: Prentice-Hall.

WILLIAMS, J. 1969. *C.E.R.C. wave gages.* Tech. Memo. 30. U.S. Army Corps of Engineers, Coastal Engineering Research Centre, Washington, D.C.

WILSON, B.N., & STROM, D.E. 1993. Fractal analysis of surface drainage networks for small upland areas. *Trans. ASAE*, **36**(5), 1319–26.

WILSON, M.D. 1978. *Descartes.* London: Routledge & Kegan Paul.

WILSON, T.H., & DOMINIC, J. 1998. Fractal interrelationships between topography and structure. *Earth Surface Processes and Landforms*, **23**(6), 509–25.

WOLDENBERG, M.J. 1966. Horton's laws justified in terms of allometric growth and steady state in open systems. *Geol. Soc. Am. Bull.*, **77**, 431–34. Cited in (Gregory & Walling, 1973).

WOLF, A., SWIFT, J.B., SWINNEY, H.L., & VASTANO, J.A. 1985. Determining Lyapunov exponents from a time series. *Physica*, **16D**, 285–317.

WOOD, A.M.M. 1969. *Coastal Hydraulics.* Macmillan.

WORONOW, P. 1981. Morphometric consistency with the Hausdorff-Besicovitch dimension. *Math. Geol.*, **13**, 201–16.

XIA, Z. 1993. *The Use and Limitation of Fractal Geometry in Digital Terrain Modeling.* Ph.D. thesis, City University of New York. Cited in (Gao & Xia, 1996).

YAMAZAKI, H. 1988. Chaos and strange attractors of Magnons observed by parallel pumping. *J. Applied Phys.*, **64**(10), 5391–95.

YAMBE, T., NANKA, S., NAGANUMA, S., KOBAYASHI, S., AKIHO, H., KAKINUMA, Y., OHSAWA, N., NITTA, S., FUKUJU, T., MIURA, M., UCHIDA, N., TABAYASHI, K., TANAKA, A., YOSHIZUMI, N., ABE, K., TAKAYASU,

M., Takayasu, H., Yoshizawa, M., & Takeda, H. 1995. Can the artificial heart make the circulation become fractal? *Int. J. Artificial Organs*, **18**(4), 190–96.

Yambe, T., Kobayashi, S., Sonobe, T., Naganuma, S., Nanka, S., Hashimoto, H., Yoshizawa, M., Tabayashi, K., Takayasu, H., Takeda, H., & Nitta, S. 1997. Nonlinear mathematical analysis of the hemodynamics parameters during left ventricular assistance with oscillated blood flow. *Artificial Organs*, **21**(7), 625–29.

Yasue, S., Munakata, K., Kato, M., & Mori, S. 1996. Calculation of power law index for a time series by means of its fractal dimension. *Fractals–An Interdisciplinary J. Complex Geom.*, **4**(3), 265–71.

Yeragani, U.K., Srinivasan, K., Vempati, S., Pohl, R., & Balon, R. 1993. Fractal dimension of heart rate time series: an effective measure of autonomic function. *I. Appl. Physiology*, **75**(6), 2429–38.

Young, B.M., & Harvey, L.E. 1996. A spatial analysis of the relationship between mangrove (*Avicennia marina* var australasica) physiognomy and sediment accretion in the Hauraki Plains, New Zealand. *Estuarine, Coastal and Shelf Sci.*, **42**, 231–46.

Zahn, W., & Zosch, A. 1997. Characterization of thin film surfaces by Fractal Geometry. *Fresenius J. Analyt. Chem.*, **358**(1-2), 119–21.

Zeide, B. 1991. Fractal Geometry is forestry applications. *Forest Ecol. Manage.*, **46**(3-4), 179–88.

Zeng, X., Pielke, R.A., & Eykholt, R. 1992. Estimating the fractal dimension and the predictability of the atmosphere. *J. Atmospheric Sci.*, **49**(8), 649–59.

Zhang, Q. 1997. The transitional time scale from stochastic to chaotic behavior for solar activity. *Solar Phys.*, **178**(2), 423–31.

Zilsel, E. 1941. Problems of Empiricism. *In:* (Santillana & Zilsel, 1941).

Appendix

Appendix A

An introduction to Chaos Theory

The historical development of Chaos Theory is introduced, then followed by its definitions, then the route to chaos.[1] The use of the phase portrait is the means to illustrate the dynamics of a system. However, in order to reduce the dimensionality, one has to apply the technique called "Poincaré sectioning".

Chaos Theory was formulated from the chaotic phenomena arising from a non-linear deterministic system. The other key element of deterministic chaos is its sensitivity to the initial conditions, popularised as the "Butterfly Effect" (Lorenz, 1963; Gleick, 1987). Work by Feigenbaum (1980) revealed the route to chaos. The conventional "phase portrait" technique is popularly used in order to display the dynamics of a system. "Poincaré sectioning" can reduce the dimensionality of an object; therefore, it is very useful in quantifying objects of self-similar structures. Because of self-similarity, it is always possible to derive the dimensions of the whole object from its sections in lower dimensional space.

[1] Refer to page 16.

A.1 Brief History of Chaos Theory

The idea that the earth was stationary and that the sun, the planets and the stars moved in circular orbits about the earth can be traced back to Aristotle's (381-322 BC) teaching at the Lyceum, a temple to Apollo, in 334 BC. After a number of centuries, the final blow to Aristotelian theory came. In 1638, Galileo's (1554-1642) *Discoursi e demonstrazione mathematiche intorno à due nuove* (Mathematical discourses and demonstrations on two new sciences) corrected many of Aristotle's errors. Just before that, in 1609, Johannes Kepler (1571-1630) had published *Astronomia nova* (New Astronomy) revealing that elliptical orbits fit the observations well. Also, he suggested that the planets were made to orbit the sun by magnetic forces. Refer to Hellemans & Bunch (1988, pp.34-36,117,137,138).

In 1687, Sir Isaac Newton (1630-1727) published his *Philosophiae Naturalis Principia Mathematica* (The mathematical principles of natural philosophy) and postulated a law of universal gravitation, according to which, bodies of mass in the universe were attracted to each other by gravitation. Pierre Simon de Laplace (1749-1827) helped to found the theory of disorder or probability at the beginning of the nineteenth century, although he had a thoroughly Newtonian view of the universe (Hellemans & Bunch, 1988, pp.167,261).

Percil (1992, p.13) summarised the development related to chaos phenomena before the twentieth century as follows: "... during the 19th century, there were two kinds of theory for changing systems, the deterministic theories and the theory of probability. The two approaches appeared incompatible. In the first, the future is determined from the past... In the second, the future depends in some random way on the past, and cannot be determined from it. The first challenge to this picture

came with the quantum theory in the 1920s and the 1930s. ... theorists describe the behaviour of an electron in terms of a 'probability wave'. The second challenge came from the theory of chaos. Simple mathematical analysis shows that even in simple systems, which obey Newton's laws of motion, you cannot always predict what is going to happen next. The reason is that there is persistent instability."

According to Gleick (1987), many of the modern developments in chaos theory can be traced back to Henri Poincaré's work (1899) on celestial mechanics at the end of the nineteenth century. He developed a new kind of mathematics called topology, a sort of geometry that deals with continuities and connections among varying quantities. Dancer (1988, p.13) noted that "it was first realized by the French mathematician Poincaré late last century that very complicated behaviour could occur for some simple equations." This was developed further by the American mathematician Birkhoff in the 1920s, and the English mathematicians Mary Cartwright and Littlewood in the late 1940s (Dancer, 1988, p.13). In the 1920s, European mathematicians, for example, Gaston Julia (1893-1978) (Julia, 1918) and Pierre Fatou (1878-1929) (Fatou, 1919) in Paris studied a special kind of abstract motion, which led to the beautiful "fractal" pictures that Benoit Mandelbrot (1983) created in the 1970s.

Approaches that follow the work of Poincaré take the topological pictures of complex dynamic behaviour and use them to probe how oscillating systems become chaotic. Myrberg (1958) started a line of research to plot how such dynamics evolve, which helped Robert May (1976) to understand how populations of animals oscillate then become chaotic (Holton & May, 1993). The American mathematician Smale (1967) showed that there really was chaotic behaviour in a rather precise sense.

The behaviour of dripping taps was analysed by Packard and his colleagues (1980). The most important complications of this kind of motion were unravelled by Šarkovskii (1964) and Mitchell Feigenbaum (1979). A similar system helped David Ruelle and Floris Takens (1971) to analyse the behaviour of turbulent fluids, and Edward Lorenz (1963) to analyse the chaos in the weather system. Lorenz produced some equations which were a rough approximation to the behaviour of the atmosphere and found numerically that chaotic behaviour occurred (Lorenz, 1993).

A.2 The Definition of Chaos

Chaos can be interpreted as a system being deterministic and sensitive to initial conditions, although there are various definitions. Some examples, quoted from Gleick's (1987, p.306) book "Chaos Making a New Science" are: "A kind of order without periodicity" (Hao, 1984); "Apparently random recurrent behaviour in a simple deterministic (clockwork-like) system" (Stewart, 1984); and the "irregular, unpredictable behaviour of deterministic, nonlinear dynamical systems" (Jensen, 1987). In one of the most recent attempts to define chaos, Mullin (1993c) stated "it represents a universe that is deterministic, obeying the fundamental physical laws, but with a predisposition for disorder, complexity and unpredictability."

Another definition of chaos was proposed by Field & Györgyi (1993, p.v) as follows: "Chaos is the word we apply to oscillatory but aperiodic, apparently random behavio[u]r appearing in a system not subject to stochastic perturbation but entirely governed by a deterministic dynamic law." It is intimately related to periodic oscillation, and periodicity may decompose to chaos when some varying parameter constraining an oscillatory system crosses a critical value. The resulting complex,

chaotic waveform may be regarded as periodic but with a repetition time approaching infinity. Indeed one of the major routes from periodicity to chaos involves a repetitive doubling of the period as a parameter is monotonically varied.

The amplitudes and/or periods of the individual cycles of a chaotic waveform seem to be random and are unpredictable and irreproducible over an extended period of time. A chaotic system will remain apparently noisy regardless of how well experimental conditions are controlled. However, a chaotic waveform results from a quite ordinary deterministic dynamic law and has considerable order related to the presence of a so-called **strange attractor** that attracts trajectories in the same way as do simpler attractors such as steady state or limit cycle. Field & Györgyi (1993, p.v) pointed out that "order is present because a chaotic waveform stays within a finite region in phase space in the close neighbourhood of the strange attractor." Various maps, e.g., return maps constructed from Poincaré sections (or maps) and next amplitude maps, may be constructed and used to show the underlying orderliness of chaos, which often has a fractal nature.

The unpredictability of a chaotic waveform results because trajectories starting from arbitrarily close initial conditions diverge. The measure of this divergence is the Lyapunov exponent. The fundamental mathematical definition of a chaotic system is one with a positive Lyapunov exponent. This definition and similar measures can be calculated for an experimental waveform, but practical problems often arise that cloud their interpretation. Chaos is thus usually identified in an experimental system or situation by construction of the sorts of maps mentioned above and by the investigation of the route from periodicity to aperiodicity (Field & Györgyi, 1993, p.v).

Chaos Theory has gained wide popularity, and attempts have been made to identify the phenomenon in many different branches of science. Articles related to chaos accumulated quickly in traditional fields such as biology (Rogers, 1981; Tsonis & Tsonis, 1989; Kyriazis, 1991; Philippe, 1993; Engbert & Drepper, 1994; Velanovich, 1994; Lloyd & Lloyd, 1995), physics (Bohigas & Weidenmuller, 1988; Lauterborn & Parlitz, 1988; Teitsworth, 1989; Monteiro, 1994; Nicholis & Nicholis, 1995), chemistry (Vidal, 1981; Scott, 1991; Roux, 1993; Györgyi & Field, 1993; Scott, 1994), mathematics (Taubes, 1984; May, 1989; Schwabe, 1990), economics (hausman & McPherson, 1990; Lebaron, 1994) and geomorphology (Malanson *et al.*, 1992; Gaffney, 1993; Phillips, 1994; Phillips, 1995; Land & Richards, 1997).

There are also articles that relate chaos to art and design (Lansdown, 1991) or to medicine (Velanovich, 1994). In fact, there are books devoted to the discussion of DNA (Walter, 1994), the I-ching (Legge, 1990) and Chaos Theory. Although the focus is mainly on the chaos arising from deterministic systems, conferences have been held and dedicated to the discussion of order and chaos in quantum systems (Exner & Neidhardt, 1990). Scientific articles related to quantum physics and chaos are available (Efetov, 1995; Jensen, 1995; Elnaschie, 1996).

Sensitive to Initial Conditions

An essential element of chaos in nonlinear deterministic systems is the extreme sensitivity of the system to initial conditions (Lorenz, 1963; Crilly, 1991; Peitgen *et al.*, 1992). This means that two sets of conditions of a system initially very close together can give rise to widely different states in the long term.

In nature, the initial condition cannot be known exactly but only with limited

accuracy. It follows that the predictability of long-term behaviour must fail for those nonlinear systems that exhibit chaos (Crilly, 1991, p.196). Crutchfield *et al.* (1986) stated, "it may happen that small differences in the initial conditions produce very great ones in the final phenomena. A small error in the former will produce an enormous error in the latter. Prediction becomes impossible." Henri Poincaré was aware of this phenomenon in 1903 in his study of planetary motion (Hellemans & Bunch, 1988; Crilly, 1991). However, the sensitivity of nonlinear systems to initial conditions was explained by Edward Lorenz (1963) and became popularly known as the **butterfly effect** shown in Figure A.1, which is derived from Equation A.1.

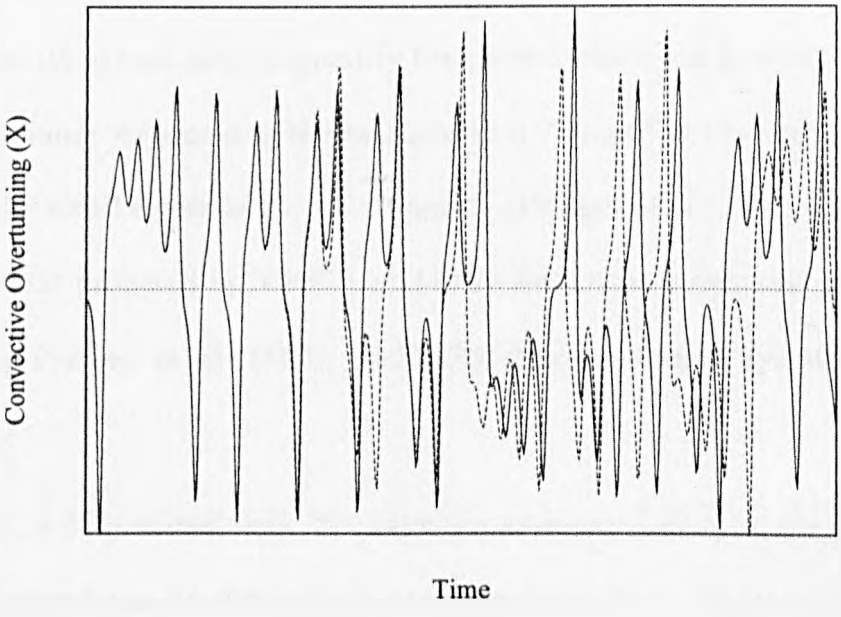

Figure A.1: The Butterfly Effect.
The parameters a, b, and c in Equation A.1 are 10, 28, and 8/3, respectively. The initial values of x are 0.6 (—) and 0.6001 (- - -). However, the difference between subsequent values becomes significant after a few iterations.

In 1960s, Edward Lorenz used a computer to model weather patterns, using a

set of ordinary nonlinear differential equations,

$$\begin{aligned} \dot{x} &= a(y-x) \\ \dot{y} &= bx - y - xz \\ \dot{z} &= xy - cz \end{aligned} \quad , \tag{A.1}$$

where a, b and c are empirical parameters. The variables x, y and z are related to "convective overturning", "horizontal temperature" and "vertical temperature", respectively (Crilly, 1991, p.200). The significance of the equations lies in their exhibition of chaos. "It is a reminder of the subject's intrinsic mathematical difficulty that very little of the behaviour of the solutions can be proved with strict mathematical rigour" (Sparow, 1982).

The mathematical tool used to quantify the phenomena is the **Lyapunov exponent**. The Lyapunov exponent is the measure that "quantifies the average growth of infinitesimally small errors in the initial point" (Peitgen *et al.*, 1992, p.516). The algorithm was first proposed by Wolf *et al.* (1985) for a time series, and generalised for example by Peitgen *et al.* (1992, pp.715,751) for continuous systems such as Lorenz system.

Shaw (1981, p.224) stated that "for an n-dimensional system, 'Lyapunov characteristic exponents' can be defined, at least operationally." These numbers can easily be computed numerically for simple systems whose equations of motion are known, and can be experimentally measured at least in some cases. The spectrum of Lyapunov numbers provides a partial classification scheme for dynamic systems. For instance, if all the Lyapunov numbers are negative, the system will approach **a stable equilibrium**. A system in **a stable oscillation** does not contract volume along the direction of the trajectory through stable phase space, thus one of the characteristic numbers is zero. If any of the Lyapunov numbers is positive, the

system will be **chaotic** (Shaw, 1981; Field & Györgyi, 1993, for example).

A.3 Routes to Chaos

The study of chaotic systems was made popular by the computer experiments of May (1974) and Feigenbaum (1980) and fully described by Peitgen *et al.* (1992) on a mapping known as the **logistic map** (May, 1976; Feigenbaum, 1980; Bland & Rowlands, 1986; Scott, 1991; Field & Golubitsky, 1992). A **map** which allows us to predict the next value x_{n+1} from the current measurement x_n is known as an **iterative, recursive,** or **logistic map** (May, 1976; Field & Golubitsky, 1992; Hardisty *et al.*, 1993, for example.). This mapping is one of the typical models in population dynamics,

$$x_{n+1} = g(x) \equiv \lambda x_n(1 - x_n), \tag{A.2}$$

where g is the logistic mapping, λ is the effective growth rate, and $x_n \subset [0, 1]$ is the relative population at generation n. The remarkable features of the logistic map are "the contrast between the simplicity of its form (it is a polynomial mapping of degree two) and the complexity of its dynamics" (Field & Golubitsky, 1992, p.100).

The route to chaos can be illustrated by Figure A.2 which shows how the dynamics of the logistic mapping g change as the effective growth rate λ is varied (May, 1974; May, 1976; Gleick, 1987; Field & Golubitsky, 1992; Peitgen *et al.*, 1992). The mathematical analysis by Feigenbaum (1980; 1992) provides a detailed understanding of the route to chaos. The route advances in three stages, that is, stationary states, period-doublings, and chaotic regions.

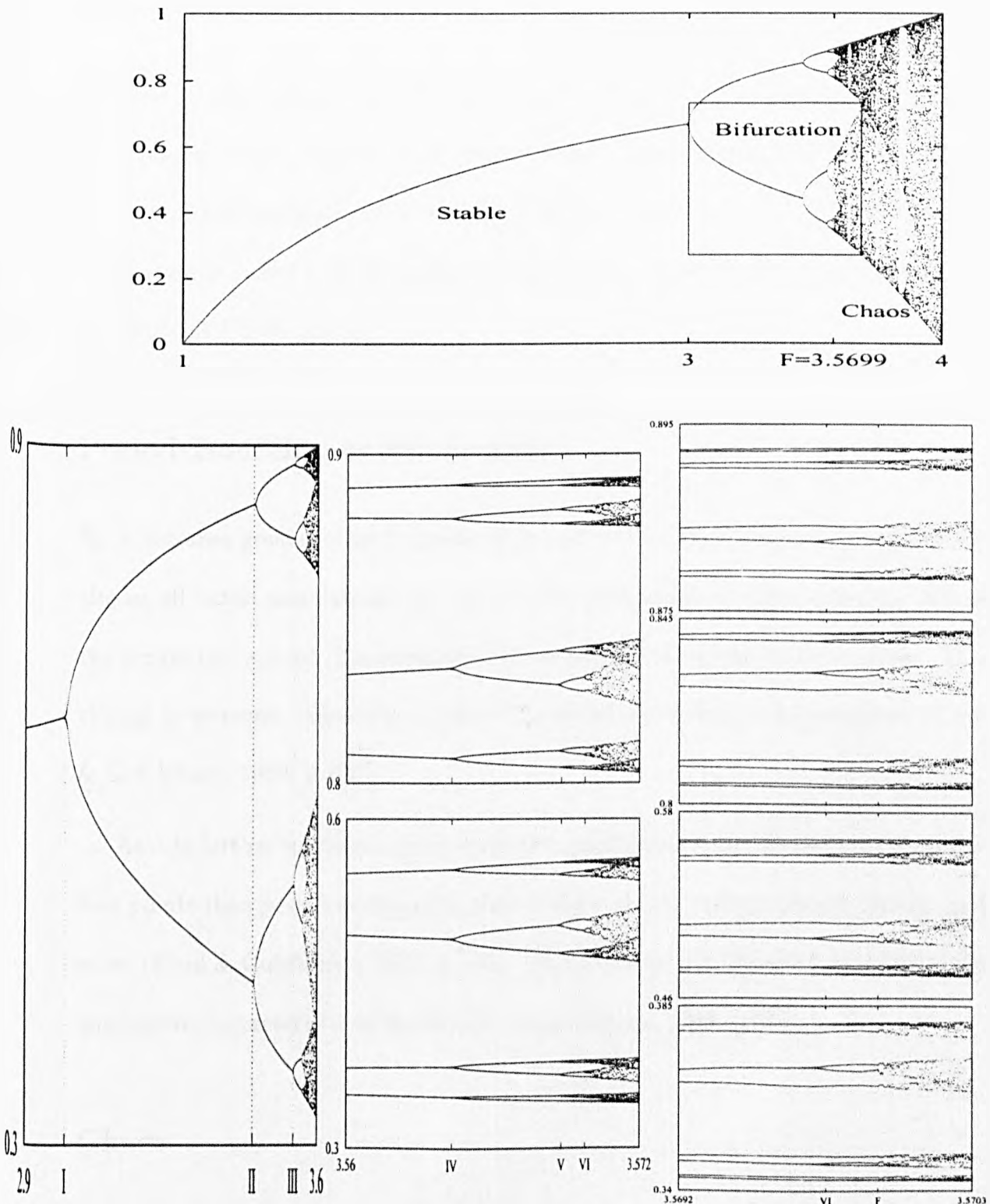

Figure A.2: Feigenbaum Map: The Route to Chaos.

The route to chaos is illustrated by the bifurcation scenario which is represented by a logistic equation. The attracting sets include fixed points, period-doubled points. The chaotic dynamics appears at parameters larger than 3.5699456..., the Feigenbaum point (F).

Stationary States

Suppose at the effective growth rate $\lambda < 1$, the population decreases to zero as n increases. Next, suppose λ is greater than 1 and smaller than 3. There is a critical relative population that remains constant time after time. The value of such population is called a **fixed point** or **stationary state** for the mapping g (Field & Golubitsky, 1992, p.104).

Period-Doubling or Bifurcation

As λ becomes greater than 3, a pair of period-two points is created. Moreover, for almost all initial populations, i.e., $x_0 > 0$, the population x_n approaches the pair of the period-two points. The population alternates between high and low values. This change in dynamic behaviour is called a **period-doubling** or **bifurcation** (Field & Golubitsky, 1992, p.104).

As λ is further increased, the period-two point itself period-doubles to a period-four points then period-doubling to period-eight occurs, then to period sixteen, and so on (Field & Golubitsky, 1992, p.106). The phenomenon of period-doubling is the qualitative characteristic of the logistic map (Scheck, 1990, p.362).

Chaos

When the effective growth rate reaches a critical value λ_c, period points of an arbitrarily large period have appeared in the dynamics of g and chaotic dynamics has set in (Field & Golubitsky, 1992, p.106). This threshold marks the end of the period-doubling regime. It was discovered by Feigenbaum (1979) and has become

known as the **Feigenbaum point** $\lambda_c = 3.5699456...$ (Gleick, 1987; Peitgen *et al.*, 1992, p.588).

A.4 Feigenbaum's Number

This bifurcation scenario which illustrates the route to chaos is summarised by the famous bifurcation diagram, redrawn relatively easily here in Figure A.2. In this figure the horizontal axis shows the parameter λ and the vertical axis shows the final population x. For each value of the parameter, the attracting sets are shown: first the fixed points, then the period-doubling points, then the chaotic region.

Dancer (1988, p.9) said that "bifurcations have been studied for a long time beginning with the work of Euler in the 18th century. An increase in interest followed the work of Poincaré late last century. ... [Focusing on] where the bifurcation takes place started with the work of the Russian mathematician Krasnosel'skiĭ (1946) in the late 1940s, and has been pursued by a number of authors since then."

However, it was not until 1978 that Feigenbaum made another remarkable discovery about the logistic map and mappings like the logistic map: "there is a universal constant of mathematics (akin to π and e) that can be associated with period-doubling cascade and, moreover, this constant can even be determined experimentally", recalled Field & Golubitsky (1992, p.108). Feigenbaum (1979) discovered that the ratio,

$$\frac{\lambda_m - \lambda_{m-1}}{\lambda_{m+1} - \lambda_m}, \tag{A.3}$$

appears to be a constant as m becomes large and this constant is now known as **Feigenbaum's number** (Field & Golubitsky, 1992, p.108) or **Feigenbaum's con-**

stant (Peitgen *et al.*, 1992, p.588). What is important is that there is a large class of mappings, which include the logistic map, for which this number is the same (Feigenbaum, 1979; Feigenbaum, 1980; Feigenbaum, 1992; Field & Golubitsky, 1992). The number is $\delta = 4.6692016...$

A.5 Making the Image of Chaos

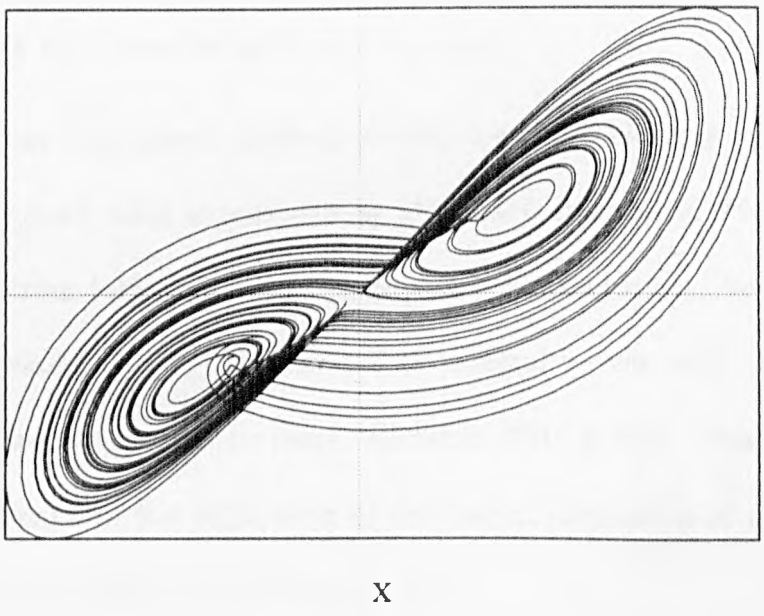

Figure A.3: The Lorenz Attractor.
The parameters a, b, and c in Equation A.1 are 10, 28, and 8/3, respectively. The initial values for x, y, and z are 0.6, 0.6, and 0.6, respectively. The trajectories are projected onto the XY-plane. The trajectories consist of 5000 points. Note that there is no crossover in the attractor.

Classical dynamical systems can be thought of as possessing attractors in phase space. For the system described by Lorenz's equations (Equation A.1) an attractor exists, although it is not simply a point attractor. The way a trajectory winds around an attractor for this case is indicated by a two-dimensional projection in Figure A.3. There are 5000 points plotted in the figure using Equation A.1. The parameters a, b,

and c are 10, 28, and 8/3, respectively. The initial values for x, y, and z are 0.6, 0.6, and 0.6, respectively. The trajectories are projected onto the XY-plane, and there is no crossover in the attractor. Crilly (1991, p.200) stated that "if trajectories of Lorenz's equations are plotted in three-dimensional phase space, Lorenz found that they are attracted towards a bounded 'ellipsoid', which all trajectories eventually enter and from which they never escape." A curious mathematical property of the ellipsoid is that it possesses zero volume. It is now known that the Lorenz attractor is an infinitely nested layered structure, and that the zero volume is consistent with cross sections through the layers being fractal in nature.

A particularly clear topological method of studying the trajectory flow in the neighbourhood of a closed orbit is provided by **Poincaré mapping**. "In essence, it consists in considering local transverse sections of the [trajectory] flow, rather than the flow as a whole, i.e., the intersection of integral curves with some local hyper-surfaces that are not tangent to them" (Scheck, 1990, p.342). This mapping technique effectively enables the estimation of the fractal dimension of a complex fractal object from its sections in lower dimensions.

Appendix B

Programme Listing of the Logistic Equation

The following C programme is compiled by C compiler on SunOS (4.1.3_U1), using the script "*acc $1.c -o $1 -lm -xCC -w*".[1] Example usage, *may 0.6 3 4*, produces a logistic map of an initial population of 0.6 and growth rates between 3 and 4.

```
/*  MAY.C
Usage: may x0 a1 a2
Desc:  x_{n+1}=a x_n (1 - x_n)
*/
#include <stdio.h>
#include <stdlib.h>
#include <math.h>
#define ISTART 500 // run-in iterations
#define ISTOP 50 // No. of iterations
#define ASTEP 1000 // Steps of para a
#define VMINUTE 0.000001 /* min.diff of
vmin and xdat */
#define VWILD 999.9 // Wild value
/*************** main ***************/
void main(int argc, char **argv)
{
int     i, j, k;
double x0, a1, a2;
double xn, xnew;
double anew, ainterval;
double xdat[ASTEP][ISTOP],
adat[ASTEP]; // a_val x x_val
double vmin;
if(argc < 2){
   printf("Usage: %s x0 a1 a2\n", argv[0]);
   printf("\tx0:      Initial population
(0<x0<1)-- 0.5\n");
   printf("\ta1,a2:  Range of parameter
(0<a<4)-- 0-4\n");
   exit(-1);
} // warning
x0 = atof(argv[1]);
a1 = atof(argv[2]);
a2 = atof(argv[3]);
ainterval = fabs(a2 - a1) / ASTEP;
for(i=0; i<ASTEP;i++){
   anew    = a1 + i * ainterval;
   xn      = x0;
   adat[i] = anew;
   for(j = 0; j < ISTART; j++){
      xnew = anew * xn * (1 - xn);
      xn   = xnew;
   } // j: skipping
   for(j = 0; j < ISTOP;j++){
      xnew = anew * xn * (1 - xn);
      xn   = xnew;
      xdat[i][j] = xnew;
   } // j: calculating
} // i
for(i = 0; i < ASTEP; i++){
   for(j = 0; j < ISTOP; j++){
      if(xdat[i][j] != VWILD){
         vmin = xdat[i][j];
         for(k = 0; k < ISTOP; k++){
            if(k == j){ xdat[i][k] = vmin; }
            else {
               if(fabs(xdat[i][k]- vmin) <
VMINUTE){ xdat[i][k] = VWILD; } // if
            } // if-else
         } // k
      } // if
   } // j
} // i
for(i=0; i < ASTEP;i++){
   for(j=0;j<ISTOP;j++){
      if(xdat[i][j] != VWILD){
         printf("%f %f  %2d\n", adat[i],
xdat[i][j], j);
      } // if
   } // j
}  // printout
} // main
```

[1] Refer to page 16.

Appendix C

Fractals in Buddhist Literature

According to Harvey (1990, p.1), the history of Buddhism spans almost 2500 years from its origin in India with Siddhattha Gotama (*c.* 566-486 BC or 448-368 BC), who became the Buddha (Pali *sammā-sambuddha*), or "perfect fully Awakened One" and taught for 49 years in India.[1] Our knowledge of Buddhism, the teachings of the Buddha, is based on several canons of scripture, which derive from the early oral transmission of *Sangha*[2]. In its long history, Buddhism has used a variety of teachings. Around the beginning of the Christian era, a movement began which led to a new style of Buddhism known as Mahāyāna[3], or "Great Vehicle". One of the schools of Mahāyāna philosophy is based on the *Avataṃsaka*, or "Flower Ornament" *Sūtra* (Chinese *Hua-yen Ching*) (Harvey, 1990, p.118). This is a huge work, many of whose chapters circulated as separate *Sūtras*. The most important

[1] Refer to page 19.

[2] The most important bearers of the Buddhist tradition have been the monks and nuns who make up the *Sangha* or "Community" (Harvey, 1990, p.2).

[3] The Mahāyāna is characterised, on the one hand, by devotion to a number of holy Saviour beings, and on the other by several sophisticated philosophies, developed by extending the implications of the earlier teachings of Buddhism (Harvey, 1990, p.2).

books are the *Daśa-bhūmika Sūtra*, on the "Ten Stages" of the *Bodhisattva*[4]-path, and the *Gaṇḍavyūha*, or "Array of Flowers" *Sūtra*, which comprises more than a quarter of the whole *Avataṃsaka*. The *Gaṇḍavyūha* deals with the spiritual pilgrimage of the youth Sudhana, who is sent on a journey to fifty-two teachers to learn the secrets of the *Bodhisattva*-path. Near his journey's end, he comes to the *Bodhisattva* Maitreya[5], who shows him the huge tower of the Buddha Vairocana ("The Resplendent One").

Sudhana enters the tower, where he finds a wondrous world, as vast as space, full of countless paths, palaces, banners and trees, all made of jewels, along with countless mirrors, burning lamps, and singing birds. Moreover, Harvey (1990, pp.118-19) described, "the tower is also found to contain countless other towers, each as vast as itself, yet these do not interfere with each other in any way, but harmoniously intermingle and preserve their separate identities. All are contained in one and one in all; and in each Sudhana sees himself, so that he feels as if his body and mind had melt away. In an especially large tower, of exquisite beauty, Sudhana sees all the worlds of the universe, with Buddhas active in each." Therefore, Sudhana sees himself, as a self-similar structure, in both inward and outward scaled towers. This image is almost identical to the description of objects of a fractal nature.

---

[4] A being (Pali *satta*) who is dedicated to attaining perfect enlightenment (*bodhi*) (Harvey, 1990, p.15).

[5] Maitreya means "The Kindly One". In Eastern Buddhism, he is portrayed in the form of his recognised manifestation, the tenth-century Pu-tai. In the West, his images are known as "Laughing Buddha" (Harvey, 1990, p.131).

Appendix D

Multifractal Dimensions

D.1 Introduction

The number of scientific papers on multidimensional fractals is increasing rapidly (Lovejoy & Schertzer, 1986; Feder, 1988; Mandelbrot, 1988; Mandelbrot, 1989; Evertsz & Mandelbrot, 1992; Borgani *et al.*, 1993; Lee *et al.*, 1993; Nagatani, 1993; Platt & Family, 1993; Radons, 1993; Tessier *et al.*, 1993a; Tessier *et al.*, 1993b, for example).[1] There are two ways to extend the idea of fractal dimensions to multifractal dimensions. One is the generalised dimension D_q and the other is the introduction of the singularity spectrum $f(\alpha)$ (Halsey *et al.*, 1986).

D.2 Generalised Dimensions

Consider a structure (or any fractal measure) embedded in a E-dimensional space. Let $\{X_i\}_{i=1}^{N}$ be the points of the structure as a long time series. The number of

[1] Refer to page 27.

points representing the space is equal to or greater than the points of the structure N. Cover the space with a mesh of E-dimensional spheres of size r. Let $M(r)$ be the number of spheres that contain points of the series $\{X_i\}_{i=1}^{N}$ and let $P_k(r) \equiv N_k/N$ where N_k is the number of points in the k-th sphere of size r.

The similarity dimension was defined by Mandelbrot (1983). However, he regretted using the term because "it does not carry over to the self-affine fractals" and suggested the box dimension, D_B, instead (Mandelbrot, 1985).

$$D_B = -\lim_{r\to 0}\lim_{N\to\infty} \log M(r)/\log r, \tag{D.1}$$

which describes the scaling of the density.

The information dimension, D_I, is defined as

$$D_I = -\lim_{r\to 0}\lim_{N\to\infty} S(r)/\log r, \tag{D.2}$$

where

$$S(r) = -\sum_{k=1}^{M(r)} P_k(r)\log P_k(r), \tag{D.3}$$

which gives the information gained by the knowledge of each P_k with accuracy r. D_I tells us how the information (or the morphology) increases as $r \to 0$.

The correlation dimension, D_C, is defined by

$$D_C = \lim_{r\to 0}\lim_{N\to\infty} \log C(r)/\log r, \tag{D.4}$$

where

$$C(r) = \frac{1}{N^2}\sum_{i\neq j} \theta(r - |X_i - X_j|), \tag{D.5}$$

where θ is the Heaviside function (Hentschel & Procaccia, 1983).

In case of a two dimensional space, this quantity is the probability that two points lie within the sphere of size r, i.e., the probability that two points that are separated

by a distance smaller than r. Therefore, $C(r)$ could be rewritten as (Blacher *et al.*, 1993)

$$C(r) = \sum_{k=1}^{M(r)} (P_k(r))^2, \tag{D.6}$$

for an image.

The uncountable infinity of generalised dimensions is given as (Hentschel & Procaccia, 1983)

$$D_q = \frac{1}{q-1} \lim_{r \to 0} \frac{\log \sum_k (P_k(r))^q}{\log r}. \tag{D.7}$$

Equation D.7 could be rewritten as

$$D_q = \frac{1}{q-1} \lim_{r \to 0} \frac{\log \sum P_k(r) \exp^{q-1} \log P_k(r)}{\log r}. \tag{D.8}$$

In the limit $q \to 1$ one expands the exponential and Equation D.2 is obtained.

Most natural fractals are not completely or even statistically self-similar. For such fractals, dimensions estimated by various methods are different from each others (Hirabayashi *et al.*, 1992). For such fractals, $D_q > D_{q'}$ if $q' > q$. Then a single value of the fractal dimension is not enough to characterise the fractals.

The singularity spectrum $f(\alpha)$ is the fractal dimension of the subsets with the same singularity strength α. When we formulate the singularity spectrum $f(\alpha)$, we cover the space with spheres of size r and define $P_i(r)$ to be the probability in the i-th sphere. This singularity α_i is defined as (Hirabayashi *et al.*, 1992)

$$P_i(r) \approx r^{-\alpha_i} \tag{D.9}$$

and then the exponent $f(\alpha)$ can be defined by

$$N_\alpha(r) \approx r^{-f(\alpha)} \tag{D.10}$$

where $N_\alpha(r)$ is the number of spheres with size r in which the $P_i(r)$ has the singularity strength between and α and $\alpha + d\alpha$.

The generalised dimension D_q is obtained as an extension of some definitions of the fractal dimensions, and can be defined as (Hirabayashi *et al.*, 1992)

$$D_q = \frac{1}{q-1} \lim_{r \to 0} \frac{\log \sum_0 (P_i(r))^q}{\log r}. \tag{D.11}$$

The parameter q can take any real number ranging from $-\infty$ to ∞.

The relation between the generalised dimension D_q and the singularity spectrum $f(\alpha)$ is expressed by

$$D_q = \frac{1}{q-1} [q\alpha(q) - f(\alpha(q))], \tag{D.12}$$

which is deduced from Equation D.11 by the use of the method of the steepest descent (Hirabayashi *et al.*, 1992). The reverse expression is the Legendre transformation of Equation D.12, such that (Halsey *et al.*, 1986)

$$\alpha(q) = \frac{d}{dq} [(q-1)D_q], \tag{D.13}$$

and

$$f(\alpha(q)) = q\alpha(q) - (q-1)D_q. \tag{D.14}$$

It has been customary to determine the D_q of interest and then to evaluate the singularity spectrum $f(\alpha)$ by transformations, because the direct determination of $f(\alpha)$ from a limited number of data often yields inaccurate answers.

D.3 Implementation Methods

Implementation methods are similar to those for monofractal objects.

Box-counting Method

This method is based directly on the definition of D_q. We cover the E-dimensional space with sphere of size r and decide $P_i(r)$. Then, D_q is estimated from the slope of the *log-log* plot between the values $\sum_i (P_i(r))^q$ and r. The slope corresponds to $(q-1)D_q$, see Eq. D.11. It is simple but often impractical for the small number of points (Greenside *et al.*, 1982; Hirabayashi *et al.*, 1992).

Fixed-centre Method

This is a generalisation of the correlation method (Jensen *et al.*, 1985). The total mass (points) $M(< r)$ within the circle of the radius r is measured with the increase of r. then, D_q is estimated from (Hirabayashi *et al.*, 1992)

$$\log < M(< r)^{q-1} > \approx (q-1)\log r, \tag{D.15}$$

where $<>$ is the average of the mass for the circle centre.

Fixed-mass Method

This is also a generalisation of the correlation method and is essentially equal to the fixed-centre method. We find how the smallest radius $R(< m)$, within which a fixed-mass m is included, increases as the mass m increases. D_q is decided by,

$$\log < R(< m)^{1(q-1)D-q} > \approx -(q-1)\log m, \tag{D.16}$$

the relation proposed by Hirabayashi *et al.* (1992), who found this method was superior in calculating $D-q$ for negative q of earthquakes.

Appendix E

Programme Listing of the Box-Counting Method

The following script is used to compile C programme incorporating NAG FORTRAN library routines (Hann & Hounam, 1991), whose resulting object programme is further compiled by FORTRAN compiler.[1] That is, "*acc -c -lm $1.c*" and "*f77 $1.o -o $1 -lnag*". It includes the main programme (*boxfd.c*), the user-defined header file (*TS.h*) and its source code (*TS.c*). The user-defined header file is first given.

```
/* TS.h
//TS_data_extrap - extrapolate raw data
*/
#ifndef _TS_h
#define _TS_h
extern void TS_data_extra(/* double x[],
double y[], int n */);
#endif
```

The source code of the user-defined header file is given below. It is a simple C programme which is compiled as a user-defined library.

```
/*
// TS.c - implementation file for TS.h
*/
#include <stdio.h>
#include <stdlib.h>
#include <math.h>
#include "TS.h"
#define MU (0.01)
/*********************************
// extrapolation
// X_i = 2*X_{i-1} - X_{i-2}
*********************************/
void
TS_data_extra(
   double x[], /* input  array */
   double y[],/* output array */
   int    n)   /* length of array  */
{
   int i;
   y[0] = 0.0; y[1] = 0.0;
   for(i=0; i < n; i++){
      if(x[i] >= 0.0){ y[i] = x[i];
      } else {
         y[i] = 2*y[i-1] - y[i-2];
         if( y[i] < 0.0 ) {  y[i] = MU; }
      }
}
} /* TS_data_extra */
```

Here follows the main programme.

```
/* boxfd.c
// Usage: boxfd col row
// Ref: Turcotte, 1993
// Input:stdin (col x row)
// Output:stdout
*/
#include <stdio.h>
#include <math.h>
#include <nagmk15.h> // NAGF lib.
#include <TS.h>
/*********************************
// Box-counting: Brownian method
// Count boxes between max and min
// width decreased by 2^n
//height is given
*********************************/
void
TS_brown_box_counting(
   double x[],  /* input data */
   int    length, /* length of data */
   double std,  /* height of data */
   double result[20]) /* result */
{
int    i,u,v;
```

[1] Refer to Section 3.2.4.

```
int     paces;
double *tmpp, *size, *count, *ind, *dep;
double width, height, val;
double scal;
/* declarations for G01AAF, G02CAF */
int     n, iwt, ifail;
double
*wt, xmean, s2, s3, s4, xmin, xmax, wtsum;
paces= (int) floor(log2((double)length));
size  = malloc(paces * sizeof(int));
count= malloc(paces * sizeof(int));
for(i = 0; i < paces; i++){
   scal   = pow(2.0, (double)i );
   width  = length / scal;
   height = std / scal;
   size[i] = scal;
   count[i] = 0.0;
   tmpp = malloc((int)width *
sizeof(double));
   wt   = malloc((int)width *
sizeof(double));
   for(u = 0; u < scal; u++){
      for(v = 0; v < width; v++) {
         tmpp[v] = x[u * (int)width + v];
      }
      n = (int) width; iwt = 0; ifail = 1;
      g01aaf_(&n, tmpp, &iwt, wt, &xmean, &s2,
&s3, &s4, &xmin, &xmax, &wtsum, &ifail);
      val= ceil(xmax/height) -
floor(xmin/height);
      count[i] += val;
   }
   free(tmpp); free(wt);
}
for(i=0; i<paces; i++){
   size[i] = log2(size[i]);
   count[i]= log2(count[i]);
}
n = paces; ifail = 1;
g02caf_(&n, size, count, result, &ifail);
free(size); free(count);
} // TS_brown_box_counting //
/************************************
*************** main ****************
************************************/
void main(int argc, char **argv)
{
int     i, j, size_d;
int     width, leng, new_leng, size;
double *dat;
/* NAGF: G01AAF etc */
int     n, iwt, ifail;
double *y, *x, *wt,
xmean, s2, s3, s4, xmin, xmax, wtsum,
result[20];
if(argc < 2){
   printf("Usage: %s col row\n", argv[0]);
   printf("\tcol:number of columns\n");
   printf("\trow:number of rows\n");
   exit(1);
}
width    = atoi(argv[1]);
leng     = atoi(argv[2]);
new_leng = (int)exp2( floor( log2(
(double)leng ) ) ); // leng = 2^n
size     = width * leng;
size_d   = sizeof(double);
/***** read data from stdin *****/
y   = malloc(size * size_d);
dat = malloc(size * size_d);
for(i = 0; i < leng; i++){
   for(j = 0; j < width; j++){
      n = i + j * leng;
      if(scanf("%lf ", &y[n]) == NULL)
y[n] = 0.0;
   } // j
} // i
TS_data_extra(y, dat, size); free(y);
/*********************************
// Computations of means and std
// G01AAF: means, std's
// Box-counting, then
//   G02CAF: y = a + bx
*********************************/
/*** results of the whole *******/
wt = malloc(size * size_d); /* A MUST! */
n = size; iwt = 0; ifail = 1;
g01aaf_(&n, dat, &iwt, wt, &xmean, &s2, &s3,
&s4, &xmin, &xmax, &wtsum, &ifail);
TS_brown_box_counting(dat, size, s2,
result); // b = result[5]
free(wt);
/**** results for each profile ******/
x  = malloc(new_leng*size_d); /* MUST! */
wt= malloc(new_leng*size_d); /* MUST! */
for(i = 0; i < width; i++){
   for(j = 0; j < new_leng; j++){
      x[j] = dat[i*leng + j]; // skipping!
   } /* j */
   n = new_leng; iwt = 0;  ifail = 1;
   g01aaf_(&n, x, &iwt, wt, &xmean, &s2, &s3,
&s4, &xmin, &xmax, &wtsum, &ifail);
   TS_brown_box_counting(x, new_leng, s2,
result);
   if(i != 0) // skipping first line
   printf("%3d %5d %.3f %.3f %.3f\n",
(int)log2(new_leng), new_leng, xmean, s2,
result[5]);
} /* i */
free(x); free(wt); free(dat);
} // main
```

Appendix F

Programme Listing of Statistical Methods

The computer programmes for conducting statistical tests are listed below.[1] First of all, the data are organised by a pre-test programme that produces compatible format of output for tests. All the statistical tools used in the thesis are included in the last programme which generates the test results and comparative data, i.e., random numbers and normal scores. The results are stored in a text file. the camparative data can be piped to, as it is conventionally called in Unix, other devices such as "gnuplot".
Example scripts are given here to illustrate how these programmes are linked. In Chapter Four, one of the tests is performed by the script "*pretest p_jh.fd tw1.fd 27 84 83 4 4 4 4 | tstats c 27 27 > wave_test_raw.txt*". In Chapter Five, an example script is like "*pretest spdem_fd.dat syn28n_fd_h.dat 1024 175 0 5 4 2 4 | tstats c 1024 1024 > dem_test_raw_all.txt*". Whereas in Chapter Six, it is like "*pretest fernredh.dat ferngrnh.dat 1024 70 70 4 4 4 4 | tstats c 1024 1024 > fern_test_raw_c.txt*". They differ mainly in the setting of parameters.

F.1 Pretest

The following C programme is compiled by C compiler on SunOS (4.1.3_U1), using the script "*acc $1.c -o $1 -lm -xCC -w*".

```
/* PRETEST.C
Syntax: pretest hdr1 hdr2 row col target
file1 file2
Dec:    organise data for <tstats>
Input:  file1, files
Output: (stdout) 2 col x row_no
hdr_no: Waves = 83; DEM = ;
*/
#include <stdio.h>
#include <stdlib.h>
#include <math.h>
/*******************************
************ main *************
*******************************/
main(int argc, char **argv)
{
FILE   *fin1,*fin2;
int
row,hdr1,hdr2,col1,col2,target1,target2;
int    i,j;
int    d_size=sizeof(double);
double tmpx,tmpy;
double *x,*y;
if(argc < 2){
   printf("Syntax: %s file1 file2 row hdr1
hdr2 col1 col2 target1 target2\n",argv[0]);
   printf("\tfile*:input files\n");
   printf("\trow:rows\n");
   printf("\thdr*:number of header in
rows\n");
   printf("\tcol*: cols\n");
   printf("\ttarget*: target col\n");
   exit(-1);
} // warning
/*** open input files ***/
if((fin1=fopen(argv[1],"rt")) == NULL){
   printf("# Can't open input file 1:
%s\n",argv[1]);
   exit(0);
} // open file1
if((fin2=fopen(argv[2],"rt")) == NULL){
   printf("# Can't open input file 2:
%s\n",argv[2]);
   exit(0);
} // open file2
/*** read in para's ***/
row    = atoi(argv[3]);
hdr1   = atoi(argv[4]);
hdr2   = atoi(argv[5]);
col1   = atoi(argv[6]);
col2   = atoi(argv[7]);
```

[1] Refer to Section 3.3.

```
target1 = atoi(argv[8]);
target2 = atoi(argv[9]);
/*** extract target col ***/
x = malloc(row * d_size);
y = malloc(row * d_size);
fseek(fin1,hdr1,SEEK_SET);
fseek(fin2,hdr2,SEEK_SET);
for(i=0;i<row;i++){
   for(j=1;j<=col1;j++){
      fscanf(fin1,"%lf ",&tmpx);
      if(j==target1){x[i]=tmpx;}
   } // j
   for(j=1;j<=col2;j++){
      fscanf(fin2,"%lf ",&tmpy);
      if(j==target2){y[i]=tmpy;}
   } // j
} // i
fclose(fin1); fclose(fin2);
for(i=0;i<row;i++){
   printf("%8.3f %8.3f\n",x[i],y[i]);
} free(x); free(y);
} // main
```

F.2 Statistical Tools

The following script is used to compile C programme incoporating NAG FORTRAN library routines (Hann & Hounam, 1991), whose resulting object programme is further compiled by FORTRAN compiler; that is, "*acc -c -lm $1.c* and *f77 $1.o -o $1 -lnag*".

```
/* TSTATS.C
Syntax: tstats c/r col row
Desc:   statistical tests
NB1:    Pre-process: <pretest>
*/
#include <stdio.h>
#include <stdlib.h>
#include <math.h>
#include <nagmk15.h> // NAGF lib.
#define VAL_ON (1)
#define VAL_OFF (0)
#define CLEVEL (0.95)
/*********************************
**************** main *************
*********************************/
void main (int argc, char **argv)
{
char    ch; // choice btw R/C
int     i,j; // loop indicators
int     leng,leng1; // data length
int     d_size=sizeof(double);
double  *x,*y,*xy;
/*** nagf var. ***/
int     ntype,ifail;
double  d,z,p,*sx,*sy; // dist.t
int     calwts;
double  *a,wx,pwx,wy,pwy; // norm.t
int     iwt; // stats
double  *wt,xmean,ymean,xstd,
ystd,xs3,ys3,xs4,ys4,
xmin,ymin,xmax,ymax,wtsum;
char    *tail,*equal;
double  clevel,t,df,prob,dl,du; // mean.t
double  *pp; // normal scores
double  xme,xmd,xsd,yme,ymd,ysd;
int     n,i1,i2;
double  *tmpx,*tmpw,tmpp; // median test
int     ties;
double  u,unor,up0,*ranks,*wrk; // MW.t
if(argc < 2){
   printf("Syntax:  %s R/C
leng\n",argv[0]);
   printf("\tR/C:   row/column type of
stdin\n");
   printf("\tleng:  row no./no. of first
data\n");
   printf("\tleng1: row no./total no. of
data\n");
   printf("\t");
   exit(-1);
} // warning
ch   = argv[1][0]; /* read in para's */
leng  = atoi(argv[2]);
leng1 = atoi(argv[3]);
switch(ch){ /* read in data from stdin */
   case 'c':
   case 'C':
      x = malloc(d_size * leng);
      y = malloc(d_size * leng);
      for(i=0;i<leng;i++){
        scanf("%lf %lf\n",&x[i],&y[i]);
      } break;
   case 'r':
   case 'R':
      x = malloc(d_size * leng);
      y = malloc(d_size * leng);
      xy = malloc(leng1 * d_size);
      for(i=0;i<leng1;i++){
        scanf("%lf ",&xy[i]);
      }
      for(i=0;i<leng;i++){
        x[i]=xy[i]; y[i]=xy[i+leng];
      } free(xy); break;
   default: break;
} // ch
/*** distribution test: F(x) = G(x) ***/
sx    = malloc(d_size * leng);
sy    = malloc(d_size * leng);
ntype = VAL_ON; ifail = VAL_OFF;
g08cdf_(&leng,x,&leng,y,&ntype,&d,&z,&p,
```

```
sx,sy,&ifail);
if(ifail == VAL_OFF){;
} else {printf("# check ifail of
g08cdf\n");}
/*** Normality test; sorted first ***/
printf("#\n# Normality test:  W-value
Sig.Level\n");
a      = malloc(d_size * leng);
ifail  = VAL_OFF; calwts = VAL_ON;
g01ddf_(sx,&leng,&calwts,a,
&wx,&pwx,&ifail);
if(ifail == VAL_OFF){ printf("# Real
Sample (X): %.3f %f\n",wx,pwx);}
else { printf("# Check g01ddf for real
sample\n"); }
ifail  = VAL_OFF; calwts = VAL_OFF;
g01ddf_(sy,&leng,&calwts,a,
&wy,&pwy,&ifail);
free(a);
if(ifail == VAL_OFF){ printf("# Syn.
Sample (Y): %.3f %f\n",wy,pwy);}
else { printf("# Check g01ddf for synthetic
sample\n"); }
/*** basic stats ***/
printf("#\n# Basic stats: mean std skew
kurt min max N\n");
wt  = malloc(d_size * leng);
iwt = VAL_OFF; ifail= VAL_OFF;
g01aaf_(&leng,x,&iwt,wt,
&xmean,&xstd,&xs3,&xs4,
&xmin,&xmax,&wtsum,&ifail);
if(ifail == VAL_OFF){ printf("# Sample X:
%6.3f %6.3f %6.3f %6.3f %6.3f %6.3f
%6d\n", xmean, xstd, xs3, xs4, xmin,
xmax, leng);}
else {printf("# Check g01aaf for X\n");}
iwt = VAL_OFF; ifail = VAL_OFF;
g01aaf_(&leng,y,&iwt,wt,&
ymean,&ystd,&ys3,&ys4,
&ymin,&ymax,&wtsum,&ifail);
if(ifail == VAL_OFF){ printf("# Sample Y:
%6.3f %6.3f %6.3f %6.3f %6.3f %6.3f
%6d\n", ymean, ystd, ys3, ys4, ymin,
ymax, leng); }
else {printf("# Check g01aaf for Y\n");}
free(wt);
/*** obtain medians ***/
ifail = VAL_OFF;
g07daf_(&leng,x,sx,&xme,&xmd,&xsd,&ifail);
if(ifail != VAL_OFF){printf("# Check
g07daf for X\n");}
ifail = VAL_OFF;
g07daf_(&leng,y,sy,&yme,&ymd,&ysd,&ifail);
if(ifail != VAL_OFF){printf("# Check
g07daf for Y\n");}
/*** t-test: Ux = Uy ***/
tail  = "T"; // two tail: HO: Ux = Uy
equal = "E"; // pop. var.: Un/Equal?
clevel = CLEVEL; ifail = VAL_OFF;
g07caf_(tail,equal,&leng,&leng,&xmean,
&ymean,&xstd,&ystd,&clevel,
&t,&df,&prob,&dl,&du, &ifail,leng,leng);
if(ifail == VAL_OFF){
   printf("#\n# t-test at %.2f level: t-value
df sig.level/L.conf. U.conf. Eq? Tail\n",
clevel);
   printf("# Ux ?= Uy %6.3f %6.0f %f %6.3f
%6.3f %s %s\n", t, df, prob, dl, du, equal,
tail);
} else {printf("# Check g07caf \n");}
/*** Median test: 2 smaples ***/
n = leng + leng; ifail = VAL_OFF;
tmpx = malloc(n * d_size);
tmpw = malloc(n * d_size);
for(i=0;i<leng;i++){
   tmpx[i]      = x[i];
   tmpx[i+leng] = y[i];
} // i
g08acf_(tmpx,&n,&leng,tmpw,&i1,&i2,
&tmpp,&ifail);
free(tmpx);free(tmpw);
if(ifail == VAL_OFF){ printf("#\n# Median
test: %d < MeX = %6.3f; %d < MeY =
%6.3f; sig.level = %f\n", i1, xme, i2, yme,
tmpp); }
else {printf("# Check g08acf \n");}
/*** Mann-Whitney test ***/
tail = "T"; ifail = VAL_OFF;
ranks = malloc((leng + leng) * d_size);
wrk   = malloc((leng + leng) * d_size);
g08ahf_(&leng,x,&leng,y,tail,&u,&unor,&up0,
&ties,ranks,wrk,&ifail,leng);
ifail= VAL_OFF;
if(ifail == VAL_OFF){
   printf("#\n# Man-Whitney test: U-value
Z-stats appr.P\n");
   printf("# %10.2f %6.3f %f\n",
u,unor,up0);
} else { printf("# Check g08ahf \n"); }
free(ranks); free(wrk); free(x); free(y);
/*** Normal scores ***/
pp= malloc(leng * d_size); ifail = VAL_OFF;
g01dbf_(&leng,pp,&ifail);
if(ifail != VAL_OFF){printf("# Check
g01dbf \n");}
printf("#\n# Normal.scores X.data Y.data
-> normal prob. plot\n");
for(i=0;i<leng;i++) { printf("\t%8.3f %8.3f
%8.3f\n",pp[i],sx[i],sy[i]); }
free(pp); free(sx); free(sy);
} // main
```

F.3 Histogram

The following script is used to compile C programme incoporating NAG FORTRAN library routines (Hann & Hounam, 1991), whose resulting object programme is further compiled by FORTRAN compiler; that is, "*acc -c -lm $1.c* and *f77 $1.o -o $1 -lnag*".

```
/*
// freq.c
// Usage: freq lhdr col row target noc
// Desc: frequency table by noc classes
// In: (stdin) including header
// Out: (stdout)
//      min class freq -> class max freq
*/
#include <stdio.h>
#include <stdlib.h>
#include <math.h>
#include <nagmk15.h> // NAGF lib.
#define HDR_WIDTH (256)
#define AUTO_BOUND (0) // auto
boundaries
#define G01PARA (1)
#define FDMIN (1.0)
#define FDMAX (1.6)

/*****************************
******* main() ***************
*****************************/
void main(int argc, char **argv)
{
char hdr[HDR_WIDTH];
int i, j, lhdr, col, row, target, count;
int size_d=sizeof(double),
size_i=sizeof(int);
double tmp;
/***** g01aef para ******/
int noc, iclass, ifail, n, nprob, *jfreq;
double *A, *C, xmin, xmax;
/***** warning msg *********/
if(argc < 2){
printf("Usage: %s lhdr col row target noc
\n", argv[0]);
printf("\tlhdr col row targt\n");
printf("\tnoc: number of classes\n");
printf("\tAuto generated boundaries
according to noc.\n");
exit(-1);
}
/***** get para *****/
lhdr   = atoi(argv[1]);
col    = atoi(argv[2]);
row    = atoi(argv[3]);
target = atoi(argv[4]);
noc    = atoi(argv[5]);
A = malloc((n+1) * size_d);
C = malloc(noc * size_d);
jfreq = malloc((noc+1) * size_i);
for(i=0; i<=n; i++){A[i]=0.0;}
/***** skip hdr *****/
for(i=0; i<lhdr; i++){ // skip hdr lines
gets(hdr);
} // i
/**** read in data *****/
target--;
count = 0;
for(i=0; i<row; i++){
for(j=0; j<col; j++){
scanf("%lf ", &tmp);
if(j==target) {
if(tmp <= FDMIN) { A[count++]=FDMIN; }
else if(tmp>=FDMAX) {
A[count++]=FDMAX; }
else { A[count++] = tmp; }
} // if
} // j
} // i
// for(i=0;i<=n;i++){printf("%6.3f \n",
A[i]);}
n = row; ifail = G01PARA;
nprob=G01PARA;
iclass = AUTO_BOUND;
g01aef_(&n,&noc,A,&iclass,C,jfreq,
&xmin,&xmax,&ifail);
/******* output *********/
printf("#  no    low  upper freq\n");
noc--;
for(i=0;i<=noc;i++){
if(i==0) {
printf("%5d %6.3f %6.3f %4d", i+1, xmin,
C[i], jfreq[i]);
} else if (i==noc) {
printf("%5d %6.3f %6.3f %4d", i+1, C[i-1],
xmax, jfreq[i]);
} else { printf("%5d %6.3f %6.3f %4d",
i+1, C[i-1], C[i], jfreq[i]); }
printf("\n");
} // i
free(A); free(C); free(jfreq);
} // main
```

Appendix G

An Introduction to Devonshire

The name of Devon is derived ultimately from a Celtic tribal name–"the people of the land," dating from the earliest days of the shire in the ninth century (Hoskins, 1954).[1] The people of the land living north of Port Isaac and Teignmouth will witness a near total solar eclipse in the twentieth century, for two minutes six seconds at around 11.11 am on August 11th, 1999 (Gibbs, 1998). Although "nature denied [Teignmouth] a deep water harbour" (Norway, 1898, p.64), Dartmouth, Dawlish and Teignmouth were much engaged in pilchard fishery from the seventeenth century until the early nineteenth century (Hoskins, 1954, p.213).

The chances of rain in Devon depend on altitude and exposure to the westerly winds. Thus, Plymouth has about 40 inches (around 1000 mm) of rain a year and the high moorland village of Princetown 82 inches (2082 mm), but Exeter, sheltered partly from the rain by the mass of Dartmoor, has only 30 inches (750 mm) (Knapp, 1984).

The mean annual temperature inland is 50.5 degrees Fahrenheit and 51.5 degrees

[1] Refer to page 109.

on the coast, and the mean annual temperature for January at sea level is 42 to 44 degrees (Hoskins, 1954). Because of the fairly mild weather, it was reported, as early as 1759, that "the air [is] very wholesome here [in Teignmouth] especially in summer" (Travis, 1993, p.10). In 1817 one local guidebook (Travis, 1993, p.61) declared that "invalids will not find more real benefit than in the healthy town of Teignmouth, the enclosed vale of Dawlish, or the warmer region of Torquay." Teignmouth was a fashionable seaside resort in the late eighteenth century–early nineteenth century (Hoskins, 1954, p.492), and has remained so until now.

The geology around Teignmouth mainly consists of Permian sandstones and Breccia, see Figure 4 of Hoskins (1954, p.17).

Appendix H

Programme Listing of Synthetic Waves

The following C programme is compiled by C compiler on SunOS (4.1.3_U1), using the script "*acc $1.c -o $1 -lm -xCC -w*".[1] One example use is such that "*synwave 27 2048 2 4 2.0 > synwave.d*", which generates a synthetic wave, stored as 27 columns and 2048 rows in file *synwave.d*, with sampling rate of 2 Hz, four compound waves and an offset of two metres.

```
/* synwave.c
// Syn: synwave out_cols leng Hz wave_no
wave_offset
*/
#include <stdio.h>
#include <stdlib.h>
#include <math.h>
#define MAX_PTS  5000
#define MAX_WAVE 4
#define PI 3.14159
/*********************************
************* main *************
*********************************/
void main(int argc, char **argv)
{
int    i,j,k,tmp;
int    out_cols, leng, Hz, wave_no;
double wave_offset;
double
omega[MAX_WAVE],plag[MAX_WAVE];
double val,new_T,sample_ratio;
double wave_T[MAX_WAVE] =
{10.0,11.0,21.0,27648};
double wave_Lag[MAX_WAVE] =
{0,5.0,10,20736};
double wave_A[MAX_WAVE] =
{1.0,0.5,0.25,2.0};
/******* Warning *********/
if(argc < 2){
   printf("Usage:%s out_cols leng in_col lag
out_cols\n", argv[0]);
   printf("\tout_cols:out_cols of stdout\n");
   printf("\tleng:length of stdout
(55296)\n");
   printf("\tHz:sampling rate
(Hz=2)-->T=leng/Hz\n");
   printf("\twave_no: wave numbers
(4)\n");
   printf("\toffset: tide offset (double)\n");
   exit(-1);
} // if
out_cols = atoi(argv[1]);
leng     = atoi(argv[2]);
Hz       = atoi(argv[3]);
wave_no  = atoi(argv[4]);
wave_offset = atof(argv[5]);
/******* trasform parameters *********/
new_T = (out_cols*leng)/(double)Hz;
wave_T[MAX_WAVE-1] = new_T;
wave_Lag[MAX_WAVE-1] = new_T*3/4;
for(i=0;i<MAX_WAVE;i++){
   omega[i] = 2*PI/wave_T[i];
   plag[i] = 2*PI*wave_Lag[i]/wave_T[i];
} // if
/****** calculation & output ********/
for(i=0;i<leng;i++){
   for(j=0;j<out_cols;j++){
      tmp = i+j*leng;
      val = 0.0;
      sample_ratio = tmp/(double)Hz;
      for(k=0;k<wave_no;k++){
         val += wave_A[k]*sin(sample_ratio *
omega[k] + plag[k]);
      } // i
      val += wave_offset;
      printf("%.3f ", val);
   } // j
   printf("\n");
} // i
} // main
```

[1] Refer to Section 4.3.1.

Appendix I

Programme Listing of Time Series Analyses

The following C programmes are compiled on SunOS (4.1.3_U1) either by using the script "*acc $1.c -o $1 -lm -xCC -w*" if it contains no NAG routines, or by "*acc $1.c -c -lm -w -xCC*" and "*f77 $1.o -o $1 -lnag*" if it includes NAG library routines.[1] Some FORTRAN programmes are compiled using "*f77 $1.f -o $1 -lm -lnag*".

I.1 Qualitative Method

One of the typiccal qualitative approaches to a time series is the reconstruction of phase portraits. Here are the reconstruction methods.

Methods of Delay

Example: *cat wave.dat | opdelay 27 2048 1 200 synop.dat*

```
/* opdelay.C
// Syn:  opdelay col leng col
// Desc: Optimal Delay Time algorithms
//       Read in data
//      log of Fill of Volme of Matrix of
Displacements
// Out:  [f_E(t), t/T, dim] i.e., ||:
t/T, f_E :||
*/
#include <stdio.h>
#include <stdlib.h>
#include <math.h>
#include <nagmk15.h>/* NAGF libraries
*/
#define HDR 55
#define MU 0.0001
#define DIM 9 /* Embedding dimensions */
#define M2CM 1.0 /* meter to cm */
#define NV 0.1 /* nv = % of total */
#define CONST (0.5) // tau=0.5 T_c
int RM[DIM+1]  /* reference points */
/*** data_correction **********/
// X_i = 2*X_{i-1} - X_{i-2}
*******************************/
void data_correction(
   int    n, /* length of array  */
   double x[], /* input  array */
   double y[] /* output array */
   )
{
int i;
for(i=0; i < n; i++){
   if(x[i] > MU) { y[i] = M2CM*x[i]; }
   else {
      y[i] = M2CM*(2*y[i-1] - y[i-2]);
      if( y[i] <= MU ) {  y[i] = y[i-1]; }
   }
} /* End of data_correction */
/**** get_det_f ************/
double get_det_f(
   int    dim, /* dim of array */
   double A[][] /* 2D array */
   )
{
int    ia, n,  ifail;
double det, *wkspce;
wkspce = malloc(2*dim*sizeof(double));
n = dim; ia = dim; ifail = 1;
f03aaf_(A, &ia, &n, &det, wkspce, &ifail);
free(wkspce);
return(fabs(det));
} /* get_det_f() */
/****** get_matrix_f  ******/
double get_matrix_f(
   int    dim,
   double diff,
   double dat_in[],
   int    leng, /* length of data */
   int    tau,/* value of tau */
   int    nv /* j-th point */
```

[1] Refer to Section 4.4.1.

```
   )
{
int    j, d, t, rm0, tmp;
double sum = 0.0, space_vol, f_val;
double *A;
double B[3][3] = {{33, 16,
72},{-24,-10,-57}, {-8,-4,-17}};
space_vol = pow(diff, (double)dim);
tmp = leng - tau * (dim - 1);
A = (double *) malloc(dim * dim *
sizeof(double));
for(j = 1; j <= nv; j++){
   rm0 = RM[0] * j;
   for(d = 0; d < dim; d++){
      for(t = 0; t < dim; t++){
         A[d*dim+t] = dat_in[(rm0 +
t*tau)%tmp] - dat_in[(RM[d] +
t*tau)%tmp];
      } /* for: t*/
   } /* for: d */
   sum += get_det_f(dim, A);
} /* j */
f_val = log( (sum / (double) nv ) /
space_vol);
if(f_val < -10000.0) f_val = -100.0;
free(A);
return(f_val);
} /* get_matrix_f */
/**** fill_f *******/
void fill_f(
   int    dim,
   double diff,
   double dat_in[], /* input data */
   int    n, /* length of data: nv */
   double dat_out[],/* log of Fill */
   int    tau /* TAU */
   )
{
int    t, nv;
double val;
nv = (int)n * NV; /* large no: 2
percents of N */
for(t = 1; t <= tau; t++){
   dat_out[t-1] = get_matrix_f(dim, diff,
dat_in, n, t, nv );
} /*  t */
} /* fill_f */
/**********************************
********** main ******************
**********************************/
void main(int argc, char **argv)
{
FILE *fout;
int  type_label, col_no, col_leng, tau, start,
nv;
char hdr[HDR];
int  i,j,k;
int  total_leng,  width, leng_step,
scale_step;
int  tmp_scale, tmp_width, tmp_step,
tmp_s;
double *tmp, *data;
double *f_dim,f_result[DIM+1][500],val;
int  iwt,ifail;
double *wt,
xmean,s2,s3,s4,xmin,xmax,wtsum;
double diff;
/********** warning *********/
if(argc < 2){
   printf("Usage:%s width col_leng col_no
tau\n",argv[0]);
   printf("\twidth: nimber of column\n");
   printf("\tcol_leng: length of column\n");
   printf("\tcol_no:which column is
used?\n");
   printf("\ttau(200): tau=0.5*T_c\n");
   exit(-1);
} // if
/******** Read in paras *********/
width= atoi(argv[1]);
col_leng= atoi(argv[2]);
col_no = atoi(argv[3]);
tau = atoi(argv[4]);
total_leng = col_leng;
/* RM[i]: i < S+N-tau/T_a * (E-1) */
/** locate memory for data[] ***/
RM[0] = 1;
tmp_s = total_leng - tau*(DIM-1);
for(i = 1; i <= DIM; i++){
   RM[i] = rand() % tmp_s;
}
data = malloc(total_leng*sizeof(double));
/**** Read in data from stdin *****/
tmp =  malloc(col_leng * sizeof(double));
col_no--;
k = 0;
for(i=0;i<col_leng;i++){
   data[i] = 0.0;// initialising
   for(j=0;j<width;j++){
      scanf("%lf ", &val);
      if(j == col_no){
         tmp[k] = val;
         k++;
      } // if
   } // j
} // i
/****** data correction *******/
data_correction(col_leng, tmp, data);
free(tmp);
/******* compute dims ********/
iwt = 0; ifail = 1;
wt = malloc(total_leng * sizeof(double));
g01aaf_(&total_leng, data, &iwt, wt,
&xmean, &s2, &s3, &s4, &xmin, &xmax,
```

```
&wtsum, &ifail);
diff = (xmax - xmin);
f_dim = malloc(tau * sizeof(double));
for(i = 1; i <= DIM; i++){
   fill_f(i, diff, data, total_leng, f_dim,
tau);
   for(j = 0; j < tau; j++){
      f_result[i][j]  = f_dim[j];
   } // j
} // i
free(f_dim); free(data);
/******** output **********/
if((fout = fopen(argv[5], "wt")) == NULL){
   printf("Can't open output file %s\n",
argv[5]);
   exit(1);
} /* if */
fprintf(fout, "# width %d  col_no %d
col_leng %d  tau %d  NV %.2f\n", width,
col_no, col_leng, tau, NV);
fprintf(fout, "# tau dim1 ...
dim%d\n",DIM);
for(j = 0; j < tau; j++){
   fprintf(fout, "%.3f ", (double)(j+1) /
(double)tau);
   for(i = 1; i <= DIM; i++){
      fprintf(fout, "%8.3f ", f_result[i][j]);
   } // i
   fprintf(fout, "\n");
} // j
} // main
```

Singular Value Decomposition (SVD)

There are two FORTRAN programmes to compute SVD. The first is to calculate the SVD values, and the second is to construct SVD vectors, which can be used to draw phase portraits.

Example: *cat wave.dat | lag4f77 27 2048 0 1 1 32 | svdval > svdval.dat* for calculating SVD values or *cat wave.dat | lag4f77 27 2048 0 1 1 32 | svdvec > svdvec.dat* for constructing SVD vectors, where *lag4f77* is the data organising programme (see below).

```
/* lag4f77.c
// Syntax: lag4f77 width leng hdr col
lag win_dim_
// Desc:  Prepare lagged vectors for f77
process
// Output: stdout
*/
#include <stdio.h>
#include <stdlib.h>

/*****************************
************* main **********
*****************************/
void main(int argc, char **argv)
{
char ch[];
int  i,j,k;
int  width,leng,hdr,col,lag,win_dim;
int  new_leng;
double *data,val;
/********* Warning *******/
if(argc < 2){
   printf("Usage:%s width leng col M N\n",
argv[0]);
   printf("\twidth: input width\n");
   printf("\tleng: input leng\n");
   printf("\thdr: length of header in
characters (0). One line at most.\n");
   printf("\tcol:selected col\n");
   printf("\tlag: lag\n");
   printf("\twin_dim: window dimension
(col)\n");
   exit(-1);
} // if
/* Read in paras from stdin */
width = atoi(argv[1]);
leng = atoi(argv[2]);
hdr = atoi(argv[3]);
col = atoi(argv[4]);
lag = atoi(argv[5]);
win_dim = atoi(argv[6]);
/******* Read in data ***/
if(hdr == 0){;}
else {scanf("%s\n",ch);} // skip header
data = malloc(leng * sizeof(double));
k = 0; col--;
for(i=0;i<leng;i++){
   for(j=0;j<width;j++){
   scanf("%lf ", &val);
      if(j == col){
         data[k] = val; k++;
      } // if
   } // j
} // i
/***** output ******/
new_leng = leng / lag - win_dim;
printf(" %d  %d\n", new_leng, win_dim);
// M, N in f77
for(i=0;i<new_leng;i++){
   for(j=0;j<win_dim;j++){
      printf("%.3f ", data[(i+j)*lag]);
   } // j
   printf("\n");
} // i
free(data);
} // main
```

The Computation of SVD Values

```
*       SVDVAL.F
*       WANTQ .FALSE. FOR L-H SV
*       WANTP .FALSE. FOR R-H SV
*            LWORK=N^2+5(N-1)
*            LDPT >= max(1,N)
* NCOLB = 0: Array B is not referenced
*
*       ... PARAMETERS .....
        INTEGER  NIN,NOUT
        PARAMETER  (NIN=5,NOUT=6)
        INTEGER  MMAX,NMAX
        PARAMETER  (MMAX=55296,
NMAX=512)
        INTEGER  LDA,LDQ,LDPT
        PARAMETER  (LDA=MMAX,
LDQ=MMAX, LDPT=NMAX)
        INTEGER  LWORK
        PARAMETER  (LWORK =
2*(NMAX-1))
*       ... LOCAL SCALARS ...
        INTEGER  I, IFAIL, J, M, N,
NCOLB
        LOGICAL  WANTP,WANTQ
*       ... LOCAL ARRAYS ....
        DOUBLE PRECISION
A(LDA,NMAX), DUMMY(1),
Q(LDQ,MMAX), SV(MMAX),
WORK(LWORK), PT(LDPT,NMAX)
*       ... EXTERNAL SUBROUTINE ...
        EXTERNAL  F02WEF
*... SKIPPING HEADER ...
*       READ  (NIN,*)
        READ  (NIN,*) M,N
        IF((M.GT.MMAX) .OR.
(N.GT.NMAX)) THEN
          WRITE (NOUT,*)'M OR N IS
OUT OF RANGE.'
          WRITE (NOUT,99999)'M = ',
M, '     N = ',N
        ELSE
          READ  (NIN,*)(
(A(I,J),J=1,N), I=1,M)
*       ... FIND SVD OF A ...
          WANTQ = .FALSE.
          WANTP = .FALSE.
          NCOLB = 0
          IFAIL = 0
          CALL F02WEF(M, N, A, LDA,
NCOLB, DUMMY, 1, WANTQ, Q, LDQ,
SV, WANTP, PT, LDPT, WORK, IFAIL)
*       ... OUTPUT ...
          WRITE (NOUT,99997)'#
SINGULAR VALUE (SV), log(SV)'
          WRITE (NOUT,99998)
(SV(I),LOG(SV(I)),I=1,N)
        ENDIF
        STOP
99999FORMAT (1X,A,I5,A,I5)
99998 FORMAT (2F10.4)
99997 FORMAT (A)
      END
```

The Construction of SVD Vectors

```
*       SVDVEC.F
*       WANTQ .TRUE. FOR L-H SV
*       WANTP .TRUE. FOR R-H SV
*            LWORK=N^2+5(N-1)
*            LDPT >= max(1,N)
* NCOLB = 0: Array B is not referenced
*
*       ... PARAMETERS .....
        INTEGER  NIN,NOUT
        PARAMETER  (NIN=5,NOUT=6)
        INTEGER  MMAX,NMAX
        PARAMETER  (MMAX=55296,
NMAX=64)
        INTEGER  LDA,LDQ,LDPT
        PARAMETER  (LDA=MMAX,
LDQ=MMAX, LDPT=NMAX)
        INTEGER  LWORK
        PARAMETER  (LWORK =
2*(NMAX-1))
*       ... LOCAL SCALARS ...
        INTEGER  I, IFAIL, J, M, N,
NCOLB
        LOGICAL  WANTP,WANTQ
*       ... LOCAL ARRAYS ....
        DOUBLE PRECISION
A(LDA,NMAX), DUMMY(1),
Q(LDQ,MMAX), SV(MMAX),
WORK(LWORK), PT(LDPT,NMAX)
*       ... EXTERNAL SUBROUTINE ...
        EXTERNAL  F02WEF
*       ... SKIPPING HEADER ...
*       READ  (NIN,*)
        READ  (NIN,*) M,N
        IF((M.GT.MMAX) .OR.
(N.GT.NMAX)) THEN
          WRITE (NOUT,*)'M OR N IS
OUT OF RANGE.'
          WRITE (NOUT,99999)'M = ',
M, '     N = ',N
        ELSE
          READ  (NIN,*) (
(A(I,J),J=1,N), I=1,M)
*       ... FIND SVD OF A ...
          WANTQ = .TRUE.
```

```
      WANTP = .FALSE.
      NCOLB = 0
      IFAIL = 0
      CALL F02WEF(M, N, A, LDA,
NCOLB, DUMMY, 1, WANTQ, Q, LDQ,
SV, WANTP, PT, LDPT, WORK, IFAIL)
*          ... OUTPUT ...
      WRITE (NOUT,99997)'# R-H
SINGULAR VALUE VECTOR, BY COLUMN'
      IF(M.GT.(MMAX/2)) THEN
         DO 10 I = 1, M/5
            WRITE (NOUT,99996)
(A(I,J),J=1,NIN)
   10       CONTINUE
      ELSE
         DO 20 I = 1, M
            WRITE (NOUT,99996)
(A(I,J),J=1,NIN)
   20       CONTINUE
      ENDIF
    ENDIF
    STOP
99999FORMAT (1X,A,I5,A,I5)
99998 FORMAT (3F10.4)
99997 FORMAT (A)
99996 FORMAT (5(1X,F10.4))
    END
```

Poincaré Sectioning

Example: *cat waveall.dat | phase 2 55296 2 22 3 > synlag22.dat*, where *waveall.dat* contains the wave data in *time-height* pairs.

```
/* phase.c
// Syn:  phase width leng in_col lag
out_cols
// Desc:Organise data into columns with
lagged time.
// Input: stdin;  width * leng
// Output: stdout
*/
#include <stdio.h>
#include <stdlib.h>
#include <math.h>
#include <TS.h>
#define MAXPTS 3000
/************************
******** main ***********
************************/
void main(int argc, char **argv)
{
int  i,j,k;
int  width, leng, in_col, lag, out_cols;
int  new_leng,out_leng;
double val, *data,*dout;
/***** Warning ***********/
if(argc < 2){
   printf("Usage:%s width leng in_col lag
out_cols\n", argv[0]);
   printf("\twidth: number of cols from
stdin\n");
   printf("\tleng: length of col from
stdin\n");
   printf("\tin_col: col to be processed\n");
   printf("\tlag: lagged time (refer to results
from opdelay.c)\n");
   printf("\tout_cols: number of column in
stdout\n");
   exit(-1);
} // if
/****** Read paras ***********/
width  = atoi(argv[1]);
leng   = atoi(argv[2]);
in_col = atoi(argv[3]);
lag    = atoi(argv[4]);
out_cols = atoi(argv[5]);
/***** Read in data from stdin ***/
out_leng= leng / lag - out_cols;
if(out_leng >= MAXPTS){
   out_leng=MAXPTS;
   new_leng=lag*out_leng;
}
else{
   new_leng=lag*out_leng;
}
data= malloc(new_leng * sizeof(double));
k  = 0; in_col--;
for(i=0;i<leng;i++){
   for(j=0;j<width;j++){
      scanf("%lf", &val);
      if(i<new_leng && j == in_col){
         data[k] = val; k++;
      } // if
   } // j
} // i
/***** data correction ***********/
dout = malloc(new_leng * sizeof(double));
TS_data_extra(data,dout,new_leng);
free(data);
/****** Output to stdout **************/
printf("# leng %d lag %d out_points
%d\n",leng, lag, out_leng);
k  = 0;
for(i=0;i<out_leng;i++){
   for(j=0;j<out_cols;j++){
      printf("%10.3f", dout[j*lag + k] );
   } // j
   printf("\n"); k += lag;
} // i
free(dout);
} // main
```

I.2 Quantitative Methods

One of the typical quantitative analyses of a time series is the spectral analysis. It consists of auto-correlation coefficient functions and power spectra.

Auto-correlation Functions

Example: *pickwavedat 2 55296 2 0 waveall.dat | autocorr 2 55296 > waveautocorr.dat*
The programe below, *pickwavedat*, is used to pre-organise the wave data.

```
/* pickwavedata.c
// Usage: pickwavedata width lengcol fin
//Input: b-band files
//Output: (stdio) chosen data from file
*/
#include <stdio.h>
#include <stdlib.h>
#define HDR 100
/*****************************
// Data correction algorithm
// X_i = 2*X_{i-1} - X_{i-2}
*****************************/
void data_correction(
      double x[], /* input  array */
      int n) /* length of array  */
{
   int i;
   for(i=0; i < n; i++){
      if(x[i] > 0.0){
         x[i] = x[i];
      } else {
         x[i] = 2*x[i-1] - x[i-2];
      }
   }
} /* data_correction */
/*****************************
******* main ***************
*****************************/
main(int argc, char **argv)
{
FILE *fin;
char ch[HDR];
int  i, j, n, k;
int  col, width, leng,hdr;
double *val, tmp;
if(argc < 2){
  printf("\nUsage: %s width leng col
fin...\n", argv[0]);
  printf("\t\twidth: no. of columns of an
individual file\n");
  printf("\t\tlength: no. of rows\n");
  printf("\t\tcol: the column to be extracted,
0 ~\n");
  printf("\t\thdr: header length\n");
  printf("\t\tin file.\n");
  exit(1);
} /* warning */
width = atoi(argv[1]);
leng = atoi(argv[2]);
col = atoi(argv[3]);
hdr = atoi(argv[4]);
val = malloc(leng * sizeof(double));
col = col - 1;
/***** Read in data ********/
fin = fopen(argv[5], "rt");
if(hdr <= 0) {;}
else { fgets(ch, HDR, fin);}
k = 0;
for(i = 0; i < leng; i++){
      for(j = 0; j < width; j++){
         fscanf(fin, "%lf ", &tmp);
         if(j == col) {
            val[k] = tmp;
            k += 1;
         }// pick the right col
      } // j
} // i
fclose(fin);
data_correction(val, leng);
for(i = 0; i < leng; i++){
   printf("%6d %6.3f\n", i+1, val[i]);
} // i
free(val);
} /* main */
```

ACC Main Programme

```
/* autocorr.c
// Syn:  autocorr col row
// Desc: Estmate auto.corr coef.
// Input: stdin
// Ouput: stdout
// NB: NAGF--g13abf_()
*/
#include <stdio.h>
#include <stdlib.h>
#include <math.h>
#include <nagmk15.h>
/*********************************
********* main() *****************
*********************************/
void main(int argc, char **argv)
{
```

```
int     i, j, n;
int     xcol, xrow, xsize;
int     size_d = sizeof(double);
double *xdat; // arary to hold data
int     nx, nk, ifail;
double *x, xm, xv, *r, stat;
/** Read stdin into a large array **/
if(argc < 2){
   printf("Usage: %s col row\n", argv[0]);
   printf("\tcol:number of columns\n");
   printf("\trow:number of rows\n");
   exit(-1);
} // warning
xcol= atoi(argv[1]);
xrow= atoi(argv[2]);
xsize= xcol * xrow;
xdat= malloc(xsize * size_d);
/*** read data int: row after row ***/
for(i = 0; i < xrow; i++){
   for(j = 0; j < xcol; j++){
      n = i + j * xrow;
      scanf("%lf ", &xdat[n]);
   } // j
} // i
/******* autocorr ************/
x  = malloc(xrow * size_d);
nx = xrow;
nk = xrow / 2;
r  = malloc(nk * size_d);
for(i = 0; i < xcol; i++){
   for(j = 0; j < xrow; j++){
      n    = i * xrow + j;
      x[j] = xdat[n];
} // row
   if(i != 0) {
     ifail = 0;
     g13abf_(x, &nx, &nk, &xm, &xv, r,
&stat, &ifail);
     printf("# mean %f varaince %f stat
%f\n", xm, xv);
     printf("# No.       R   log2R\n");
     for(n = 0; n < nk; n++){
     if(r[n] > 0.0) {
       printf("%5d %6.3f %6.3f\n", n+1,
r[n], log2(r[n]));
       } else if(r[n] == 0.0) {
       printf("%5d %6.3f 0.000\n", n+1,
r[n]);
       } else {
         printf("%5d %6.3f %6.3f\n", n+1,
r[n], log2( fabs(r[n]) ));
       } // else-if
     }// n
  } // if
}  // i: col
free(x); free(r); free(xdat);
} // main
```

Power Spectra

There are two programmes here. One is C programme which prepares the data and the other is F77 programme which calculates DPS.

Example: *cat wave.dat | predps 27 2048 0 1 | dps > dps.dat*

The programme below, *predps*, is used to pre-organize the data.

```
/* predps.c
// Syntax: predps width leng hdr col
// Desc:  Prepare lagged vectors for f77
process
// Output: stdout
*/
#include <stdio.h>
#include <stdlib.h>
#define  OUT_COL(16)
/************************
************ main *******
************************/
void main(int argc, char **argv)
{
char ch[];// header
int  i,j,k;
int  width,leng,hdr,col;
double *data,val;
/****** Warning ********/
if(argc < 2){
   printf("Usage:%s width leng col M N\n",
argv[0]);
   printf("\twidth: input width\n");
   printf("\tleng:  input leng\n");
   printf("\thdr: length of header in
characters (0). One line at most.\n");
   printf("\tcol: selected col\n");
   printf("\tnote: output in 16 cols\n");
   exit(-1);
} // if
/* Read in paras from stdin */
width= atoi(argv[1]);
leng = atoi(argv[2]);
hdr = atoi(argv[3]);
col = atoi(argv[4]);
/******* Read in data *********/
if(hdr == 0){;}
else {scanf("%s\n",ch);} // skip header
data = malloc(leng * sizeof(double));
k = 0; col--;
for(i=0;i<leng;i++){
   for(j=0;j<width;j++){
      scanf("%lf ", &val);
      if(j == col){
```

```
        data[k] = val; k++;
      } // if
    } // j
} // i
/******** output *******/
printf(" %d\n", leng); // M in f77
for(i=0;i<leng;i++){
   printf("%6.3f", data[i]);
   if( (i % OUT_COL)==(OUT_COL-1)) {
      printf("\n");
   }
} // i
printf("\n"); free(data);
} // main
```

DPS Main Programme

```
*     DPS.F
*     .. Parameters ..
      INTEGER MW0, MW1, NG,NX
      INTEGER KCMAX, NXMAX
      PARAMETER (KCMAX=221184,
NXMAX=KCMAX/2)
      INTEGER NIN, NOUT
      PARAMETER (NIN=5,NOUT=6)
*     .. Local Scalars ..
      DOUBLE PRECISION PW, PX
      INTEGER I, IFAIL, KC, L, LG0,
LG1, MTX0, MTX1, MTX2
*     .. Local Arrays ..
      DOUBLE PRECISION STATS(4),
XH(NXMAX)
*     XGabc: a: correction; b: un/smoothed;
*     c: un/log
      DOUBLE PRECISION
XG000(KCMAX), XG001(KCMAX)
      DOUBLE PRECISION
XG100(KCMAX), XG101(KCMAX)
      DOUBLE PRECISION
XG200(KCMAX), XG201(KCMAX)
      DOUBLE PRECISION
XG010(KCMAX), XG011(KCMAX)
      DOUBLE PRECISION
XG110(KCMAX), XG111(KCMAX)
      DOUBLE PRECISION
XG210(KCMAX), XG211(KCMAX)
*     .. External Subroutines ..
      EXTERNAL          G13CBF
*     .. Executable Statements ..
      READ (NIN,*) NX
      IF (NX.GT.0 .AND.
NX.LE.NXMAX) THEN
         READ (NIN,*) (XH(I), I=1,NX)
         MTX0 = 0
         MTX1 = 1
         MTX2 = 2
         PX = 0.2D0
         PW = 0.5D0
         MW0 = NX
         MW1 = NX/8
         KC = 4 * NX
         L = NX
         LG0 = 0
         LG1 = 1
*        .. READ DATA IN ..
         DO 40 I = 1, NX
            XG000(I) = XH(I)
            XG100(I) = XH(I)
            XG200(I) = XH(I)
            XG010(I) = XH(I)
            XG110(I) = XH(I)
            XG210(I) = XH(I)
            XG001(I) = XH(I)
            XG101(I) = XH(I)
            XG201(I) = XH(I)
            XG011(I) = XH(I)
            XG111(I) = XH(I)
            XG211(I) = XH(I)
   40    CONTINUE
* DO NOT USE WRITE (NOUT,*)
* which gives ' # 123...' on stdout
* THE LEADING SPACE IN ' # 123...'
* WILL CAUSE PROBLEMS TO gnuplot
*        .. MW0 = NX: un-smoothed ..
         WRITE (NOUT,99996) '#
UnLog/Corr(no, mean, trend)
Log/Corr(...)'
         WRITE (NOUT,99996) '#    DF
bandwidth lower upper ifail'
         WRITE (NOUT,99999) '# Not
smoothed: MW =', MW0
         IFAIL = 1
         CALL G13CBF(NX, MTX0, PX,
MW0, PW, L, KC, LG0, XG000, NG,
STATS, IFAIL)
         WRITE(NOUT,99998) '# ',
STATS(1), STATS(4), STATS(2), STATS(3),
IFAIL
         IFAIL = 1
         CALL G13CBF(NX, MTX1, PX,
MW0, PW, L, KC, LG0, XG100, NG,
STATS, IFAIL)
         WRITE(NOUT,99998) '# ',
STATS(1), STATS(4), STATS(2), STATS(3),
IFAIL
         IFAIL = 1
         CALL G13CBF(NX, MTX2, PX,
MW0, PW, L, KC, LG0, XG200, NG,
STATS, IFAIL)
         WRITE(NOUT,99998) '# ',
STATS(1), STATS(4), STATS(2), STATS(3),
IFAIL
```

```
      IFAIL = 1
      CALL G13CBF(NX, MTX0, PX,
MW0, PW, L, KC, LG1, XG001, NG,
STATS, IFAIL)
      WRITE(NOUT,99998) '# ',
STATS(1), STATS(4), STATS(2), STATS(3),
IFAIL
      IFAIL = 1
      CALL G13CBF(NX, MTX1, PX,
MW0, PW, L, KC, LG1, XG101, NG,
STATS, IFAIL)
      WRITE(NOUT,99998) '# ',
STATS(1), STATS(4), STATS(2), STATS(3),
IFAIL
      IFAIL = 1
      CALL G13CBF(NX, MTX2, PX,
MW0, PW, L, KC, LG1, XG201, NG,
STATS, IFAIL)
      WRITE(NOUT,99998) '# ',
STATS(1), STATS(4), STATS(2), STATS(3),
IFAIL
*
      WRITE (NOUT,99999) '#
Smoothed: window (freq.width) = /', MW1
     IFAIL = 1
      CALL G13CBF(NX, MTX0, PX,
MW1, PW, L, KC, LG0, XG010, NG,
STATS, IFAIL)
      WRITE(NOUT,99998) '# ',
STATS(1), STATS(4), STATS(2), STATS(3),
IFAIL
      IFAIL = 1
      CALL G13CBF(NX, MTX1, PX,
MW1, PW, L, KC, LG0, XG110, NG,
STATS, IFAIL)
      WRITE(NOUT,99998) '# ',
STATS(1), STATS(4), STATS(2), STATS(3),
IFAIL
      IFAIL = 1
      CALL G13CBF(NX, MTX2, PX,
MW1, PW, L, KC, LG0, XG210, NG,
STATS, IFAIL)
      WRITE(NOUT,99998) '# ',
STATS(1), STATS(4), STATS(2), STATS(3),
IFAIL
      IFAIL = 1
      CALL G13CBF(NX, MTX0, PX,
MW1, PW, L, KC, LG1, XG011, NG,
STATS, IFAIL)
      WRITE(NOUT,99998) '# ',
STATS(1), STATS(4), STATS(2), STATS(3),
IFAIL
      IFAIL = 1
      CALL G13CBF(NX, MTX1, PX,
MW1, PW, L, KC, LG1, XG111, NG,
STATS, IFAIL)
      WRITE(NOUT,99998) '# ',
STATS(1), STATS(4), STATS(2), STATS(3),
IFAIL
      IFAIL = 1
      CALL G13CBF(NX, MTX2, PX,
MW1, PW, L, KC, LG1, XG211, NG,
STATS, IFAIL)
      WRITE(NOUT,99998) '# ',
STATS(1), STATS(4), STATS(2), STATS(3),
IFAIL
*
      WRITE (NOUT,99996) '# No.
Corr(raw mean trend) SmCorr(ibid)
LogCorr(ibid) LogSmCorr(ibid)'
      WRITE(NOUT,99997)
     +  (I, XG000(I), XG100(I),
XG200(I),
     +  XG010(I), XG110(I), XG210(I),
     +  XG001(I), XG101(I), XG201(I),
     +  XG011(I), XG111(I), XG211(I),
I=1, NG-1)
    END IF
  60 STOP
*
99999 FORMAT (A,I)
99998 FORMAT (A,F5.1,3F8.4,I2)
99997 FORMAT (I5,12F10.3)
99996 FORMAT (A)
    END
```

Appendix J

Attractors Reconstructed from Some Singular Vectors

A Synthetic Wave

A Natural Wave

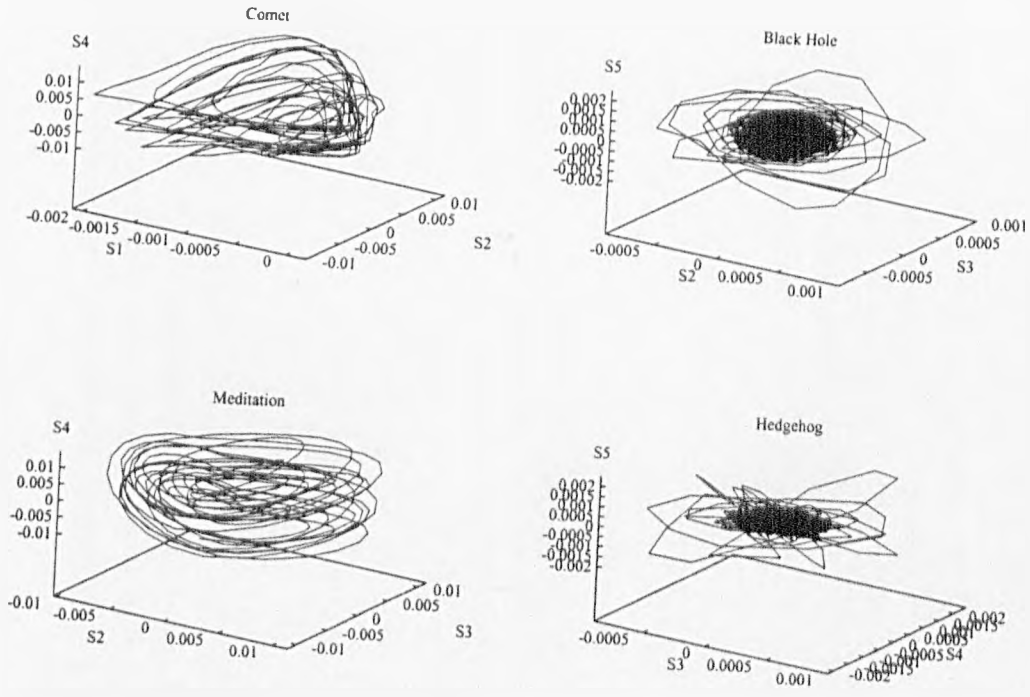

Appendix K

Comparisons of Regression Lines

		R1	R2	R3	R4	R5	R6	R7	R8	R9	R10	R11	R12	R13	R14	R15	R16	R17	R18	R19	R20	R21	R22	R23	R24	R25	R26	R27
	SE	.023	.019	.037	.041	.040	.041	.043	.040	.041	.042	.040	.044	.044	.046	.044	.046	.044	.045	.044	.044	.045	.044	.044	.046	.046	.037	.031
R1	.023	.00																										
R2	.019	.13	.00																									
R3	.037	.32	.43	.00																								
R4	.041	.38	.49	.07	.00																							
R5	.040	.37	.47	.06	.02	.00																						
R6	.041	.38	.49	.07	.00	.02	.00																					
R7	.043	.41	.51	.11	.03	.05	.03	.00																				
R8	.040	.37	.47	.06	.02	.00	.02	.05	.00																			
R9	.041	.38	.49	.07	.00	.02	.00	.03	.02	.00																		
R10	.042	.40	.50	.09	.02	.03	.02	.02	.03	.02	.00																	
R11	.040	.37	.47	.06	.02	.00	.02	.05	.00	.02	.03	.00																
R12	.044	.42	.52	.12	.05	.07	.05	.02	.07	.05	.03	.07	.00															
R13	.044	.42	.52	.12	.05	.07	.05	.02	.07	.05	.03	.07	.00	.00														
R14	.046	.45	.54	.15	.08	.10	.08	.05	.10	.08	.06	.10	.03	.03	.00													
R15	.044	.42	.52	.12	.05	.07	.05	.02	.07	.05	.03	.07	.00	.00	.03	.00												
R16	.046	.45	.54	.15	.08	.10	.08	.05	.10	.08	.06	.10	.03	.03	.00	.03	.00											
R17	.044	.42	.52	.12	.05	.07	.05	.02	.07	.05	.03	.07	.00	.00	.03	.00	.03	.00										
R18	.045	.44	.53	.14	.07	.08	.07	.03	.08	.07	.05	.08	.02	.02	.02	.02	.02	.02	.00									
R19	.044	.42	.52	.12	.05	.07	.05	.02	.07	.05	.03	.07	.00	.00	.03	.00	.03	.00	.02	.00								
R20	.044	.42	.52	.12	.05	.07	.05	.02	.07	.05	.03	.07	.00	.00	.03	.00	.03	.00	.02	.00	.00							
R21	.045	.44	.53	.14	.07	.08	.07	.03	.08	.07	.05	.08	.02	.02	.02	.02	.02	.02	.00	.02	.02	.00						
R22	.044	.42	.52	.12	.05	.07	.05	.02	.07	.05	.03	.07	.00	.00	.03	.00	.03	.00	.02	.00	.00	.02	.00					
R23	.044	.42	.52	.12	.05	.07	.05	.02	.07	.05	.03	.07	.00	.00	.03	.00	.03	.00	.02	.00	.00	.02	.00	.00				
R24	.046	.45	.54	.15	.08	.10	.08	.05	.10	.08	.06	.10	.03	.03	.00	.03	.00	.03	.02	.03	.03	.02	.03	.03	.00			
R25	.046	.45	.54	.15	.08	.10	.08	.05	.10	.08	.06	.10	.03	.03	.00	.03	.00	.03	.02	.03	.03	.02	.03	.03	.00	.00		
R26	.037	.32	.43	.00	.07	.06	.07	.11	.06	.07	.09	.06	.12	.12	.15	.12	.15	.12	.14	.12	.12	.14	.12	.12	.15	.15	.00	
R27	.031	.21	.33	.12	.19	.18	.19	.23	.18	.19	.21	.18	.24	.24	.27	.24	.27	.24	.26	.24	.24	.26	.24	.24	.27	.27	.12	.00

t values for the test between two slopes (FDs of the real wave)

t = ABS(SE1 - SE2) / SQRT(SE1*SE1 + SE2*SE2)

n = (N1-2) + (N2-2) = (11-2) + (11-2) = 18

where SE is the standard error of slope and n is the number of sample.

	SE	R1	R2	R3	R4	R5	R6	R7	R8	R9	R10	R11	R12	R13	R14	R15	R16	R17	R18	R19	R20	R21	R22	R23	R24	R25	R26	R27
		.069	.070	.069	.070	.070	.072	.067	.065	.067	.065	.068	.067	.066	.065	.068	.067	.068	.065	.067	.065	.067	.068	.070	.070	.069	.070	.070
R1	.069	.01																										
R2	.070	.00	.01																									
R3	.069	.01	.00	.01																								
R4	.070	.00	.01	.00	.00																							
R5	.070	.00	.01	.00	.00	.02																						
R6	.072	.02	.03	.02	.02	.00	.05																					
R7	.067	.03	.02	.03	.03	.05	.00	.02																				
R8	.065	.05	.04	.05	.05	.07	.02	.00	.02																			
R9	.067	.03	.02	.03	.03	.05	.00	.02	.00	.02																		
R10	.065	.05	.04	.05	.05	.07	.02	.00	.02	.00	.03																	
R11	.068	.02	.01	.02	.02	.04	.01	.03	.01	.03	.00	.01																
R12	.067	.03	.02	.03	.03	.05	.00	.02	.00	.02	.01	.00	.01															
R13	.066	.04	.03	.04	.04	.06	.01	.01	.01	.01	.02	.01	.00	.01														
R14	.065	.05	.04	.05	.05	.07	.02	.00	.02	.00	.03	.02	.01	.00	.03													
R15	.068	.02	.01	.02	.02	.04	.01	.03	.01	.03	.00	.01	.02	.03	.00	.01												
R16	.067	.03	.02	.03	.03	.05	.00	.02	.00	.02	.01	.00	.01	.02	.01	.00	.01											
R17	.068	.02	.01	.02	.02	.04	.01	.03	.01	.03	.00	.01	.02	.03	.00	.01	.00	.03										
R18	.065	.05	.04	.05	.05	.07	.02	.00	.02	.00	.03	.02	.01	.00	.03	.02	.03	.00	.02									
R19	.067	.03	.02	.03	.03	.05	.00	.02	.00	.02	.01	.00	.01	.02	.01	.00	.01	.02	.00	.02								
R20	.065	.05	.04	.05	.05	.07	.02	.00	.02	.00	.03	.02	.01	.00	.03	.02	.03	.00	.02	.00	.02							
R21	.067	.03	.02	.03	.03	.05	.00	.02	.00	.02	.01	.00	.01	.02	.01	.00	.01	.02	.00	.02	.00	.01						
R22	.068	.02	.01	.02	.02	.04	.01	.03	.01	.03	.00	.01	.02	.03	.00	.01	.00	.03	.01	.03	.01	.00	.02					
R23	.070	.00	.01	.00	.00	.02	.03	.05	.03	.05	.02	.03	.04	.05	.02	.03	.02	.05	.03	.05	.03	.02	.00	.00				
R24	.070	.00	.01	.00	.00	.02	.03	.05	.03	.05	.02	.03	.04	.05	.02	.03	.02	.05	.03	.05	.03	.02	.00	.00	.01			
R25	.069	.01	.00	.01	.01	.03	.02	.04	.02	.04	.01	.02	.03	.04	.01	.02	.01	.04	.02	.04	.02	.01	.01	.01	.00	.01		
R26	.070	.00	.01	.00	.00	.02	.03	.05	.03	.05	.02	.03	.04	.05	.02	.03	.02	.05	.03	.05	.03	.02	.00	.00	.01	.00	.00	
R27	.070	.00	.01	.00	.00	.02	.03	.05	.03	.05	.02	.03	.04	.05	.02	.03	.02	.05	.03	.05	.03	.02	.00	.00	.01	.00	.00	1.00

t values for the test between two slopes (FDs of the synthetic wave)

t = ABS(SE1 - SE2) / SQRT(SE1*SE1 + SE2*SE2)

n = (N1-2) + (N2-2) = (11-2) + (11-2) = 18

where SE is the standard error of slope and n is the number of sample.

Appendix L

Land Use and Conservation of Taiwan, R.O.C.

The Republic of China is situated in Eastern Asia, and includes islands bordering the East China Sea, Philippines Sea, South China Sea, and Taiwan Strait, north of the Philippines, off the southern coast of China.[1] The total area is 35980 square kilometres, roughly the same size as the Netherlands (WCMC, 1994). The land, including the Pescadores, Matsu, and Quemoy, is 32260 square kilometre long. The coast line is 1448 kilometres. Mean temperatures range from 25° to 28°*c*, from June to September, respectively. The average temperature in winter, that is, from November to April, is 20°*c*. The annual rainfall exceeds 2000 millimetres or 78.7 inches (Tsai & Simpson, 1992).

The tropical and marine climate reflects the fact that the Tropic of Cancer passes through the middle of the main island, Taiwan. The rainy season is during the southwest monsoon from June to August. Cyclones occur frequently. Cloudiness, except in the south, is persistent and extensive all year. Two-thirds of Taiwan, mainly in the east, is mostly rugged mountainous terrain. However, the terrain descends to gently rolling plains in the west (Tsai & Simpson, 1992).

[1] Refer to page 163.

	TW	UK	(TW : UK)	US	(TW : US)
Population (*million*)	21*	58**	(1 : 2.8)	264*	(1 : 12.6)
Land Area (km^2)	32.3e3	241.6e3	(1 : 7)	9.2e6	(1 : 284)
Population Density($head/km^2$)	651.0	240.1	(2.7 : 1)	28.8	(22.6 : 1)
Land Use I (%)					
Arable Land	24	29	(1 : 1.2)	20	(1.2 : 1)
Meadows & Pastures	5	48	(1 : 9.6)	26	(1 : 5.2)
Forest & Woodland	55	9	(6.1 : 1)	29	(1.9 : 1)
Other	16	14	(1.1 : 1)	25	(1 : 1.6)
Land Use II ($ha/10^3$)					
Food Production	44.5	320.7	(1 : 7.2)	1597.2	(1 : 35.9)
Potential Conservation	84.5	37.5	(2.3 : 1)	1006.9	(1 : 12.0)
Conservation/Food	1.89	0.12	(16 : 1)	0.63	(3 : 1)

Table L.1: Comparison of Land Uses Between Taiwan, the UK and the US. Symbols * and ** indicate the populations estimated in 1995 and 1992, respectively. The digraphs TW, UK and US represent Taiwan, the Republic of China, the United Kingdom, and the United States of America, respectively. The Food Production area in Land Use II is the total of the Arable Land and Meadows & Pastures, while the Potential Conservation includes Forest & Woodland in Land Use I. Source: *The 1996 World Factbook* (1996).

A summary of basic statistics between Taiwan, the Republic of China (TW), the United States (US) and the United Kingdom (UK) is given in Table L.1. The total population of TW is rather small, compared with that of US and UK. However, the population density is relatively high, given the small land area. Twenty-nine per cent of land used for agricultural purpose confirms that two-thirds of Taiwan is mountainous (Tsai & Simpson, 1992), compared with nearly half of the land in the US, and three-quarters of the land in the UK which are of agricultural use. A much lower land area per thousand people than in the US or the UK is used for agricultural production. Also, more land per thousand people in US than in TW and the UK potentially contributes to conservation. However, the conservation/food ratio is much higher in TW than in either the UK or the US.

All figures in Table L.1 indicate that there is great potential for conservation in Taiwan. Indeed, there are more than two hundred peaks of over 3000 metres which connect to form the Central Ridge that is termed the backbone of the island. The

Central Ridge includes "Jade Mountain", the highest peak in East Asia, which rises to 3952 metres or 12965 feet. With its tropical and marine weather, Taiwan supports diverse flora of over 4000 vascular plant species (1075 endemic) and a spectrum of six forest types. This environment in turn supports rich fauna: sixty-one species of mammals (42 endemic), more than 400 species of birds (70 endemic), 92 species of reptiles, 30 species of amphibians, 140 species of freshwater fish, and an estimated 50000 insect species, including more than 400 species of butterflies (McHenry & Lin, 1984; Tsai & Simpson, 1992).

Title	Cat.	Major Protected Features	*Ha.*	Year
Kenting	V	Marine Ecosystem, Uplifted Coral Reef, Limestone Caves, Slumping Cliffs, Tropical Coastal Rainforest, Waterfowl, Migratory Birds, Butterflies.	17731	1985
Kinmen		Historical Battlefields, Traditional Ming Villages, Historical Sites, Archaeological Sites, Natural Scenic Areas.	5745	1995
Lanyu	II	n/a	29146	n/a
Shei-pa	II	High Mountains, Rugged Terrain, Cliffs, Natural Forest, Wildlife. Rare Species of Flora and Fauna.	76850	1992
Taroko	II	Marble Gorge, Sheer Cliffs, Waterfalls, High Mountains, Valleys, Streams, Wildlife, Virgin Forest, Prehistoric Relics Trail.	92000	1986
Yanmingshan	V	Volcanic Geological Forms, Meadows, Hot Springs, Waterfalls, Butterflies, Birds, Amphibians.	11456	1985
Yushan	II	High Peaks and Mountainous Terrain, Diversity of Plants and Wildlife, Virgin Forest, Large Mammals, Rare Species of Flora and Fauna.	105490	1985

Table L.2: List of National Parks in Taiwan.
IUCN Categories and the major protected features are given. Sources: Tsai & Simpson (1992) and IUCN (1994).

However, it was not until 1985 that the first national parks were established. Table L.2 lists the major protected features, area and established year of the seven national parks in Taiwan. The World Conservation Union (IUCN) Management Categories to which they belong are also given. The World Conservation Union (IUCN) Management Categories I – V are listed in Table L.3 below. This classifi-

cation defines what activities are allowed or not allowed in such areas. Most of the national parks in Taiwan fall into Category II which aims to "protect outstanding natural and scenic areas of national or international significance for scientific, educational, and recreational use." Kenting and Yanmingshan national parks belong to Category V which is to "maintain nationally significant natural landscapes which are characteristic of the harmonious interaction of man and land while providing opportunities for public enjoyment through recreation and tourism within the normal life style and economic activity of these areas."

Shei-pa national park aims to protect features such as high mountains, rugged terrain, cliffs, natural forest, wildlife, rare species of flora and fauna. However, this thesis focuses on its geomorphology.

I. Strict Nature Reserve/Scientific Reserve. To protect nature and maintain natural processes in an undisturbed state in order to have ecologically representative examples of the natural environment available for scientific study, environmental monitoring, education, and for the maintenance of genetic resources in a dynamic and evolutionary state.

II. National Parks. To protect outstanding natural and scenic areas of national or international significance for scientific, educational, and recreational use. These are relatively large natural areas not materially altered by human activity where extractive resource uses are not allowed.

III. Natural Monuments/Natural Landmarks. To protect and preserve nationally significant natural features because of their special interest or unique characteristics. These are relatively small areas focused on the protection of specific features.

IV. Managed Nature Reserves/Wildlife Sanctuary. To assure the natural conditions necessary to protect nationally significant species, groups of species, biotic communities, or physical features of the environment where these may require specific human manipulation for their perpetuation. Controlled harvesting of some resources can be permitted.

V. Protected Landscapes and Seascapes. To maintain nationally significant natural landscapes which are characteristic of the harmonious interaction of man and land while providing opportunities for public enjoyment through recreation and tourism within the normal life style and economic activity of these areas. These are mixed cultural/natural landscapes of high scenic value where traditional land uses are maintained.

Table L.3: The IUCN Management Category.
Here Categories VI to VIII are not included. Note that a revised Category system is under construction at the time of writing. Source: The World Conservation Union (IUCN) (1994).

Appendix M

Programme Listing of Converting DEM to IDRISI

The computer programme for converting the digital elevation model files to files of Idrisi format is listed below.[1] The following script is used to compile the C programme, that is, "*acc -c -lm $1.c*".

```
/*
// DEM2IDRISI.C
// Usage: DEM2IDRISI in.img out.bin
out.doc
// Desc: Read TWN DEM image file and
convert it into Unix recognisable file,
//*.bin and idrisi *.doc.
// Input: TWN DEM: *.img -> *.dem 'cos
idrisi uses .img. See below.
// Output: Unix binary file: *.bin ->
idrisi .img
//idrisi document file: *.doc
*/
#include <stdio.h>
#include <stdlib.h>
#defineSTART60
#defineHDR22
#defineROWS75
#defineINFO11
#defineBLK400
/*************** main *************/
void main(int argc, char **argv)
{
FILE*fin, *ftmp, *fbin, *fdoc;
charhdr[HDR], sour[4], dest[4],
ch_in[BLK], ch_out[BLK];
intval0, val1=0, para[11],
xmin, ymin, xmax, ymax, resol, rows,
cols,zmax, zmin;
short int hgt;
floatval;
inti, j, k, l, m;
intstart, char_size, int_size, short_size,
float_size;
if(argc < 2){
printf("Syntax: %s in.img output.bin
input.doc\n", argv[0]);
printf("\tin.img:  input files\n");
printf("\toutput.bin: output file.\n");
printf("\t\tto be converted into idrisi image
by dd\n");
printf("\toutput.doc: output idrisi document
file.\n");
exit(0);
} /* if */
/* char: 1; short int: 2; int/float: 4;
double: 8 bytes */
char_size = sizeof(char);
int_size = sizeof(int);
short_size  = sizeof(short int);
float_size  = sizeof(float);
if((fin = fopen(argv[1], "rb")) == NULL){
printf("Can't open input file %s\n",
argv[1]);
exit(0);
} /* if */
/* open a temporary file to hold data */
if((ftmp = fopen("temp.img", "wb")) ==
NULL){
printf("Can't open temp bianry file:
temp.img\n");
exit(1);
}
/*
// Convert bytes into desirable order
and output as a file
// keep the header: 60 bytes
// mirror each 4 bytes between 60-th and
400-th byte: 1234 becomes 4321
// swab each 4 bytes afterwards: 1234
becomes 3412,
//minus 1 from element 2 of original
before put into new order
*/
fseek(fin, 0L, SEEK_SET); fseek(ftmp, 0L,
```

[1] Refer to section 5.3.1.

```
SEEK_SET);
fread(ch_in, char_size, BLK, fin);
for( k = 0; k < START; k++){
ch_out[k] = ch_in[k];
} // k: 0-60
for(k = START; k < BLK; ){
for(l = 0, m = 3; l < 4, m >= 0; l++,
m--){
ch_out[k + m] = ch_in[k + l];
} // l: mirror
k += 4;
} // k: 60-400
fwrite( ch_out, char_size, BLK, ftmp);
fseek(fin, BLK, SEEK_SET);
fseek(ftmp, BLK, SEEK_SET);
for(l = 0; l < ROWS; l++){
fread(ch_in, char_size, BLK, fin);
for(k = 0; k < BLK;){
ch_out[k+0] = ch_in[k+1]-1;
ch_out[k+1] = ch_in[k+0];
ch_out[k+2] = ch_in[k+3];
ch_out[k+3] = ch_in[k+2];
k += 4;
} // k: swab
fwrite(ch_out, char_size, BLK, ftmp);
}
fclose(fin); fclose(ftmp);
/*
// read the data from corrected file
// put it into a file
*/
ftmp = fopen("temp.img", "rb");
if((fbin = fopen(argv[2], "wb")) ==
NULL){
printf("Can't open output image file: %s\n",
argv[2]);
exit(1);
}
fseek(ftmp, 0L, SEEK_SET); fscanf( ftmp,
"%s", hdr);
fseek(ftmp, START, SEEK_SET);
fread(para, int_size, 11, ftmp);
xmin = para[0];
ymin = para[3];
xmax = para[4];
ymax = para[1];
resol = para[8];
rows = para[9];
cols = para[10];
zmin = 9999;
zmax = 0;
fseek(ftmp, BLK, SEEK_SET);
fseek(fbin, 0L, SEEK_SET);
for(k = 0; k < rows; k++){
fseek(ftmp, k*BLK, SEEK_SET);
for( l = 0; l < cols; l++){
fread(&val, float_size, 1, ftmp);
hgt = (short int) val;
if(hgt > 0 && hgt > zmax) zmax = hgt;
if(hgt > 0 && hgt < zmin) zmin = hgt;
if(hgt < 0)  hgt = 0;
fwrite(&hgt, short_size, 1, fbin);
} /* l */
} /* k */
fclose(ftmp); fclose(fbin);
if((fdoc = fopen(argv[3], "wt")) ==
NULL){
printf("Can't open output doc file: %s\n",
argv[3]);
exit(1);
}
/*** write out idrisi .doc file ***/
fprintf(fdoc, "file title  : %s\n", argv[1]);
fprintf(fdoc, "data type   : integer\n");
fprintf(fdoc, "file type   : binary\n");
fprintf(fdoc, "columns     : %d\n", cols);
fprintf(fdoc, "rows        : %d\n", rows);
fprintf(fdoc, "ref. system : plane\n");
fprintf(fdoc, "ref. units  : m\n");
fprintf(fdoc, "unit dist.  : 1\n");
fprintf(fdoc, "min. X      : %d\n", xmin -
resol);
fprintf(fdoc, "max. X      : %d\n", xmax +
resol);
fprintf(fdoc, "min. Y      : %d\n", ymin -
resol);
fprintf(fdoc, "max. Y      : %d\n", ymax +
resol);
fprintf(fdoc, "pos'n error : unknown\n");
fprintf(fdoc, "resolution  : unknown\n");
fprintf(fdoc, "min. value  : %d\n", zmin);
fprintf(fdoc, "max. value  : %d\n", zmax);
fprintf(fdoc, "value units : classes\n");
fprintf(fdoc, "value error : unknown\n");
fprintf(fdoc, "flag value  : none\n");
fprintf(fdoc, "flag def'n  : none\n");
fprintf(fdoc, "legend cats : 0\n");
fclose(fdoc);
} /* main */
```

Appendix N

Programme Listing of Synthetic DEMs

The following C programme is compiled by C compiler on SunOS (4.1.3_U1), using the script "*acc $1.c -o $1 -lm -xCC -w*".[1] The example use of this programme is like "*syndem 0.2 0.8 n syn28n.bin syn28n.doc*", which generates the landscape with the offset of 0.2, H of 0.8, and no random addition, which is stored in the files of syn28syn.bin and syn28syn.doc .

```
// syndem.c
// Usage: syndem Sigma H y/n .bin .doc
// Desc: Terrain model by mid-point
displacement
// Source: p.77 & p.100, the science of
fratal images, 1988.
*/
#include <stdio.h>
#include <stdlib.h>
#include <math.h>
#define Nrand (4)
#define Arand ((int)((pow(2,15))-(1)))
#define GaussAdd (sqrt((3.0)*(Nrand)))
#define GaussFac ((2.0)*(GaussAdd) /
((Nrand)*(Arand)))
#define SEED (100)
#define MAX_LEVEL (10)
#define MAP_SIZE (1024)
#define BASE (0.1)
#define SCAL (0.5)
#define MAG (4000.0)
#define OFFST (1)
#define MIN(x, y)(((x)<=(y))?(x):(y))
#define MAX(x, y)(((x)>(y))?(x):(y ))
/****** InitGauss() ******/
void
InitGauss(unsigned int seed)
{
    srand(seed);
}// InitGauss()
/******* Gauss() ******/
double
Gauss()
{
int i;
int sum = 0;

for(i = 0; i < Nrand; i++){
    sum += rand();
}
return(GaussFac * (double)sum -
GaussAdd);
}// Gauss()
/****** f4() ******/
double
f4( double delta, double x0, double x1,
double x2, double x3)
{
double resul, *ran;
resul= (x0 + x1 + x2 + x3)/4.0 + delta *
Gauss();
return(resul);
} // f4()
/****** f3() ******/
double
f3( double delta, double x0, double x1,
double x2)
{
double resul, *ran;
resul= (x0 + x1 + x2)/3.0 + delta *
Gauss();
return(resul);
} // f3()
/************************
****** main() ***********
************************/
void main(int argc, char **argv)
{
FILE    *f01, *f02;
char    ch;
int     i,x,y, *z;
int     N, D, d;
```

[1] Refer to Section 5.4.3.

```
short int itmp[MAP_SIZE][MAP_SIZE],
imin, imax;
float   X[MAP_SIZE][MAP_SIZE];
double delta, sigma, H_const, val, vmax,
vmin, vrange, vcentre;
if(argc < 2){
   printf("Usage: %s sigma H_constant
no/yes\n", argv[0]);
   printf("\tsigma:initial std (0.5)\n");
   printf("\tH_const: Parameter H(0.8), D =
3 - H\n");
   printf("\tNo/Yes: Turn random addition
on? [N]o/[Y]es\n");
   printf("Note: map size = %d x %d\n",
MAP_SIZE, MAP_SIZE);
   exit(-1);
} // warning msg
sigma   = atof(argv[1]);
H_const = atof(argv[2]);
ch      = argv[3][0];
InitGauss(SEED);
N       = (int)exp2(MAX_LEVEL);
delta   = sigma;
for(x = 0; x < MAP_SIZE;x++){
   for(y = 0; y < MAP_SIZE;y++){
      X[x][y] = BASE;
   } // y
} // x
X[0][0] = delta * Gauss();
X[0][N] = delta * Gauss();
X[N][0] = delta * Gauss();
X[N][N] = delta * Gauss();
/*
// DEM generation
//Going from grid type I to type II
//then type II to type I
*/
D = N;
d = N/2;
for(i=0;i<MAX_LEVEL;i++){
/*** type I to type II ***/
   delta *= pow(SCAL, SCAL*H_const);
   for(x = d; x <= N-d; x += D){
      for(y = d; y <= N-d; y += D){
         X[x][y] =
f4(delta,X[x+d][y+d],X[x+d][y-d],
X[x-d][y+d],X[x-d][y-d]);
      } // y
   } // x

   if( (ch == 'y') || (ch == 'Y') ){
      for(x = 0; x <= N; x += D){
         for(y = 0; y <= N; y += D){
            X[x][y] += delta * Gauss();
         } // y
      } // x
   }
/**** type II to type I ****/
   delta *= pow(SCAL, SCAL*H_const);
/** Interpolate and offset boundary grid
points **/
   for(x = d; x < N-d; x += D){
      X[x][0] = f3(delta, X[x+d][0],
X[x-d][0], X[x][d]);
      X[x][N] = f3(delta, X[x+d][N],
X[x-d][N], X[x][N-d]);
      X[0][x] = f3(delta, X[0][x+d],
X[0][x-d], X[d][x]);
      X[N][x] = f3(delta, X[N][x+d],
X[N][x-d], X[N-d][x]);
   }
/** Interpolate and offset interior grid
points **/
   for(x = d; x <= N-d; x += D){
      for(y = D; y <= N-d; y += D){
         X[x][y] =
f4(delta,X[x][y+d],X[x][y-d],
X[x+d][y],X[x-d][y]);
      } // y
   } // x
   for(x = D; x <= N-d; x += D){
      for(y = d; y <= N-d; y += D){
         X[x][y] =
f4(delta,X[x][y+d],X[x][y-d],
X[x+d][y],X[x-d][y]);
      } // y
   } // x
   if( (ch == 'y') || (ch == 'Y') ){
      for(x = 0; x <= N; x += D){
         for(y = 0; y <= N; y += D){
            X[x][y] += delta * Gauss();
         } // y
      } // x
      for(x = d; x <= N-d; x += D){
         for(y = d; y <= N-d; y += D){
            X[x][y] += delta * Gauss();
         } // y
      } // x

   } // turns random addition on
   D = D/2;
   d = d/2;
} // i
/*** scaling: -10000 to 10000 ****/
vmax = -999.0;
vmin = 999.0;
for(x = 0; x < MAP_SIZE;x++){
   for(y = 0; y < MAP_SIZE;y++){
      vmin = MIN(vmin, X[x][y]);
      vmax = MAX(vmax, X[x][y]);
   } // y
} // x
for(x = 0; x < MAP_SIZE;x++){
   for(y = 0; y < MAP_SIZE;y++){
```

```
      X[x][y] -= vmin; // all positive
now!
   } // y
} // x
vmax = -999.0;
vmin = 999.0;
for(x = 0; x < MAP_SIZE;x++){
   for(y = 0; y < MAP_SIZE;y++){
      vmin = MIN(vmin, X[x][y]);
      vmax = MAX(vmax, X[x][y]);
   } // y
} // x
vcentre = (vmax + vmin)/2.0;
vrange  = fabs(vmax - vmin);
for(x = 0; x < MAP_SIZE;x++){
   for(y = 0; y < MAP_SIZE;y++){
      val = X[x][y]/vrange;
      if(val > 0.0){
         val *= MAG;
         itmp[x][y] = (short int) val;
      } else {
         itmp[x][y] = OFFST;
      } // if-else
   } // y
} // x
/*** output binary .bin file ***/
if((f01 = fopen(argv[4], "wb")) == NULL){
   printf("Can't open output .bin file\n");
   exit(1);
}
for(x = 0; x < MAP_SIZE;x++){
   fwrite(itmp[x], sizeof(short int),
MAP_SIZE, f01);
} // x
fclose(f01);
imax = -999;
imin = 999;
for(x = 0; x < MAP_SIZE;x++){
   for(y = 0; y < MAP_SIZE;y++){
      imin = MIN(imin, itmp[x][y]);
      imax = MAX(imax, itmp[x][y]);
   } // y
} // x
if((f02 = fopen(argv[5], "wt")) == NULL){
   printf("Can't open output .doc file\n");
   exit(1);
} // if
/*** output idrisi .doc file ***/
fprintf(f02, "file title  : Synthetic DEM by
mid-point method\n");
fprintf(f02, "data type   : integer\n");
fprintf(f02, "file type   : binary\n");
fprintf(f02, "columns     : %d\n",
MAP_SIZE);
fprintf(f02, "rows        : %d\n",
MAP_SIZE);
fprintf(f02, "ref. system : plane\n");
fprintf(f02, "ref. units  : m\n");
fprintf(f02, "unit dist.  : 1\n");
fprintf(f02, "min. X      : 0\n");
fprintf(f02, "max. X      : %d\n",
MAP_SIZE*40);
fprintf(f02, "min. Y      : 0\n");
fprintf(f02, "max. Y      : %d\n",
MAP_SIZE*40);
fprintf(f02, "pos'n error : unknown\n");
fprintf(f02, "resolution  : unknown\n");
fprintf(f02, "min. value  : %d\n",  imin);
fprintf(f02, "max. value  : %ld\n", (short
int)imax);
fprintf(f02, "value units : classes\n");
fprintf(f02, "value error : unknown\n");
fprintf(f02, "flag value  : none\n");
fprintf(f02, "flag def'n  : none\n");
fprintf(f02, "legend cats : 0\n");
fclose(f02);
} // main()
```

Appendix O

Programme Listing of DEMs' Dimensions

The computer programme for estimating the fractal dimension of DEMs is listed below.[1] The following script is used to compile C programme incoporating NAG FORTRAN library routines (Hann & Hounam, 1991), whose resulting object programme is further compiled by FORTRAN compiler. That is, "*acc -c -lm $1.c*" and "*f77 $1.o -o $1 -lnag*".
Example: "*demfd dem.doc dem.bin 1 > fd.dat*", where *dem.doc* is an IDRISI header file and *dem.bin* is a Unix binary file, converted from the IDRISI image file by "*dd if=dem.img of=dem.bin conv=swab*" on the Unix machine.

```
/* demfd.c
// Usage: demfd in.doc(Idrisi)
in.bin(Unix) 1 > file
// Desc: Get info from Idrisi .doc
//  Read image into an array row * col
//  Get profile of 2^n points
// Out: (stdout)
//     no mean std fd(h) mean std fd(v)
*/
#include <stdio.h>
#include <stdlib.h>
#include <math.h>
#include <nagmk15.h> // NAGF lib.
#include <TS.h>
#define MX_IMG_SIZE (1024)
#define HDR_LINE_NO  (21)
#define HDR_LINE_SIZE (100)
#define HDR_INFO_START (14)
#define MX_SUB_SET (20)
#define OUT_BASE  (0.0)
/* col, row, etc from header */
int extract_info(
   char out[], // input string
   char in[])  // output string
{
int  i, j;
for(i=HDR_INFO_START, j=0; j<5;
i++,j++){ out[j] = in[i]; }
} // extrac_info()
/*********************************
// Box-counting: Brwnian method
// Count boxes between max and min
//    width decreased by 2^n!
//   height is given
*********************************/
void
TS_brown_box_counting(
   double x[], /* input data */
   int    length,/* length of data */
   double std, /* height of data */
   double result[20]) /* dimensions */
{
int  i,u,v;
int  paces;
double *tmpp, *size, *count, *ind, *dep;
double width, height,val;
double scal;
/* declarations for G01AAF, G02CAF */
int  n,iwt,ifail;
double *wt,
xmean,s2,s3,s4,xmin,xmax,wtsum;
paces = (int) floor(log2((double)length));
size  = malloc(paces * sizeof(int));
count= malloc(paces * sizeof(int));
for(i = 0; i < paces; i++){
   scal   = exp2((double)i );
   width = length / scal;
   height = std / scal;
   size[i] = scal; /* from scale to size */
   count[i] = 0.0;
   tmpp = malloc((int)width *
sizeof(double));
wt  = malloc((int)width * sizeof(double));
for(u = 0; u < scal; u++){
   for(v = 0; v < width; v++) { tmpp[v] =
x[u * (int)width + v]; }
   n = (int) width;
```

[1] Refer to Section 5.5.2.

```
    iwt = 0;
    ifail = 1;
    g01aaf_(&n, tmpp, &iwt, wt, &xmean,
&s2, &s3, &s4, &xmin, &xmax, &wtsum,
&ifail);
    val = ceil(xmax/height) -
floor(xmin/height);
    count[i] += val;
} // u
free(tmpp); free(wt);
} // i
for(i=0;i<paces;i++){
    size[i] = log2(size[i]);
    count[i]= log2(count[i]);
} // i
n = paces; ifail = 1;
g02caf_(&n, size, count, result, &ifail);
free(size); free(count);
} // TS_brown_box_counting //
/*******************************
********* main() ****************
*******************************/
void main(int argc, char **argv)
{
FILE *fin;
char hdr[HDR_LINE_SIZE], tmp[5], ch;
int  sub;// number of subsets
int  i, j, k;
int  col, row, new_col, new_row;
int  diff_c, diff_r, start_c, start_r,
val[2][MX_SUB_SET];
int  size_s, size_d;
short int
img[MX_IMG_SIZE][MX_IMG_SIZE],
*temp;
double
out[2][MX_SUB_SET][MX_IMG_SIZE];
double vremn1, vremn2;
/* NAGF: G01AAF etc */
int     m, n,iwt,ifail;
double *y, *x,*wt,
xmean,s2,s3,s4,xmin,xmax,wtsum,
result[20];
double *tmpx, *tmpy;
size_s = sizeof(short int);
size_d = sizeof(double);
/***** warning msg *************/
if(argc < 2){
    printf("Usage: %s in.doc in.bin no >
file\n", argv[0]);
    printf("\tin.doc:Input document
(Idrisi)\n");
    printf("\tin.bin:Input image (Unix)\n");
    printf("\tno.:Number of points. 1 means
an img. of 2^n\n\n");
    printf("\t\t-> to be dd conv=swab (Unix)
-> .img (Idrisi)\n");
    printf(".Note: output (stdout) should be
redirected to a file\n");
    printf("\ti.e., ... | more > file\n");
    printf("\tno: Number of sub-sets used <
%d\n", MX_SUB_SET);
    exit(-1);
}
/****** parameter *********/
sub = atoi(argv[3]); // to see if N != 2^n
/* get col & row from .doc header */
if((fin = fopen(argv[1], "rt")) == NULL){
    printf("Can't open input Idrisi .doc file:
%s\n", argv[1]);
    exit(-1);
} // open file
for(i = 0; i < HDR_LINE_NO; i++){
    fgets(hdr, HDR_LINE_SIZE, fin);
    if(i == 3) {
        extract_info(tmp, hdr);
        col = atoi(tmp);
    }
    if ( i == 4){
        extract_info(tmp, hdr);
        row = atoi(tmp);
    }
} // i
fclose(fin);
/*** scan image into an arry ***/
if((fin = fopen(argv[2], "rb")) == NULL){
    printf("Can't open input image file:
%s\n", argv[2]);
    exit(-1);
}
temp = malloc(col * size_s);
for(i = 0; i < row; i++){
    fread(temp, size_s, col, fin);
    for(j = 0; j < col; j++){
        if(temp[j] > 0) {
            img[i][j] = temp[j];
        }else { img[i][j] = 0; }
} // j
} // i
free(temp);
fclose(fin);
/* Decide the size of profile for fd */
xmean= floor(log2( (double) col ));
vremn1 = remainder((double) col, 2.0);
new_col = (int) exp2(xmean);
xmean= floor(log2( (double) row ));
vremn2 = remainder((double) row, 2.0);
new_row = (int) exp2(xmean);
/****** fd calculation ********/
x = malloc(new_col * size_d);
y = malloc(new_row * size_d);
tmpx = malloc(new_col * size_d);
tmpy = malloc(new_row * size_d);
wt= malloc(new_col * size_d);
```

```
diff_c = (col - new_col)/2;
diff_r = (row - new_row)/2;
for(k = 0; k < sub; k++){
   if(vremn1 != 0.0) {
      start_c= random() % diff_c;
      val[0][k] = start_c;
   } else {
      val[0][k] = start_c = 0;
   }
   if(vremn2 != 0.0){
      start_r= random() % diff_r;
      val[1][k] = start_r;
   } else {
      val[0][k] = start_r = 0;
   }
   for(i = start_c, m = 0; m < new_col;
i++, m++){
      for(j = start_r, n = 0; n < new_row;
j++, n++){
         tmpx[n] = img[i][j];
         tmpy[n] = img[j][i];
      } // j
      n= new_row; iwt = 0; ifail = 1;
      TS_data_extra(tmpx,x,n);
      g01aaf_(&n, x, &iwt, wt, &xmean,
&s2, &s3, &s4, &xmin, &xmax, &wtsum,
&ifail);
      TS_brown_box_counting(x, n, s2,
result);
      out[0][k][m] = result[5]; // [0]:
horizontal
      n= new_row; iwt = 0; ifail = 1;
      TS_data_extra(tmpy,y,n);
      g01aaf_(&n, y, &iwt, wt, &xmean,
&s2, &s3, &s4, &xmin, &xmax, &wtsum,
&ifail);
      TS_brown_box_counting(y, n, s2,
result);
      out[1][k][m] = result[5]; // [1]:
vertical
      } // i
} // k
free(x); free(y); free(wt);
/********** Result *************/
printf("# fd (h v) results from %s %s;
subimage size: %d\n", argv[1], argv[2],
new_col);
printf("# %d pairs of top-left corners: ",
sub);
for(i = 0; i < sub; i++){
printf("(%d %d) ", val[0][i], val[1][i]);
}
printf("\n");
printf("# no. h_fd v_fd delta_h_fd+%.1f
delta_v_fd+%.1f\n", OUT_BASE,
OUT_BASE);
for(i = 0; i < new_col; i++){ // orignal &
delta
   printf("%5d ", i+1);
   for(j = 0; j < sub; j++){
      printf("%5.3f ", out[0][j][i]);
   }
   for(j = 0; j < sub; j++){
      printf("%6.3f ", out[0][j][i] -
out[0][0][i] + OUT_BASE);
   }
   for(j = 0; j < sub; j++){
      printf("%5.3f ", out[1][j][i]);
   }
   for(j = 0; j < sub; j++){
      printf("%6.3f ", out[1][j][i] -
out[1][0][i] + OUT_BASE);
   }
   printf("\n");
} // i
} // main
```

Appendix P

Some Synthetic Landforms

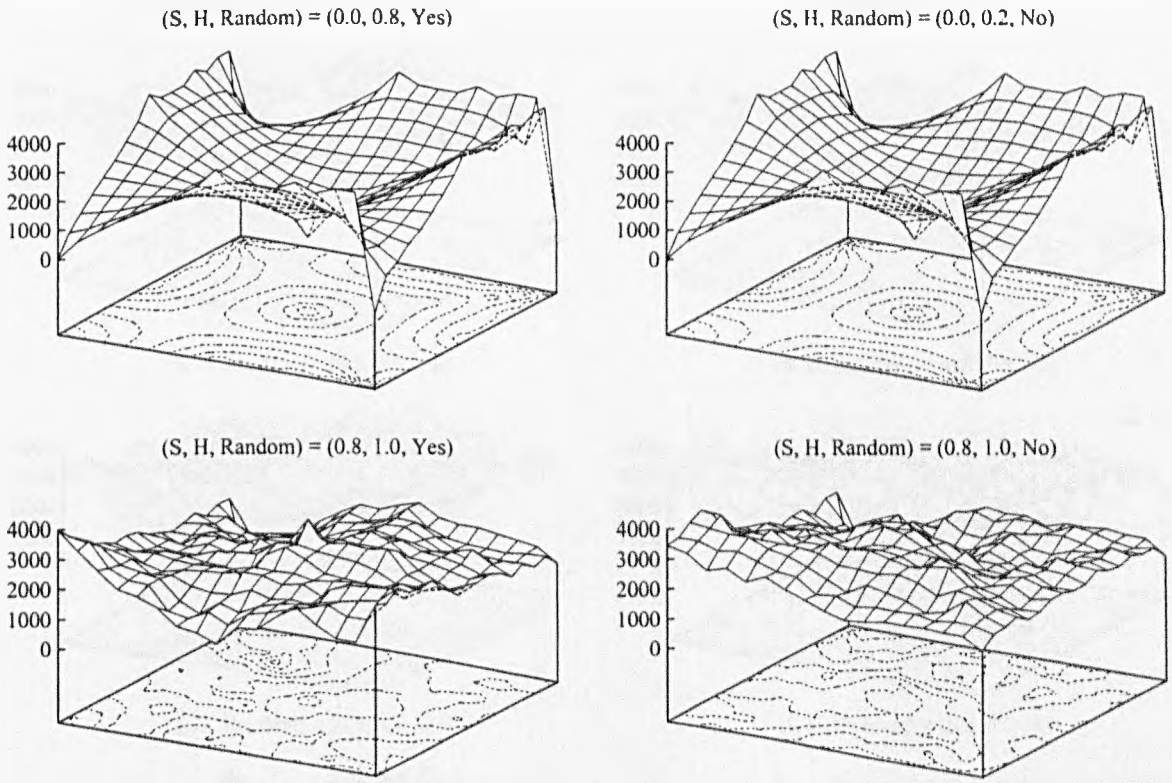

Parameters controlling the simulation include the initial variation of landform, S, the Hurst exponent, H, and the addition of randomness. The image size is 16×16 pixels and eight levels of contours are plotted for each image.

An initial flat landform produces same resultant landforms, regardless of H values or random additions. As H decreases, landforms become more complicated, seen from the pattern of contours. The effect of random addition is also shown. There is little difference between landforms with other initial variations.

(S, H, Random) = (0.8, 0.9, Yes)

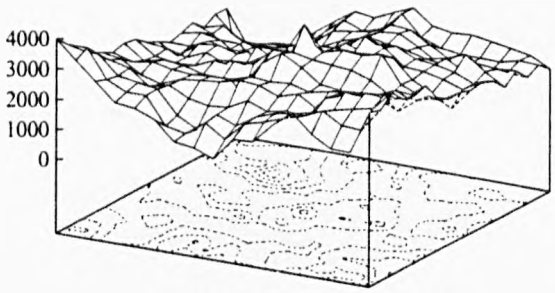

(S, H, Random) = (0.8, 0.9, No)

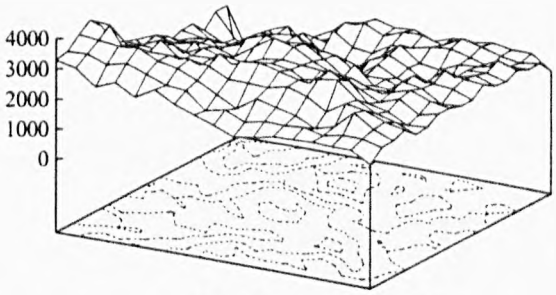

(S, H, Random) = (0.8, 0.8, Yes)

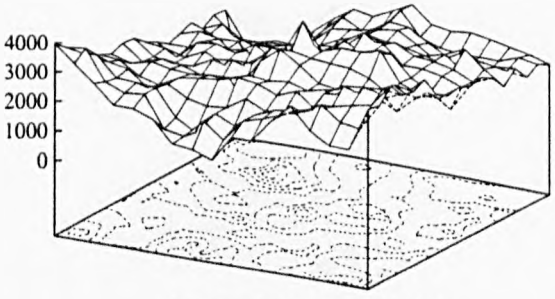

(S, H, Random) = (0.8, 0.8, No)

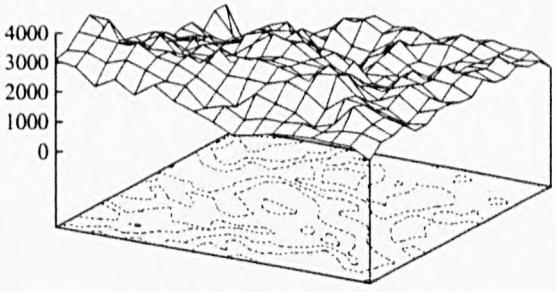

(S, H, Random) = (0.8, 0.7, Yes)

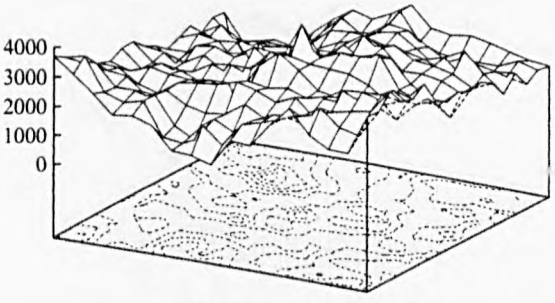

(S, H, Random) = (0.8, 0.7, No)

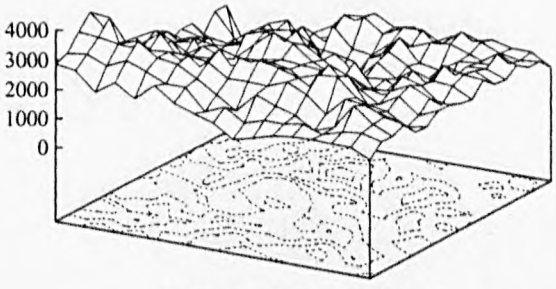

(S, H, Random) = (0.8, 0.6, Yes)

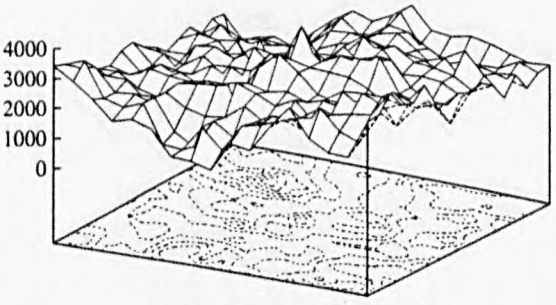

(S, H, Random) = (0.8, 0.6, No)

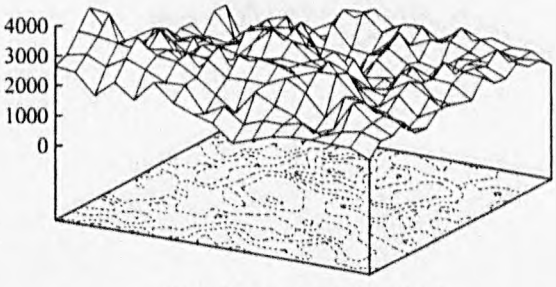

(S, H, Random) = (0.8, 0.5, Yes)

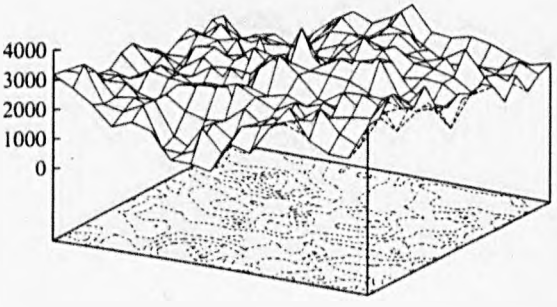

(S, H, Random) = (0.8, 0.5, No)

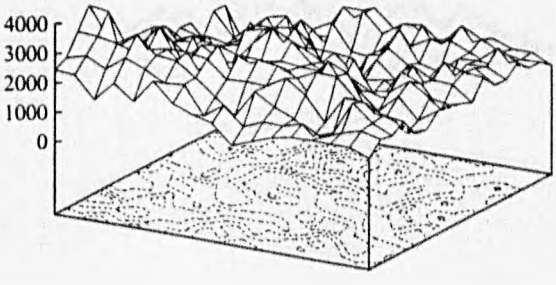

(S, H, Random) = (0.8, 0.4, Yes)

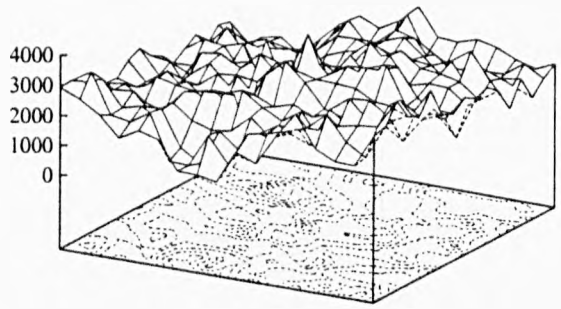

(S, H, Random) = (0.8, 0.4, No)

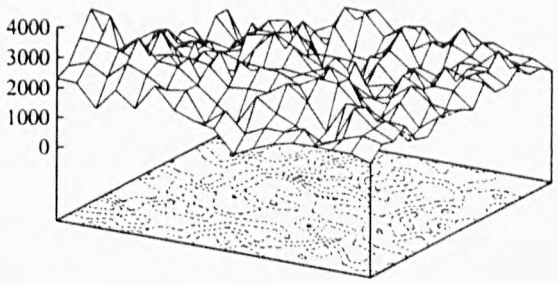

(S, H, Random) = (0.8, 0.3, Yes)

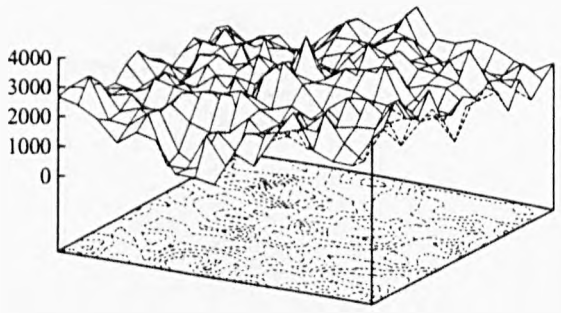

(S, H, Random) = (0.8, 0.3, No)

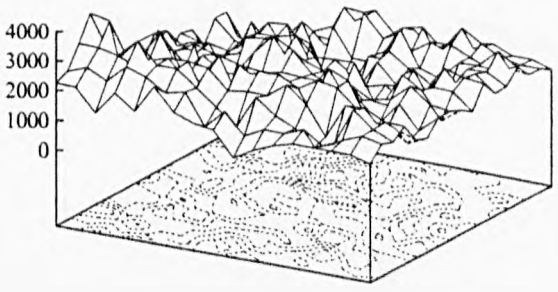

(S, H, Random) = (0.8, 0.2, Yes)

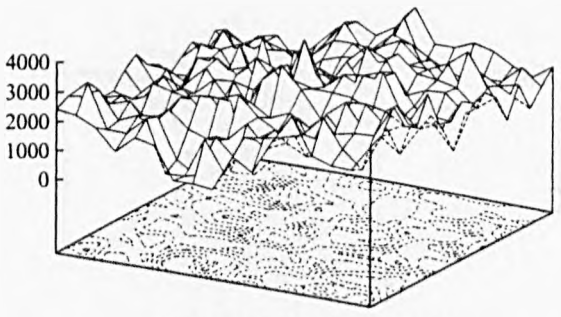

(S, H, Random) = (0.8, 0.2, No)

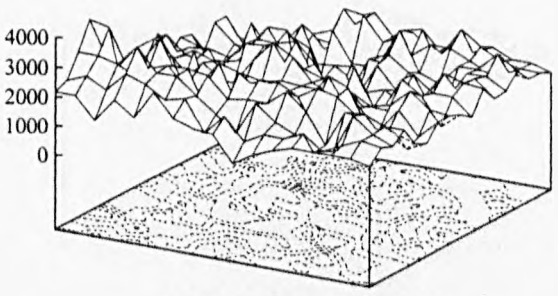

(S, H, Random) = (0.8, 0.1, Yes)

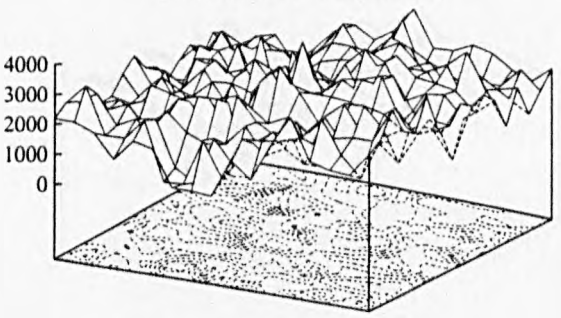

(S, H, Random) = (0.8, 0.1, No)

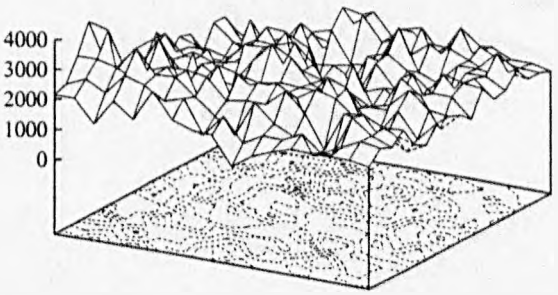

(S, H, Random) = (0.8, 0.0, Yes)

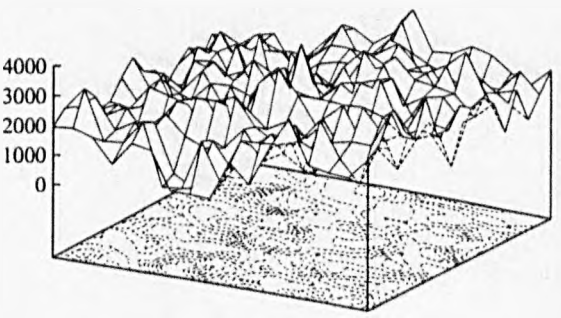

(S, H, Random) = (0.8, 0.0, No)

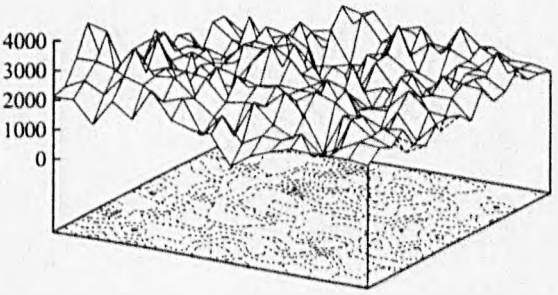

(S, H, Random) = (0.2, 0.9, Yes)

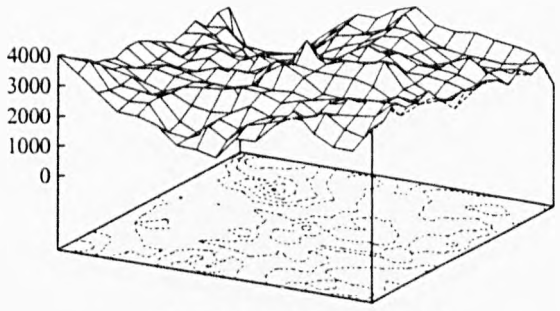

(S, H, Random) = (0.2, 0.9, No)

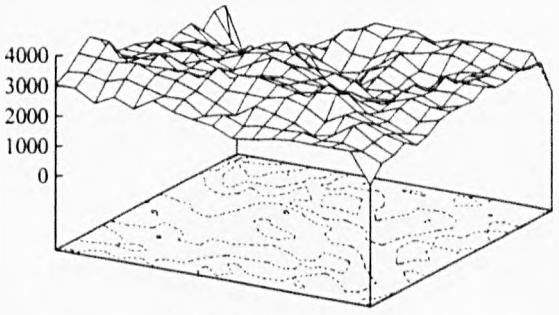

(S, H, Random) = (0.2, 0.8, Yes)

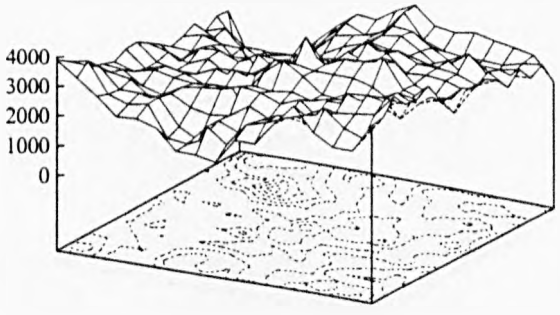

(S, H, Random) = (0.2, 0.8, No)

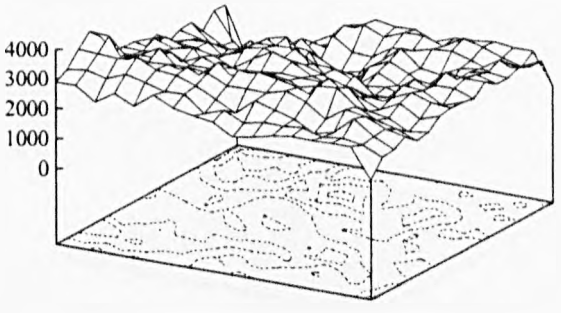

(S, H, Random) = (0.2, 0.7, Yes)

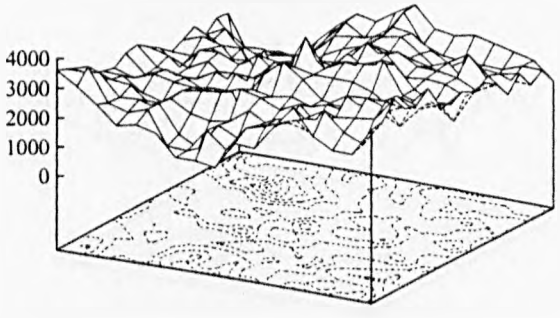

(S, H, Random) = (0.2, 0.7, No)

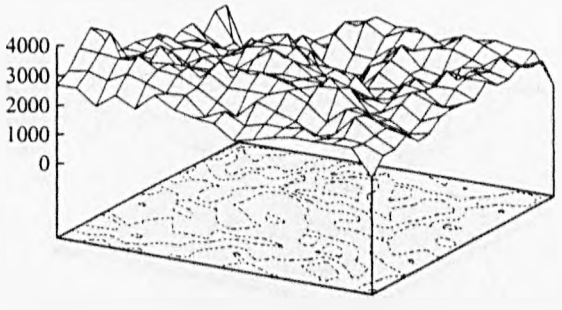

(S, H, Random) = (0.2, 0.6, Yes)

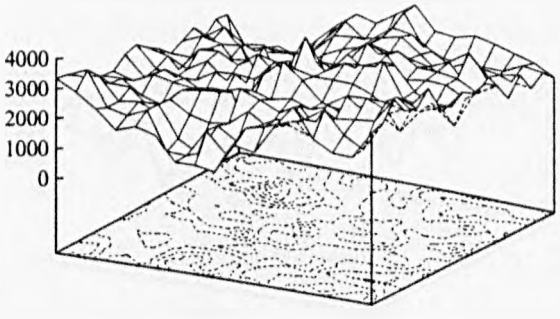

(S, H, Random) = (0.2, 0.6, No)

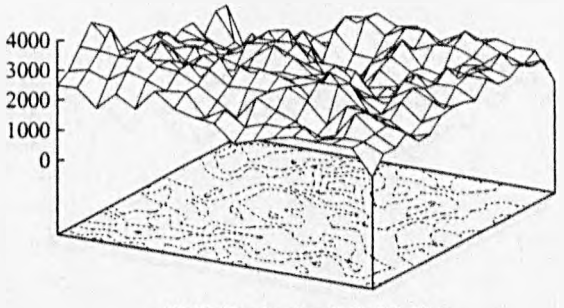

(S, H, Random) = (0.2, 0.5, Yes)

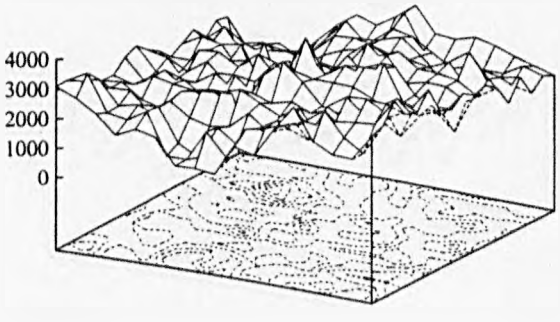

(S, H, Random) = (0.2, 0.5, No)

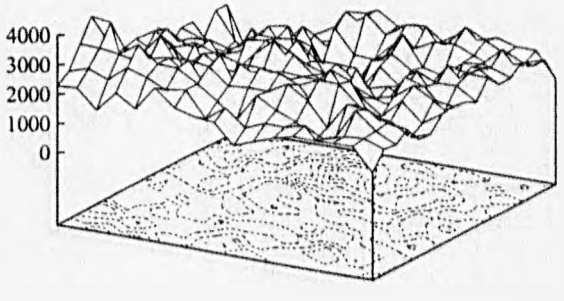

(S, H, Random) = (0.2, 0.4, Yes)

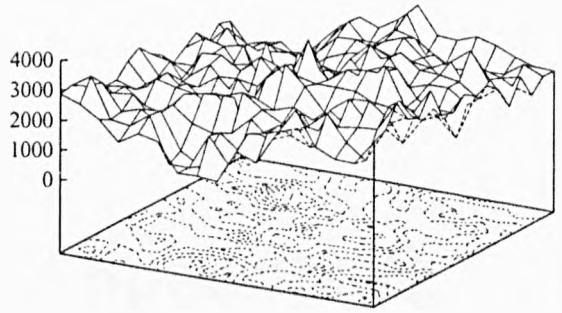

(S, H, Random) = (0.2, 0.4, No)

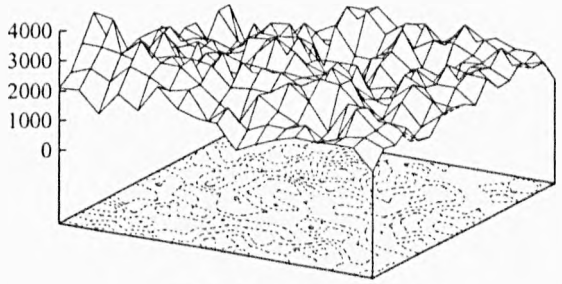

(S, H, Random) = (0.2, 0.3, Yes)

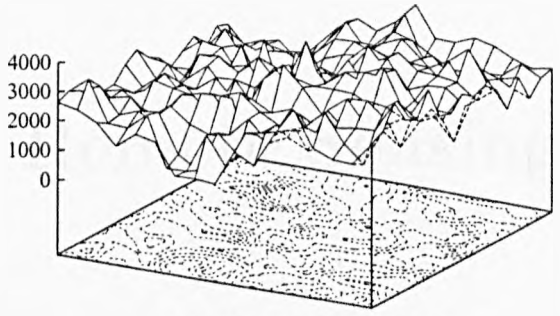

(S, H, Random) = (0.2, 0.3, No)

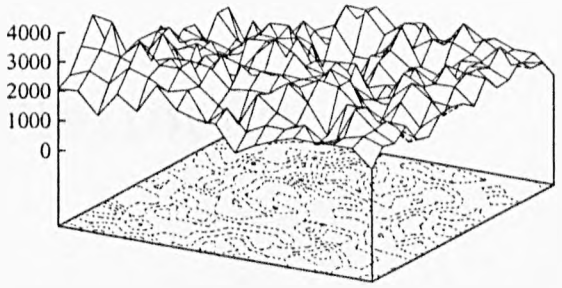

(S, H, Random) = (0.2, 0.2, Yes)

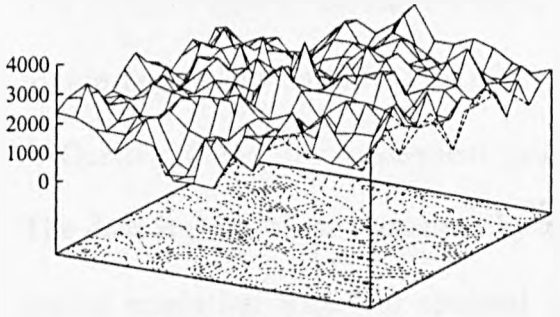

(S, H, Random) = (0.2, 0.2, No)

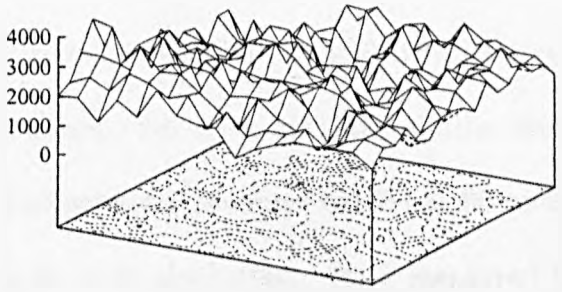

(S, H, Random) = (0.2, 0.1, Yes)

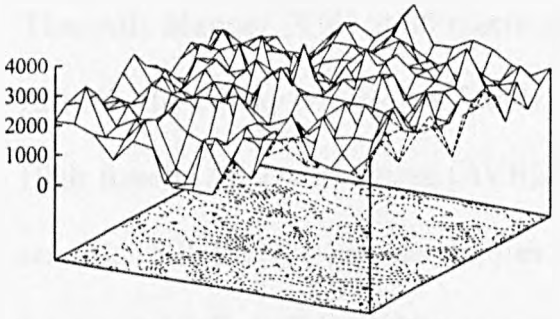

(S, H, Random) = (0.2, 0.1, No)

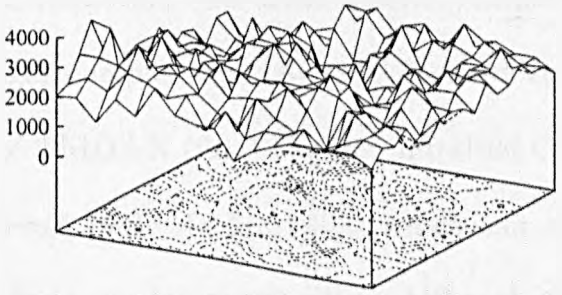

(S, H, Random) = (0.2, 0.0, Yes)

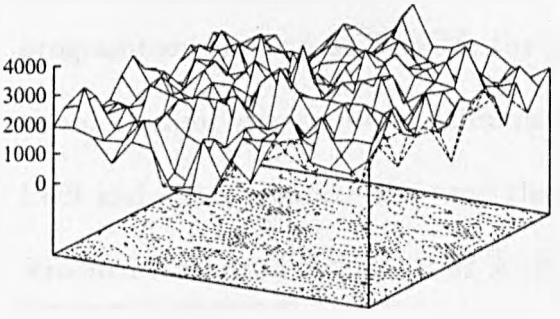

(S, H, Random) = (0.2, 0.0, No)

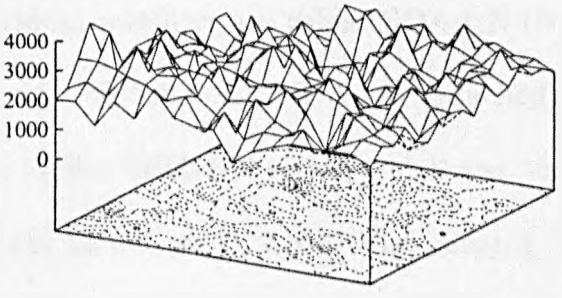

Appendix Q

Remote Sensing Platforms

The satellite view of the earth's surface began in 1972 with the launch of Earth Resource Technology Satellite (ERTS-1), later renamed Landsat (NASA, 1972; Barrett & Curtis, 1974).[1] In subsequent years, Landsats 2-5 have obtained similar data. The data include those measured by the Multispectral Scanners (MSS) at 80-metre spatial resolution with four spectral channels, and, since 1982, those measured by Thematic Mapper (TM) at 30-metre spatial resolution with seven spectral channels. In 1979, the 16-day coverage of Landsat began complemented by the Advanced Very High Resolution Radiometres (AVHRR) of TIROS-N (for Television InfraRed Observation Satellites) series of satellites (Kidwell, 1981; Mather, 1987), which acquires 1.1 *km* spatial resolution data in four or five spatial channels daily. Although the programme is known as TIROS, the individual satellites are called NOAA-N (National Oceanic Atmospheric Administration). NOAA-6 and NOAA-7, launched in 1979 and 1981, respectively, were the last in the TIROS-N series, which was then renamed Advanced TIROS-N or ATN on the launch of NOAA-8. The imaging in-

[1] Refer to page 201.

strument carried by the ATN satellites is the AVHRR (Mather, 1987, p.68). In 1986 two High Resolution Visible (HRV) sensors onboard the French *Satellite Pour l'Observation de la Terre* (SPOT) have begun to obtain data suitable for monitoring vegetation at 10-metre spatial resolution with a visible "panchromatic" channel or at 20-metre spatial resolution with three thermal channels (Price, 1987, p.15).

Other spacecraft and sensors were developed to monitor the earth's surface, too. Explorer-A carries the HCMMR (Heat Capacity Mapping Mission Radiometre), with spatial resolutions of 500 and 600 metres for channels 1 and 2, respectively (Mather, 1987). Nimbus-7, which was launched in 1978 and continued to operate for ten years, had onboard CZCS (Coastal Zone Color Scanner). Seasat was launched in 1978 and operated for only 106 days. Nevertheless, it was the first spaceborne active microwave mapping sensor, a Synthetic Aperture Radar or SAR, with 25-metre spatial resolution (Cracknell & Hayes, 1991). The Meteosat is geostationary. It carries one visible channel with 2.4-metre spatial resolution and two thermal infrared channels with five-metre spatial resolution (Mather, 1987).

Th optics and optical systems of remote sensing are detailed, for example, by Slater (1980), whereas the physical principles of remote sensing can be seen, for example, in Rees (1990). Price (1987) gave a detailed account of wavelengths and bandwidths of the scanners, and vegetation indices related to the spectral channels.

Appendix R

The Natural History of Ferns

In the Palaeozonic era, the typical palaeophytic formations were "carboniferous forests" composed of tree-like clubmosses, horsetails and ferns.[1] Over a long period of 350 million years, these sporophytes evolved, died out or adapted to the change from life in water and bogs to life on dry land. The plant bodies of clubmosses, horsetails and ferns are the asexual phase, which is entirely independent of the sexual phase. These plant bodies are already clearly differentiated into a root, stem and leaves, hence also have a relatively complicated morphological and anatomical structure. Besides the leaves which manufacture food, the plants also have leaves called sporophylls that develop sporangia. Present-day ferns are not as large as their ancestors, although, in the tropics, they may have immensely large fronds. Ferns also include dwarf species only five centimetre high, more like a liverwort or moss in appearance, that grow on rocks. Ferns also include plants that long ago gave up life on dry land and went back to living in water, e.g., the water-fern (*Salvinia*) used in aquaria. Refer to Toman & Felix (1990) for more details.

---

[1] Refer to page 203.

Appendix S

Programme Listing of Virtual Plants

The computer programmes for generating two virtual plants are listed below.

S.1 A Virtual Tree

The following C programme generates a virtual tree using the "chaos game" approach.[1] This programme is incorporated with the SunGKS 4.1 Graphic library using the following script, "*acc -Bdynamic -I$GKSHOME/include -I$OPENWINHOME/include $1.c -o $1 -xCC -L$OPENWINHOME/lib -L$GKSHOME/lib -lgks -lxgl -lxview -lX11 -lm -lF77*".

```
/*
// GKTREE.C
// Des.: a chaotic tree.
*/
#include <gks/ansicgks.h>
#include <stdio.h>
#include <stdlib.h>
#include <math.h>
#define MAXCLR 15
#define NUMITS 50000
#define DAMMY 100
#define RNUM 1000
#define PARA_SIZE 5
/* the window and viewport dimensions */
Gnlimit viewport = { 0.0, 1.0, 0.0, 1.0 };
Gwlimit window = { -0.1, 1.1, -0.1, 1.1
};
/* Frame of viewport. */
Gwpoint square[5] = {0.0, 0.0,
                     0.0, 1.0,
                     1.0, 1.0,
                     1.0, 0.0,
                     0.0, 0.0};

Gwpoint val, newval;

/* IFS code: a,b,c,d,e,f and p */
floatta[PARA_SIZE] = { 0.195,  0.462,
-0.058, -0.035, -0.637},
tb[PARA_SIZE] = {-0.488,  0.414,
-0.070,  0.070,  0.000},
tc[PARA_SIZE] = { 0.344, -0.252,
0.453, -0.469,  0.000},
td[PARA_SIZE] = { 0.443,  0.361,
-0.111, -0.022,  0.501},
te[PARA_SIZE] = { 0.4431, 0.2511,
0.5976, 0.4884, 0.8562},
tf[PARA_SIZE] = { 0.2452, 0.5692,
0.0969, 0.5069, 0.2513},
tp[PARA_SIZE] = { 0.049,  0.6,    0.05,
0.001,  0.3};
/*********************************
************** main ************
*********************************/
void main()
{
Gasfs asfs;
Gks_ws_config config;
Gchar *conn = NULL;
Gchar *wstype = "xgl_tool";
Gint  transform = 1;
Gws  ws1 = 1;
Gmktype  marker = 1;
Gcobundl colour_rep;
Gindex  fill_colour = 0;
long int i;
int r;
int map;
float mag;
/* either INDIVIDUAL or BUNDLED */
asfs.mk_type   = INDIVIDUAL;
asfs.mk_size   = INDIVIDUAL;
asfs.mk_colour = INDIVIDUAL;
asfs.ln_colour = INDIVIDUAL;
asfs.ln_type   = INDIVIDUAL;
asfs.ln_width  = INDIVIDUAL;
```

[1] Refer to page 199 and Section 6.3.2.

```
/*
// Open GKS.
// Set up and configure the workstation.
//  Open and activate workstation
*/
if (gopengks(stdout, GMEMORY))
{ exit(2); }
config = gks_ws_config_get_installed(wstype);
gks_ws_config_set(config,
GKS_TOOL_X,       10,
GKS_TOOL_Y,       10,
GKS_TOOL_WIDTH,   600,
GKS_TOOL_HEIGHT,  600,
GKS_TOOL_LABEL,  "GKS #1",
0);
gks_ws_config_install(config);
gopenws(ws1, conn, wstype);
gactivatews(ws1);
/* set attribute; activate wrkstn */
gsetasf(asfs);
/* Set up colourmap for each ws */
for(fill_colour = 0; fill_colour <= MAXCLR;
fill_colour++){
colour_rep.red = colour_rep.green =
colour_rep.blue =
(float)fill_colour/MAXCLR;
gsetcolourrep(ws1, fill_colour, colour_rep);
}
/* the window and viewport using # */
gsetwindow(transform, window); // no &
gsetviewport(transform, viewport); // no &
gselnormtran(transform);
/* Set colour, type, style, etc. */
gsetmarkertype(marker);
gsetmarkercolour(15);
gsetlinecolour(15);
val.x = 0.0;
val.y = 0.0;
gpolyline(5, square);
for(i = 0; i < NUMITS; i++){
r = rand() % RNUM;
map = 0;
if(r > (int)(tp[0] * RNUM))
map = 1;
if(r > (int)((tp[0]+tp[1]) * RNUM))
map = 2;
if(r > (int)((tp[0]+tp[1]+tp[2]) * RNUM))
map = 3;
if(r > (int)((tp[0]+tp[1]+tp[2]+tp[3]) *
RNUM)) map = 4;
newval.x = (float)ta[map] * val.x +
tb[map] * val.y + te[map];
newval.y = (float)tc[map] * val.x +
td[map] * val.y + tf[map];
val.x = newval.x;
val.y = newval.y;
if(i > DAMMY){
gpolymarker(1, &newval);
}
}
gmessage(ws1, "Quits after five seconds");
sleep(15);
/* Clean up */
gdeactivatews(ws1);
gclosews(ws1);
gclosegks();
} // main
```

S.2 Synthetic Ferns

The two computer programmes for generating synthetic ferns are listed below: one using deterministic while the other using random algorithms.[2] The following script is used to compile both C programmes incorporating NAG FORTRAN library routines (Hann & Hounam, 1991), whose resulting object programme is further compiled by FORTRAN compiler. That is, "*acc -c -lm $1.c*" and "*f77 $1.o -o $1 -lnag*".

Deterministic Synthetic Ferns

Example: *detfern 10 0*

```
/* detfern.C
// Santax: detfern level 3/2/0(Idrisi)
// Desc: Generating a fern: peitetal92
//  Using Deterministic algorithm
// Range: [0.0 1.0]x[0.0 1.0]
// Output: 3D (z only) or 2D (x y)
// file: a fern in IDRISI format
//Note:Img set to WIN_SIZE x WIN_SIZE
*/
#include <stdio.h>
#include <stdlib.h>
#include <math.h>

#define PARA_SIZE (4)
#define WIN_SIZE (1024)
#define VAL_OFF (0)
#define VAL_ON (1)
#define MIN(x, y)(((x)<=(y))?(x):(y))
#define MAX(x, y)(((x)>(y))?(x):(y))

unsigned short int
fern[WIN_SIZE][WIN_SIZE];
unsigned short int
img[WIN_SIZE][WIN_SIZE];
```

[2] Refer to Section 6.3.2.

```
/*** peitetal92: 295 ***/
floata[4]={ 0.849, 0.197,-0.15, 0.0},
      b[4]={ 0.037,-0.226, 0.283,0.0},
      c[4]={-0.037, 0.226, 0.26, 0.0},
      d[4]={ 0.849, 0.197, 0.237,0.16},
      e[4]={ 0.075, 0.4,   0.575,0.5},
      f[4]={ 0.183, 0.049,-0.084,0.0};
/*** Det_tansformation() ***/
void Det_transformation(
   int iter, // iteration
   floatx,// coord
   float y)
{
   int  trans, level,i,j;
   float newx[PARA_SIZE],
newy[PARA_SIZE];
   float tmpx,tmpy;
/* Calculate first set of trans */
   for(trans = 0; trans < PARA_SIZE;
trans++){
      newx[trans] = a[trans] * x + b[trans]
* y + e[trans];
      newy[trans] = c[trans] * x + d[trans]
* y + f[trans];
      tmpx = newx[trans];
      tmpy = newy[trans];
      if((tmpx>=0.0) && (tmpx<=1.0) &&
(tmpy>=0.0) && (tmpy<=1.0)){
/*float to pixel (int) location */
         i = (short int)
(rint(tmpx*WIN_SIZE));
         j = (short int)
(rint(tmpy*WIN_SIZE));
         if((i>=0) && (i<WIN_SIZE) &&
(j>=0) && (j<WIN_SIZE)){
            fern[i][j] += VAL_ON;
         } // if: i,j
      } // if: tmpx, tmpy
   } // trans
/* calculate the second set of trans */
   level = iter - 1;
   if(level > 0){
      for(trans = 0; trans < PARA_SIZE;
trans++){
         x = newx[trans];
         y = newy[trans];
         Det_transformation(level, x, y);
      } // trans
   } // if: level
} // Det_transformation()
/*********************************
************ Main ****************
*********************************/
main(int argc, char **argv)
{
FILE *fout;
int  iter,out_choice;
int  i,j;
int  size_us = sizeof(unsigned short int);
unsigned short int zmin,zmax,z;
float x,y;
if(argc != 3){
   printf("Usage: %s iter 3/2/0\n",argv[0]);
   printf("\titer: Iterations (10)\n");
   printf("\t3/2/0: 3D, 2D or IDRISI files
(default).\n");
   exit(-1);
} // warning
iter = atoi(argv[1]);
out_choice = atoi(argv[2]);
/*** Initialising array ***/
for(i=0;i<WIN_SIZE;i++){
   for(j=0;j<WIN_SIZE;j++){
      img[i][j] = VAL_OFF;
      fern[i][j] = VAL_OFF;
   } // j
} // i
img[WIN_SIZE/2][WIN_SIZE/4] =
VAL_ON;
img[WIN_SIZE/2][0] = VAL_ON;
/*** CAlculations ***/
for(i=0;i<WIN_SIZE;i++){
   for(j=0;j<WIN_SIZE;j++){
      if(img[i][j] != VAL_OFF){
         x = (float) i / WIN_SIZE;
         y = (float) j / WIN_SIZE;
         Det_transformation(iter, x, y);
      } // if
   } // j
} // i
/*** Output routine ***/
switch(out_choice){
case 3:
   for(i=0;i<WIN_SIZE;i++){
      for(j=0;j<WIN_SIZE;j++){
         printf(" %u\n",fern[i][j]);
      } // j
      printf("\n");// gnuplot: z only
   } // i
   break;
case 2:
   for(i=0;i<WIN_SIZE;i++){
      for(j=0;j<WIN_SIZE;j++){
         if(fern[i][j] != VAL_OFF){
            printf("%d %d",i,j);
            printf("\n");
         } // if
      } // j
   } // i
   break;
default:
   printf("# Default: Write to IDRISI .doc
and .img files.\n");
   if((fout = fopen("DetFern.bin", "wb"))
```

PAGE MISSING IN ORIGINAL

```
/*** Initialising array ***/
fern = malloc(sizeof(int) * img_size *
img_size);
for(i=0;i<img_size;i++){
   for(j=0;j<img_size;j++){
      fern[i*img_size+j]=VAL_OFF;
   } // j
} // i
/*** Initail set ***/
// x = e[0]; y = f[0];
 x = 0.5; y = 0;
/*** intervals ***/
p1 = p[0];
p2 = p[0] + p[1];
p3 = p[0] + p[1] + p[2];
for(iter = 0; iter < num_point; iter++){
   r = r_lcran_();
   trans = 0; // stem; peitetal93: 351
   if(r > p1) trans = 1; // right leaf
   if(r > p2) trans = 2; // left leaf
   if(r > p3) trans = 3; // top
   newx = a[trans] * x + b[trans] * y +
e[trans];
   newy = c[trans] * x + d[trans] * y +
f[trans];
   m = (unsigned short int)rint(newx *
img_size);
   n = (unsigned short int)rint(newy *
img_size);
   if((m>=0) && (m<img_size) && (n>=0) &&
(n<img_size)){
      fern[m * img_size + n] += VAL_ON;
   } // i,j
   x = newx;  y = newy;
} // iter
switch(out_choice){
   case 3: /*** 3D: z only ***/
      for(i=0;i<img_size;i++){
         for(j=0;j<img_size;j++){
            printf("%d\n",
fern[j*img_size+i]);
         } // j
         printf("\n");
      } // i
      break;
   case 2:/*** 2D: xy ***/
      for(i=0;i<img_size;i++){
         for(j=0;j<img_size;j++){
            if((k=fern[i*img_size+j]) > 0){
               printf("%d %d ", i,j);
               printf("\n");
            } // if
         } // j
      } // i
      break;
   default:/*** IDRISI files ***/
         printf("# Default: Write to IDRISI
.doc and .img files.\n");
         if((fout = fopen("RanFern.bin",
"wb")) == NULL){
            printf("# Can't open IDRISI
image file: ansifern.img\n");
            exit(-1);
         } // opening a file
         zmin = fern[0]; zmax = fern[0];
         for(i = 0; i < img_size; i++){
            for(j = 0; j < img_size; j++){
               k = i * img_size + j;
               fwrite(&fern[k], size_us, 1,
fout);
               zmin = MIN(zmin, fern[k]);
               zmax = MAX(zmax, fern[k]);
            } // y
         } // x
         fclose(fout);
         if((fout = fopen("RanFern.doc",
"wt")) == NULL){
            printf("# Can't open IDRISI .doc
file: ansifern.doc\n");
            exit(-1);
         } // opening a file
   fprintf(fout, "file title : RanFern\n");
   fprintf(fout, "data type : integer\n");
   fprintf(fout, "file type : binary\n");
   fprintf(fout, "columns : %d\n", img_size);
   fprintf(fout, "rows : %d\n", img_size);
   fprintf(fout, "ref. system : plane\n");
   fprintf(fout, "ref. units : m\n");
   fprintf(fout, "unit dist. : 1\n");
   fprintf(fout, "min. X : 0\n");
   fprintf(fout, "max. X:%d\n",img_size-1);
   fprintf(fout, "min. Y : 0\n");
   fprintf(fout, "max. Y:%d\n",img_size-1);
   fprintf(fout, "pos'n error : unknown\n");
   fprintf(fout, "resolution : unknown\n");
   fprintf(fout, "min. value : %d\n", zmin);
   fprintf(fout, "max. value : %d\n", zmax);
   fprintf(fout, "value units : classes\n");
   fprintf(fout, "value error : unknown\n");
   fprintf(fout, "flag value : none\n");
   fprintf(fout, "flag def'n : none\n");
   fprintf(fout, "legend cats : 0\n");
   fclose(fout);
  break;
} // switch
free(fern);
} // main
```

Appendix T

Programme Listing of Fern's Dimensions

The computer programme for calculating the fractal dimensions of the fern is listed below.[1] The following script is used to compile the C programme, that is, "*acc -c -lm $1.c*" and "*f77 $1.o -o $1 -lnag*".

T.1 Fractal Dimensions of Profiles

```
/*
// fernfd.c    <-- from dem_fd.c
// Usage: dem_fd in.doc in.bin 1 > file
// Out:(stdout)
*/
#include <stdio.h>
#include <stdlib.h>
#include <math.h>
#include <nagmk15.h> // NAGF lib.
#include <TS.h>

#define MAX_IMG_SIZE (1024)
#define HDR_LINE_NO (21)
#define HDR_LINE_SIZE (100)
#define HDR_INFO_START (14)
#define REGR_RESULTS (20)
#define OUT_RESULTS (9)
#define MAX_SUB_SETS (20) s
#define OUT_BASE (1.0)

/*** col, row, etc from header ***/
int extract_info(
char out[],// input string
char in[]) // output string
{
inti, j;
for(i=HDR_INFO_START, j=0; j<5; i++,
j++) { out[j]=in[i]; }
} // extrac_info()
```

[1] Refer to Section 6.4.

```
/************************************
// Box-counting: Brownian method
************************************/
void TS_brown_box_counting(
double x[],        /* input data */
int length,        /* length of data */
double std,        /* height of data */
double result[20])     /* resultant
dimension */
{
int i,u,v;
int paces;
double *tmpp, *size, *count, *ind, *dep;
double width, height,val;
double scal;
/* declarations for G01AAF, G02CAF */
int n,iwt,ifail;
double *wt, xmean,s2,s3,s4,
xmin,xmax,wtsum;
paces= (int) floor(log2((double)length));
size  = malloc(paces * sizeof(int));
count= malloc(paces * sizeof(int));
for(i = 0; i < paces; i++){
scal = exp2((double)i );
width= length / scal; height = std / scal;
size[i] = scal; count[i]= 0.0;
tmpp = malloc((int)width *
sizeof(double));
wt = malloc((int)width * sizeof(double));
for(u = 0; u < scal; u++){
for(v = 0; v < width; v++) {
tmpp[v] = x[u * (int)width + v];
}
n = (int) width; iwt= 0; ifail = 1;
g01aaf_(&n, tmpp, &iwt, wt, &xmean, &s2,
&s3, &s4, &xmin, &xmax, &wtsum, &ifail);
val = ceil(xmax/height) - floor(xmin/height);
count[i] += val;
}
free(tmpp); free(wt);
}
```

```
for(i=0;i<paces;i++){
size[i] = log2(size[i]);
count[i]= log2(count[i]);
}
n= paces; ifail = 1;
g02caf_(&n, size, count, result, &ifail);
free(size); free(count);
} // TS_brown_box_counting //


/************************************
********** main() ******************
************************************/

void main(int argc, char **argv)
{
FILE *fin;
char hdr[HDR_LINE_SIZE], tmp[5], ch;
int sub;// number of subsets
int i, j, k;
int col, row, new_col, new_row;
int diff_c, diff_r, start_c, start_r,
val[2][MAX_SUB_SETS];
int size_s, size_d;// 2 bytes
short int *temp,
img[MAX_IMG_SIZE][MAX_IMG_SIZE];
double
hout[REGR_RESULTS][MAX_IMG_SIZE],
vout[REGR_RESULTS][MAX_IMG_SIZE];
double vremn1, vremn2;

/* NAGF: G01AAF etc */
int m, n,iwt,ifail;
double *y, *x,*wt, xmean,s2,s3,s4,
xmin,xmax,wtsum, result[20];
double *tmpx, *tmpy;
size_s = sizeof(short int);
size_d = sizeof(double);

/****** warning msg *****************/
if(argc < 2){
printf("Usage: %s in.doc in.bin no > file\n",
argv[0]);
printf("\tin.doc:Input document (Idrisi)\n");
printf("\tin.bin:Input image (Unix)\n");
printf("\tno.:Number of points. 1 means an
img. of 2^n\n");
printf("\t\t-> to be dd conv=swab (Unix) ->
.img (Idrisi)\n");
printf("Note: output (stdout) should be
redirected to a file\n");
printf("\ti.e., ... | more > file\n");
printf("\tno: Number of sub-sets used <
%d\n", MAX_SUB_SETS);
exit(-1);
}

/********** parameter *********/
sub = atoi(argv[3]);
/*** col & row from .doc header **/
if((fin = fopen(argv[1], "rt")) == NULL){
printf("Can't open input Idrisi .doc file:
%s\n", argv[1]); exit(-1);
} // open file
for(i = 0; i < HDR_LINE_NO; i++){
fgets(hdr, HDR_LINE_SIZE, fin);
if(i == 3) {
extract_info(tmp, hdr);
col= atoi(tmp);
}
if ( i == 4){
extract_info(tmp, hdr);
row= atoi(tmp);
}
} // i
fclose(fin);

/****** scan image into an arry *******/
if((fin = fopen(argv[2], "rb")) == NULL){
printf("Can't open input image file: %s\n",
argv[2]); exit(-1);
}
temp = malloc(col * size_s);
img[0][0]=0.0; temp[0]=0.0; temp[1]=0.0;
for(i = 0; i < row; i++){
fread(temp, size_s, col, fin);
for(j = 0; j < col; j++){
if(temp[j] > 0.0) {
img[i][j] = temp[j];
}else {
temp[j]=2*temp[j-1]-temp[j-2];
if(temp[j]<0.0) { temp[j]=temp[i-1]; }
img[i][j] = temp[j];
}
} // j
} // i
free(temp); fclose(fin);
/** the size of profile for fd **/
xmean= floor(log2( (double) col ));
vremn1= remainder((double) col, 2.0);
new_col= (int) exp2(xmean);
xmean= floor(log2( (double) row ));
vremn2= remainder((double) row, 2.0);
new_row= (int) exp2(xmean);

/******** fd calculation ********/
x= malloc(new_col * size_d);
y= malloc(new_row * size_d);
tmpx= malloc(new_col * size_d);
tmpy= malloc(new_row * size_d);
wt= malloc(new_col * size_d);
diff_c= (col - new_col)/2;
diff_r= (row - new_row)/2;
for(k = 0; k < sub; k++){
```

```
if(vremn1 != 0.0) {
start_c= random() % diff_c;
val[0][k] = start_c;
} else {
val[0][k] = start_c = 0;
}
if(vremn2 != 0.0){
start_r= random() % diff_r;
val[1][k] = start_r;
} else {
val[0][k] = start_r = 0;
}
for(i = start_c, m = 0; m < new_col; i++,
m++){
for(j = start_r, n = 0; n < new_row; j++,
n++){
tmpx[n]= img[i][j];
tmpy[n]= img[j][i];
} // j
n= new_row; iwt = 0; ifail = 1;
TS_data_extra(tmpx,x,n);
g01aaf_(&n,x,&iwt,wt,&xmean,&s2,&s3,&s4,
&xmin,&xmax,&wtsum,&ifail);
TS_brown_box_counting(x, n, s2, result);
for(j=0;j<REGR_RESULTS;j++){
if(xmean > xmin){
hout[j][i] = result[j];
} else { hout[j][i] = OUT_BASE; }
} // j
n= new_row; iwt = 0; ifail = 1;
TS_data_extra(tmpy,y,n);
g01aaf_(&n,y,&iwt,wt,&xmean,&s2,&s3,&s4,
&xmin,&xmax,&wtsum,&ifail);
TS_brown_box_counting(y, n, s2, result);
for(j=0;j<REGR_RESULTS;j++){
if(xmean > xmin){
vout[j][i] = result[j];
} else { vout[j][i] = OUT_BASE; }
} // j
} // i
} // k
free(x); free(y); free(wt);

/*************** Result **********/
printf("# fd (h v) results from %s %s;
subimage size: %d\n", argv[1], argv[2],
new_col);
printf("# %d pairs of top-left corners: ",
sub);
for(i = 0; i < sub; i++){
printf("(%d %d) ", val[0][i], val[1][i]);
} printf("\n");
printf("# no. 12 h_results... 12
v_result...\n");
for(i = 0; i < new_col; i++){
printf("%5d ", i+1);
for(j = 0; j < OUT_RESULTS; j++)
{printf("%.3lf ", hout[j][i]);}
for(j = 0; j < OUT_RESULTS; j++)
{printf("%.3lf ", vout[j][i]);}
printf("\n");
} // i
} // main
```

T.2 Fractal Dimensions of 2D & 3D Features

```
/*
// FERNBOXFD.C
// Santax: fernboxfd in_img img_size R/S
// Desc:FD of 2D and 3D
// Output:2D 3D
*/
#include <stdio.h>
#include <stdlib.h>
#include <math.h>
#include <nagmk15.h> // NAGF lib.

#define MAX_IMG_SIZE (1024)
#define VAL_OFF (0)
#define VAL_ON (1)
#define MIN(x,y) (((x)<=(y))?(x):(y))
#define MAX(x,y) (((x)>(y))?(x):(y))

/******** box_fd() *********/
void box_fd(
int max_level, // iteration
double x[], // x variable
double y[], // y variable
double result[20]) // output: fd
{
int i, size_d=sizeof(double);
/* declarations for G01AAF, G02CAF */
int n,iwt,ifail;
double *xx,*yy,*wt;
n = max_level - 1;
xx = malloc(n * size_d);
yy = malloc(n * size_d);
for(i=1;i<max_level;i++){
n = i - 1; xx[n] = log(1.0/x[i]);
yy[n] = log(y[i]);
} // i
ifail = 1;
g02caf_(&n, xx, yy, result, &ifail);
free(xx); free(yy);
} // box_fd()

/************************************
```

```
************* main *****************
************************************/
void main(int argc, char **argv)
{
FILE *fdoc,*fimg;
char ch;
int img_size,box_size;
int iter,max_iter,level,max_level;
int i,j,m,n,u,v,i_str,j_str;
int size_d=(sizeof(double)),size_us=
(sizeof(unsigned short int));

unsigned short int *temp,
img[MAX_IMG_SIZE][MAX_IMG_SIZE];
unsigned short int z_count,box_count,
z,zmin,zmax;
unsigned long int count,box_count_3D;

double *y, *x,*wt,xmean,s2,s3,s4,xmin,
xmax,wtsum,result[20],iwt,ifail;
double *yy,*xx, height,fd;

if(argc != 4){
printf("Usage: %s in_img img_size R/S\n",
argv[0]);
printf("\tin_img:input IDRISI image (don't
need .doc)\n");
printf("\timg_size: size of image\n");
printf("\tR/S:Real/Synthetic\n"); exit(-1);
} // warning
img_size = atoi(argv[2]); ch = argv[3][0];
max_level = (int)log2((double)img_size);

if((fimg=fopen(argv[1],"rb")) == NULL){
printf("Can't open input image.\n");
exit(-1);
} // open image file
/*** Read file into array array ***/
temp = malloc(size_us * img_size);
zmin = 0; zmax = 0;
for(i=0;i<img_size;i++){
fread(temp,size_us,img_size,fimg);
for(j=0;j<img_size;j++){
z = temp[j]; img[i][j] = z;
zmin=MIN(zmin,z); zmax=MAX(zmax,z);
} // j
} // i
free(temp); fclose(fimg);
printf("# zmin %d zmax %d\n",
zmin,zmax);

switch(ch) /* real or synthetic */
{
case 'R': case 'r':
count = VAL_OFF;
for(i=0;i<img_size;i++){
for(j=0;j<img_size;j++){ z = img[i][j];
if(z < zmax) { count++; } // if
img[i][j] = abs(zmax - z);
} // j
} // i
printf("# Non-empty pixels: %d\n",count);
break;
case 'S': case 's':
count = VAL_OFF;
for(i=0;i<img_size;i++){
for(j=0;j<img_size;j++){ z = img[i][j];
if(z > VAL_OFF) { count++; } // if
} // j
} // i
printf("# Non-empty pixels: %d\n",count);
break;
defult: break;
} // switch

x = malloc(count * size_d);
wt= malloc(count * size_d);
count = VAL_OFF;

for(i=0;i<img_size;i++){
for(j=0;j<img_size;j++){
z = img[i][j];
if(z > VAL_OFF) { x[count]=(double)z;
count++; } // if
} // j
} // i

/*** get stats ***/
iwt = VAL_OFF; ifail = VAL_ON;
g01aaf_(&count,x,&iwt,wt,&xmean,&s2,&s3,
&s4,&xmin,&xmax,&wtsum,&ifail);
printf("# mean  std  min max\n");
printf("# %4.2f  %4.2f %3.0f %3.0f\n",
xmean,s2, xmin,xmax);
free(wt); free(x);

/*** iter -> box_count (col -> row);
output: size[] & count[] ***/
x = malloc(size_d * (max_level+1));
y = malloc(size_d * (max_level+1));
xx = malloc(size_d * (max_level+1));
yy = malloc(size_d * (max_level+1));
x [0] = (double)MAX_IMG_SIZE;
xx [0] = (double)MAX_IMG_SIZE;
x [10] = (double)VAL_ON;
xx [10] = (double)VAL_ON;
y [0] = 1.0; yy [0] = (xmax-xmin)/s2;
y [10] = (double)img_size * img_size;
yy [10] = (double)img_size * img_size *
(xmax-xmin)/s2*exp2(10);

/*** setting size ***/
for(level=1;level<max_level;level++){
max_iter = (int)exp2(level);
```

```
box_size  = img_size/max_iter;
height = s2/(double)max_iter;
x[level] = (double)box_size;
xx[level] = (double)box_size;

/*** counting routine ***/
box_count = VAL_OFF;
box_count_3D = VAL_OFF;
for(u=0; u<max_iter; u++){
j_str=u*box_size;
for(v=0; v<max_iter; v++){
i_str = v * box_size; z_count = VAL_OFF;
zmin = 999; zmax = VAL_OFF;
for(i=0; i<box_size; i++){ m = i_str + i;
for(j=0; j<box_size; j++){
n = j_str + j; z = img[m][n];
if(z > VAL_OFF) { z_count++;
zmin = MIN(zmin,z);
zmax = MAX(zmax,z); } // if
} // j
} // i
if(z_count > VAL_OFF) { box_count++; }
count = (unsigned long int)
(ceil(xmax/height) - floor(xmin/height));
box_count_3D += count;
} // v
} // u
y[level] = (double)box_count;
yy[level] = (double)box_count_3D;
} // level
printf("# size  2D_counts   3D_counts
(log2 vs real scales)\n");

for(i=0;i<=max_level;i++){
printf("%4.0f \t%9.3f %11.3lf\t",
log2(x[i]),log2(y[i]),log2(yy[i]));
printf("%4.0f \t%9.0f %11.0lf\n",
x[i],y[i],yy[i]);
} // i

printf("# D  fd (log-log)\n");
box_fd(max_level,x,y,result);
printf("# 2 %.3f\n", result[5]);
box_fd(max_level,xx,yy,result);
printf("# 3 %.3f\n", result[5]);
free(x); free(y); free(xx);free(yy);
} // main
```